

**SYNTHESIS AND REACTIVITY OF
DINITROGEN, OXO, AND NITRIDO COMPLEXES
OF FIRST ROW TRANSITION METALS
SUPPORTED BY HYRDOTRIS(PYRAZOLYL)BORATE LIGANDS**

by

Daniel Clayton Cummins

A dissertation submitted to the Faculty of the University of Delaware in partial fulfillment of the requirements for the degree of Doctor of Philosophy in Chemistry and Biochemistry

Fall 2017

© 2017 Daniel Clayton Cummins
All Rights Reserved

**SYNTHESIS AND REACTIVITY OF
DINITROGEN, OXO, AND NITRIDO COMPLEXES
OF FIRST ROW TRANSITION METALS
SUPPORTED BY HYRDOTRIS(PYRAZOLYL)BORATE LIGANDS**

by

Daniel C Cummins

Approved: _____
Brian J. Bahnson, Ph.D.
Chair of the Department of Chemistry and Biochemistry

Approved: _____
George H. Watson, Ph.D.
Dean of the College of Arts and Sciences

Approved: _____
Ann L. Ardis, Ph.D.
Senior Vice Provost for Graduate and Professional Education

I certify that I have read this dissertation and that in my opinion it meets the academic and professional standard required by the University as a dissertation for the degree of Doctor of Philosophy.

Signed:

Klaus H. Theopold, Ph.D.
Professor in charge of dissertation

I certify that I have read this dissertation and that in my opinion it meets the academic and professional standard required by the University as a dissertation for the degree of Doctor of Philosophy.

Signed:

Svilen Bobev, Ph.D.
Member of dissertation committee

I certify that I have read this dissertation and that in my opinion it meets the academic and professional standard required by the University as a dissertation for the degree of Doctor of Philosophy.

Signed:

Mary P. Watson, Ph.D.
Member of dissertation committee

I certify that I have read this dissertation and that in my opinion it meets the academic and professional standard required by the University as a dissertation for the degree of Doctor of Philosophy.

Signed:

Daniel J. Mindiola, Ph.D.
Member of dissertation committee

Dedicated to my family, without whom I'd have nothing

ACKNOWLEDGMENTS

First I'd like to thank my research advisor, Klaus H. Theopold, for the chance to contribute to his group. His advice and guidance have made possible my growth as a chemist, and afforded me a greater breadth of synthetic acumen.

I'd also like to extend my deepest gratitude to the members of my dissertation committee, Dr. Mary P. Watson, Dr. Svilen Bobev, and Dr. Daniel Mindiola for reviewing my research and providing me with valuable advice as I progressed through my time in graduate school. I also thank Dr. Shi Bai for helping familiarize me with operating the NMR spectrometers and adjoining software, Dr. Joel Rosenthal and his group for assisting me in running cyclic voltammetry experiments, and all the members of the Theopold lab group, past and present, for their advice and day to day assistance in research. I also give special thanks to Dr. Glenn P. A. Yap, for his assistance in crystallography, his advice concerning the many problems I encountered with my chemistry, and his continued friendship and kind remarks.

To all my friends, family, and especially my partner Hiu-Tung Candy Wong, I can't express with words how grateful I am for your understanding and support, without which I couldn't have made it to where I am today. I will never forget how I got to be here, or how instrumental you all were in making that happen.

Lastly, I'd like to give special thanks to Dr.'s Swiatoslaw Trofimenko and Eric R. Sirianni, whose work built the fundamental underpinnings of my own. Eric told me to carry the legacy of his ligand forward, and to that end I have done all I could.

TABLE OF CONTENTS

LIST OF TABLES	ix
LIST OF FIGURES	xiii
LIST OF SCHEMES	xxi
ABSTRACT	xxiii

Chapter

1	INTRODUCTION	1
	REFERENCES	9
2	SYNTHESIS AND CHARACTERIZATION OF MONO-VALENT IRON AND COBALT COMPLEXES OF FERROCENYL SUBSTITUTED TRIS(PRAZOLYL)BORATE LIGANDS	12
	Introduction	12
	Results and Discussion	14
	Synthesis and characterization of iron halides supported by $\text{Tp}^{\text{Fc,Me}}$ ligand	14
	Synthesis and characterization of cobalt halides supported by $\text{Tp}^{\text{Fc,Me}}$ ligand	25
	Synthesis and characterization of iron alkyls supported by $\text{Tp}^{\text{Fc,Me}}$ ligand	29
	Synthesis and characterization of formally univalent $\text{Tp}^{\text{Fc,Me}}\text{Fe}(\text{CO})$..	41
	Synthesis of univalent dinitrogen complexes	45
	Activation of ferrocenyl moiety by way of supposed hydride intermediate	69
	Conclusions	84
	Experimental	85
	Preparation of $\text{Tp}^{\text{Fc,Me}}\text{FeCl}$ (1).....	87
	Preparation of $\text{Tp}^{\text{Fc,Me}}\text{FeBr}$ (2)	87
	Preparation of $\text{Tp}^{\text{Fc,Me}}\text{FeI}$ (3)	88
	Preparation of $\text{Tp}^{\text{Fc,Me}}\text{CoBr}$ (4).....	89
	Preparation of $\text{Tp}^{\text{Fc,Me}}\text{FeBn}$ (5).....	90

Preparation of $\text{Tp}^{\text{Fc,Me}}\text{FeEt}$ (6).....	91
Preparation of $\text{Tp}^{\text{Fc,Me}}\text{Fe}(\text{CO})$ (7).....	91
Preparation of $\text{Tp}^{\text{Fc,Me}}\text{Fe}(\text{PzH}^{\text{Fc,Me}})(\text{Pz}^{\text{Fc,Me}})$ (8).....	92
Preparation of $[\text{Tp}^{\text{Fc,Me}}\text{Fe}^{\text{I}}]_2(\mu_2\text{-}\eta^1\text{:}\eta^1\text{-N}_2)$ (9).....	93
Preparation of $[\text{Tp}^{\text{Fc,Me}}\text{Fe}^{\text{I}}]_2(\mu_2\text{-}\eta^1\text{:}\eta^1\text{-N}_2)$ (10).....	94
Preparation of $\text{Bp}^{\text{Fc,Me}}(\text{Me-pz-CpFe}(\text{C}_5\text{H}_4))\text{Co}$ (11).....	95
Preparation of $\text{Bp}^{\text{Fc,Me}}(\text{Me-pz-CpFe}(\text{C}_5\text{H}_4))\text{Co}(\text{CO})$ (12).....	96
REFERENCES.....	97
3 REACTIONS OF MONO-VALENT IRON AND COBALT COMPLEXES SUPPORTED BY HYDROTRIS(3-FERROCENYL-5-METHYL)PYRAZOLYL BORATO LIGANDS WITH OXO AND IMIDO TRANSFER REAGENTS.....	100
Introduction.....	100
Results and Discussion.....	100
Synthesis of triphenylmethyl chalcogenide iron complexes supported by $\text{Tp}^{\text{Fc,Me}}$ and reaction to form novel bridging sulfide complex.....	102
Reactions of single atom oxygen transfer reagents with $[\text{Tp}^{\text{Fc,Me}}\text{Fe}]_2(\mu\text{-}\eta^1\text{:}\eta^1\text{-N}_2)$ (9).....	115
Reactions of $[\text{Tp}^{\text{Fc,Me}}\text{Fe}]_2(\mu\text{-}\eta^1\text{:}\eta^1\text{-N}_2)$ (9) with oxygen gas as an oxygen atom transfer reagent.....	122
Reaction of $[\text{Tp}^{\text{Fc,Me}}\text{Co}]_2(\mu\text{-}\eta^1\text{:}\eta^1\text{-N}_2)$ (10) with O_2 and single oxygen atom transfer reagents.....	144
Reactions of $[\text{Tp}^{\text{Fc,Me}}\text{Fe}]_2(\mu\text{-}\eta^1\text{:}\eta^1\text{-N}_2)$ (9) and $[\text{Tp}^{\text{Fc,Me}}\text{Co}]_2(\mu\text{-}\eta^1\text{:}\eta^1\text{-N}_2)$ (10) with organic azides, general considerations.....	129
Synthesis of $\text{Tp}^{\text{Fc,Me}}\text{MN}(\text{H})\text{Ph}$ complexes, general considerations, and reactions with hydrogen abstraction reagents.....	139
Conclusions.....	147
Experimental.....	148
Preparation of $\text{Tp}^{\text{Fc,Me}}\text{FeO}(\text{CPh}_3)$ (13).....	149
Preparation of $\text{Tp}^{\text{Fc,Me}}\text{FeS}(\text{CPh}_3)$ (14).....	150
Preparation of $[\text{Tp}^{\text{Fc,Me}}\text{Fe}]_2(\mu_2\text{-}\eta^1\text{:}\eta^1\text{-S})$ (15).....	151
Preparation of $[\text{Tp}^{\text{Fc,Me}}\text{Fe}]_2(\mu_2\text{-}\eta^1\text{:}\eta^1\text{-O})$ (16).....	151
Preparation of $\text{Tp}^{\text{Fc,Me}}\text{CoN}_4\text{Bn}_2$ (17).....	152
Preparation of $\text{Tp}^{\text{Fc,Me}}\text{FeN}(\text{H})\text{Ph}$ (18).....	153
Preparation of $\text{Tp}^{\text{Fc,Me}}\text{CoN}(\text{H})\text{Ph}$ (19).....	153
REFERENCES.....	154

4	SYNTHESIS OF NITRIDO COMPLEXES SUPPORTED BY TRYS(PYRAZOLYL)BORATO LIGANDS, THEIR CHARACTERIZATION AND REACTIVITY	157
	Introduction	157
	Results and Discussion	159
	Synthesis of Iron and Cobalt azide complexes supported by $\text{Tp}^{\text{Fc,Me}}$ ligand	159
	Reactions of nitride transfer reagent with iron and cobalt halides, supported by $\text{Tp}^{\text{Fc,Me}}$ ligand	164
	Reactions of Fe and Co complexes supported by $\text{Tp}^{\text{tBu,Me}}$ ligand with dbabh	166
	Reactions of Li-dbabh and H-dbabh with $\text{Tp}^{\text{tBu,Me}}\text{CrCl}$ and $\text{Tp}^{\text{tBu,Me}}\text{CrEt}$, synthesis of $\text{Tp}^{\text{tBu,Me}}\text{CrN}$	178
	Kinetic and thermodynamic data related to $\text{Tp}^{\text{tBu,Me}}\text{CrN}$	183
	Reactivity of $\text{Tp}^{\text{tBu,Me}}\text{CrN}$ (24) with various substrates, general considerations	189
	Conclusion	203
	Experimental	203
	Preparation of $\text{Tp}^{\text{Fc,Me}}\text{FeN}_3$ (20)	205
	Preparation of $\text{Tp}^{\text{Fc,Me}}\text{CoN}_3$ (21)	206
	Preparation of $\text{Tp}^{\text{tBu,Me}}\text{FeN}(\text{C}_{14}\text{H}_{10})$ (22)	206
	Preparation of $\text{Tp}^{\text{tBu,Me}}\text{CoN}(\text{C}_{14}\text{H}_{10})$ (23)	207
	Preparation of $\text{Tp}^{\text{tBu,Me}}\text{CrN}$ (24)	208
	Preparation of $\text{Tp}^{\text{tBu,Me}}\text{Cr}(\text{I})(\text{N})$ (25)	208
	Preparation of $\text{Tp}^{\text{tBu,Me}}\text{CrNMe}$ (26)	209
	REFERENCES	210
	Appendix	
	A, Chapter 2	214
	B, Chapter 3	234
	C, Chapter 4	247

LIST OF TABLES

Table 1.1: Selected interatomic distances (Å) and angles (°) for $\text{Tp}^{\text{Fc,Me}}\text{FeCl}$ (1)	18
Table 1.2: Selected interatomic distances (Å) and angles (°) for $\text{Tp}^{\text{Fc,Me}}\text{CoBr}$ (4).....	27
Table 1.3: Selected interatomic distances (Å) and angles (°) for $\text{Tp}^{\text{Fc,Me}*}\text{MgMe}$ (A1.1)	31
Table 1.4: Selected interatomic distances (Å) and angles (°) for $\text{Tp}^{\text{Fc,Me}}\text{FeBn}$ (5).....	34
Table 1.5: Selected interatomic distances (Å) and angles (°) for $\text{Tp}^{\text{Fc,Me}}\text{FeEt}$ (6).....	38
Table 1.6: Comparison of Fe-N and Fe-C bonds and angles of compounds (5), (6), and analogous $\text{Tp}^{\text{tBu,Me}}\text{Fe}$ alkyl complexes	40
Table 1.7: Comparison of $\text{Tp}^{(\text{R,R})}\text{Fe}(\text{CO})$ bonds and angles of compounds	42
Table 1.8: Selected interatomic distances (Å) and angles (°) for $\text{Tp}^{\text{Fc,Me}}\text{Fe}(\text{CO})$ (7) ...	43
Table 1.9: Selected interatomic distances (Å) and angles (°) for $\text{Tp}^{\text{Fc,Me}}\text{Fe}(\text{PzH}^{\text{Fc,Me}})(\text{Pz}^{\text{Fc,Me}})$ (8)	49
Table 1.10: Selected interatomic distances (Å) and angles (°) for $[\text{Tp}^{\text{Fc,Me}}\text{Fe}]_2(\mu\text{-}\eta^1:\eta^1\text{-N}_2)$ (9).....	54
Table 1.11: Selected interatomic distances (Å) and angles (°) for $[\text{Tp}^{\text{Fc,Me}}\text{Co}]_2(\mu\text{-}\eta^1:\eta^1\text{-N}_2)$ (10).....	61
Table 1.12: Alpha angles and M-N ₂ -M torsions of (9) and (10), and their respective V_{NN} stretching frequencies	63
Table 1.13: Comparison of N ₂ activation and select structural parameters of $[\text{Tp}^{(\text{R,R}')}]\text{M}]_x\text{N}_2$ complexes (R= tBu, Fc, Np, iPr, Ph, or Ad; R'= Me or H; M=Co or Fe; X= 1 or 2)	65
Table 1.14: Selected interatomic distances (Å) and angles (°) for $\text{Bp}^{\text{Fc,Me}}(\text{Me-pz-CpFe}(\text{C}_5\text{H}_4))\text{Co}$ (11).....	71

Table 1.15: Selected interatomic distances (Å) and angles (°) for $\text{Bp}^{\text{Fc,Me}}(\text{Me-pz-CpFe}(\text{C}_5\text{H}_4)\text{Co}(\text{CO}))$ (12).....	80
Table 2.1: Selected interatomic distances (Å) and angles (°) for $\text{Tp}^{\text{Fc,Me}}\text{FeO}(\text{CPh}_3)$ (13)	124
Table 2.2: Selected interatomic distances (Å) and angles (°) for $\text{Tp}^{\text{Fc,Me}}\text{FeS}(\text{CPh}_3)$ (14)	127
Table 2.3: Comparison of relevant structural features of (NNN)FeER complexes, (E = S or O, R = CPh ₃ , C ₆ F ₅ , C(CH ₃) ₂ Ph or Benzyl)	130
Table 2.4: Selected interatomic distances (Å) and angles (°) for $[\text{Tp}^{\text{Fc,Me}}\text{Fe}]_2(\mu\text{-}\eta^1:\eta^1\text{-S})$ (15).....	133
Table 2.5: Selected interatomic distances (Å) and angles (°) for $[\text{Tp}^{\text{Fc,Me}}\text{Fe}]_2(\mu\text{-}\eta^1:\eta^1\text{-O})$ (16).....	138
Table 2.6: Selected interatomic distances (Å) and angles (°) for $\text{Tp}^{\text{Fc,Me}}\text{Co}(\text{N}_4\text{Bn}_2)$ (17)	151
Table 2.7: Selected interatomic distances (Å) and angles (°) for $\text{Tp}^{\text{Fc,Me}}\text{Fe}(\text{N}_4\text{Ad}_2)$ (A2.1).....	156
Table 2.8: Selected interatomic distances (Å) and angles (°) for $\text{Tp}^{\text{Fc,Me}}\text{FeNHPH}$ (18)	161
Table 2.9: Selected interatomic distances (Å) and angles (°) for $\text{Tp}^{\text{Fc,Me}}\text{CoNHPH}$ (19)	164
Table 3.1: Selected interatomic distances (Å) and angles (°) for $\text{Tp}^{\text{Fc,Me}}\text{FeN}_3$ (20)...	195
Table 3.2: Comparison of triclinic and orthorhombic polymorphs of $\text{Tp}^{\text{Fc,Me}}\text{FeN}_3$ (20)	196
Table 3.3: Selected interatomic distances (Å) and angles (°) for $\text{Tp}^{\text{tBu,Me}}\text{Fe-dbabh}$ (22)	202
Table 3.4: Selected interatomic distances (Å) and angles (°) for $\text{Tp}^{\text{tBu,Me}}\text{Co-dbabh}$ (23)	206
Table 3.5: Comparison of bond lengths and angles for LM(dbabh) complexes (M= Cr, Mn, Fe, or Co)	208
Table 3.6: Selected interatomic distances (Å) and angles (°) for $\text{Tp}^{\text{tBu,Me}}\text{CrN}$ (24) ...	214

Table 3.7: Rate constants taken at temperatures between 278.15 K and 328.15 K for the decomposition of $\text{Tp}^{\text{tBu,Me}}\text{Cr-dbabh}$ to $\text{Tp}^{\text{tBu,Me}}\text{CrN}$ (24), ($R = 8.31446 \text{ J/Kmol}$, $h = 6.626 \cdot 10^{-34} \text{ Js}$, $K_b = 1.38065 \cdot 10^{-23} \text{ J/K}$).....	221
Table 3.8: Selected interatomic distances (\AA) and angles ($^\circ$) for $\text{Tp}^{\text{tBu,Me}}\text{Cr(N)(I)}$ (25)	228
Table 3.9: Selected interatomic distances (\AA) and angles ($^\circ$) for $\text{Tp}^{\text{tBu,Me}}\text{CrNMe}$ (26)	235
Table A.1: Selected interatomic distances (\AA) and angles ($^\circ$) for $[\text{Tp}^{\text{Fc,Me}}]_2\text{Co}$ (A1.2).....	215
Table A.2: Selected interatomic distances (\AA) and angles ($^\circ$) for $\text{Tp}^{\text{Fc,Me}}\text{Co}(\text{PzH}^{\text{Fc,Me}})(\text{Pz}^{\text{Fc,Me}})$ (A1.3).....	217
Table A.3: Crystal data and structure refinement for $\text{Tp}^{\text{Fc,Me}}\text{FeCl}$ (1)	220
Table A.4: Crystal data and structure refinement for $\text{Tp}^{\text{Fc,Me}}\text{CoBr}$ (4)	221
Table A.5: Crystal data and structure refinement for $\text{Tp}^{\text{Fc,Me}}\text{FeBn}$ (5)	222
Table A.6: Crystal data and structure refinement for $\text{Tp}^{\text{Fc,Me}}\text{FeEt}$ (6)	223
Table A.7: Crystal data and structure refinement for $\text{Tp}^{\text{Fc,Me}}\text{Fe}(\text{CO})$ (7).....	224
Table A.8: Crystal data and structure refinement for $\text{Tp}^{\text{Fc,Me}}\text{Fe}(\text{PzH}^{\text{Fc,Me}})(\text{Pz}^{\text{Fc,Me}})$ (8)	225
Table A.9: Crystal data and structure refinement for $[\text{Tp}^{\text{Fc,Me}}\text{Fe}]_2(\mu\text{-}\eta^1\text{:}\eta^1\text{-N}_2)$ (9) ...	226
Table A.10: Crystal data and structure refinement for $[\text{Tp}^{\text{Fc,Me}}\text{Co}]_2(\mu\text{-}\eta^1\text{:}\eta^1\text{-N}_2)$ (10)	227
Table A.11: Crystal data and structure refinement for $[\text{Tp}^{\text{Fc,Me}}\text{Co}]_2(\mu\text{-}\eta^1\text{:}\eta^1\text{-N}_2)$ (10)	228
Table A.12: Crystal data and structure refinement for $\text{Bp}^{\text{Fc,Me}}(\text{Me-pz-CpFe}(\text{C}_5\text{H}_4))\text{Co}$ (11).....	229
Table A.13: Crystal data and structure refinement for $\text{Bp}^{\text{Fc,Me}}(\text{Me-pz-CpFe}(\text{C}_5\text{H}_4))\text{Co}(\text{CO})$ (12)	230
Table A.14: Crystal data and structure refinement for $\text{Tp}^{\text{Fc,Me}}\text{*MgMe}$ (A1.1)	231

Table A.15: Crystal data and structure refinement for $[\text{Tp}^{\text{Fc,Me}}]_2\text{Co}$ (A1.2).....	232
Table A.16: Crystal data and structure refinement for $\text{Tp}^{\text{Fc,Me}}\text{Co}(\text{PzH}^{\text{Fc,Me}})(\text{Pz}^{\text{Fc,Me}})$ (A1.3).....	233
Table B.1: Selected interatomic distances (Å) and angles (°) for $\text{Tp}^{\text{Fc,Me}}\text{Co}(\text{TEMPO})$ (A2.2)	236
Table B.2: Crystal data and structure refinement for $\text{Tp}^{\text{Fc,Me}}\text{FeO}(\text{CPh}_3)$ (13).....	238
Table B.3: Crystal data and structure refinement for $\text{Tp}^{\text{Fc,Me}}\text{FeS}(\text{CPh}_3)$ (14)	239
Table B.4: Crystal data and structure refinement for $[\text{Tp}^{\text{Fc,Me}}\text{Fe}]_2(\mu_2\text{-}\eta^1:\eta^1\text{-S})$ (15) ..	240
Table B.5: Crystal data and structure refinement for $[\text{Tp}^{\text{Fc,Me}}\text{Fe}]_2(\mu_2\text{-}\eta^1:\eta^1\text{-O})$ (16) .	241
Table B.6: Crystal data and structure refinement for $\text{Tp}^{\text{Fc,Me}}\text{CoN}_4\text{Bn}_2$ (17)	242
Table B.7: Crystal data and structure refinement for $\text{Tp}^{\text{Fc,Me}}\text{FeNHPH}$ (18)	243
Table B.8: Crystal data and structure refinement for $\text{Tp}^{\text{Fc,Me}}\text{CoNHPH}$ (19).....	244
Table B.9: Crystal data and structure refinement for $\text{Pz}^{\text{Fc,Me}}\text{Bp}^{\text{Fc,Me}}\text{FeN}_4\text{Ad}_2$ (A2.1)	245
Table B.10: Crystal data and structure refinement for $\text{Tp}^{\text{Fc,Me}}\text{Co}(\text{TEMPO})$ (A2.2) ..	246
Table C.1: Selected interatomic distances (Å) and angles (°) for $\text{Tp}^{\text{Fc,Me}}\text{Li}(\text{THF})$ (A3.1).....	248
Table C.2: Crystal data and structure refinement for $\text{Tp}^{\text{Fc,Me}}\text{FeN}_3$ (20)	251
Table C.3: Crystal data and structure refinement for $\text{Tp}^{\text{Fc,Me}}\text{FeN}_3$ (20)	252
Table C.4: Crystal data and structure refinement for $\text{Tp}^{\text{tBu,Me}}\text{Fe-dbabh}$ (22)	253
Table C.5: Crystal data and structure refinement for $\text{Tp}^{\text{tBu,Me}}\text{Co-dbabh}$ (23)	254
Table C.6: Crystal data and structure refinement for $\text{Tp}^{\text{tBu,Me}}\text{CrN}$ (24)	255
Table C.7: Crystal data and structure refinement for $\text{Tp}^{\text{tBu,Me}}\text{Cr}(\text{N})(\text{I})$ (25).....	256
Table C.8: Crystal data and structure refinement for $\text{Tp}^{\text{tBu,Me}}\text{CrNMe}$ (26)	257

LIST OF FIGURES

Figure I.1: Qualitative frontier molecular orbital diagrams of 3 ligand fields common to M-O complexes	2
Figure I.2: Graphical representation of the “Oxo wall”, between groups 8 and 9	2
Figure I.3: Structure of oxotrimesityliridium (V).....	3
Figure I.4: Structure of Cytochrome P450 active site in the pre catalyst stage, and simplified mechanism of aliphatic hydrocarbon hydroxylation	4
Figure I.5: Both reaction pathways theorized to be used by nitrogenase enzymes	5
Figure I.6: Reaction mechanism for the formation of molybdenum terminal nitride from molybdenum di-nitrogen complex.....	6
Figure I.7: Reaction of monovalent iron complexes supported by the $\text{Tp}^{\text{tBu,Me}}$ ligand, where L is either CO, C_2H_4 , or N_2	7
Figure I.8: Comparison of $\text{Tp}^{\text{tBu,Me}}$ and $\text{Tp}^{\text{Fc,Me}}$ ligands and their BDEs	8
Figure 1.1: ^1H -NMR spectrum of $\text{Tp}^{\text{Fc,Me}}\text{FeCl}$ (1) recorded in $^*\text{THF-d}_8$ at 400MHz..	16
Figure 1.2: ^1H -NMR spectrum of $\text{Tp}^{\text{Fc,Me}}\text{FeBr}$ (2) recorded in $^*\text{THF-d}_8$ at 400MHz, (Inset: close up of resonances between 0 and 5 ppm)	17
Figure 1.3: Molecular structure of $\text{Tp}^{\text{Fc,Me}}\text{FeCl}$ (1) represented as 50% probability thermal ellipsoids. Hydrogen atoms (with the exception of the hydrogen attached to the boron, H1) have been omitted for clarity	18
Figure 1.4: ^1H -NMR spectrum of $\text{Tp}^{\text{Fc,Me}}\text{FeI}$ (3) recorded in $^*\text{C}_6\text{D}_6$ at 400MHz	22
Figure 1.5: ^1H -NMR Comparison of $\text{Tp}^{\text{Fc,Me}}\text{FeCl}$ (1) (Bottom), the same sample after 24 hours at room temperate had passed (Middle), and then the same sample left at 60 °C for 12 hours (top)	23

Figure 1.6: $^1\text{H-NMR}$ Comparison of $\text{Tp}^{\text{Fc,Me}}\text{FeBr}$ (2) (Bottom), the same sample after 24 hours at room temperature had passed (Middle), and then the same sample left at 60 °C for 12 hours (top)	24
Figure 1.7: $^1\text{H-NMR}$ Comparison of $\text{Tp}^{\text{Fc,Me}}\text{FeI}$ (3) (Bottom), the same sample after 24 hours at room temperature had passed (Middle), and then the same sample left at 60 °C for 40 hours (top)	25
Figure 1.8: Molecular structure of $\text{Tp}^{\text{Fc,Me}}\text{CoBr}$ (4) represented as 50% probability thermal ellipsoids. Hydrogen atoms (with the exception of the hydrogen attached to the boron, H1) have been omitted for clarity	27
Figure 1.9: Molecular structure of $\text{Tp}^{\text{Fc,Me}}\text{MgMe}$ (A1.1) represented as 50% probability thermal ellipsoids. Hydrogen atoms (with the exception of the hydrogen attached to the boron, H1) have been omitted for clarity	31
Figure 1.10: Molecular structure of $\text{Tp}^{\text{Fc,Me}}\text{FeBn}$ (5) represented as 50% probability thermal ellipsoids. Hydrogen atoms (with the exception of the hydrogen attached to the boron, H1), and 1 molecule of toluene, have been omitted for clarity	33
Figure 1.11: Molecular structure of $\text{Tp}^{\text{Fc,Me}}\text{FeEt}$ (6) represented as 50% probability thermal ellipsoids. Hydrogen atoms (with the exception of the hydrogen attached to the boron, H1) have been omitted for clarity	37
Figure 1.12: LIFDI-MS of complex (5), displaying peaks for its molecular ion $[\text{M}^+ : 954.1369]$ and $[\text{M}^+ - \text{C}_7\text{H}_7 : 863.1214]$	41
Figure 1.13: Molecular structure of $\text{Tp}^{\text{Fc,Me}}\text{Fe}(\text{CO})$ (7) represented as 50% probability thermal ellipsoids. Hydrogen atoms (with the exception of the hydrogen attached to the boron, H1) have been omitted for clarity	43
Figure 1.14: Cyclic voltammograms of compounds 1 (blue, top), 2 (red, middle), and 3 (green, bottom), in 0.1 M solutions of $[\text{NBu}_4]\text{ClO}_4$ and $(\text{Cp}^*)_2\text{Fe}$ in THF, (working electrode = GC, reference electrode = Ag/Ag ⁺ , counter electrode = Pt).....	47
Figure 1.15: Molecular structure of $\text{Tp}^{\text{Fc,Me}}\text{Fe}(\text{PzH}^{\text{Fc,Me}})(\text{Pz}^{\text{Fc,Me}})$ (8) represented as 50% probability thermal ellipsoids. Hydrogen atoms (with the exception of the hydrogens attached to the boron, H1, and to N10, H2), and 1 molecule of Et ₂ O have been omitted for clarity	48

- Figure 1.16: Molecular structure of $[\text{Tp}^{\text{Fc,Me}}\text{Fe}]_2(\mu\text{-}\eta^1\text{:}\eta^1\text{-N}_2)$ (**9**) represented as 30% probability thermal ellipsoids. Hydrogen atoms (with the exception of the hydrogens attached to boron, H1 and H2,) and 1 molecule of THF and 1.5 molecules of n-Pentane have been omitted for clarity..... 53
- Figure 1.17: Cyclic voltammogram of compound (**4**), in 0.1 M solution of $[\text{NnBu}_4]\text{ClO}_4$ and $(\text{Cp}^*)_2\text{Fe}$ in THF, (working electrode = GC, reference electrode = Ag/Ag^+ , Counter electrode = Pt) 59
- Figure 1.18: Molecular structure of $[\text{Tp}^{\text{Fc,Me}}\text{Co}]_2(\mu\text{-}\eta^1\text{:}\eta^1\text{-N}_2)$ (**10**) represented as 50% probability thermal ellipsoids. Hydrogen atoms (with the exception of the hydrogens attached to boron, H1 and H2), and 10 molecules of THF have been omitted for clarity 60
- Figure 1.19: IR spectroscopy of compounds **9** (blue, $\nu_{\text{NN}}=1970$) and **10** (red, $\nu_{\text{NN}}=2069\text{ cm}^{-1}$), with their B-H and N-N stretching frequencies annotated..... 62
- Figure 1.20: Comparison of α -angles and M-N₂-M torsions of compounds (**9**) and (**10**), atoms displayed as 50% thermal ellipsoids, all other atoms omitted for clarity 63
- Figure 1.21: ¹H-NMR of crystals of **9** taken in C₆D₆, co-crystallized with *THF/pentanes, with some impurities from oxidation (bottom), and that sample when placed under an N₂ atmosphere (top) 66
- Figure 1.22: ¹H-NMR of crystals of **10** in C₆D₆, co-crystallized with pentanes*, with some impurities from oxidation (bottom), and that sample when placed under an N₂ atmosphere (top) 67
- Figure 1.23: Cyclic voltammogram of **9**, in a solution of 0.1 M $[\text{NnBu}_4]\text{ClO}_4$ and 0.1 M $(\text{Cp}^*)_2\text{Fe}$ in THF, (working electrode = GC, reference electrode = Ag/Ag^+ , counter electrode = Pt) 68
- Figure 1.24: Cyclic voltammogram of **10**, in a solution of 0.1 M $[\text{NnBu}_4]\text{ClO}_4$ and 0.1 M $(\text{Cp}^*)_2\text{Fe}$ in THF, (working electrode = GC, reference electrode = Ag/Ag^+ , counter electrode = Pt) 69
- Figure 1.25: Molecular structure of $\text{Bp}^{\text{Fc,Me}}(\text{Me-pz-CpFe}(\text{C}_5\text{H}_4))\text{Co}$ (**11**) represented as 50% probability thermal ellipsoids. Hydrogen atoms (with the exception of the hydrogen attached to boron, H1), and one molecule of n-pentane have been omitted for clarity 71

- Figure 1.26: $^1\text{H-NMR}$ spectrum of $\text{Bp}^{\text{Fc,Me}}(\text{Me-pz-CpFe}(\text{C}_5\text{H}_4))\text{Co}$ (**11**) recorded in C_6D_6 at 400MHz, with some *THF/Ether/Pentanes present in crystals used for collection 75
- Figure 1.27: $^1\text{H-NMR}$ spectrum of $\text{Bp}^{\text{Fc,Me}}(\text{Me-pz-CpFe}(\text{C}_5\text{H}_4))\text{Co}$ (**11**) recorded in C_6D_6 (bottom), the same sample with 1 atm of D_2 gas added and heated at 45 °C for 16 hours (top), Cp rings effected by deuterium incorporation highlighted with red arrows, (inset: HD resonances highlighted with red arrows) 77
- Figure 1.28: $^2\text{H-NMR}$ spectrum of $\text{Bp}^{\text{Fc,Me}}(\text{Me-pz-CpFe}(\text{C}_5\text{H}_4))\text{Co}$ (**11**) after heating at 45 °C under 1 atm of D_2 , recorded in C_6H_6 , D_2 still present at 4.5 ppm 78
- Figure 1.29: Molecular structure of $\text{Bp}^{\text{Fc,Me}}(\text{Me-pz-CpFe}(\text{C}_5\text{H}_4))\text{Co}(\text{CO})$ (**12**) represented as 50% probability thermal ellipsoids. Hydrogen atoms (with the exception of the hydrogen attached to boron, H1) have been omitted for clarity 80
- Figure 1.30: $^1\text{H-NMR}$ spectrum of $\text{Bp}^{\text{Fc,Me}}(\text{Me-pz-CpFe}(\text{C}_5\text{H}_4))\text{Co}$ (**11**) recorded in C_6D_6 (spectrum A), the same sample with 1 atm of O_2 gas added (spectrum B), the same sample after 1 FPT degas cycle (spectrum C), the same sample after a second FPT degas cycle (spectrum D) 84
- Figure 2.1: Molecular structure of $\text{Tp}^{\text{Fc,Me}}\text{FeO}(\text{CPh}_3)$ (**13**) represented as 50% probability thermal ellipsoids. Hydrogen atoms (with the exception of the hydrogens attached to boron, H1), and a second molecule of **13** present in the asymmetric unit have been omitted for clarity 104
- Figure 2.2: Molecular structure of $\text{Tp}^{\text{Fc,Me}}\text{FeS}(\text{CPh}_3)$ (**14**) represented as 50% probability thermal ellipsoids. Hydrogen atoms (with the exception of the hydrogens attached to boron, H1) have been omitted for clarity 107
- Figure 2.3: Predicted isotope model for the molecular ion of $[\text{Tp}^{\text{Fc,Me}}\text{Fe}]_2(\mu\text{-}\eta^1\text{:}\eta^1\text{-S})$ (**15**) [M^+ : 1758.1375] LIFDI-MS, and a sample taken from the crystallization mother liquor used to produce crystals of **15** 111
- Figure 2.4: Molecular structure of $[\text{Tp}^{\text{Fc,Me}}\text{Fe}]_2(\mu\text{-}\eta^1\text{:}\eta^1\text{-S})$ (**15**) represented as 30% probability thermal ellipsoids. Hydrogen atoms (with the exception of the hydrogens attached to borons, H1 and H2), and one molecule of ether have been omitted for clarity 112
- Figure 2.5: LIFDI-MS of the result of reaction of **14** with DHA (bottom), the calculated isotope pattern of the desired $\text{Tp}^{\text{Fc,Me}}\text{FeSH}$ complex (top) 115

- Figure 2.6: Molecular structure of $[\text{Tp}^{\text{Fc,Me}}\text{Fe}]_2(\mu\text{-}\eta^1\text{:}\eta^1\text{-O})$ (**16**) represented as 50% probability thermal ellipsoids. Hydrogen atoms (with the exception of the hydrogens attached to boron, H1A and H2A), and 2 molecules of THF have been omitted for clarity 118
- Figure 2.7: $^1\text{H-NMR}$ spectrum of $[\text{Tp}^{\text{Fc,Me}}\text{Fe}]_2(\mu\text{-}\eta^1\text{:}\eta^1\text{-O})$ (**16**) recorded in C_6D_6 (+) at 400 MHz, with THF (*) present in crystals used for collection 121
- Figure : 2.8: LIFDI-MS of the result from a reaction of **16** with oxygen gas (Bottom), calculated isotope pattern for $\text{C}_{42}\text{H}_{39}\text{B}_1\text{N}_6\text{Fe}_4\text{O}$, the apparent activation of on of the ferrocene arms of the ligand (top) 122
- Figure 2.9: $^1\text{H-NMR}$ spectrum of THF extracts from a reaction of **9** with 1 Eq of O_2 at $-78\text{ }^\circ\text{C}$ in Ether, (**8** = red arrows), (**16** = blue arrows)..... 123
- Figure 2.10: $^1\text{H-NMR}$ spectrum of the starting material, **10** (bottom), for the reaction with excess O_2 at RT in C_6D_6 (Top), ($\text{Tp}^{\text{Fc,Me}}\text{CoOH}$ = green arrows, **10** = red arrows, $\text{Tp}^{\text{Fc,Me}}\text{Co}(\text{O}_2)$ = blue arrows)..... 127
- Figure 2.11: $^1\text{H-NMR}$ spectrum of an aliquot taken from the reaction of $\text{Tp}^{\text{Fc,Me}}\text{Co}(\text{O}_2)$ with **10** at $60\text{ }^\circ\text{C}$ in THF for 21 days, ($\text{Tp}^{\text{Fc,Me}}\text{CoOH}$ = green arrows, $\text{Tp}^{\text{Fc,Me}}\text{Co}(\text{O}_2)$ = blue arrows) 128
- Figure 2.12: $^1\text{H-NMR}$ spectrum of $\text{Tp}^{\text{Fc,Me}}\text{CoN}_4\text{Bn}_2$ (**17**) recorded in C_6D_6 (7.16 ppm (+)) at 400 MHz, with some THF, ether, and pentane (*) present in the spectrum, (Inset - left: close up of resonances between 7 and 7.4 ppm; Inset – right: Close up of resonance between 3.74 and 3.86 ppm) . 131
- Figure 2.13: Molecular structure of $\text{Tp}^{\text{Fc,Me}}\text{Co}(\text{N}_4\text{Bn}_2)$ (**17**) represented as 50% probability thermal ellipsoids. Hydrogen atoms (with the exception of the hydrogen attached to boron, H1), and another molecule of **17** have been omitted for clarity 132
- Figure 2.14: Molecular structure of $\text{Tp}^{\text{Fc,Me}}\text{Fe}(\text{N}_4\text{Ad}_2)$ (**A2.1**) represented as 50% probability thermal ellipsoids. Hydrogen atoms (with the exception of the hydrogen attached to boron, H1) omitted for clarity 136
- Figure 2.15: Molecular structure of $\text{Tp}^{\text{Fc,Me}}\text{FeNHPH}$ (**18**) represented as 50% probability thermal ellipsoids. Hydrogen atoms (with the exception of the hydrogen attached to boron, H1, and the hydrogen attached N7, H2), and one molecule of ether omitted for clarity 141

- Figure 2.16: Molecular structure of $\text{Tp}^{\text{Fc,Me}}\text{CoNHPH}$ (**19**) represented as 50% probability thermal ellipsoids. Hydrogen atoms (with the exception of the hydrogen attached to boron, H1, and the hydrogen attached N7, H2), and one molecule of ether omitted for clarity 144
- Figure 2.17: LIFDI-MS of the result from a reaction of (**19**) with 2,4,6-tri-tert-butylphenoxy radical (bottom), calculated isotope pattern for $\text{C}_{60}\text{H}_{69}\text{B}_1\text{N}_6\text{Fe}_3\text{Co}_1\text{O}_1$ (top)..... 147
- Figure 3.1: Molecular structure of $\text{Tp}^{\text{Fc,Me}}\text{FeN}_3$ (**20**) represented as 50% probability thermal ellipsoids. Hydrogen atoms (with the exception of the hydrogen attached to boron, H1), and one molecule of THF omitted for clarity..... 161
- Figure 3.2: IR spectra of both polymorphs of $\text{Tp}^{\text{Fc,Me}}\text{FeN}_3$ (**20**), triclinic (red, $\nu_{\text{N}_3} = 2100 \text{ cm}^{-1}$) and orthorhombic (purple, $\nu_{\text{N}_3} = 2092 \text{ cm}^{-1}$), with their B-H and N_3 stretching frequencies annotated 163
- Figure 3.3: LIFDI-MS of the product of a reaction of **3** with Li-dbabh (Bottom), calculated isotope pattern for $\text{Tp}^{\text{Fc,Me}}\text{Li}$ (top, $\text{M}^+ - \text{C}_{42}\text{H}_{40}\text{B}_1\text{N}_6\text{Fe}_3\text{Li}$)..... 165
- Figure 3.4: LIFDI-MS of the products from a reaction of $\text{Tp}^{\text{tBu,Me}}\text{FeI}$ with dbabh (Bottom), calculated isotope pattern for $\text{Tp}^{\text{tBu,Me}}\text{Li}$ (Middle, $\text{M}^+ - \text{C}_{42}\text{H}_{40}\text{B}_1\text{N}_6\text{Fe}_3\text{Li}$), calculated isotope pattern for $\text{Tp}^{\text{tBu,Me}}\text{Fe-dbabh}$ (top, $\text{M}^+ - \text{C}_{38}\text{H}_{50}\text{B}_1\text{N}_7\text{Fe}_1$)..... 167
- Figure 3.5: Molecular structure of $\text{Tp}^{\text{tBu,Me}}\text{Fe-dbabh}$ (**22**) represented as 50% probability thermal ellipsoids. Hydrogen atoms (with the exception of the hydrogen attached to boron, H1) omitted for clarity 168
- Figure 3.6: Molecular structure of $\text{Tp}^{\text{tBu,Me}}\text{Co-dbabh}$ (**23**) represented as 50% probability thermal ellipsoids. Hydrogen atoms (with the exception of the hydrogen attached to boron, H1) omitted for clarity 172
- Figure 3.7: $^1\text{H-NMR}$ spectrum of the starting material, **22** (bottom), and the resulting spectrum after heating the material at $75 \text{ }^\circ\text{C}$ for 24 hours (Top), (**22** = blue arrows, $\text{Tp}^{\text{tBu,Me}}\text{FeI}$ = purple arrows, free $\text{Tp}^{\text{tBu,Me}}$ = black arrows)..... 176
- Figure 3.8: $^1\text{H-NMR}$ spectrum of the starting material, $\text{Tp}^{\text{tBu,Me}}\text{Co-dbabh}$ (**23**) (bottom), and the resulting spectrum after heating the material at $100 \text{ }^\circ\text{C}$ for 24 hours (Top), (**23** = blue arrows, $\text{Tp}^{\text{tBu,Me}}\text{CoI}$ = purple arrows)..... 177

- Figure 3.9: $^1\text{H-NMR}$ spectrum of solid residue from reaction of $\text{Tp}^{\text{tBu,Me}}\text{Cr}(\text{Cl})(\text{Py})$ with Li-dbabh in C_6D_6 (**24** = green arrows, Anthracene = blue arrows, $\text{Tp}^{\text{tBu,Me}}\text{Li}$ = black arrows, unidentified Cr dbabh complex = red arrows) 179
- Figure 3.10: Molecular structure of $\text{Tp}^{\text{Fc,Me}}\text{Cr}$ (**24**) represented as 50% probability thermal ellipsoids. Hydrogen atoms (with the exception of the hydrogen attached to boron, H1) were omitted for clarity 180
- Figure 3.11: Histogram of chromium bond lengths, using the search query drawn in the upper left, Avg. = 1.539 Å, Std. Dev. = .008 Å, Range = 1.516 – 1.560 Å, the Cr-N bond length of $\text{Tp}^{\text{tBu,Me}}\text{CrN}$ (**24**) is 1.544(3) Å 182
- Figure 3.12: $^1\text{H-NMR}$ of the reaction of $\text{Tp}^{\text{tBu,Me}}\text{CrEt}$ with H-dbabh in C_6D_6 , starting 5 minutes after transfer of solvent, with spectra taken every 10 minutes. Inset (left): disappearance of intermediate chemical shift at 47.3 ppm and growth of **24** chemical shift at 50.3 ppm; Inset (right): growth of anthracene chemical shifts at 8.2, 7.8, and 7.2ppm 184
- Figure 3.13: $^1\text{H-NMR}$ spectra before (bottom) and after sublimation done at 110 °C for 6 hours and one crystallization from a solution of **24** in ether and pentane (top) 185
- Figure 3.14: Stacked plot of UV-Vis data showing the loss of the intermediate ($\lambda_{\text{max}} = 830$ nm), growth of **24** ($\lambda_{\text{max}} = 455$ nm), and isosbestic point at 645 nm 187
- Figure 3.15: Eyring plot for the decomposition of $\text{Tp}^{\text{tBu,Me}}\text{Cr-dbabh}$ to $\text{Tp}^{\text{tBu,Me}}\text{CrN}$, plotted as $R \cdot \ln(kh)/(K_b T)$ vs $1/T$, ($R = 8.31446$ J/Kmol, $h = 6.626 \cdot 10^{-34}$ Js, $K_b = 1.38065 \cdot 10^{-23}$ J/K) 188
- Figure 3.16: $^1\text{H-NMR}$ spectra of the reaction of $\text{Tp}^{\text{tBu,Me}}\text{CrN}$ (**24**) with 9,10-dihydroanthracene, with chemical shifts for anthracene marked with blue arrows (bottom – starting material, middle – 7 hours at 75 °C, top – 7 additional hours at 75 °C) 190
- Figure 3.17: $^1\text{H-NMR}$ for the reaction of $\text{Tp}^{\text{tBu,Me}}\text{CrN}$ (**24**) (bottom) with 1 atm of NO (top), ($\text{HPz}^{\text{tBu,Me}}$ highlighted with red arrows [inset], chromium containing product highlighted with blue arrows) 191
- Figure 3.18: LIFDI-MS for the result of the reaction of $\text{Tp}^{\text{tBu,Me}}\text{CrN}$ (**24**) with 1 atm of NO (bottom), with isotope model for a compound have the formula corresponding to $\text{Tp}^{\text{tBu,Me}}\text{Cr}(\text{N})(\text{Pz}^{\text{tBu,Me}})$ (top) 192

- Figure 3.19: Cyclic voltammogram of $\text{Tp}^{\text{tBu,Me}}\text{CrN}$ (**24**), in 0.1 M THF solution of $[\text{NnBu}_4]\text{PF}_6$ referenced with Fc^+/Fc to SHE at $V = 0$, (working electrode = GC, reference electrode = Ag/Ag^+ , Counter electrode = Pt)..... 193
- Figure 3.20: Molecular structure of $\text{Tp}^{\text{tBu,Me}}\text{Cr}(\text{N})(\text{I})$ (**25**) represented as 50% probability thermal ellipsoids. Hydrogen atoms (with the exception of the hydrogen attached to boron, H1) omitted for clarity 195
- Figure 3.21: ^1H -NMR spectrum of crystals grown from pentane, from the reaction of $\text{Tp}^{\text{tBu,Me}}\text{CrN}$ with MeI, showing 7 broad paramagnetic chemical shifts, with some anthracene having also been present in the unit cell 198
- Figure 3.22: LIFDI-MS spectrum of the pentane extract from the reaction of $\text{Tp}^{\text{tBu,Me}}\text{CrN}$ (**24**) with MeI (bottom), predicted isotope pattern for a complex with a formula corresponding to $\text{Tp}^{\text{tBu,Me}}\text{CrNMe}$ ($\text{C}_{25}\text{H}_{43}\text{N}_7\text{B}_1\text{Cr}_1$ middle), and the predicted isotope pattern complex with a formula corresponding to $\text{Tp}^{\text{tBu,Me}}\text{CrI}$ ($\text{C}_{24}\text{H}_{40}\text{N}_6\text{B}_1\text{Cr}_1\text{I}_1$ top)..... 199
- Figure 3.23: Molecular structure of $\text{Tp}^{\text{tBu,Me}}\text{CrNMe}$ (**26**) represented as 50% probability thermal ellipsoids. Hydrogen atoms (with the exception of the hydrogen attached to boron, H1) omitted for clarity 201
- Figure A.1: Molecular structure of $[\text{Tp}^{\text{Fc,Me}}]_2\text{Co}$ (**A1.2**) represented as 50% probability thermal ellipsoids. Hydrogen atoms (with the exception of the hydrogens attached to the boron, H1 and H2), have been omitted for clarity 214
- Figure A.2: Molecular structure of $\text{Tp}^{\text{Fc,Me}}\text{Co}(\text{PzH}^{\text{Fc,Me}})(\text{Pz}^{\text{Fc,Me}})$ (**A1.3**) represented as 50% thermal ellipsoids. Hydrogen atoms (with the exception of the hydrogens attached to the boron, H1, and to N2, H2A), and 1 molecule of THF and n-Pentane have been omitted for clarity 216
- Figure B.1: Molecular structure of $\text{Tp}^{\text{Fc,Me}}\text{Co}(\text{TEMPO})$ (**A2.2**) represented as 50% probability thermal ellipsoids. Hydrogen atoms (with the exception of the hydrogen attached to boron, H1), and one molecule of Ether omitted for clarity 135
- Figure C.1: Molecular structure of $\text{Tp}^{\text{Fc,Me}}\text{Li}(\text{THF})$ (**A3.1**) represented as 50% probability thermal ellipsoids. Hydrogen atoms (with the exception of the hydrogen attached to boron, H1) omitted for clarity 247

LIST OF SCHEMES

Scheme 1.1: Previously published synthesis of $\text{Tp}^{(\text{R},\text{R}')} \text{ML}$ ($\text{M} = \text{Cr}, \text{Mn}, \text{Fe}, \text{or Co}$, $\text{R} = t\text{Bu}, i\text{Pr}, \text{neopentyl}, \text{or Ad}$; $\text{R}' = \text{Me}, i\text{Pr}, \text{or H}$, $\text{X} = \text{Cl}, \text{I}$; $\text{L} = \text{CO}, \text{N}_2$) complexes	13
Scheme 1.2: Solid state synthesis of $\text{Tp}^{\text{Fc,Me}} \text{FeX}$ ($\text{X} = \text{Cl}$ (1), Br (2))	15
Scheme 1.3: Solution state synthesis of $\text{Tp}^{\text{Fc,Me}} \text{FeI}$, (3)	21
Scheme 1.4: Synthesis of $\text{Tp}^{\text{Fc,Me}} \text{CoBr}$, (4)	26
Scheme 1.5: Production of magnesium di-alkyl complexes by precipitation of MgX_2	30
Scheme 1.6: Synthesis of $\text{Tp}^{\text{Fc,Me}} \text{FeR}$, where $\text{R} = \text{Bn}$ (5), Et (6)	33
Scheme 1.7: Synthesis of $\text{Tp}^{\text{Fc,Me}} \text{Fe}(\text{CO})$ (7), [$0 < \text{N} < .5$]	42
Scheme 1.8: Synthesis of $\text{Tp}^{\text{Fc,Me}} \text{Fe}(\text{PzH}^{\text{Fc,Me}})(\text{Pz}^{\text{Fc,Me}})$ (8)	46
Scheme 1.9: Synthesis of $[\text{Tp}^{\text{Fc,Me}} \text{Fe}]_2(\mu_2\text{-}\eta^1\text{:}\eta^1\text{-N}_2)$ (9)	52
Scheme 1.10: Synthesis of $[\text{Tp}^{\text{Fc,Me}} \text{Co}]_2(\mu\text{-}\eta^1\text{:}\eta^1\text{-N}_2)$ (10)	58
Scheme 1.11: Synthesis of $\text{Bp}^{\text{Fc,Me}}(\text{Me-pz-CpFe}(\text{C}_5\text{H}_4))\text{Co}$ (11)	70
Scheme 1.12: Incorporation of deuterium into the ferrocene moieties of 11 , elimination of HD and equilibrium under deuterium atmosphere ($x = 0$ to 5, $y = 0$ to 4)	76
Scheme 1.13: Synthesis of $\text{Bp}^{\text{Fc,Me}}(\text{Me-pz-CpFe}(\text{C}_5\text{H}_4))\text{Co}(\text{CO})$ (12)	79
Scheme 1.14: reversible binding of O_2 to $\text{Bp}^{\text{Fc,Me}}(\text{Me-pz-CpFe}(\text{C}_5\text{H}_4))\text{Co}$ (11)	83
Scheme 2.1: Suggested mechanism for the formation of an $\text{Fe}^{\text{III}}/\text{Fe}^{\text{III}}$ bridging oxo species supported by $\text{Tp}^{t\text{Bu,Me}}$, taken from the thesis of Dr. Fernando Jove ($\text{L} = \text{CO}, \text{N}_2, \text{or C}_2\text{H}_4$)	101

Scheme 2.2: Synthesis of $\text{KE}(\text{CPh}_3)$ ($\text{E} = \text{O}, \text{S}$) and their reaction with 3 , synthesis of $\text{Tp}^{\text{Fc,Me}}\text{FeE}(\text{CPh}_3)$, $\text{E} = \text{O}$ (13), $\text{E} = \text{S}$ (14)	103
Scheme 2.3: Reaction of $[\text{Tp}^{\text{Fc,Me}}\text{Fe}]_2(\mu\text{-}\eta^1\text{:}\eta^1\text{-N}_2)$ (9) with various single atom oxygen transfer reagents, synthesis of $[\text{Tp}^{\text{Fc,Me}}\text{Fe}]_2(\mu\text{-}\eta^1\text{:}\eta^1\text{-O})$ (16)	117
Scheme 2.4: Reaction of 9 with 1 Eq of oxygen gas at low temperature, synthesis of trace amounts of $[\text{Tp}^{\text{Fc,Me}}\text{Fe}]_2(\mu\text{-}\eta^1\text{:}\eta^1\text{-O})$ (16)	124
Scheme 2.5: Reaction of $[\text{Tp}^{\text{iPr,Me}}\text{Co}]_2(\mu\text{-}\eta^1\text{:}\eta^1\text{-N}_2)$ with oxygen gas	126
Scheme 2.6: Reaction of $\text{Tp}^{\text{tBu,Me}}\text{Co-N}_2$ with oxygen gas	126
Scheme 2.7: Reaction of $[\text{Tp}^{\text{Fc,Me}}\text{Co}]_2(\mu\text{-}\eta^1\text{:}\eta^1\text{-N}_2)$ (10) with benzyl azide to make $\text{Tp}^{\text{Fc,Me}}\text{CoN}_4\text{Bn}_2$ (17) by elimination of N_2	130
Scheme 2.8: Reaction of $[\text{Tp}^{\text{Fc,Me}}\text{Co}]_2(\mu\text{-}\eta^1\text{:}\eta^1\text{-N}_2)$ (10) benzyl azide, the formation of $\text{Tp}^{\text{Fc,Me}}\text{Co}(\text{N}_3)$ by the formation of an organic radical	135
Scheme 2.9: Synthesis of $\text{Tp}^{\text{Fc,Me}}\text{FeNHPH}$ (18) and $\text{Tp}^{\text{Fc,Me}}\text{CoNHPH}$ (19)	140
Scheme 3.1: Synthesis of first row transition metal di-nitrogen complexes supported by various hydrotris(3-R,5-R'pyrazolyl)borate ligands, ($\text{M} = \text{Cr}, \text{Mn}, \text{Fe}, \text{or Co}; \text{R} = \text{tBu}, \text{Me}; \text{R}' = \text{Me}, \text{iPr}, \text{or H}; \text{X} = \text{Cl}, \text{I}$)	158
Scheme 3.2: Synthesis of 20 ($\text{M} = \text{Fe}$) and 21 ($\text{M} = \text{Co}$)	160
Scheme 3.3: Synthesis of 22 ($\text{M} = \text{Fe}$) and 23 ($\text{M} = \text{Co}$)	166
Scheme 3.4: Reaction of $\text{Tp}^{\text{tBu,Me}}\text{Cr}(\text{Cl})(\text{Py})$ with Li-dbabh	178
Scheme 3.5: Reaction of $\text{Tp}^{\text{tBu,Me}}\text{CrEt}$ with H-dbabh.....	183
Scheme 3.6: Expected equilibrium of 24 with $[\text{Tp}^{\text{tBu,Me}}\text{Cr}^{\text{I}}]_2(\mu\text{-}\eta^1\text{:}\eta^1\text{-N}_2)$, which is observed to not occur.....	186
Scheme 3.7: Reaction of $\text{Tp}^{\text{tBu,Me}}\text{CrN}$ (24) with MeI, synthesis of $\text{Tp}^{\text{tBu,Me}}\text{Cr}(\text{N})(\text{I})$ (25), $\text{Tp}^{\text{tBu,Me}}\text{CrNMe}$, and $\text{Tp}^{\text{tBu,Me}}\text{CrI}$	200

ABSTRACT

Following previous work done by members of the Theopold Lab, which was limited by the propensity for C-H bond activation on the hydrotris(3-*tert*-butyl-5-methylpyrazolyl)borate ligand, this work is a continuation of efforts to produce oxo complexes with the more robust hydrotris(3-ferrocenyl-5-methylpyrazolyl)borate ligand. $\text{Tp}^{\text{Fc,Me}}\text{FeX}$ ($\text{X} = \text{Cl}$ (**1**), Br (**2**), I (**3**)) and $\text{Tp}^{\text{Fc,Me}}\text{CoBr}$ (**4**) have been synthesized and used to produce $[\text{Tp}^{\text{Fc,Me}}\text{Fe}^{\text{I}}]_2(\mu_2\text{-}\eta^1\text{:}\eta^1\text{-N}_2)$ (**9**) and $[\text{Tp}^{\text{Fc,Me}}\text{Co}^{\text{I}}]_2(\mu_2\text{-}\eta^1\text{:}\eta^1\text{-N}_2)$ (**10**) to act as synthons for activation of oxygen. In a similar effort, alkyl complexes $\text{Tp}^{\text{Fc,Me}}\text{FeBn}$ (**5**) and $\text{Tp}^{\text{Fc,Me}}\text{FeEt}$ (**6**) were synthesized and reacted with carbon monoxide to produce a formally univalent $\text{Tp}^{\text{Fc,Me}}\text{Fe}(\text{CO})$ (**7**), to act as a synthon.

When **9** is reacted with oxygen atom transfer reagents the novel bridging oxo complex in the form of $[\text{Tp}^{\text{Fc,Me}}\text{Fe}]_2(\mu_2\text{-}\eta^1\text{:}\eta^1\text{-O})$ (**16**) is produced. **16** is only the second instance of such a $\text{Fe}^{\text{II}}\text{-O-Fe}^{\text{II}}$ compound to have been isolated and structurally characterized. In the effort to produce additional chalcogenide compounds the complexes $\text{Tp}^{\text{Fc,Me}}\text{FeOCPh}_3$ (**13**) and $\text{Tp}^{\text{Fc,Me}}\text{FeSCPh}_3$ (**14**) were produced by salt metathesis with **3**. The reaction of **14** with KH in the presence of 18-crown-6 to produce a bridging sulfide, $[\text{Tp}^{\text{Fc,Me}}\text{Fe}]_2(\mu_2\text{-}\eta^1\text{:}\eta^1\text{-S})$ (**15**). Attempts to produce imide compounds to act as isoelectronic models for terminal oxo compounds by reacting organic azides with **9** and **10** resulted in the production of tetrazene complex $\text{Tp}^{\text{Fc,Me}}\text{CoN}_4\text{Bn}_2$ (**17**), as well as metallated azides $\text{Tp}^{\text{Fc,Me}}\text{FeN}_3$ (**20**) and $\text{Tp}^{\text{Fc,Me}}\text{CoN}_3$ (**21**).

Reactions of **3** and **4** with the lithiated nitride transfer reagent 2,3:5,6-Dibenzo-7-azabicyclo[2.2.1]hepta-2,5-diene (dbabh) resulted only in transmetallation of production of $\text{Tp}^{\text{Fc,Me}}\text{Li}$. Reactions of $\text{Tp}^{\text{tBu,Me}}\text{FeI}$ and $\text{Tp}^{\text{tBu,Me}}\text{CoI}$ with Li-dbabh resulted in $\text{Tp}^{\text{tBu,Me}}\text{Fe-dbabh}$ (**22**) and $\text{Tp}^{\text{tBu,Me}}\text{Co-dbabh}$ (**23**), which do not decompose under heating to produce terminal nitrides. $\text{Tp}^{\text{tBu,Me}}\text{CrEt}$ reacts with H-dbabh to produce the first example of a first row

transition metal nitride compound supported by a Tp ligand, $\text{Tp}^{\text{tBu,Me}}\text{CrN}$ (**24**), which reacts with MeI to produce a rare example of a methyl imide, $\text{Tp}^{\text{tBu,Me}}\text{CrNMe}$ (**26**).

Chapter 1

INTRODUCTION

Small molecule activation via oxidative processes is important for the production of many industrially relevant compounds. Most such transformations utilize late transition metals, and few utilize metals from the first row. Such late 2nd and 3rd row transition metals are often expensive, and their high demand contributes to the deleterious effect mining and refining those metals has on the environment. Two small molecules of notable importance are O₂ and N₂ gases, both of which are exceptionally abundant and environmentally benign.¹ Various routes to the activation of either O₂ or N₂ involve an intermediate terminal oxo or nitrido complex. Terminal oxo complexes on late transition metals (group 9 and higher) violate the principle of the ‘oxo wall’. First described in relation to tetragonal crystal field splitting, metals with more than 5 d electrons will no longer effectively participate in π bonding, having the anti-bonding orbitals for that interaction partially or completely filled. Although not in name, the principles behind the oxo wall apply to all ligands that participate in π bonding with metals, including the nitride ligand (N³⁻).² For these reasons, metals in group 9 and above have been postulated as being incapable of producing stable terminal oxo complexes.³ This is true of all ligand fields, but decreasing the coordination number of the complex can lower the total electron count, remove trans-influence, and/or making orbitals available to host electrons in a state that is either non-bonding or only weakly anti-bonding.⁴

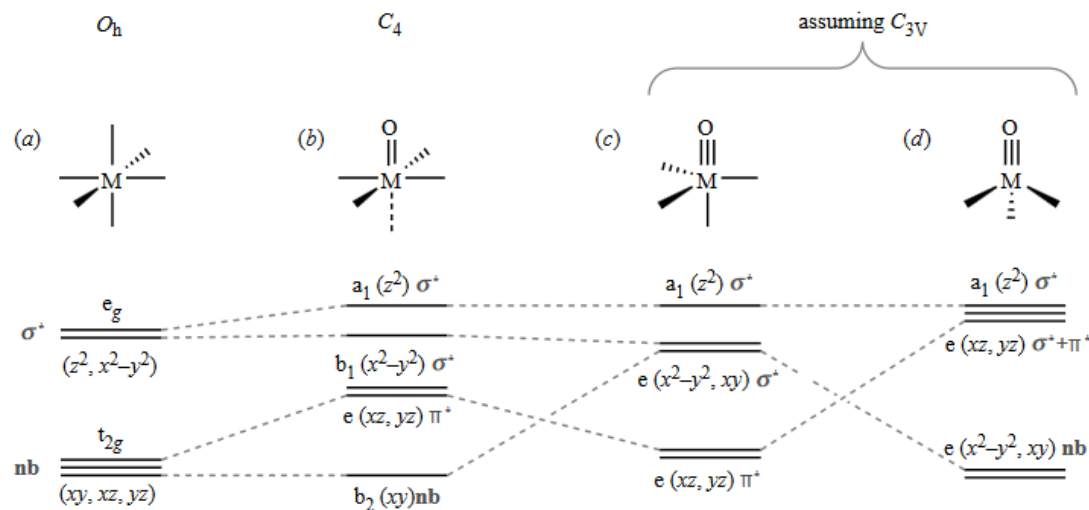


Figure I.1: Qualitative frontier molecular orbital diagrams of 3 ligand fields common to M-O complexes.⁴

H																				He
Li	Be													B	C	N	O	F		Ne
Na	Mg													Al	Si	P	S	Cl		Ar
K	Ca	Sc	Ti	V	Cr	Mn	Fe	Oxo wall	Co	Ni	Cu	Zn	Ga	Ge	As	Se	Br		Kr	
Rb	Sr	Y	Zr	Nb	Mo	Tc	Ru	Oxo wall	Rh	Pd	Ag	Cd	In	Sn	Sb	Te	I		Xe	
Cs	Ba	La	Hf	Ta	W	Re	Os	Oxo wall	Ir	Pt	Au	Hg	Tl	Pb	Bi	Po	At		Rn	

Figure I.2: Graphical representation of the “Oxo wall”, between groups 8 and 9.³

By utilizing either non-tetragonal ligand fields, or especially strong field ligands, terminal oxo compounds on group 9 and 10 metals have been produced. The first of these was isolated by Wilkinson in the 1990s, in the form of $\text{Ir}(\text{mes})_3(\text{O})$, produced from the reaction of an Ir^{III} precursor with the single oxygen atom transfer

reagent trimethylamine N-oxide.⁵ With an additional terminal oxo complex of Pt supported by the $C_6H_3[CH_2P(tBu)_2](CH_2)_2N(CH_3)_2$ (PCN) pincer ligand having also been described.⁶

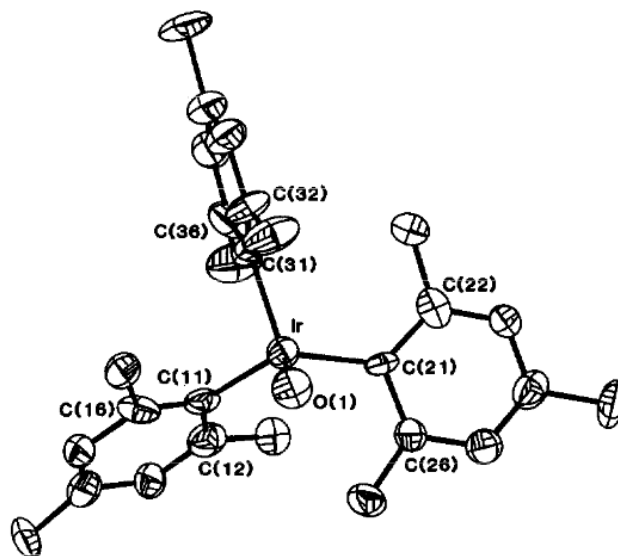


Figure I.3: Structure of oxotrimesityliridium (V).⁵

The concept of the oxo wall also implies that metal centers with higher electron counts produce oxo, or other π bonded anionic ligand complexes of greater reactivity (and thus less stability) than earlier or lower oxidation state metals. Of particular interest then, especially given the precedent with iridium, is the activation of oxygen with abundant group 8 and 9 metal centers. Iron and cobalt are the most abundant metals of those respective families, and iron is utilized heavily in nature for oxygen activation by way of functionalizing aliphatic hydrocarbons using the enzyme cytochrome P450, which is theorized to have a terminal oxo or oxyl intermediate.⁷

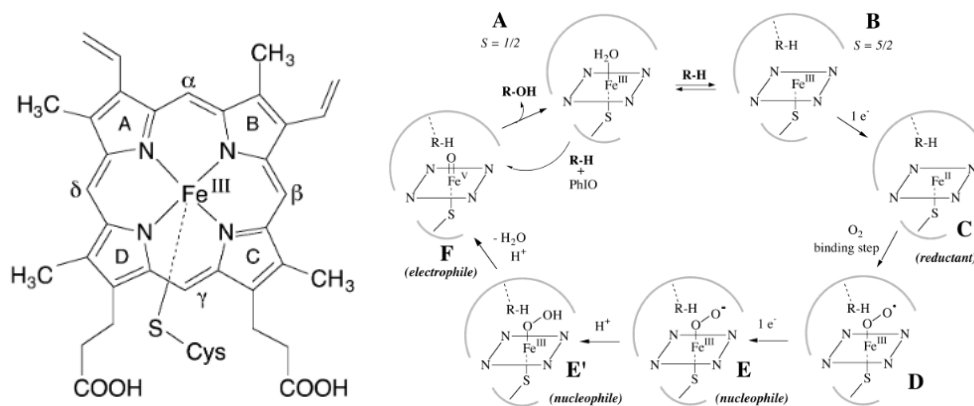


Figure I.4: Structure of Cytochrome P450 active site in the pre catalyst stage, and simplified mechanism of aliphatic hydrocarbon hydroxylation.⁸

Nitrogen activation shares many qualities in common with oxygen activation, by virtue of its also being a diatomic molecule and also because the resulting N^{3-} ligand participates in π bonding to metal centers. N_2 activation is accomplished in nature by nitrogenase enzymes at the iron centers of its active sites. The iron at which the nitrogen is activated alternates between a tetrahedral and trigonal bipyramidal coordination environment, by alternating its binding to an encapsulated carbide ligand.⁹ Nitrogenase accomplishes the synthesis of NH_3 through one of two mechanisms, termed the distal and alternating pathways. The distal pathway includes the formation of a nitride intermediate, while the alternating pathway has both a diazene and hydrazine as intermediate N_2 derived ligands, only completely cleaving the N-N bond upon formation of ammonia, see **Figure I.5.**¹⁰

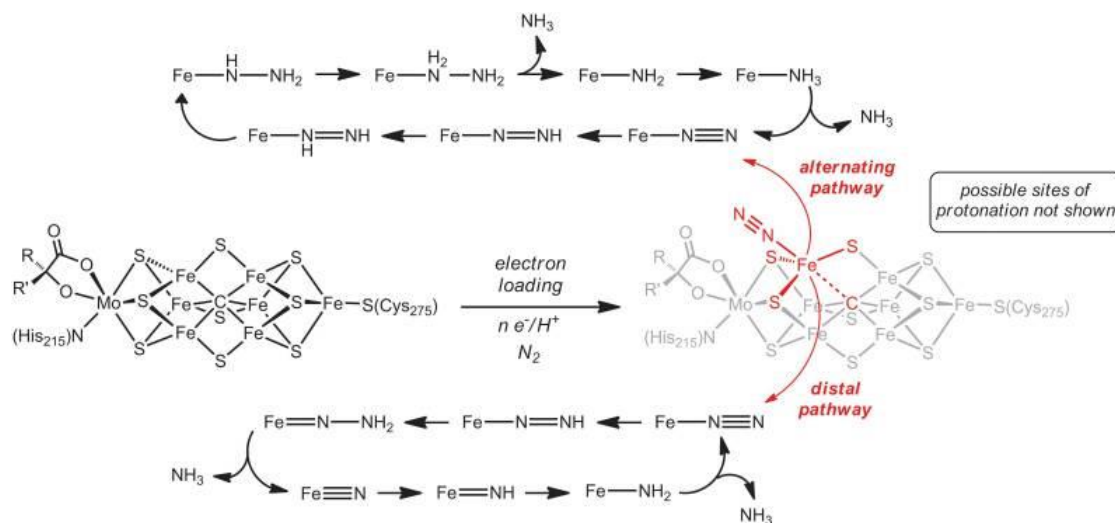


Figure I.5: Both reaction pathways theorized to be used by nitrogenase enzymes.¹⁰

While the role of terminal nitrido ligands is somewhat ambiguous in the catalytic fixation of nitrogen by biological systems, it is less so in industrial nitrogen fixation. The most common means by which N_2 is fixed industrially is the Haber-Bosch process, utilizing an iron oxide catalyst at high nitrogen and hydrogen pressures. That catalytic cycle unambiguously involves the cleavage of N_2 to produce two terminal iron nitrides, before reactions with H_2 to produce ammonia.¹¹ Significant effort has been expended attempting to replicate this process at ambient temperatures in homogeneous systems. Similar effort has been devoted to producing metal dinitrogen complexes using atmospheric N_2 and then through either irradiation or heating produce a complementary terminal nitride by way of activating that N_2 moiety. The prototypical example was produced by Cummins et. al. on a molybdenum trisulfide amide complex. There are a total of 7 examples of isolated dinitrogen complexes

whose terminal nitride analogues have also been produced, all on early transition metals.¹²

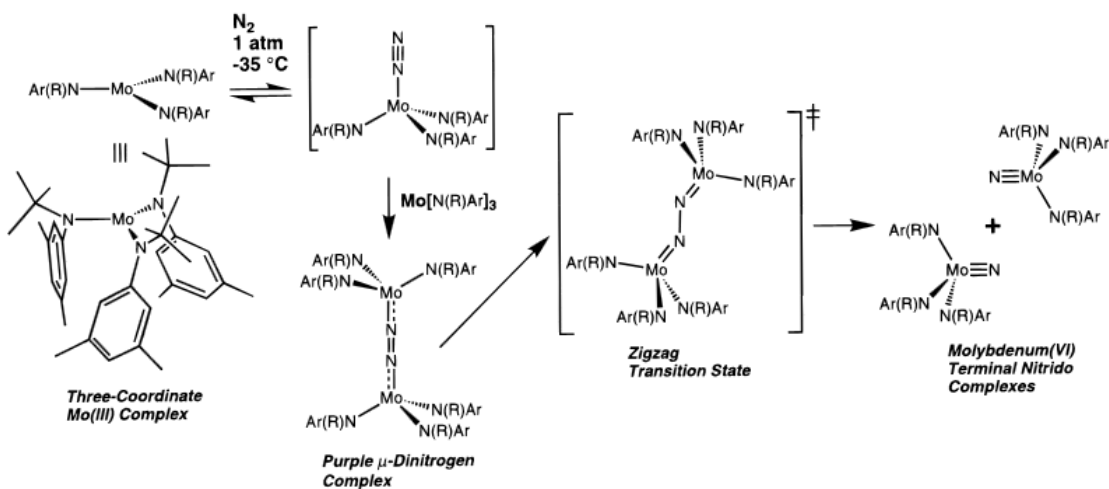


Figure I.6: Reaction mechanism for the formation of molybdenum terminal nitride from molybdenum di-nitrogen complex.¹²

In an effort to bypass issues of instability with the formation of terminal oxo and nitrido complexes, our lab has employed tetrahedral enforcing ligands, in the form of hydrotris(pyrazolyl)borates (Tp). Previous work with iron supported by hydrotris(3-*tert*-butyl,5-methylpyrazolyl)borate ($Tp^{tBu,Me}$) produced what was likely an extremely active intermediate oxo species, which then activated the *tert*-butyl groups on the ligand to produce an Fe^{III} -O- Fe^{III} moiety, with both iron atoms in a trigonal bipyramidal coordination sphere.¹³ Many bridging dinitrogen complexes supported by Tp ligands have also been produced in the Theopold Lab, however none of their terminal nitride analogues have thus far been isolated, likely due to both the stability of the N_2 molecule as well as the highly reactive nature such nitride complex would be likely to have.¹⁴

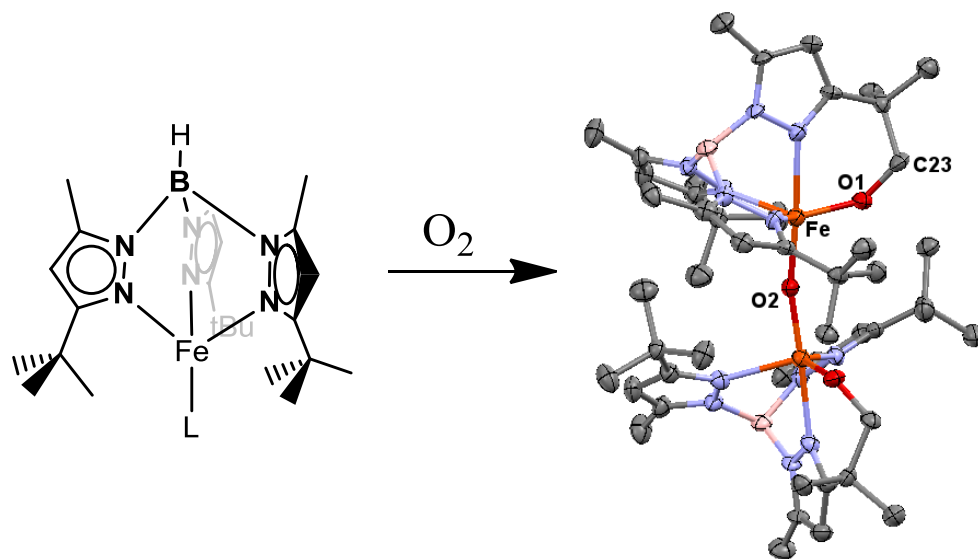


Figure I.7: Reaction of monovalent iron complexes supported by the $\text{Tp}^{\text{tBu,Me}}$ ligand, where L is either CO, C_2H_4 , or N_2 .¹³

In an effort to address the problem of terminal oxo complexes activating the aliphatic C-H bonds of the ligand, a Tris(pyrazolyl)borate compound was produced by the Theopold lab with ferrocenes at the 3-position of the pyrazole arm.¹⁵ This ligand takes advantage of ferrocenes C-H bonds high bond dissociation energy to prevent their activation and to isolate moieties that are otherwise too reactive to study.

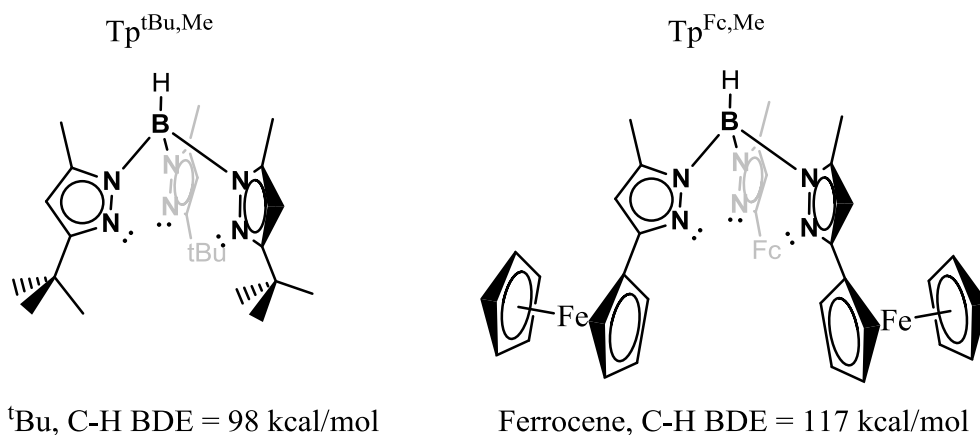


Figure I.8: Comparison of $\text{Tp}^{\text{tBu,Me}}$ and $\text{Tp}^{\text{Fc,Me}}$ ligands and their BDEs.¹⁶

This work will focus on the synthesis of dinitrogen complexes of Fe and Co using the $\text{Tp}^{\text{Fc,Me}}$ ligand system. Those complexes act as synthons for the investigation into the possibility of isolating novel oxo complexes of metals supported by $\text{Tp}^{\text{Fc,Me}}$ ligand. The work will also investigate the possibility of producing terminal nitride complexes on metals supported by tris(pyrazolyl)borate ligands for which there are known stable di-nitrogen complexes.

REFERENCES

1. a) Hess, J, *E.T.Z. Arch.*, **1922**, *43*, p. 957 – 960; b) Wataru, M.; Masao, I.; Tyozaemon, M.; Ryohei, O, *Rikagaku Kenkyusho Iho*, **1941**, *20*, p. 137 – 140; c) Sheldon, R. A.; Kochi, J. K., *Metal-Catalyzed Oxidations of Organic Compounds: Mechanistic principles and synthetic methodology including biochemical processes*; Academic Press Inc: New York, **1981**; d) Jenkinson, D. S., *Plant and Soil*, **2001**, *228*, p. 3 – 15; e) Martar, S.; Hatch, L., *Catalysis in Petrochemical Processes Second Edition*, **2001**, Chapter 7, p. 188 – 212.; f) Jankowiak, J. T.; Barteau, M. A. *Journal of Catalysis*, **2005**, *236*, p. 366 – 378; g) Meyer, F.; Tolman, W. B., *Inorg. Chem.*, **2015**, *54*, p. 5039.
2. a) Ballhausen, C. J.; Gray, H. B., *Inorg. Chem.*, **1962**, *1*, p. 111 – 123; b) Gray, H. B.; Hare, C. R., *Inorg. Chem.*, **1962**, *1*, p. 363 - 368; c) Sunil, K. K.; Harrison, J. F.; Rogers, M. T., *J. Chem. Phys.*, **1982**, *76*, p. 3087 ; d) Spaltenstein, E.; Erikson, T. K. G.; Critchlow, S. C.; Mayer, J. M. *J. Am. Chem. Soc.*, **1989**, *111*, p. 617; e) Cao, R.; Han, J. W.; Anderson, T. M.; Hillesheim, D. A.; Hardcastle, K. I.; Slonkina, E.; Hedman, B.; Hodgson, K. O.; Kirk, M. L.; Musaev, D. G.; Morokuma, K.; Geletii, Y. V.; Hill, C. L, *Advances in Inorganic Chemistry*, **2008**, *Vol 60*, p. 246 – 248; f) O'Halloran, K. P.; Zhao, C.; Ando, N. S.; Schultz, A. J.; Koetzle, T. F.; Piccoli, P. M. B.; Hedman, B.; Hodgson, K. O.; Bobyr, E.; Kirk, M. L.; Knottenbelt, S.; Depperman, E. C.; Stein, B.; Anderson, T. M.; Cao, R.; Geletii, Y. V.; Hardcastle, K. I.; Musaev, D. G.; Neiwert, W. A.; Fang, X.; Morokuma, K.; Wu, S.; Kögerler, P.; Hill, C. L., *Inorg. Chem.*, **2012**, *51*, p. 7025 – 7031.
3. Winkler, J. R.; Gray, H. B., *Struct. Bond.*, **2012**, *142*, p. 17.
4. Betley, T. A.; Surendranath, Y.; Childress, M. V.; Alliger, G. E.; Fu, R.; Cummins, C. C.; Nocera, D. G., *Phil. Trans. R. Soc. B*, **2008**, *363*, p. 1293 – 1303.
5. Hay-Motherwell, R. S.; Wilkinson, G.; Hussain-Bates, B.; Hursthouse, M. B., *Polyhedron*, **1993**, *12*, p. 2009 – 2012.

6. Poverenov, E., Efremenko, I.; Frenkel, A. I., Ben-David, Y., Shimon, L. J. W., Leitus, G., Konstantinovski, L., Martin, J. M. L., Milstein, D., *Nature*, **2008**, *455*, 1093.
7. a) Oloo, W. N.; Que, L., *Acc. Chem. Res.*, **2015**, *48*, 2612 – 2621; b) Lide, David R., editor. *CRC Handbook of Chemistry and Physics*, 88th edition. Boca Raton, Florida: Taylor & Francis Group, **2008**; c) Solomon, E. I.; Brunold, T. C.; Davis, M. I.; Kemsley, J. N.; Lee, S. K.; Lehnert, N.; Neese, F.; Skulan, A. J.; Yang, Y. S.; Zhou, J., *Chem. Rev.*, **2000**, *100*, p. 235 – 349.
8. Meunier, B.; Vissar, S. P.; Shaik, S., *Chem. Rev.*, **2004**, *104*, p. 3947 – 3980.
9. a) Macleod, K. C.; Holland, P. L., *Nature*, **2013**, *5*, p. 559 – 565; b) Kowalska, J.; Debeer, S., *Biochimica et Biophysica Acta*, **2015**, *1853*, p. 1406 – 1415.
10. a) Rittle, J.; Peters, J. C., *J. Am. Chem. Soc.*, **2016**, *138*, p. 4243 – 4248; b) Anderson, J. S.; Cutsail, G. E.; Rittle, J.; Connor, B. A.; Gunderson, W. A.; Zhang, L.; Hoffman, B. M.; Peters, J. C., *J. Am. Chem. Soc.*, **2015**, *137*, p. 7803–7809; c) Hoffman, B. M.; Lukoyanov, D.; Yang, Z. Y.; Dean, D. R.; Seefeldt, L. C., *Chem. Rev.*, **2014**, *114*, p. 4041 – 4062; d) Hoffman, B. M.; Lukoyanov, D.; Dean, D. R.; Seefeldt, L. C., *Acc. Chem. Res.*, **2013**, *46*, p. 587 – 595; e) Anderson, J. S.; Rittle, J.; Peters, J. C., *Nature*, **2013**, *501*, p. 84 – 87.
11. a) Rodriguez, M. M.; Bill, E.; Brennesel, W. W.; Holland, P. L., *Science*, **2011**, *334*, p. 780 – 783; b) Lan, R.; Alkhazmi, K. A.; Amar, I. A.; Tao, S., *Appl. Catal., B*, **2014**, *152 – 153*, p. 212 – 217.
12. a) Keane, A. J.; Yonke, B. L.; Hirotsu, M.; Zavalij, P. Y.; Sita, L. R., *J. Am. Chem. Soc.*, **2014**, *136*, p. 9906 – 9909; b) Kunkely, H.; Volger, A., *Angew. Chem. Int. Ed.*, **2010**, *49*, p. 1591 – 1593; c) Hirotsu, M.; Fontaine, P. P.; Epshteyn, A.; Zavalij, P. Y.; Sita, L. R., *J. Am. Chem. Soc.*, **2007**, *129*, p. 9282 – 9285; d) Fryzuk, M. D.; Kozak, C. M.; Bowdridge, M. R.; Patrick, B. O.; Rettig, S. J., *J. Am. Chem. Soc.*, **2002**, *124*, p. 8389 – 8397; e) Solari, E.; Silva, C. D.; Iacono, B.; Hesschenbrouck, J.; Rizzoli, C.; Scopelliti, R.; Floriani, C., *Angew. Chem. Int. Ed.*, **2001**, *40*, p. 3907 – 3909; f) Laplaza, C. E.; Cummins, C. C., *Science*, **1995**, *268*, p. 861 – 862; g) Laplaza, C. E.; Johnson, M. J. A.; Peters, J. C.; Odom, A. L.; Kim, E.; Cummins, C. C.; George, G. N.; Pickering, I. J., *J. Am. Chem. Soc.*, **1996**, *118*, p. 8623 – 8638.

13. a) F. A. Jove, Ph. D. thesis, University of Delaware (Newark, DE), **2008**;
b) Jove, F. A.; Chandi, P.; Michael, S.; Yap, G. P. A.; Theopold, K. H.,
Chem. Eur. J., **2011**, *17*, p 1310 – 1318.
14. Cummins, D. C.; Yap, G. P. A.; Theopold, K. H., *Eur. J. Inorg. Chem.*,
2016, p. 2349 – 2356.
15. a) E. R. Sirianni, Ph. D. thesis, University of Delaware (Newark, DE),
USA, **2014**; b) Sirianni, E. R.; Yap, G. P. A.; Theopold, K. H., *Inorg.*
Chem., **2014**, *53*, p. 9424 – 9430.
16. a) Elihin, K.; Larsson, K., *Thin Solid Films*, **2004**, *458*, p. 325; b)
Blanksby, S. J.; Ellison, G. B., *Acc. Chem. Res.*, **2003**, *36*, 255.

Chapter 2

**SYNTHESIS AND CHARACTERIZATION OF MONO-VALENT
IRON AND COBALT COMPLEXES OF FERROCENYL SUBSTITUTED
TRIS(PRAZOLYL)BORATE LIGANDS**

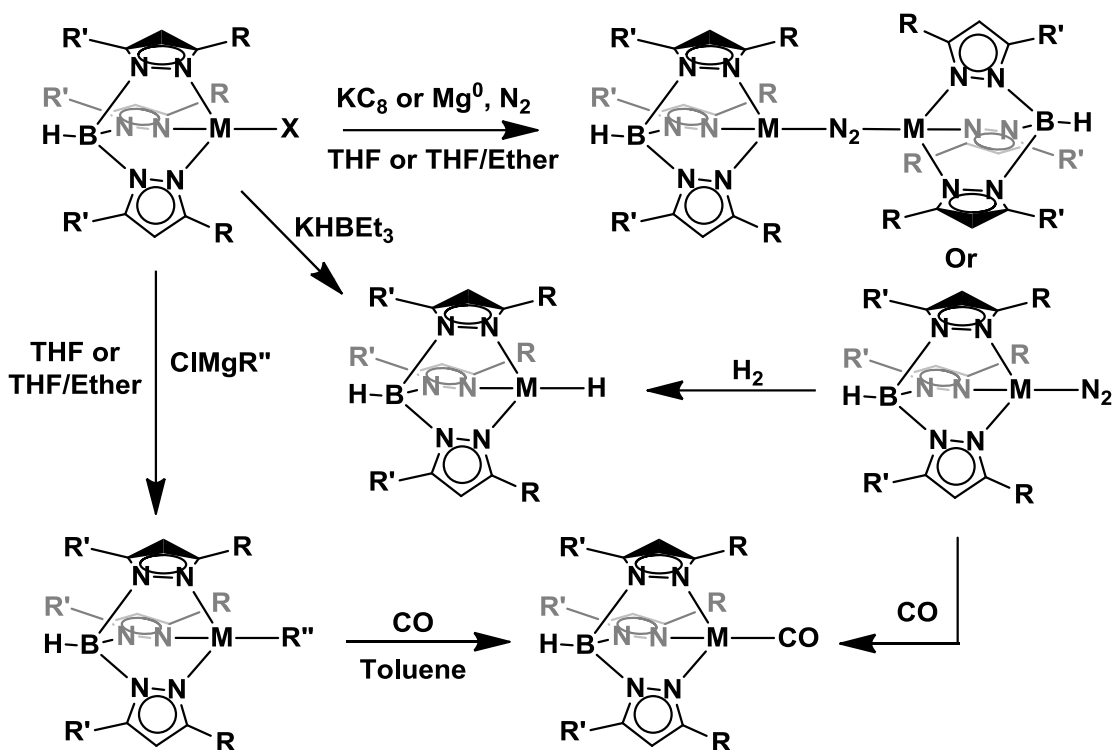
INTRODUCTION

In the service of the ultimate goal, to activate oxygen gas, I set out to produce low valent complexes of iron and cobalt, including N_2 ,¹ carbonyl,^{2,3,4} and hydride complexes.⁵ We selected these moieties because of their previous success in oxygen activation and their proficiency in facilitating oxidative addition in general. The first neutral ligand complex I set out to produce was a carbonyl complex, which, in the case of first row transition metals supported by hydrotris(pyrazolyl)borate ligands, have been shown to be accessible through bond homolysis of an alkyl complex, by the addition of carbon monoxide.⁶

Accessing those alkyl complexes, as well as either N_2 or H^- complexes, is accomplished in an often facile manner from ligated metal halides. Compounds of that type with tris(pyrazolyl)borate ligands are often made by the metathesis of an alkali metal salt of the desired Tp ligand with a metal halide salt of the desired metal.³⁻⁶ Once purified, TpMX complexes can then be reacted with Grignard reagents to afford the desired alkyl complex for later carbonylation.

An N_2 complex of cobalt has been prepared by direct reduction of $Tp^{tBu,Me}CoI$ with magnesium metal, and di-nitrogen complexes supported by chromium and iron

have been produced by reduction of their respective halide compounds with KC_8 .^{3,6} Cobalt hydride complexes supported by Tp ligands have been synthesized by either reaction of a borohydride with TpCoX or reaction of $\text{TpCo}(\text{N}_2)$ with H_2 gas.^{7,8} A general outline for the reactions to make these low valent complexes is shown in Scheme 1.1 below.



Scheme 1.1: Previously published synthesis of $\text{Tp}^{(\text{R},\text{R}')}\text{ML}$ ($\text{M} = \text{Cr}, \text{Mn}, \text{Fe}, \text{ or } \text{Co}$, $\text{R} = i\text{Bu}, i\text{Pr}, \text{ neopentyl}, \text{ or } \text{Ad}$; $\text{R}' = \text{Me}, i\text{Pr}, \text{ or } \text{H}$, $\text{X} = \text{Cl}, \text{I}$; $\text{L} = \text{CO}, \text{N}_2$) complexes.

Once in hand, carbonyl complexes have the advantage of increasing the π -acidity of the metal, making them more reactive with good π -bases, i.e. pnictogen

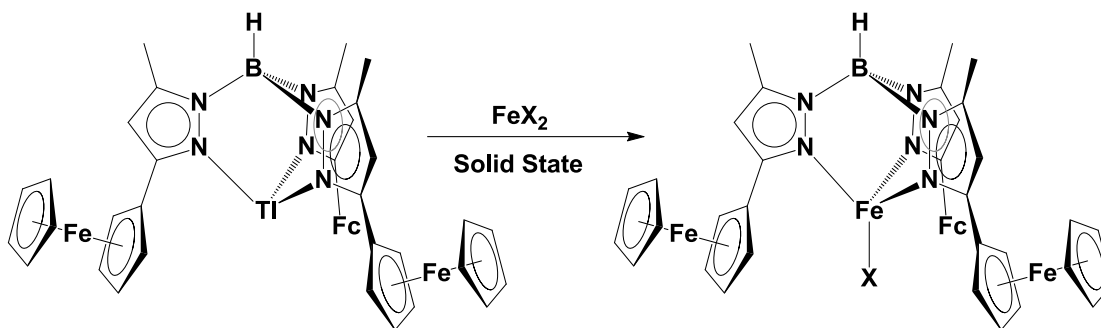
containing substrates such as nitriles. Dinitrogen complexes have the advantage of being highly labile in cases where the N₂ moiety is not considerably activated, making them ideal for dissociative reactions. Dinitrogen compounds that are more activated can also be selective for reactions that go by associative mechanisms, given the oxidizing effect such compounds have on the N₂ ligated metal center.³ Finally, cobalt hydride complexes have previously been used by members of our group to produce activated metal oxo complexes, by reacting them with oxygen atom transfer reagents.⁵

RESULTS AND DISCUSSION

Synthesis and characterization of iron halides supported by Tp^{Fc,Me} ligand.

Ligated metal halide complexes provide an easy entry into the synthesis of various classes of inorganic and organometallic compounds. The complexes Tp^{Fc,Me}FeCl (**1**) and Tp^{Fc,Me}FeBr (**2**) are accessible by reaction of the Tp^{Fc,Me}Tl^{4,9} ligand salt with anhydrous FeX₂ (X = Cl, Br) in the solid state by grinding with a mortar and pestle, followed by extraction with THF and washing with ether and pentanes solutions. This method of synthesis can be used to favor the kinetic product over the thermodynamic product of a reaction.¹⁰ This is necessary as the pure form of **1** is especially sensitive to isomerization by way of borotropic rearrangement when in THF, and was difficult to handle as a result. Analytically pure samples of the complex **1** can be prepared by slow evaporation of a solution of the compound in dichloromethane, affording bright orange crystals. ¹H-NMR spectra recorded in deuterated THF or benzene-d₆ solution of either **1** or **2** display 5 reasonably well defined resonances between -2 to 59 ppm, which are assigned to the protons of the Tp^{Fc,Me} ligand, displayed in **Figures 1.1 and 1.2**, respectively. The structure of **1** was determined by X-ray crystallography, and it

displays the same pseudotetrahedral coordination geometry of other κ^3 bound Tp complexes of iron halides.⁶ The unit cell of **2** was found to be nearly identical to that of **1** so the acquisition of a crystal structure of **2** was forgone. The effective magnetic moments of **1** and **2** taken at room temperature were found to be $4.9 \mu_B$ and $5.0 \mu_B$ respectively, consistent with the 4 unpaired electrons expected for high spin d^6 Fe^{II} ions.



Scheme 1.2: Solid state synthesis of $Tp^{Fc,Me}FeX$ ($X=Cl$ (1**), Br (**2**)).**

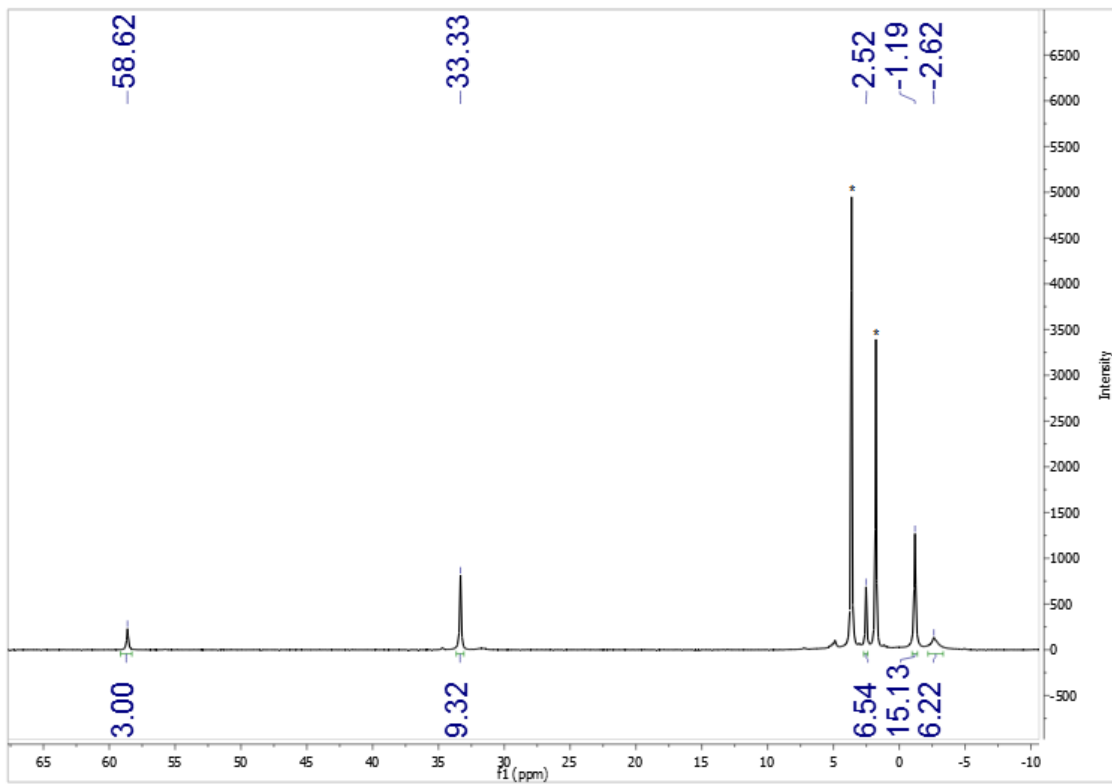


Figure 1.1: ¹H-NMR spectrum of Tp^{Fc,Me}FeCl (1) recorded in THF-d⁸ (*) at 400MHz

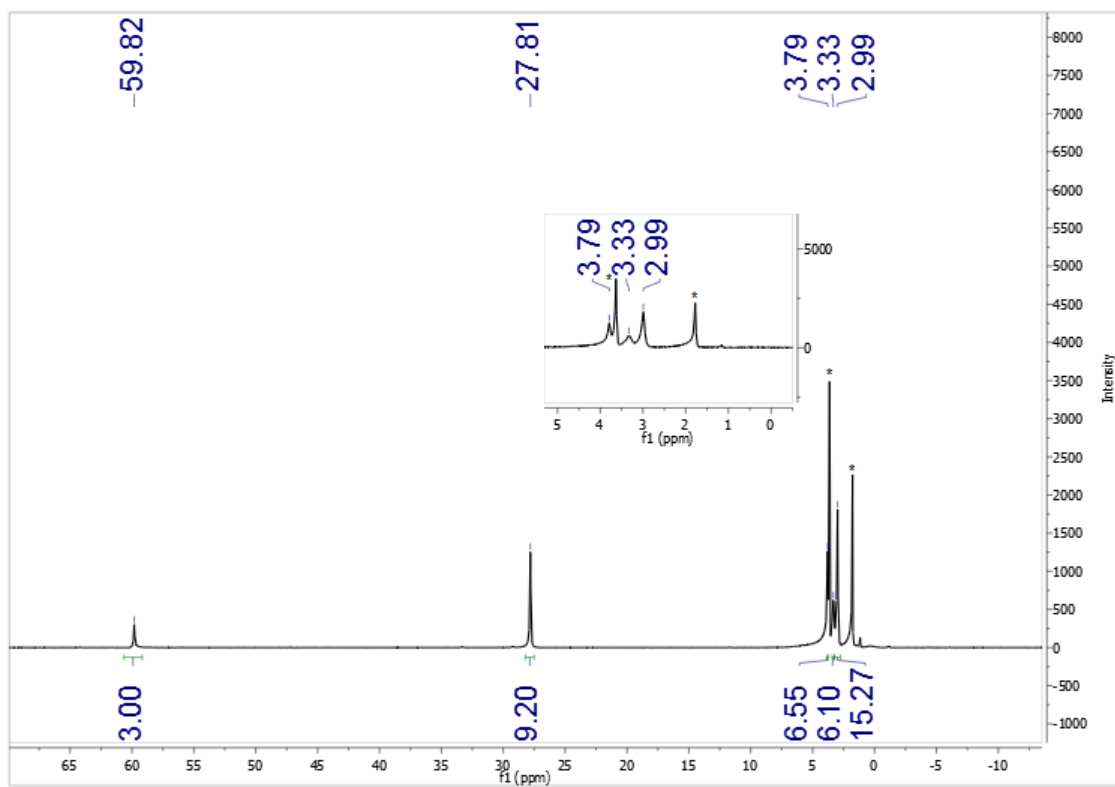


Figure 1.2: $^1\text{H-NMR}$ spectrum of $\text{Tp}^{\text{Fc,Me}}\text{FeBr}$ (2) recorded in THF-d^8 (*) at 400MHz, (Inset: close up of resonances between 0 and 5 ppm)

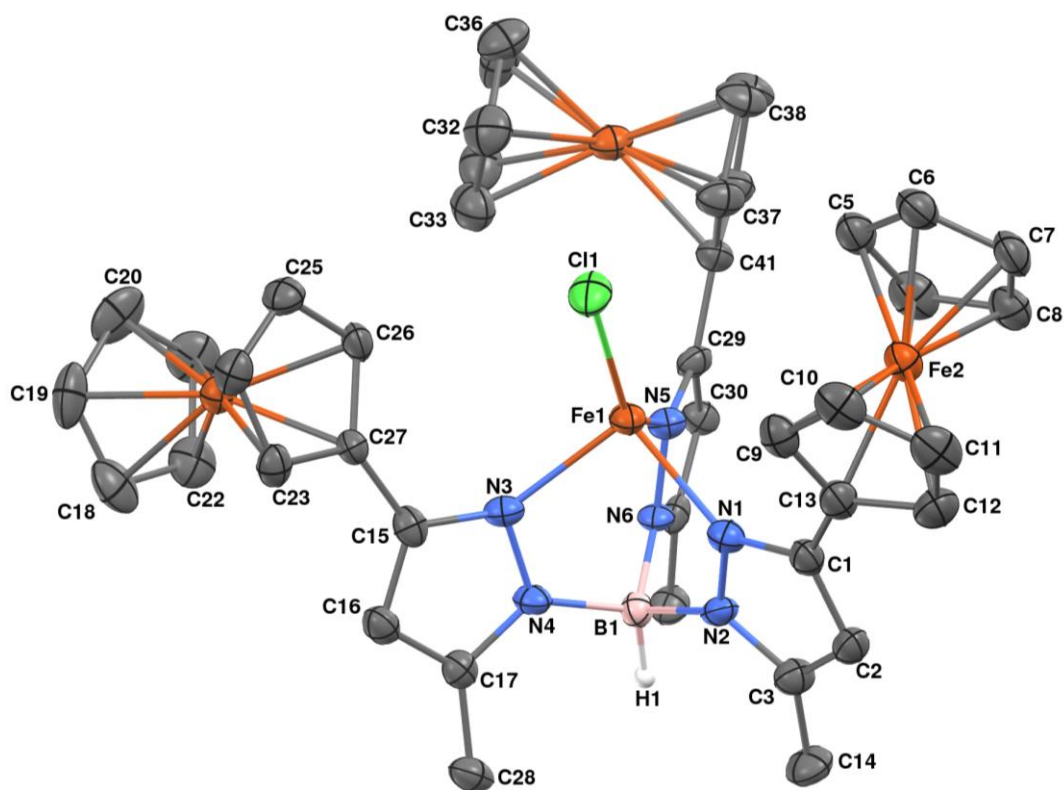


Figure 1.3: Molecular structure of $\text{Tp}^{\text{Fc,Me}}\text{FeCl}$ (1) represented as 50% probability thermal ellipsoids. Hydrogen atoms (with the exception of the hydrogen attached to the boron, H1) have been omitted for clarity.

Table 1.1: Selected interatomic distances (Å) and angles (°) for $\text{Tp}^{\text{Fc,Me}}\text{FeCl}$ (1)

Distances (Å)

Fe1-N5	2.076(4)	Fe1-N1	2.089(5)
Fe1-N3	2.095(5)	Fe1-Cl1	2.2209(16)
N1-C1	1.348(7)	N1-N2	1.376(6)
N2-C3	1.337(7)	N2-B1	1.545(8)
N3-C15	1.353(7)	N3-N4	1.377(6)
N4-C17	1.352(7)	N4-B1	1.552(7)
N5-C29	1.352(7)	N5-N6	1.375(5)
N6-C31	1.351(6)	N6-B1	1.562(8)
B1-H1	1.07(5)	C1-C2	1.397(8)

C1-C13	1.459(8)	C2-C3	1.375(8)
C4-C8	1.416(9)	C3-C14	1.495(7)
C9-C10	1.430(8)	C4-C5	1.436(9)
C15-C16	1.396(8)	C5-C6	1.416(8)
C16-C17	1.378(8)	C6-C7	1.410(9)
C17-C28	1.489(7)	C7-C8	1.424(9)
C18-C22	1.413(9)	C9-C13	1.433(8)
C19-C20	1.415(10)	C10-C11	1.416(9)
C20-C21	1.407(9)	C11-C12	1.422(9)
C21-C22	1.417(9)	C12-C13	1.441(8)
C23-C27	1.427(7)	C15-C27	1.466(7)
C24-C25	1.406(8)	C18-C19	1.402(10)
C25-C26	1.426(8)	C23-C24	1.413(8)
C26-C27	1.419(8)	C29-C30	1.406(7)
C29-C41	1.453(7)	C30-C31	1.367(7)
C32-C33	1.400(9)	C31-C42	1.504(7)
C37-C38	1.408(8)	C32-C36	1.415(9)
C37-C41	1.439(8)	C33-C34	1.404(9)
C38-C39	1.393(8)	C34-C35	1.445(10)
C39-C40	1.420(8)	C35-C36	1.401(9)
C40-C41	1.436(8)		

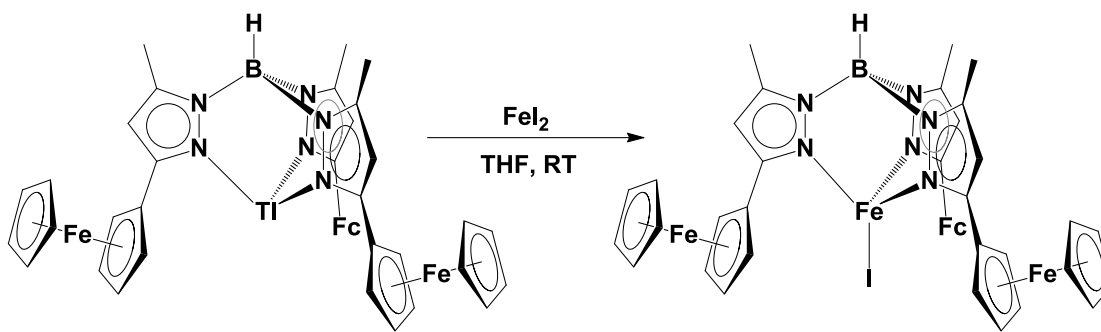
Angles (°)

B1-Fe1-C11	167.3(2)	N5-Fe1-N3	90.67(17)
N5-Fe1-N1	89.90(17)	N5-Fe1-C11	133.00(13)
N1-Fe1-N3	95.15(18)	N3-Fe1-C11	112.04(13)
N1-Fe1-C11	125.97(13)	C1-N1-N2	106.7(4)
C3-N2-N1	110.0(5)	C3-N2-B1	128.9(5)
N1-N2-B1	121.1(4)	C15-N3-N4	106.2(4)
C17-N4-N3	109.9(4)	C17-N4-B1	129.3(5)
N3-N4-B1	120.7(4)	C29-N5-N6	106.5(4)
C31-N6-N5	109.9(4)	C31-N6-B1	129.5(4)
N5-N6-B1	120.2(4)	N2-B1-N4	110.2(4)
N2-B1-N6	107.8(4)	N4-B1-N6	109.3(5)
N2-B1-H1	108.(3)	N4-B1-H1	113.(3)
N6-B1-H1	108.(3)	N1-C1-C2	108.8(5)
N1-C1-C13	125.1(5)	C2-C1-C13	126.0(5)
C3-C2-C1	106.4(5)	N2-C3-C2	108.0(5)
N2-C3-C14	123.2(5)	C2-C3-C14	128.8(6)
C8-C4-C5	107.9(6)	C9-C13-C1	128.4(5)

C6-C5-C4	107.6(6)	N3-C15-C27	122.3(5)
C7-C6-C5	108.2(6)	C17-C16-C15	106.1(5)
C6-C7-C8	108.6(6)	N4-C17-C28	122.7(5)
C4-C8-C7	107.6(6)	C19-C18-C22	107.6(7)
C10-C9-C13	107.8(6)	C18-C19-C20	108.9(6)
C11-C10-C9	108.5(6)	C21-C20-C19	107.3(6)
C12-C11-C10	108.2(6)	C20-C21-C22	108.2(6)
C11-C12-C13	108.2(6)	C18-C22-C21	107.9(6)
C9-C13-C12	107.3(5)	C24-C23-C27	108.0(5)
C12-C13-C1	123.9(6)	C25-C24-C23	108.3(5)
N3-C15-C16	109.7(5)	C24-C25-C26	108.4(5)
C16-C15-C27	128.0(5)	C27-C26-C25	107.6(5)
N4-C17-C16	108.0(5)	C26-C27-C23	107.7(5)
C16-C17-C28	129.3(5)	C23-C27-C15	123.8(5)
C26-C27-C15	128.3(5)	N5-C29-C30	109.1(5)
N5-C29-C41	123.9(5)	C30-C29-C41	127.1(5)
C31-C30-C29	106.3(5)	N6-C31-C30	108.2(5)
N6-C31-C42	122.8(5)	C30-C31-C42	129.0(5)
C33-C32-C36	108.0(6)	C37-C41-C29	128.4(5)
C34-C33-C32	108.7(6)	C38-C39-C40	108.3(5)
C33-C34-C35	107.6(6)	C39-C40-C41	107.7(5)
C36-C35-C34	106.9(6)	C37-C41-C40	107.0(5)
C35-C36-C32	108.8(6)	C40-C41-C29	124.6(5)
C38-C37-C41	107.4(5)	C39-C38-C37	109.6(5)

Tp^{Fc,Me}FeI (**3**) was more robust with respect to borotropic rearrangement than either **1** or **2**, showing only minimal isomerization when left in a solution of THF for 24 hours at room temperature. Because of this, **3** can be synthesized by salt metathesis of anhydrous FeI₂ with Tp^{Fc,Me}Tl in THF at room temperature, as seen in **Scheme 1.3**. Following filtration and washing the ppt with ether to remove any byproducts, **3** can be crystallized from mixtures of THF/pentanes at -35 °C to afford the desired compound as small orange blocks in yields that ranged from 55 to 78 %. Again, the unit cell of **3** was found to be exceedingly similar to that of **1**, so the acquisition of a

crystal structure of **3** was forgone. $^1\text{H-NMR}$ spectra taken in deuterated benzene revealed 5 resonances between 4 and 65 ppm, corresponding to the hydrogens on the $\text{Tp}^{\text{Fc,Me}}$ Ligand, shown in **Figure 1.4** below. **3** displayed an effective magnetic moment of $5.0 \mu_{\text{B}}$ at room temperature, indicating that it is a high spin Fe^{II} d^6 complex, similar to **1** and **2**.



Scheme 1.3: Solution state synthesis of $\text{Tp}^{\text{Fc,Me}}\text{FeI}$, (3**).**

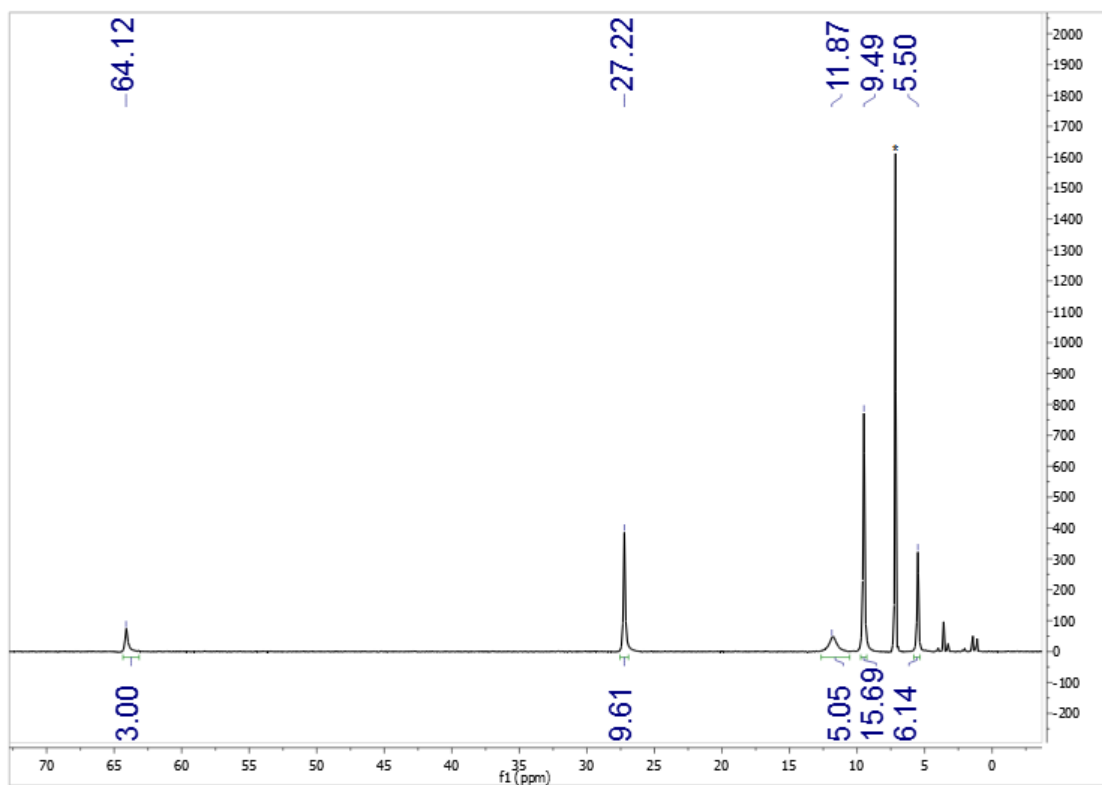


Figure 1.4: ^1H -NMR spectrum of $\text{Tp}^{\text{Fc,Me}}\text{FeI}$ (**3**) recorded in C_6D_6 (*) at 400MHz

Borotropic rearrangement of compounds **1**, **2**, and **3** is evident by loss of the C_{3v} symmetry displayed by the number of resonances in their respective ^1H -NMR spectra, shown in **Figures 1.5 – 1.7**. The rate at which these isomerizations occurred showed a clear trend of **1**>>**2**>**3**.

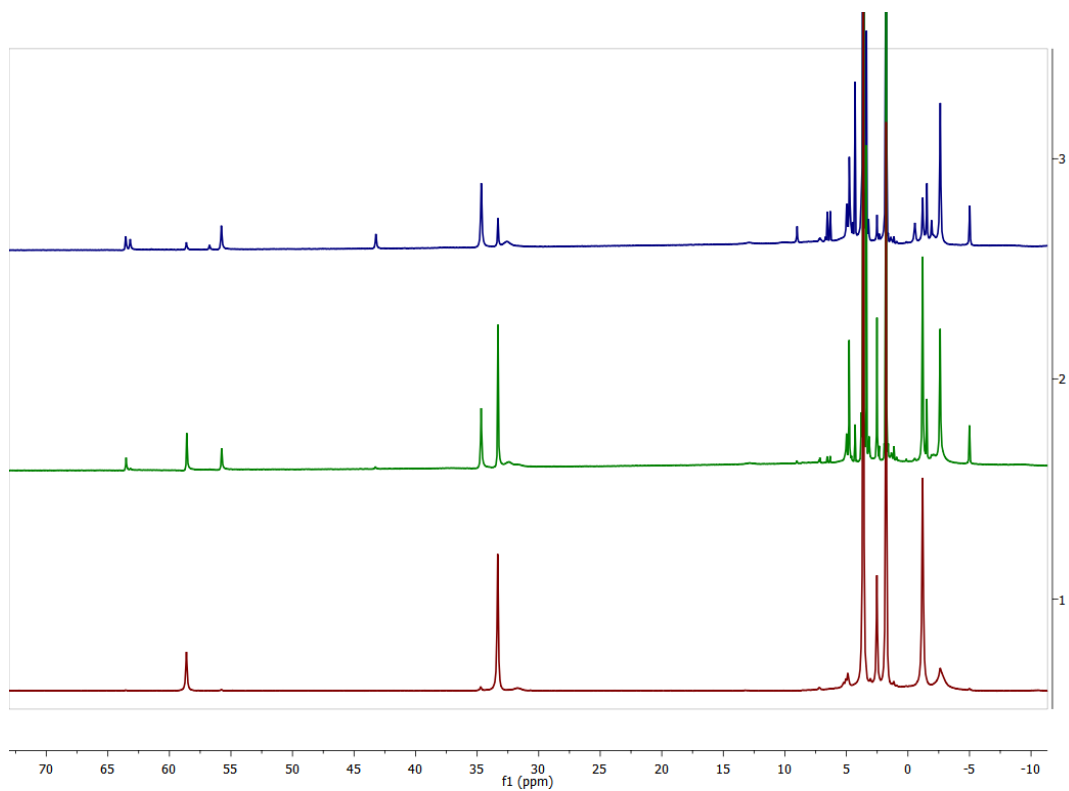


Figure 1.5: $^1\text{H-NMR}$ Comparison of $\text{Tp}^{\text{Fe,Me}}\text{FeCl}$ (1) (Bottom), the same sample after 24 hours at room temperature had passed (Middle), and then the same sample left at 60 °C for 12 hours (top), all spectra taken in THF-d^8 .

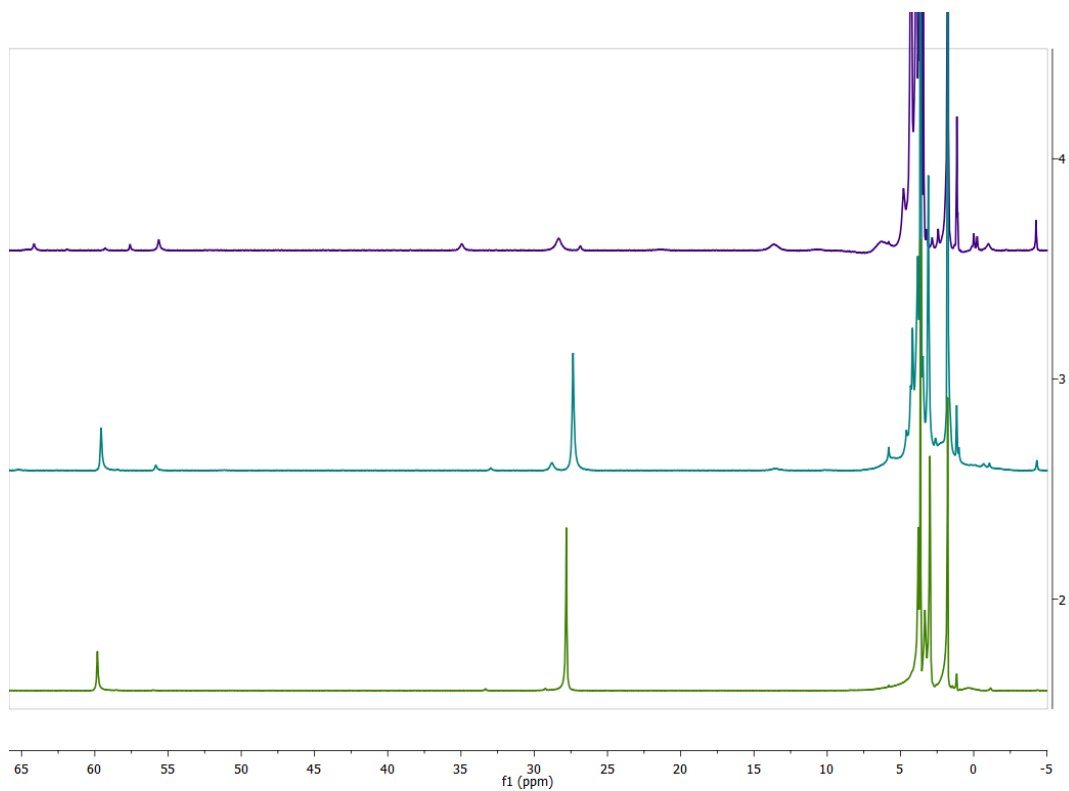


Figure 1.6: ¹H-NMR Comparison of Tp^{Fc,Me}FeBr (2) (Bottom), the same sample after 24 hours at room temperature had passed (Middle), and then the same sample left at 60 °C for 12 hours (top), all spectra taken in C₆D₆.

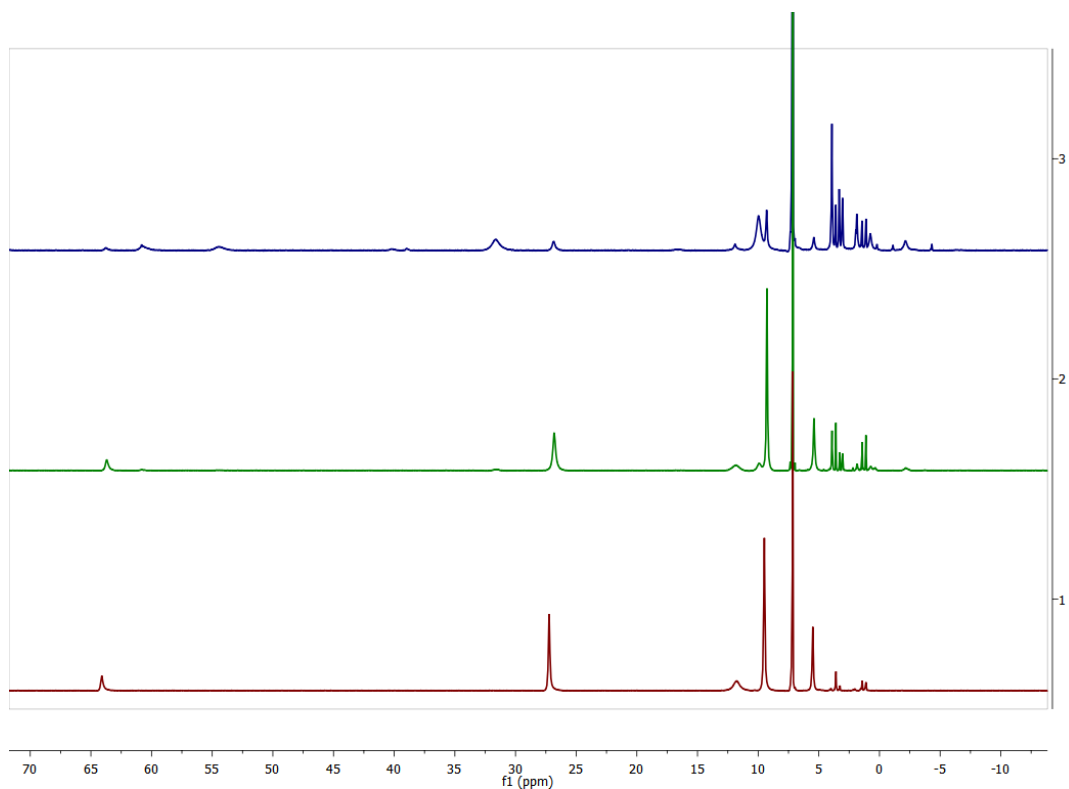
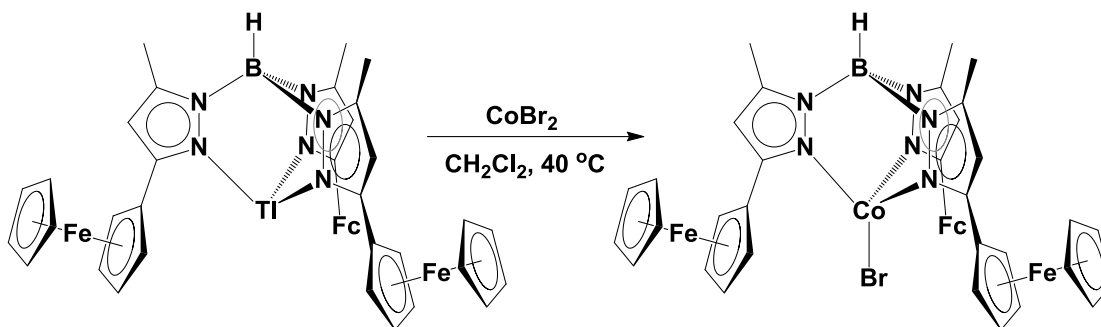


Figure 1.7: ^1H -NMR Comparison of $\text{Tp}^{\text{Fc,Me}}\text{FeI}$ (3**) (Bottom), the same sample after 24 hours at room temperature had passed (Middle), and then the same sample left at 60 °C for 40 hours (top).**

Synthesis and characterization of cobalt halide supported by $\text{Tp}^{\text{Fc,Me}}$ ligand. We set out to synthesize a cobalt halide complex analogous to **1-3**, to access formally Co^{I} compounds supported by the $\text{Tp}^{\text{Fc,Me}}$ ligand system, in order to complement our iron chemistry. The complex $\text{Tp}^{\text{Fc,Me}}\text{CoBr}$ (**4**) can be synthesized by metathesis of anhydrous CoBr_2 with $\text{Tp}^{\text{Fc,Me}}\text{I}$ in refluxing dichloromethane under a nitrogen atmosphere, **Scheme 1.4**. After filtration and concentration of the solution, an equal volume of pentanes is added and the mixture is then left at -35 °C overnight, producing **4** as analytically pure green blocks in yields ranging from 75 to 85%. The

$^1\text{H-NMR}$ spectrum of **4** displays 5 peaks between 4 and 74 ppm corresponding to the hydrogens on the $\text{Tp}^{\text{Fc,Me}}$ ligand, plus one comparatively broad resonance at -24 ppm which is assigned as the resonance of the hydrogen on the boron. The structure of **4** is similar to that of **1**, with only minor differences in bond lengths and angles about the central metal atom. The effective magnetic moment for **4** was found to be $3.9(1) \mu_{\text{B}}$ when measured at room temperature, consistent with 3 unpaired electrons of a high spin Co^{II} d^7 complex.



Scheme 1.4: Synthesis of $\text{Tp}^{\text{Fc,Me}}\text{CoBr}$, (4**).**

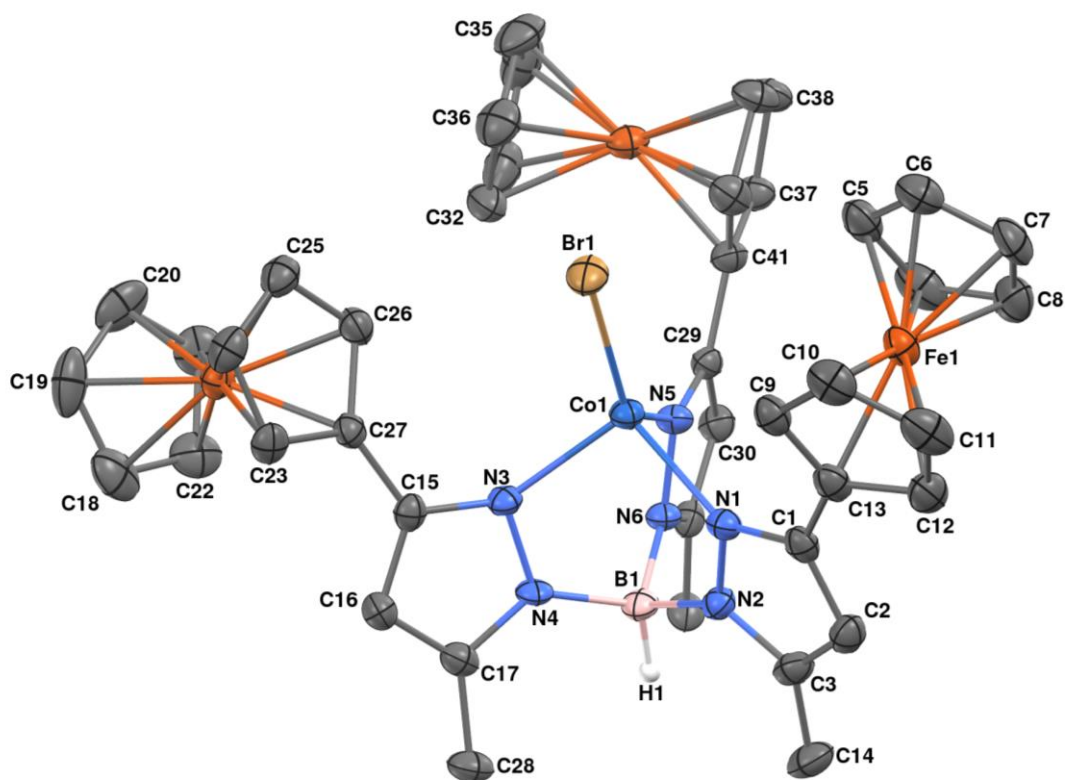


Figure 1.8: Molecular structure of $\text{Tp}^{\text{Fc,Me}}\text{CoBr}$ (4) represented as 50% probability thermal ellipsoids. Hydrogen atoms (with the exception of the hydrogen attached to the boron, H1) have been omitted for clarity.

Table 1.2: Selected interatomic distances (Å) and angles (°) for $\text{Tp}^{\text{Fc,Me}}\text{CoBr}$ (4)

Distances (Å)			
Co1-N3	2.034(3)	Co1-N1	2.047(3)
Co1-N5	2.046(3)	Co1-Br1	2.3458(6)
N1-C1	1.344(4)	N1-N2	1.395(4)
N2-C3	1.348(5)	N2-B1	1.545(5)
N3-C15	1.340(4)	N3-N4	1.385(4)
N4-C17	1.352(4)	N4-B1	1.544(5)
N5-C29	1.335(4)	N5-N6	1.390(4)
N6-C31	1.355(4)	N6-B1	1.552(5)
C1-C2	1.394(5)	C1-C13	1.475(5)
C2-C3	1.383(5)	C3-C14	1.482(5)

C4-C8	1.404(6)	C4-C5	1.420(6)
C5-C6	1.413(5)	C6-C7	1.398(6)
C7-C8	1.407(6)	C9-C13	1.426(5)
C9-C10	1.431(5)	C10-C11	1.432(6)
C11-C12	1.416(5)	C12-C13	1.435(5)
C15-C16	1.392(5)	C15-C27	1.465(5)
C16-C17	1.377(5)	C17-C28	1.492(5)
C18-C22	1.415(6)	C18-C19	1.409(6)
C19-C20	1.419(6)	C20-C21	1.405(6)
C21-C22	1.415(6)	C23-C27	1.422(5)
C23-C24	1.398(5)	C24-C25	1.411(5)
C25-C26	1.423(5)	C26-C27	1.427(5)
C29-C30	1.405(5)	C29-C41	1.457(5)
C30-C31	1.376(5)	C31-C42	1.486(5)
C32-C36	1.396(5)	C32-C33	1.408(6)
C33-C34	1.436(6)	C34-C35	1.396(6)
C35-C36	1.418(6)	C37-C38	1.418(5)
C37-C41	1.435(5)	C38-C39	1.406(5)
C39-C40	1.422(5)	C40-C41	1.440(5)

Angles (°)

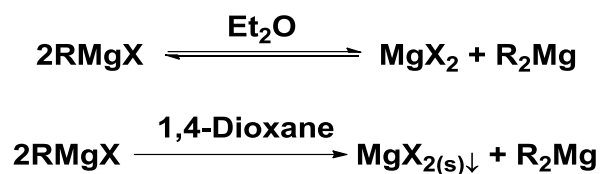
B1-Co1-Br1	168.6(1)	N3-Co1-N5	93.85(11)
N3-Co1-N1	98.43(11)	N3-Co1-Br1	111.48(8)
N1-Co1-N5	92.63(11)	N5-Co1-Br1	130.06(8)
N1-Co1-Br1	123.16(8)	C1-N1-N2	106.1(3)
C1-N1-Co1	143.5(3)	N2-N1-Co1	109.3(2)
C3-N2-N1	109.4(3)	C3-N2-B1	129.2(3)
N1-N2-B1	121.3(3)	C15-N3-N4	106.5(3)
C15-N3-Co1	140.4(2)	N4-N3-Co1	109.6(2)
C17-N4-N3	109.4(3)	C17-N4-B1	130.2(3)
N3-N4-B1	120.4(3)	C29-N5-N6	107.2(3)
C29-N5-Co1	143.5(2)	N6-N5-Co1	109.1(2)
C31-N6-N5	109.3(3)	C31-N6-B1	129.0(3)
N5-N6-B1	121.2(3)	N4-B1-N2	109.7(3)
N4-B1-N6	109.9(3)	N2-B1-N6	107.9(3)
N1-C1-C2	110.2(3)	N1-C1-C13	125.0(3)
C2-C1-C13	124.8(3)	C3-C2-C1	105.9(3)
N2-C3-C2	108.4(3)	N2-C3-C14	122.8(3)
C2-C3-C14	128.8(4)	C8-C4-C5	107.2(4)
C4-C5-C6	108.1(4)	C7-C6-C5	107.8(4)

C6-C7-C8	108.4(4)	C4-C8-C7	108.5(4)
C13-C9-C10	107.5(4)	C11-C10-C9	108.3(4)
C12-C11-C10	107.9(4)	C11-C12-C13	108.2(4)
C9-C13-C12	108.1(3)	C9-C13-C1	128.2(3)
C12-C13-C1	123.3(4)	N3-C15-C27	123.1(3)
N3-C15-C16	109.9(3)	C17-C16-C15	106.2(3)
C16-C15-C27	127.0(3)	N4-C17-C28	122.3(3)
N4-C17-C16	107.9(3)	C22-C18-C19	108.0(4)
C16-C17-C28	129.8(3)	C21-C20-C19	108.4(4)
C18-C19-C20	107.7(4)	C18-C22-C21	108.2(4)
C20-C21-C22	107.7(4)	C23-C24-C25	108.7(3)
C27-C23-C24	108.7(3)	C27-C26-C25	108.2(3)
C24-C25-C26	107.5(3)	C23-C27-C15	124.7(3)
C23-C27-C26	106.9(3)	N5-C29-C41	123.7(3)
C26-C27-C15	128.4(3)	C31-C30-C29	106.7(3)
N5-C29-C30	109.1(3)	N6-C31-C42	123.3(3)
C30-C29-C41	127.2(3)	C36-C32-C33	108.5(4)
N6-C31-C30	107.7(3)	C35-C34-C33	107.6(4)
C30-C31-C42	129.0(3)	C32-C36-C35	108.2(4)
C32-C33-C34	107.4(4)	C37-C38-C39	108.9(3)
C34-C35-C36	108.3(4)	C39-C40-C41	107.6(3)
C38-C37-C41	107.7(3)	C37-C41-C40	107.4(3)
C38-C39-C40	108.5(3)	C29-C41-C40	128.4(3)
C37-C41-C29	124.2(3)		

Synthesis and characterization of iron alkyls supported by $\text{Tp}^{\text{Fc,Me}}$ ligand.

There are many examples of organometallic complexes of the type $\text{Tp}^{\text{tBu,Me}}\text{MR}$ ($\text{M} = \text{Fe, Co}$) undergoing clean carbonylation in the presence of CO to afford their corresponding $\text{Tp}^{\text{tBu,Me}}\text{M}(\text{CO})$ or $\text{Tp}^{\text{tBu,Me}}\text{M}(\text{CO})_2$ complex.^{4,6,8,11} In an effort to produce a monovalent Fe synthon that could be used in oxygen activation we set about synthesizing alkyl complexes of iron supported by the $\text{Tp}^{\text{Fc,Me}}$ ligand. Using **3** as a starting material, I first attempted a stoichiometric reaction with Grignard reagents in ether, THF, or Toluene as solvent, but in all cases observed the formation of N-

confused magnesium alkyl complexes of the $\text{Tp}^{\text{Fc,Me}^*}$ ligand that proved impossible to separate from any paramagnetic compounds also produced. The structure for the magnesium methyl compound, $\text{Tp}^{\text{Fc,Me}^*}\text{MgMe}$ (**A1.1**), is shown in **Figure 1.9**, the crystals having been grown in minute quantity from a reaction mixture extracted with ether and layered with pentanes. Given that these complexes appeared to form with the elimination of Fe^{II} halide, I set about using magnesium di-alkyl complexes, prepared by the interaction of Grignard reagents with 1,4-dioxane.¹² This takes advantage of the Schlenk Equilibrium displayed by Grignard reagents in ethereal solvents,⁶ shown in **Scheme 1.5** below.



Scheme 1.5: Production of magnesium di-alkyl complexes by precipitation of MgX_2 .

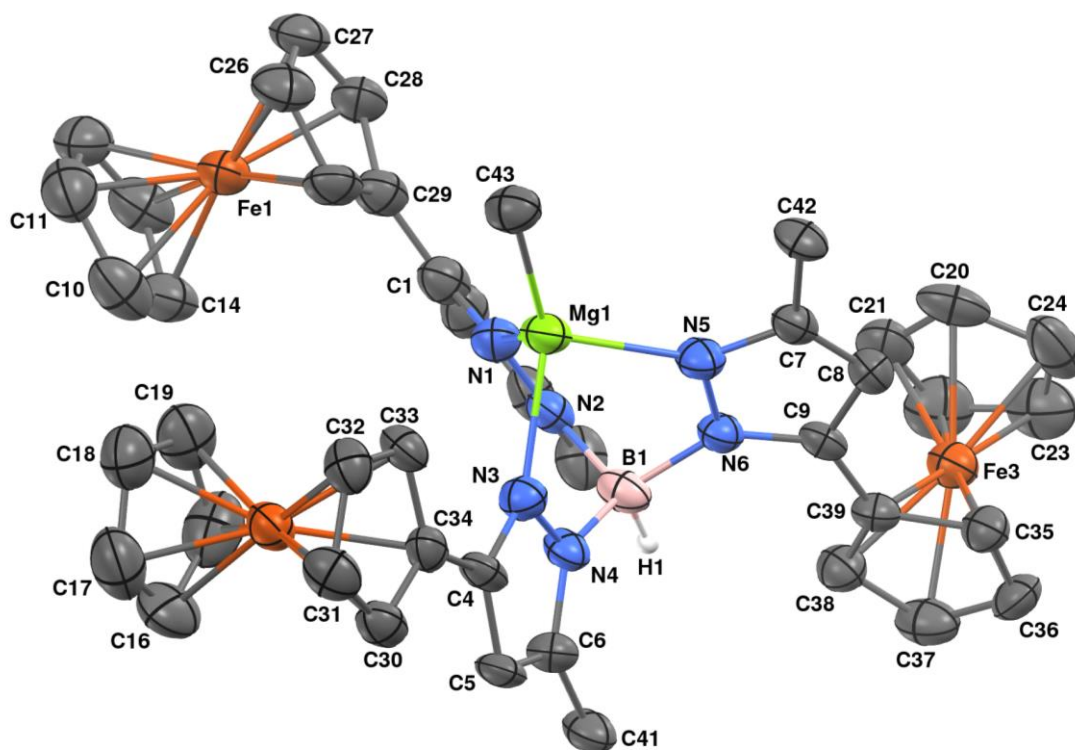


Figure 1.9: Molecular structure of $\text{Tp}^{\text{Fc,Me}^*}\text{MgMe}$ (A1.1) represented as 50% probability thermal ellipsoids. Hydrogen atoms (with the exception of the hydrogen attached to the boron, H1) have been omitted for clarity.

Table 1.3: Selected interatomic distances (\AA) and angles ($^\circ$) for $\text{Tp}^{\text{Fc,Me}^*}\text{MgMe}$ (A1.1)

Distances (\AA)			
Mg1-N5	2.099(6)	Mg1-N1	2.127(6)
Mg1-C43	2.145(7)	Mg1-N3	2.152(6)
B1-N4	1.562(9)	B1-N2	1.564(10)
B1-N6	1.576(9)	N1-C1	1.351(9)
N1-N2	1.396(7)	N2-C3	1.349(8)
N3-C4	1.356(8)	N3-N4	1.393(7)
N4-C6	1.353(8)	N5-C7	1.355(8)
N5-N6	1.393(7)	N6-C9	1.349(8)
C1-C29	1.482(10)	C4-C34	1.460(9)

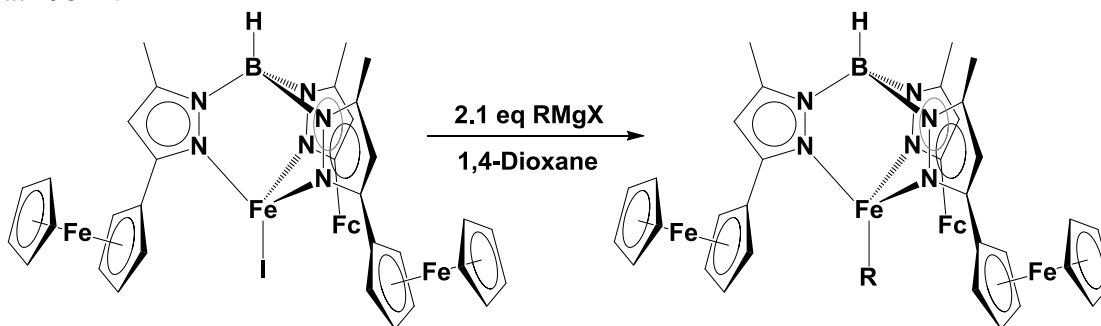
C4-C5	1.419(9)	C6-C41	1.515(9)
C5-C6	1.381(9)	C7-C42	1.533(8)
C7-C8	1.358(9)	C9-C39	1.479(9)
C8-C9	1.391(8)	C10-C14	1.427(11)
C10-C11	1.430(12)	C16-C17	1.405(13)
C17-C18	1.386(13)	C18-C19	1.386(12)
C20-C21	1.430(11)	C20-C24	1.453(12)
C23-C24	1.418(12)	C26-C27	1.434(11)
C27-C28	1.412(10)	C28-C29	1.426(10)
C30-C31	1.407(9)	C30-C34	1.432(9)
C31-C32	1.415(10)	C32-C33	1.419(9)
C33-C34	1.452(9)	C35-C36	1.419(9)
C35-C39	1.436(9)	C36-C37	1.423(10)
C37-C38	1.418(10)	C38-C39	1.439(9)

Angles (°)

N5-Mg1-N1	91.7(2)	N5-Mg1-C43	118.0(3)
N1-Mg1-C43	124.7(3)	N5-Mg1-N3	89.6(2)
N1-Mg1-N3	88.3(2)	C43-Mg1-N3	133.0(3)
N4-B1-N6	109.3(6)	N2-B1-N6	109.3(5)
C1-N1-N2	105.3(6)	C1-N1-Mg1	138.6(5)
N2-N1-Mg1	113.9(4)	C3-N2-N1	110.6(6)
C4-N3-N4	106.9(5)	N1-N2-B1	119.9(5)
N4-N3-Mg1	112.0(4)	C4-N3-Mg1	141.1(5)
C6-N4-B1	128.2(6)	C6-N4-N3	109.3(5)
C7-N5-N6	104.9(5)	N3-N4-B1	122.5(5)
N6-N5-Mg1	117.9(4)	C7-N5-Mg1	137.1(4)
C9-N6-B1	133.2(5)	C9-N6-N5	110.2(5)
N1-C1-C29	119.6(7)	N5-N6-B1	116.5(5)
N3-C4-C34	123.6(6)	N3-C4-C5	109.0(6)
C6-C5-C4	105.9(6)	C5-C4-C34	127.3(6)
N4-C6-C41	123.2(6)	N4-C6-C5	108.9(6)
C8-C7-N5	111.1(6)	C5-C6-C41	127.9(6)
N5-C7-C42	118.7(6)	C8-C7-C42	130.1(6)
N6-C9-C8	107.0(6)	C7-C8-C9	106.8(6)
C8-C9-C39	126.0(6)	N6-C9-C39	127.0(5)
C18-C17-Fe2	71.2(6)	C11-C10-C14	106.9(8)
C18-C17-C16	108.6(9)	C28-C29-C1	126.0(7)
C28-C27-C26	108.3(7)	C31-C30-C34	109.4(6)
C31-C32-C33	109.4(6)	C30-C34-C33	106.5(6)

C33-C34-C4	128.2(6)	C30-C34-C4	125.3(6)
C36-C35-C39	108.8(6)	C38-C37-C36	108.6(6)
C35-C39-C38	106.6(6)	C35-C39-C9	120.4(6)
C38-C39-C9	132.8(6)		

Taking advantage of this difference in solubility we were able to synthesize two new iron alkyl complexes, namely $\text{Tp}^{\text{Fc,Me}}\text{FeBn}$ (**5**) and $\text{Tp}^{\text{Fc,Me}}\text{FeEt}$ (**6**), by slow addition of 2.1 equiv. of the respective alkyl Grignard reagent into a solution of **3** in 1,4-dioxane, as shown in **Scheme 1.6**. Upon addition of a 2 M BnMgCl solution in THF to a stirring mixture of **3** in 1,4-dioxane over the course of several minutes a color change was observed, from light orange to dark orange. The reaction mixture was allowed to stir for an additional 3 hours, then filtered through celite and solvent removed in vacuo. The resulting orange residue was dissolved in toluene and again filtered to further remove any remaining magnesium containing compounds, and the solvent removed in vacuo. The remaining solid was then recrystallized in a mixture of THF and pentanes to afford **5** as orange rods in yields averaging 68%. Crystals more suitable to X-ray diffraction were grown from a mixture of toluene and pentanes, producing crystals containing 1 molecule of toluene per asymmetric unit, see **Figure 1.10**. The complex displayed a curiously low effective magnetic moment, of $3.9(1) \mu_{\text{B}}$ at 295 K.



Scheme 1.6: Synthesis of $\text{Tp}^{\text{Fc,Me}}\text{FeR}$, where R = Bn (**5**), Et (**6**).

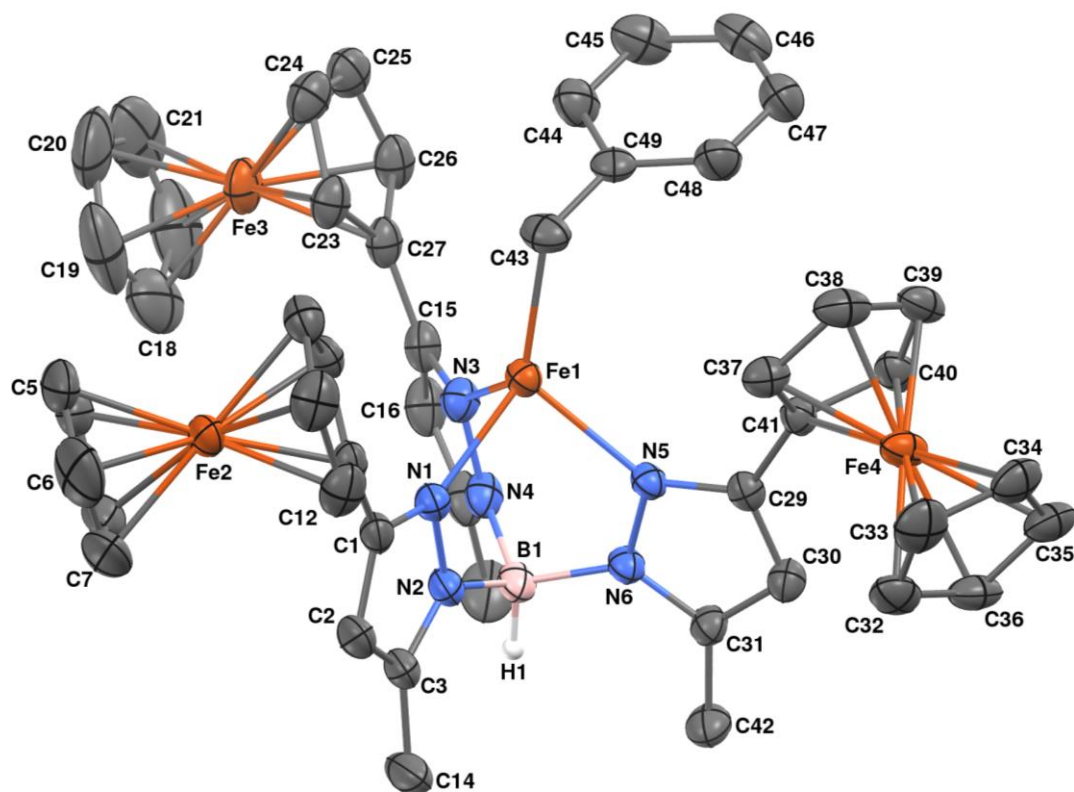


Figure 1.10: Molecular structure of $\text{Tp}^{\text{Fc,Me}}\text{FeBn}$ (**5**) represented as 50% probability thermal ellipsoids. Hydrogen atoms (with the exception of the hydrogen attached to the boron, H1), and 1 molecule of toluene, have been omitted for clarity.

Table 1.4: Selected interatomic distances (Å) and angles (°) for $\text{Tp}^{\text{Fc,Me}}\text{FeBn}$ (**5**)

Distances (Å)			
Fe1-C42	2.037(4)	Fe1-N1	2.112(3)
Fe1-N2	2.112(3)	Fe1-N3	2.138(3)
B1-N6	1.534(5)	B1-N4	1.545(5)
B1-N5	1.553(5)	B1-H1	1.10(4)
N1-C16	1.334(5)	N1-N4	1.375(4)
N2-C27	1.336(5)	N2-N5	1.380(4)
N3-C39	1.341(4)	N3-N6	1.366(4)
N4-C18	1.333(5)	N5-C29	1.329(5)

N6-C41	1.341(5)	C1-C6	1.395(6)
C1-C2	1.395(6)	C1-C42	1.489(6)
C2-C3	1.374(8)	C7-C10	1.523(6)
C3-C4	1.391(9)	C8-C12	1.521(6)
C4-C5	1.345(8)	C9-C14	1.509(6)
C5-C6	1.387(7)	C10-C15	1.377(6)
C10-C11	1.389(6)	C11-C12	1.389(5)
C13-C14	1.403(5)	C12-C13	1.405(5)
C14-C15	1.393(5)	C13-C16	1.493(5)
C16-C17	1.391(5)	C17-C18	1.382(6)
C19-C20	1.519(6)	C20-C21	1.400(6)
C20-C43	1.371(6)	C22-C25	1.515(6)
C21-C22	1.384(6)	C23-C27	1.484(5)
C22-C23	1.412(6)	C24-C26	1.504(6)
C23-C24	1.397(5)	C28-C29	1.377(6)
C24-C43	1.404(6)	C33-C34	1.381(6)
C27-C28	1.383(6)	C36-C37	1.403(5)
C30-C33	1.503(6)	C37-C38	1.406(6)
C31-C35	1.519(6)	C39-C40	1.396(5)
C32-C37	1.522(6)	C35-C36	1.400(5)
C33-C38	1.377(6)	C36-C39	1.475(5)
C34-C35	1.407(5)	C40-C41	1.363(6)

Angles (°)

C43-Fe1-N1	131.61(16)	C42-Fe1-N2	130.78(15)
B1-Fe1-C43	170.09(9)	C42-Fe1-N3	112.41(15)
N1-Fe1-N2	90.37(12)	N2-Fe1-N3	88.54(11)
N1-Fe1-N3	89.26(11)	N6-B1-N5	108.9(3)
N6-B1-N4	109.4(3)	N6-B1-H1	118.(2)
N4-B1-N5	109.6(3)	N5-B1-H1	105.(2)
N4-B1-H1	106.(2)	C16-N1-Fe1	139.1(2)
C16-N1-N4	106.6(3)	C27-N2-N5	106.7(3)
N4-N1-Fe1	114.2(2)	N5-N2-Fe1	114.0(2)
C27-N2-Fe1	139.2(3)	C39-N3-Fe1	137.9(2)
C39-N3-N6	107.0(3)	C18-N4-N1	109.5(3)
N6-N3-Fe1	115.1(2)	N1-N4-B1	121.4(3)
C18-N4-B1	129.0(3)	C29-N5-B1	129.3(3)
C29-N5-N2	109.3(3)	C41-N6-N3	109.5(3)
N2-N5-B1	121.2(3)	N3-N6-B1	120.1(3)
C41-N6-B1	130.3(3)	C6-C1-C42	122.5(4)

C6-C1-C2	115.6(4)	C3-C2-C1	121.5(5)
C2-C1-C42	121.9(4)	C5-C4-C3	118.5(5)
C2-C3-C4	121.2(5)	C5-C6-C1	122.5(4)
C4-C5-C6	120.7(5)	C15-C10-C7	120.1(4)
C15-C10-C11	118.8(4)	C12-C11-C10	121.7(4)
C11-C10-C7	121.0(4)	C11-C12-C8	120.3(3)
C11-C12-C13	118.7(4)	C14-C13-C12	120.2(3)
C13-C12-C8	121.0(3)	C12-C13-C16	119.0(3)
C14-C13-C16	120.7(3)	C15-C14-C9	120.0(4)
C15-C14-C13	119.0(4)	C10-C15-C14	121.5(4)
C13-C14-C9	121.0(4)	N1-C16-C13	122.5(3)
N1-C16-C17	110.1(3)	C18-C17-C16	105.1(4)
C17-C16-C13	127.4(3)	C43-C20-C21	117.5(4)
N4-C18-C17	108.6(3)	C21-C20-C19	121.2(4)
C43-C20-C19	121.3(4)	C21-C22-C23	119.8(4)
C22-C21-C20	121.8(4)	C23-C22-C25	120.3(4)
C21-C22-C25	119.9(4)	C24-C23-C27	120.8(4)
C24-C23-C22	119.1(4)	C23-C24-C43	119.0(4)
C22-C23-C27	120.1(3)	C43-C24-C26	119.1(4)
C23-C24-C26	121.9(4)	N2-C27-C23	122.2(3)
N2-C27-C28	109.5(4)	C29-C28-C27	106.0(4)
C28-C27-C23	128.3(4)	N5-C29-C28	108.4(4)

Using a procedure similar to that for synthesizing **5**, I also prepared $\text{Tp}^{\text{Fc,Me}}\text{FeEt}$ (**6**). A solution of **3** in 1,4-dioxane was prepared, to which 2.1 equiv. of a 2 M solution of EtMgCl in THF was added dropwise in two separate portions 30 or more minutes apart. Adding the Grignard solution all in one portion led to the formation of Tp ligated magnesium salts that proved difficult to separate; by slowing down the addition this problem is mitigated. The same workup as that used to prepare pure samples of **5** was applied, however **6** was found to be analytically pure after the extraction with toluene. Crystals for X-ray structure determination can be prepared by dissolving **6** in THF and then layering the solution with pentanes, producing bright orange blocks without incorporation of solvent molecules in the lattice. The complex

is κ_3 with respect to the Tp ligand, and does not readily isomerize to the borotropically rearranged isomer even upon heating, see **Figure 1.11**. Similar to **5**, the effective magnetic moment of **6** is $4.0(1) \mu_B$ when measured at room temperature, lower than expected for a high spin d^6 complex.

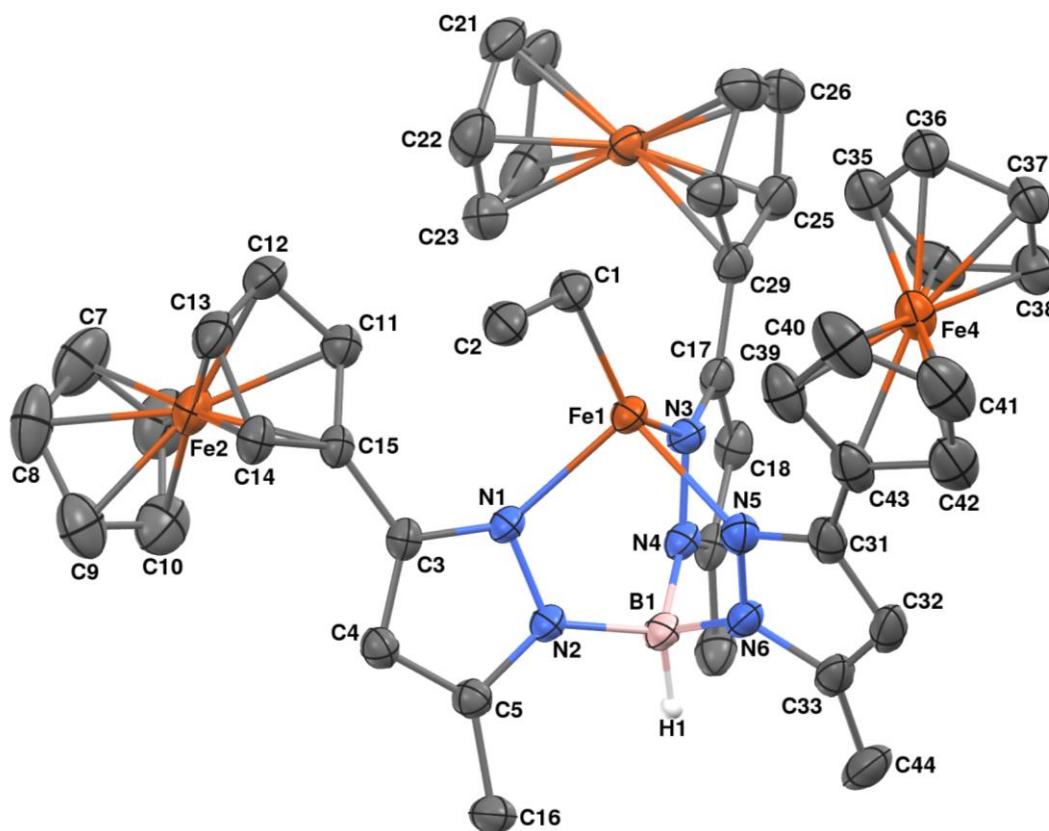


Figure 1.11: Molecular structure of $\text{Tp}^{\text{Fc,Me}}\text{FeEt}$ (**6**) represented as 50% probability thermal ellipsoids. Hydrogen atoms (with the exception of the hydrogen attached to the boron, H1) have been omitted for clarity.

Table 1.5: Selected interatomic distances (Å) and angles (°) for $\text{Tp}^{\text{Fc,Me}}\text{FeEt}$ (6)

Distances (Å)			
Fe1-C1	2.056(2)	Fe1-N3	2.1205(18)
Fe1-N1	2.1256(18)	Fe1-N5	2.1391(18)
N1-C3	1.343(3)	N1-N2	1.373(2)
N2-C5	1.354(3)	N2-B1	1.547(3)
N3-C17	1.342(3)	N3-N4	1.384(2)
N5-C31	1.344(3)	N4-B1	1.549(3)
N6-C33	1.351(3)	N5-N6	1.384(3)
B1-H1	1.08(2)	N6-B1	1.545(3)
C3-C15	1.467(3)	C1-C2	1.536(3)
C11-C15	1.422(3)	C3-C4	1.398(3)
C17-C18	1.403(3)	C4-C5	1.379(3)
C21-C22	1.403(4)	C5-C16	1.496(3)
C22-C23	1.403(4)	C7-C8	1.398(5)
C25-C29	1.433(3)	C8-C9	1.424(5)
C26-C27	1.416(4)	C9-C10	1.417(4)
C31-C43	1.461(4)	C11-C12	1.424(3)
C39-C43	1.424(4)	C12-C13	1.413(4)
C35-C36	1.417(3)	C13-C14	1.423(3)
C36-C37	1.419(3)	C14-C15	1.430(3)
C37-C38	1.414(4)	C17-C29	1.465(3)
C32-C33	1.376(4)	C25-C26	1.419(4)
C33-C44	1.493(4)	C31-C32	1.401(3)
C39-C40	1.426(4)	C40-C41	1.413(5)
C41-C42	1.408(4)	C42-C43	1.436(3)
Angles (°)			
B1-Fe1-C1	164.25(8)	C1-Fe1-N1	111.63(8)
C1-Fe1-N3	136.81(8)	C1-Fe1-N5	126.46(8)
N3-Fe1-N1	86.37(7)	N1-Fe1-N5	95.10(7)
N3-Fe1-N5	88.18(7)	C3-N1-N2	106.64(17)
Fe1-C1-C2	115.5(2)	C5-N2-B1	131.01(17)
C5-N2-N1	109.72(17)	C17-N3-N4	106.51(17)
N1-N2-B1	119.07(17)	C31-N5-N6	106.42(18)
N3-N4-B1	120.19(17)	C33-N6-B1	128.8(2)
C33-N6-N5	109.76(19)	N6-B1-N2	110.24(18)

N5-N6-B1	120.99(17)	N2-B1-N4	110.25(17)
N6-B1-N4	107.41(18)	N2-B1-H1	109.3(13)
N6-B1-H1	110.0(13)	N1-C3-C4	109.82(18)
N4-B1-H1	109.6(13)	C4-C3-C15	130.6(2)
N1-C3-C15	119.58(19)	N2-C5-C4	107.97(18)
C5-C4-C3	105.81(19)	C11-C15-C3	125.77(19)
N2-C5-C16	122.78(19)	N3-C17-C29	121.81(19)
C4-C5-C16	129.2(2)	C20-C21-C22	108.8(2)
C7-C8-C9	107.7(3)	C23-C22-C21	107.8(3)
C10-C9-C8	107.8(3)	C26-C25-C29	107.8(2)
C15-C11-C12	108.3(2)	C27-C26-C25	108.5(2)
C13-C12-C11	108.1(2)	C25-C29-C17	125.2(2)
C12-C13-C14	108.2(2)	N5-C31-C32	109.7(2)
C13-C14-C15	108.0(2)	C32-C31-C43	125.9(2)
C11-C15-C14	107.47(19)	N6-C33-C32	108.0(2)
C14-C15-C3	126.8(2)	C32-C33-C44	129.2(2)
N3-C17-C18	109.63(19)	C39-C43-C31	128.7(2)
C18-C17-C29	128.5(2)	C41-C40-C39	107.8(3)
N5-C31-C43	124.5(2)	C42-C41-C40	108.9(2)
C33-C32-C31	106.1(2)	C41-C42-C43	107.9(3)
N6-C33-C44	122.7(2)	C39-C43-C42	107.3(2)
C35-C36-C37	107.5(2)	C42-C43-C31	123.9(2)
C38-C37-C36	108.3(2)	C43-C39-C40	108.1(2)

5 and **6** display NMR resonances between -29 and 49 ppm, indicative of paramagnetic metal centers, with 5 peaks corresponding to the hydrogens on the $\text{Tp}^{\text{Fc,Me}}$ ligand. Both compounds display several peaks in the same range that correspond to the alkyl ligand, with some hydrogens not represented in the spectra, likely as a result of the peaks being too broad to be distinguished from noise. The Fe-N and Fe-C bond lengths for both **5** and **6** are nearly identical. As is the case with the halide complexes **1**, **2**, and **3**, the Fe-N bond lengths for compounds **5** and **6** are shorter than analogous compounds supported by the $\text{Tp}^{\text{tBu,Me}}$ ligand. The α -angle, defined as the angle between the boron, Tp ligated metal center, and the non-Tp

ligand,¹² of complexes **5** and **6** vary greatly from those of their $\text{Tp}^{\text{tBu,Me}}$ analogues, both of these comparisons are shown in **Table 1.6**. Mass spectra of both **5** and **6**, collected using LIFDI-MS, displayed the molecular ion peak as only a very minor contribution to the overall data collected, shown in **Figure 1.12**. This is atypical among all other $\text{Tp}^{\text{Fc,Me}}$ supported complexes examined by this method, and is indicative of the Fe-C bonds being relatively weak, thus resulting in homolytic bond cleavage under mildly ionizing conditions. **6** is stable in solution and as a solid, but both **5** and **6** decompose rapidly upon exposure to oxygen and moisture. **5** decomposes slowly over time as a solid, even when stored at -35 °C in a glove box environment, via an as yet unknown pathway.

Table 1.6: Comparison of Fe-N and Fe-C bonds and angles of compounds (5), (6), and analogous $\text{Tp}^{\text{tBu,Me}}$ Fe alkyl complexes

<i>Compound</i>	<i>Fe-N_(1,3,5) Å</i>	<i>Fe-C Å</i>	<i>α (°)</i>
$\text{Tp}^{\text{Fc,Me}}\text{FeBn}$ (5)	2.129(2), 2.103(2), 2.056(2)	2.056(2)	170.09(9)
$\text{Tp}^{\text{Fc,Me}}\text{FeEt}$ (6)	2.126(2), 2.120(2), 2.139(2)	2.056(2)	164.25(8)
$\text{Tp}^{\text{tBu,Me}}\text{FeEt}^6$	2.140(2), 2.142(2), 2.154(2)	2.069(3)	177.8(1)
$\text{Tp}^{\text{tBu,Me}}\text{FePh}^6$	2.099(3), 2.130(3), 2.141(2)	2.061(3)	163.3(1)

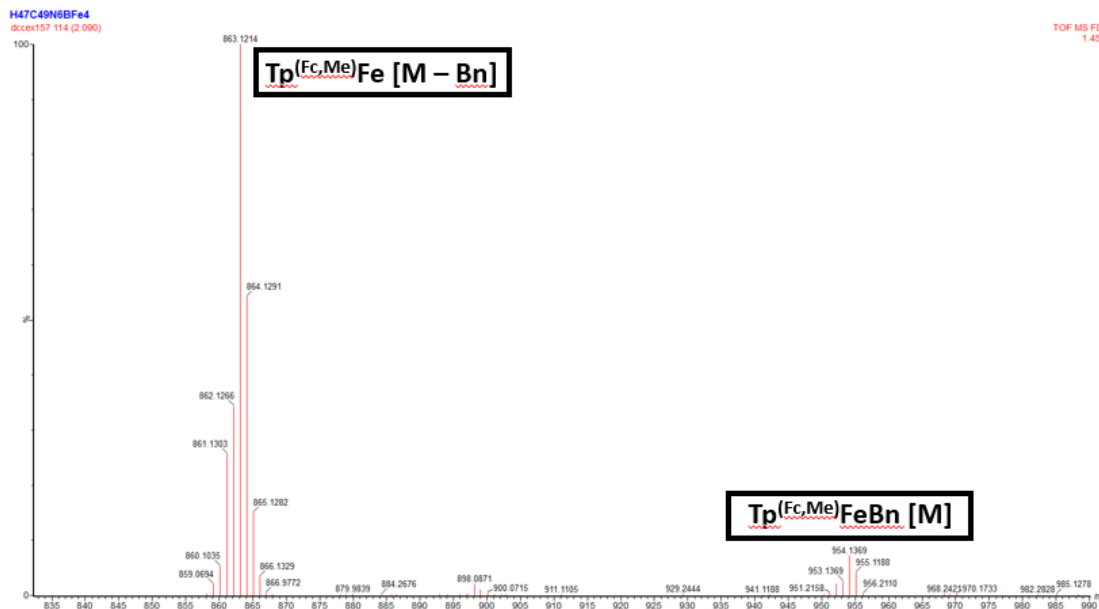


Figure 1.12: LIFDI-MS of complex (5), displaying peaks for its molecular ion $[M^+ : 954.1369]$ and $[M^+ - C_7H_7 : 863.1214]$

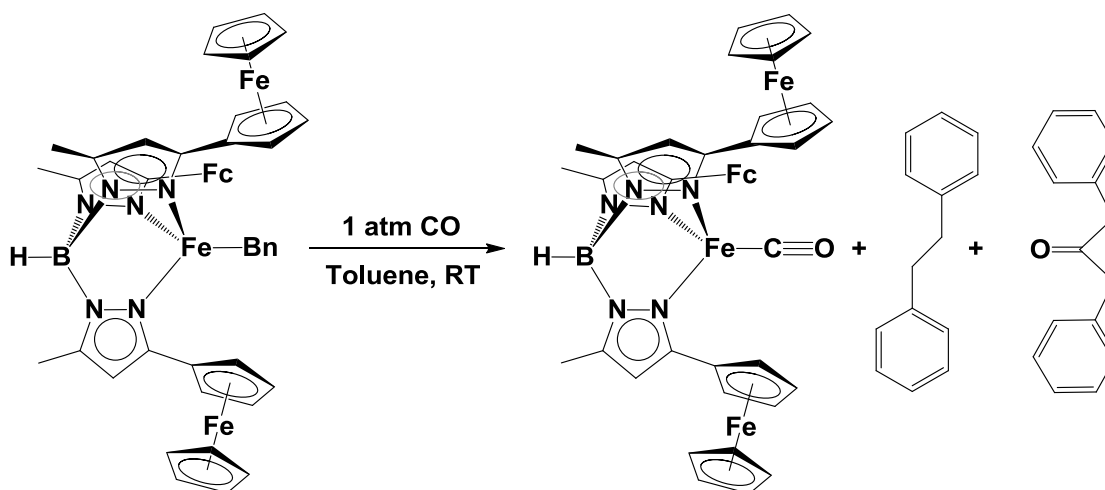
Synthesis and characterization of formally univalent $Tp^{Fc,Me}Fe(CO)$.

Having an effective means of producing alkyl complexes enabled the synthesis of a novel carbonyl, $Tp^{Fc,Me}Fe(CO)$ (**7**). This was accomplished through what was presumed to be an associative reaction of carbon monoxide gas with **5**, resulting in homolytic bond cleavage of the benzyl substituent to produce **7** along with 1,2-diphenylethane and 1,3-diphenyl acetone, as shown in **Scheme 1.7**. Both byproducts are observed when the reaction is monitored by NMR in deuterated THF, the latter of which indicating insertion of CO into the Fe-Bn bond prior to dissociation. The CO stretching frequency of **7** was found to be 1890 cm^{-1} , which overlaps well with that reported for its $Tp^{tBu,Me}Fe(CO)$ ⁶ and $PhTp^{tBu}Fe(CO)$ ¹⁴ analogues, having CO stretching frequencies at 1889 and 1863 cm^{-1} respectively. These stretching frequencies and their corresponding C-O bond lengths are listed in **Table 1.7** below, and illustrate no

obvious trend on which to compare bond length and stretching frequency. The best method for purifying compound **7** is by crystallization, which is achieved in a facile manner from mixtures of benzene, toluene, or THF with pentanes. However, once crystallized, **7** is extremely difficult to re-dissolve, which makes further use of this compound as a synthon problematic. This issue, together with the number of synthetic steps required for its production, make **7** undesirable as a synthon in reactions to make novel iron oxo or imido compounds.

Table 1.7: Comparison of $\text{Tp}^{\text{R,R}}\text{Fe}(\text{CO})$ bonds and angles of compounds

Compound	IR_{CO} (cm^{-1})	C-O (\AA)	Fe-C (\AA)	α ($^\circ$)
$\text{Tp}^{\text{Fc,Me}}\text{Fe}(\text{CO})$ (7)	1890	1.148(4)	1.783(3)	170.5(1)
$\text{Tp}^{\text{tBu,Me}}\text{Fe}(\text{CO})^6$	1889	1.113(2)	1.799(2)	180.00(6)
$\text{PhTp}^{\text{tBu}}\text{Fe}(\text{CO})^{12}$	1863	1.158(3)	1.790(4)	177.2(1)



Scheme 1.7: Synthesis of $\text{Tp}^{\text{Fc,Me}}\text{Fe}(\text{CO})$ (7**).**

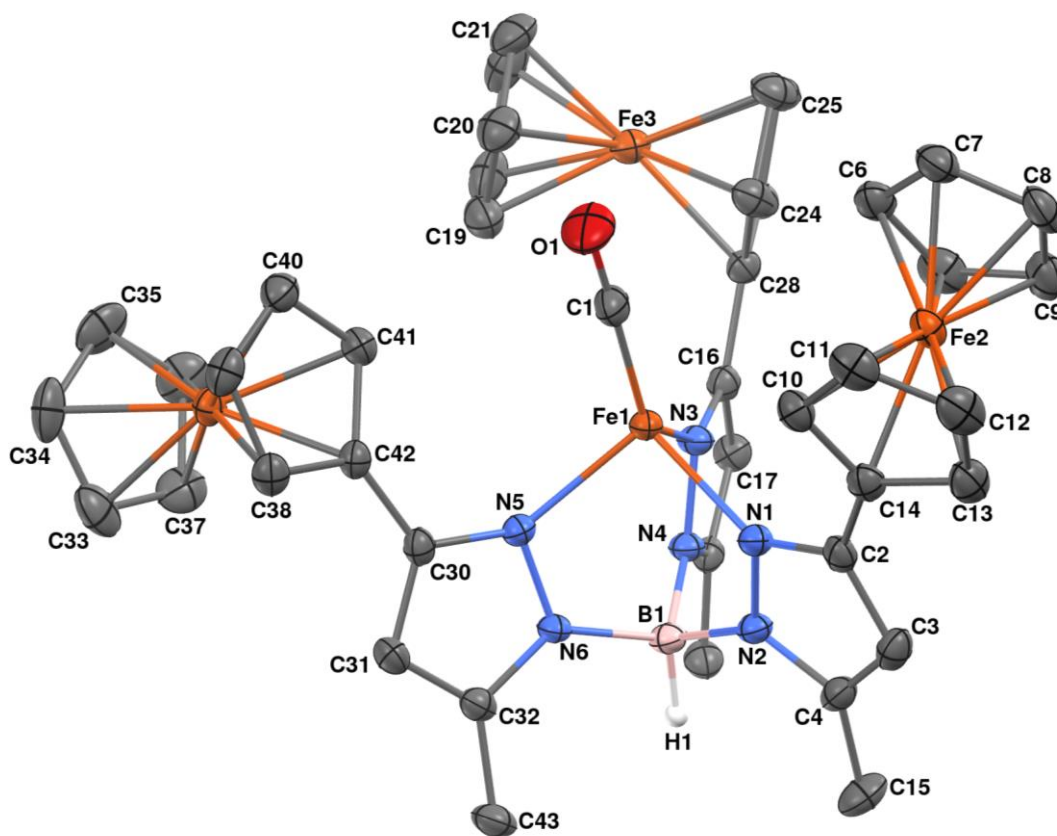


Figure 1.13: Molecular structure of $\text{Tp}^{\text{Fc,Me}}\text{Fe}(\text{CO})$ (7) represented as 50% probability thermal ellipsoids. Hydrogen atoms (with the exception of the hydrogen attached to the boron, H1) have been omitted for clarity.

Table 1.8: Selected interatomic distances (\AA) and angles ($^\circ$) for $\text{Tp}^{\text{Fc,Me}}\text{Fe}(\text{CO})$ (7)

Distances (\AA)			
Fe1-C1	1.782(2)	Fe1-N5	2.0521(18)
Fe1-N1	2.0692(18)	Fe1-N3	2.0750(18)
N1-C2	1.340(3)	N1-N2	1.387(2)
N2-C4	1.348(3)	N2-B1	1.553(3)
N3-C16	1.341(3)	N3-N4	1.381(2)

N5-C30	1.341(3)	N4-B1	1.555(3)
N6-C32	1.349(3)	N5-N6	1.382(2)
C1-O1	1.149(3)	N6-B1	1.546(3)
C2-C14	1.463(3)	C2-C3	1.395(3)
C4-C15	1.491(3)	C3-C4	1.378(3)
C7-C8	1.416(4)	C6-C7	1.421(3)
C10-C11	1.425(3)	C8-C9	1.417(4)
C11-C12	1.420(4)	C10-C14	1.429(3)
C13-C14	1.436(3)	C12-C13	1.418(4)
C16-C28	1.464(3)	C16-C17	1.402(3)
C24-C25	1.420(3)	C19-C20	1.412(3)
C25-C26	1.419(3)	C20-C21	1.413(4)
C27-C28	1.435(3)	C24-C28	1.429(3)
C30-C42	1.461(3)	C26-C27	1.420(3)
C32-C43	1.492(3)	C30-C31	1.399(3)
C33-C37	1.416(4)	C31-C32	1.370(3)
C35-C36	1.418(4)	C33-C34	1.414(4)
C38-C42	1.432(3)	C34-C35	1.409(4)
C40-C41	1.417(3)	C36-C37	1.409(4)
C41-C42	1.431(3)		

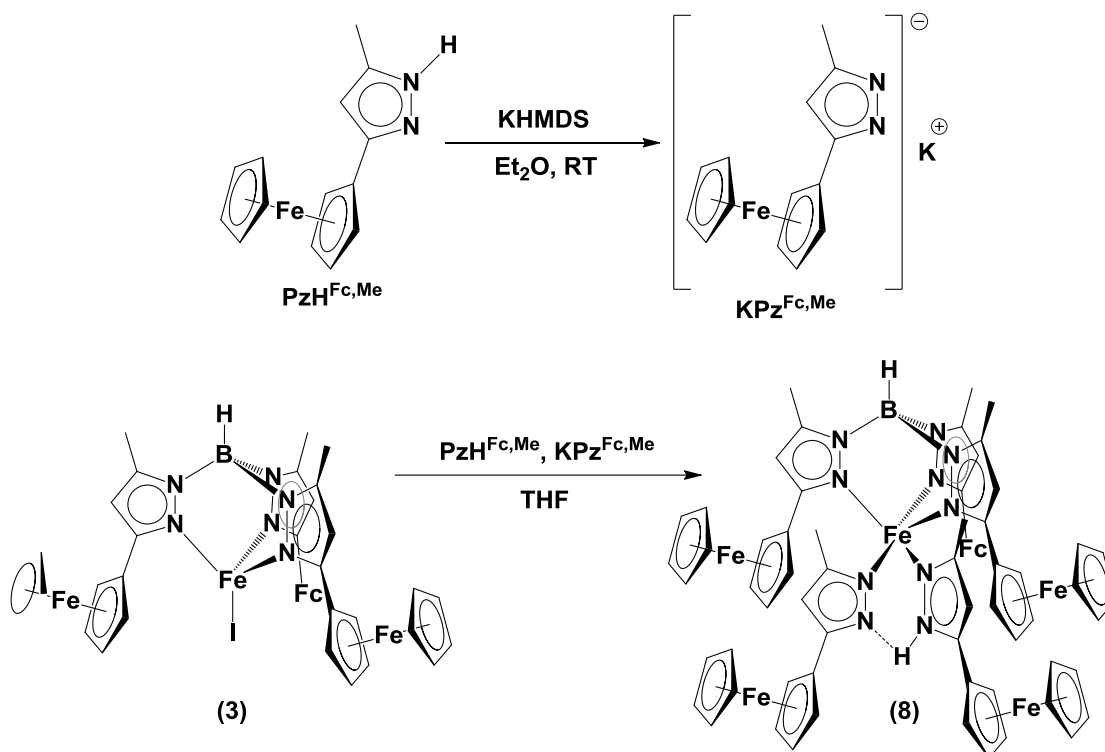
Angles (°)

C1-Fe1-N5	113.52(9)	B1-Fe1-C1	170.5(1)
N5-Fe1-N1	95.75(7)	C1-Fe1-N1	124.39(9)
N5-Fe1-N3	93.80(7)	C1-Fe1-N3	129.04(10)
C4-N2-N1	109.50(18)	N1-Fe1-N3	92.23(7)
N1-N2-B1	120.90(17)	C2-N1-N2	106.54(18)
C18-N4-N3	109.59(17)	C4-N2-B1	129.57(19)
N3-N4-B1	120.77(17)	C16-N3-N4	106.64(17)
C32-N6-N5	109.39(17)	C18-N4-B1	129.22(18)
N5-N6-B1	120.13(17)	C30-N5-N6	106.68(17)
N6-B1-N4	110.23(18)	C32-N6-B1	130.42(19)
N1-C2-C14	124.4(2)	N6-B1-N2	109.46(17)
C4-C3-C2	106.3(2)	N2-B1-N4	108.74(18)
N2-C4-C15	123.1(2)	N1-C2-C3	109.7(2)
C9-C5-C6	108.2(2)	C3-C2-C14	125.8(2)
C8-C7-C6	108.1(2)	N2-C4-C3	108.0(2)
C5-C9-C8	108.0(2)	C3-C4-C15	129.0(2)
C12-C11-C10	107.7(2)	C7-C6-C5	107.6(2)
C12-C13-C14	107.8(2)	C7-C8-C9	108.1(2)

C10-C14-C2	128.4(2)	C11-C10-C14	108.3(2)
N3-C16-C28	122.74(19)	C13-C12-C11	108.8(2)
N4-C18-C29	122.9(2)	C10-C14-C13	107.5(2)
N3-C16-C17	109.70(19)	C13-C14-C2	123.9(2)
C17-C16-C28	127.5(2)	C25-C24-C28	108.2(2)
N4-C18-C17	107.99(18)	C25-C26-C27	108.1(2)
C17-C18-C29	129.1(2)	C24-C28-C27	107.28(19)
C19-C20-C21	107.9(2)	C27-C28-C16	124.3(2)
C31-C30-C42	128.3(2)	N5-C30-C31	109.4(2)
N6-C32-C31	108.2(2)	C35-C34-C33	108.1(3)
C31-C32-C43	129.2(2)	C37-C36-C35	107.9(2)
C26-C25-C24	108.3(2)	C39-C38-C42	108.0(2)
C26-C27-C28	108.1(2)	C41-C40-C39	108.0(2)
C24-C28-C16	128.42(19)	C41-C42-C38	107.3(2)
N5-C30-C42	122.3(2)	C38-C42-C30	124.7(2)
C32-C31-C30	106.3(2)	C36-C37-C33	108.1(2)
N6-C32-C43	122.6(2)	C38-C39-C40	108.3(2)
C34-C33-C37	107.9(3)	C40-C41-C42	108.3(2)
C34-C35-C36	108.0(3)	C41-C42-C30	128.0(2)

Synthesis of univalent dinitrogen complexes. Given the difficulties faced in working with the carbonyl complex, the focus shifted to using di-nitrogen complexes as synthons. Our initial attempts to reduce **3** or **4** with potassium graphite, potassium metal, sodium metal, or magnesium metal all failed to produce the desired dinitrogen compounds. Instead these reactions produced a mixture of bis-ligand complexes, and a pyrazolyl pyrazolato complex, such as $\text{Tp}^{\text{Fc,Me}}\text{Fe}(\text{PzH}^{\text{Fc,Me}})(\text{Pz}^{\text{Fc,Me}})$ (**8**) when **3** was used as starting material. **8** can be produced through an alternate method shown in **Scheme 1.8**. This compound being present in the product mixture is indicative of ligand decomposition by cleavage of the nitrogen-boron bonds. This issue was part of the original impetus for the synthesis of iodide **3**, in the hopes that a milder reductant could be used with an iodide as opposed to a chloride or bromide. During the course of acquiring cyclic voltammetry data for compounds **1** through **4** it was discovered that

the ligand decomposed at voltages above -2.15 V vs SHE, as demonstrated by an irreversible wave at that voltage. **2** and **3** display Fe^{II}/Fe^I reduction events at -2.06 and -1.99 V vs SHE respectively, while **1** only shows reduction events associated with ligand decomposition, see **Figure 1.14** below. These values for redox potentials correspond well with the BDE reported for Fe-X bonds, those being 400, 339.7, and 279.1 kJ/mol for Fe^{II}-Cl, Fe^{II}-Br, and Fe^{II}-I bonds respectively.¹⁵ Given the peak potential of these reduction events, and their proximity to reductions that corresponded to the decomposition of the ligand, it became clear that we needed a chemical reductant with a potential between ~-1.95 and -2.05 V vs SHE. The only readily accessible chemical reductants for our purposes were .5 to 1.5% w/w Na/Hg amalgams, having potentials near -1.96 V vs SHE at 298.15 K.¹⁶



Scheme 1.8: Synthesis of $\text{Tp}^{\text{Fc,Me}}\text{Fe}(\text{PzH}^{\text{Fc,Me}})(\text{Pz}^{\text{Fc,Me}})$ (8**)**

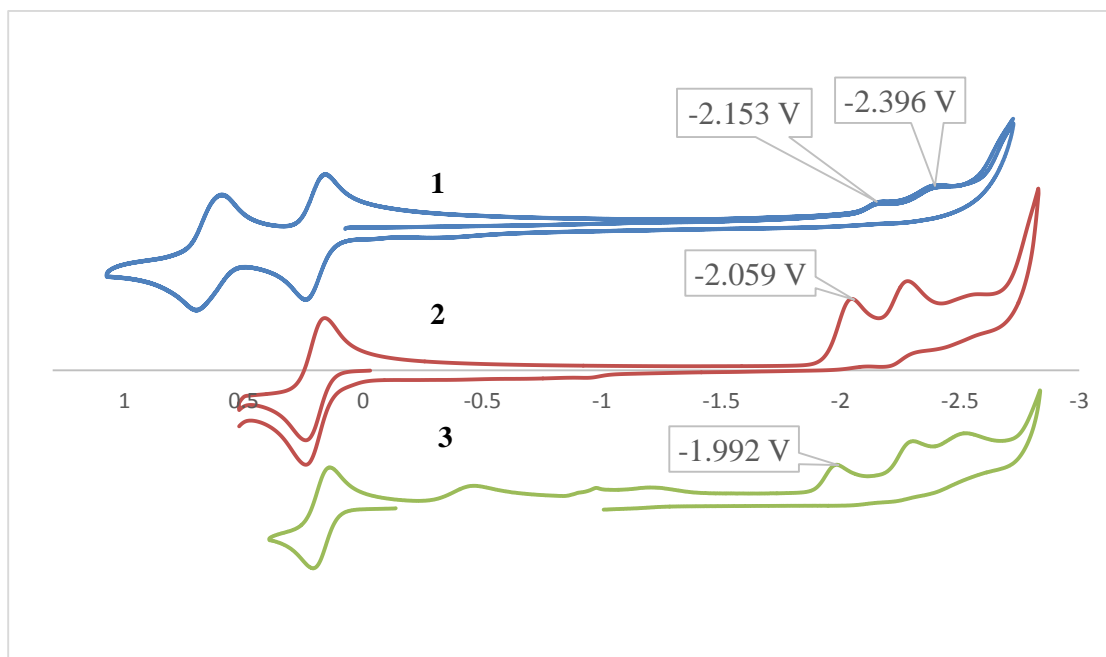


Figure 1.14: Cyclic voltammograms of 1 (blue, top), 2 (red, middle), and 3 (green, bottom), in 0.1 M solutions of $[\text{N}^{\text{t}}\text{Bu}_4]\text{ClO}_4$ and $(\text{Cp}^*)_2\text{Fe}$ (0.14 V) (used to reference voltages to SHE = 0 V) in THF, (working electrode = GC, reference electrode = Ag/Ag⁺, counter electrode = Pt)

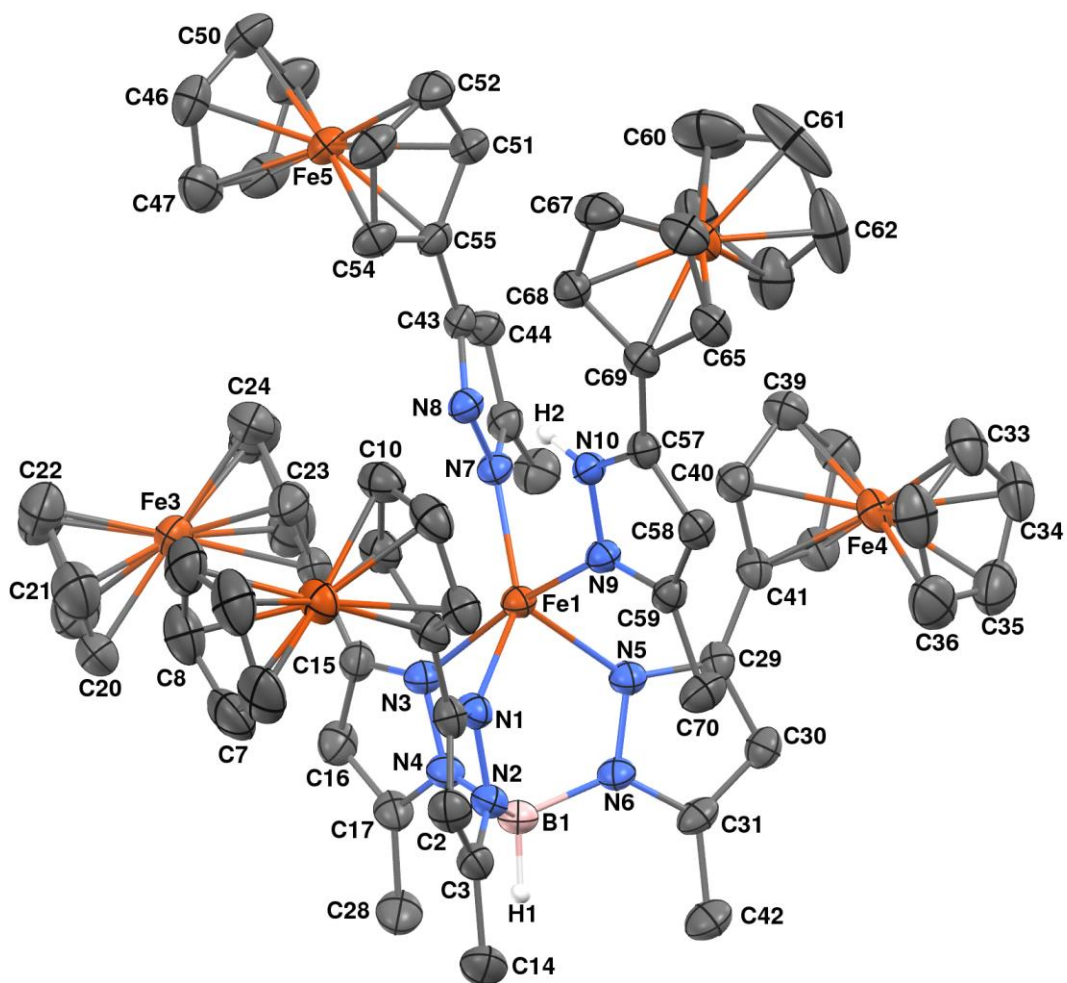


Figure 1.15: Molecular structure of $\text{Tp}^{\text{Fc,Me}}\text{Fe}(\text{PzH}^{\text{Fc,Me}})(\text{Pz}^{\text{Fc,Me}})$ (8) represented as 50% probability thermal ellipsoids. Hydrogen atoms (with the exception of the hydrogens attached to the boron, H1, and to N10, H2), and 1 molecule of Et_2O has been omitted for clarity.

Table 1.9: Selected interatomic distances (Å) and angles (°) for**Tp^{Fe,Me}Fe(PzH^{Fe,Me})(Pz^{Fe,Me}) (8)**

Distances (Å)			
Fe1-N7	2.039(2)	Fe1-N1	2.113(2)
Fe1-N5	2.113(2)	Fe1-N9	2.208(2)
Fe1-N3	2.271(2)	N2-C3	1.352(4)
N1-N2	1.378(3)	N3-C15	1.345(4)
N2-B1	1.546(4)	N4-C17	1.357(4)
N3-N4	1.381(3)	N5-C29	1.346(4)
N4-B1	1.541(4)	N6-C31	1.353(4)
N5-N6	1.380(3)	N7-C45	1.353(4)
N6-B1	1.562(4)	N8-C43	1.343(3)
N7-N8	1.380(3)	N9-N10	1.360(3)
N9-C59	1.343(3)	C2-C3	1.373(4)
N10-C57	1.345(4)	C4-C8	1.402(5)
C3-C14	1.499(4)	C5-C6	1.410(5)
C4-C5	1.417(5)	C7-C8	1.422(5)
C6-C7	1.405(5)	C9-C13	1.427(4)
C9-C10	1.422(4)	C11-C12	1.418(5)
C10-C11	1.411(5)	C15-C16	1.394(4)
C12-C13	1.428(4)	C16-C17	1.361(4)
C15-C27	1.467(4)	C18-C22	1.390(6)
C17-C28	1.500(4)	C19-C20	1.422(7)
C18-C19	1.417(5)	C21-C22	1.402(6)
C20-C21	1.409(6)	C23-C27	1.420(5)
C23-C24	1.405(6)	C25-C26	1.431(6)
C24-C25	1.386(7)	C29-C30	1.402(4)
C26-C27	1.426(5)	C30-C31	1.372(4)
C29-C41	1.463(4)	C33-C34	1.414(5)
C31-C42	1.495(4)	C35-C36	1.404(6)
C34-C35	1.400(5)	C39-C40	1.419(4)
C40-C41	1.425(4)	C43-C44	1.391(4)
C43-C55	1.472(4)	C44-C45	1.380(4)
C46-C47	1.424(5)	C46-C50	1.402(5)
C51-C55	1.419(4)	C51-C52	1.425(4)
C54-C55	1.429(4)	C57-C58	1.379(4)
C57-C69	1.459(4)	C58-C59	1.400(4)
C59-C70	1.494(4)	C61-C62	1.409(7)

C60-C61	1.420(7)	C65-C69	1.429(4)
C62-C63	1.394(6)	C67-C68	1.420(4)
C68-C69	1.424(4)	C1S-C2S	1.417(11)
C2S-O1S	1.300(9)	O1S-C3S	1.396(11)
C3S-C4S	1.280(10)		

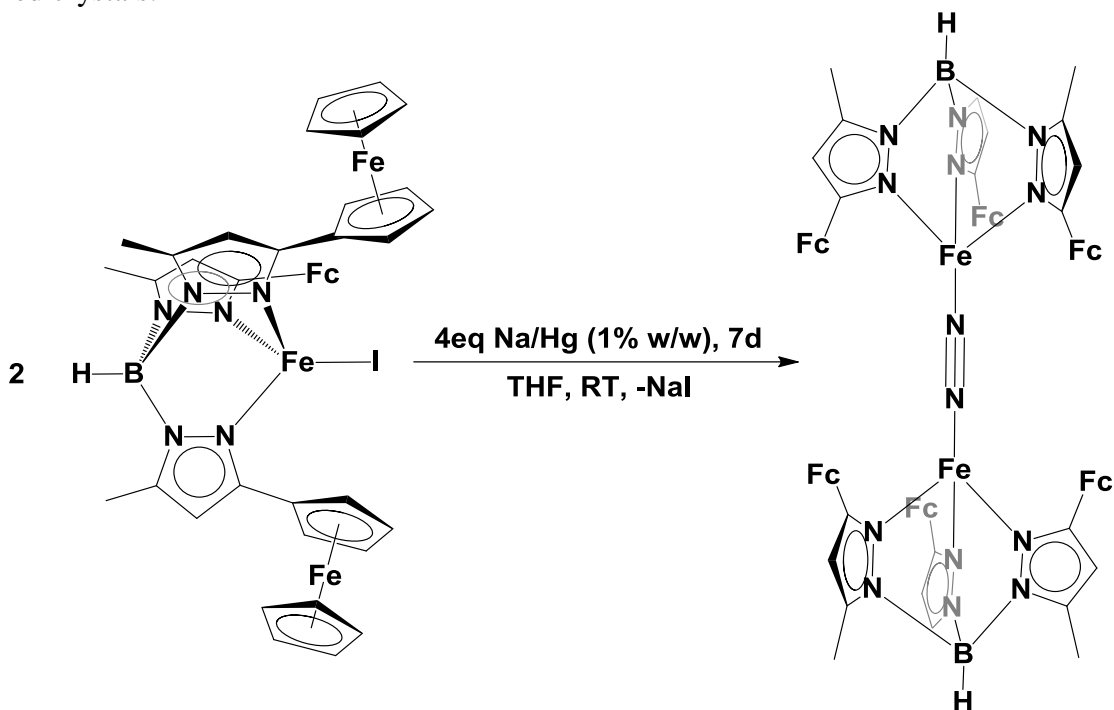
Angles (°)

N7-Fe1-N1	146.05(9)	N7-Fe1-N5	117.75(9)
N1-Fe1-N5	96.14(9)	N7-Fe1-N9	93.60(9)
N1-Fe1-N9	84.83(9)	N5-Fe1-N9	95.11(9)
N7-Fe1-N3	98.13(9)	N1-Fe1-N3	81.72(9)
N5-Fe1-N3	85.33(9)	N9-Fe1-N3	166.51(9)
C3-N2-N1	109.3(2)	C3-N2-B1	131.6(2)
N1-N2-B1	119.1(2)	C15-N3-N4	105.6(2)
C17-N4-N3	109.8(2)	C17-N4-B1	128.9(2)
N3-N4-B1	121.3(2)	C29-N5-N6	106.2(2)
C31-N6-N5	109.8(2)	C31-N6-B1	129.9(2)
N5-N6-B1	120.1(2)	C59-N9-N10	105.5(2)
C43-N8-N7	106.7(2)	N4-B1-N2	109.7(2)
C57-N10-N9	111.9(2)	N2-B1-N6	110.0(2)
N4-B1-N6	109.5(2)	N2-C3-C14	123.0(3)
N2-C3-C2	108.0(3)	C8-C4-C5	109.1(4)
C2-C3-C14	129.0(3)	C7-C6-C5	107.9(4)
C6-C5-C4	107.5(4)	C4-C8-C7	106.8(4)
C6-C7-C8	108.7(4)	C11-C10-C9	108.1(3)
C10-C9-C13	108.2(3)	C11-C12-C13	108.1(3)
C10-C11-C12	108.4(3)	C9-C13-C1	126.4(3)
C9-C13-C12	107.3(3)	N3-C15-C27	121.9(3)
C12-C13-C1	126.2(3)	C17-C16-C15	106.2(3)
N3-C15-C16	110.3(3)	N4-C17-C28	123.2(3)
C16-C15-C27	127.8(3)	C22-C18-C19	107.3(4)
N4-C17-C16	108.1(3)	C21-C20-C19	107.6(4)
C16-C17-C28	128.7(3)	C18-C22-C21	109.7(4)
C18-C19-C20	107.9(4)	C25-C24-C23	107.0(5)
C22-C21-C20	107.5(5)	C27-C26-C25	105.8(4)
C24-C23-C27	109.3(5)	C23-C27-C15	127.4(3)
C24-C25-C26	110.3(4)	N5-C29-C41	123.2(3)
C23-C27-C26	107.5(3)	C31-C30-C29	105.9(3)
C26-C27-C15	125.1(3)	N6-C31-C42	123.2(3)
N5-C29-C30	109.9(3)	C35-C34-C33	108.2(4)

C30-C29-C41	126.6(3)	C39-C40-C41	108.1(3)
N6-C31-C30	108.2(2)	C40-C41-C29	129.5(3)
C30-C31-C42	128.6(3)	N8-C43-C55	119.4(2)
C34-C35-C36	107.9(4)	C50-C46-C47	108.0(3)
N8-C43-C44	110.5(2)	C51-C55-C43	126.7(3)
C44-C43-C55	130.0(3)	N10-C57-C69	121.9(2)
C57-C58-C59	106.1(3)	C67-C68-C69	107.7(3)
N9-C59-C70	121.9(3)	C68-C69-C57	126.4(3)
C63-C62-C61	108.0(4)	N10-C57-C58	106.5(2)
C55-C51-C52	107.8(3)	C58-C57-C69	131.5(3)
C51-C55-C54	107.8(3)	N9-C59-C58	109.9(2)
C54-C55-C43	125.4(3)	C58-C59-C70	128.1(3)
C62-C61-C60	107.5(4)	C65-C69-C57	125.9(3)
C68-C69-C65	107.7(3)		

Having the appropriate redox potential in hand, synthesis of $[\text{Tp}^{\text{Fc,Me}}\text{Fe}]_2(\mu\text{-}\eta^1\text{:}\eta^1\text{-N}_2)$ (**9**) was accomplished through reduction of either **2** or **3** under different reaction conditions, both using Na/Hg amalgam as reducing agent. The reaction of **2** with a large excess (40 equiv.) of 1.2 % by weight Na/Hg amalgam over the course of 6 days resulted in yields of only 6 to 10% of **9**, with the remaining material being identified as mostly N-confused versions of the starting material. We attribute this to the increased susceptibility toward borotropic rearrangement of **2** as compared to **3**, as well as the more negative redox potential of **2**. Because it possesses a peak potential only slightly more negative than -1.96 V vs SHE, **3** will undergo complete reduction using a 2 part excess of 1% w/w Na/Hg amalgam over the course of 7 days stirring in THF. This produces a mixture of the desired compound **9** and some borotropically rearranged bis-ligand complexes, being the result of minor over-reduction or possibly disproportionation to Fe^{II} and Fe^0 . After removing solvent in vacuo, and then extracting the remaining residue with ether to remove any Na salts, produces **9** with a purity suitable for further reactivity studies, in yields varying from 60 and 90 %. Analytically pure samples of **9** were prepared by re-dissolving and concentrating in

THF, layering with pentanes, and cooling to $-35\text{ }^{\circ}\text{C}$ to produce small quantities of dark red crystals.



Scheme 1.9: Synthesis of $[\text{Tp}^{\text{Fc,Me}}\text{Fe}]_2(\mu_2\text{-}\eta^1\text{:}\eta^1\text{-N}_2)$ (**9**).

The structure of **9**, depicted in **Figure 1.16**, shows that the complex is a bridging dinuclear di-nitrogen complex, with the N_2 moiety bound to the metal centers in an end on fashion. The structure also shows a lack of inversion symmetry about the bridging N-N bond, present in many other such dinitrogen complexes. Because of this, it displays an IR stretching mode for the N-N bond at 1970 cm^{-1} , shown in **Figure 1.19**. The N-N bond distance of the ligated N_2 was $1.171(5)\text{ \AA}$, showing a degree of N_2 activation that agrees with the IR stretching frequency; both are indicative of only a weakly activated N_2 moiety having a bond order somewhere between 2 and 3.¹⁷ The complex was found to be highly paramagnetic, possessing an effective magnetic

moment of $5.9(1) \mu_B$ (293 K). This magnetic moment means it is not strongly anti-ferromagnetically coupled, but either ferrimagnetically coupled as is the case with some other bridging N_2 complexes,¹⁸ or that the two metal centers only weakly interact with one another.

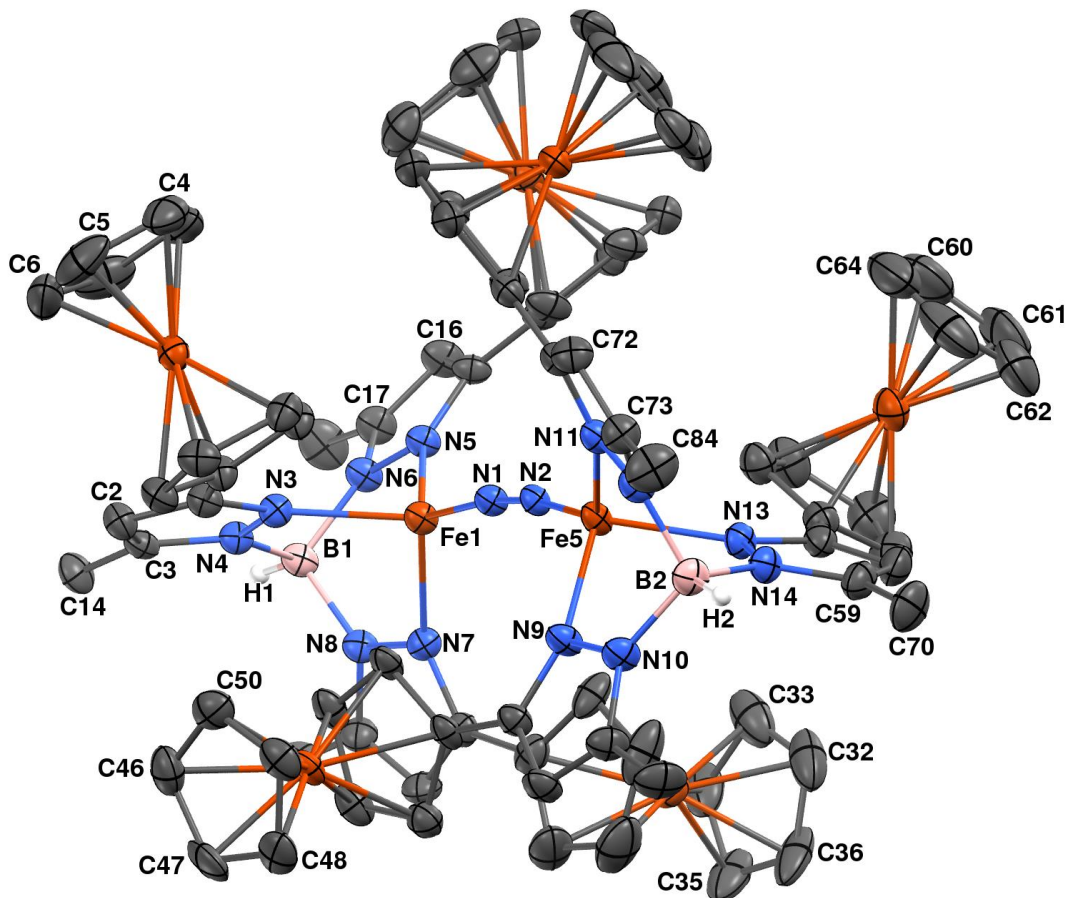


Figure 1.16: Molecular structure of $[Tp^{Fc,Me}Fe]_2(\mu\text{-}\eta^1:\eta^1\text{-}N_2)$ (9) represented as 30% probability thermal ellipsoids. Hydrogen atoms (with the exception of the hydrogens attached to boron, H1 and H2,) and 1 molecule of THF and 1.5 molecules of n-Pentane have been omitted for clarity.

Table 1.10: Selected interatomic distances (Å) and angles (°) for [Tp^{Fe,Me}Fe]₂(μ-η¹:η¹-N₂) (9)

Distances (Å)			
Fe1-N1	1.778(4)	Fe1-N5	2.063(4)
Fe1-N3	2.075(4)	Fe1-N7	2.083(4)
Fe5-N2	1.780(4)	Fe5-N11	2.066(4)
Fe5-N9	2.078(4)	Fe5-N13	2.081(4)
B1-N8	1.538(7)	B1-N4	1.546(7)
B1-N6	1.554(7)	B2-N14	1.533(8)
N1-N2	1.171(5)	B2-N10	1.545(7)
N3-N4	1.375(5)	N3-C1	1.334(6)
N5-C15	1.347(6)	N4-C3	1.359(6)
N6-C17	1.363(6)	N5-N6	1.372(5)
N7-N8	1.374(5)	N7-C29	1.341(6)
N9-C43	1.350(6)	N8-C31	1.358(6)
N10-C45	1.367(7)	N9-N10	1.373(5)
N13-C57	1.347(7)	N11-C71	1.330(7)
N14-C59	1.353(7)	N13-N14	1.382(5)
C3-C14	1.509(7)	C2-C3	1.361(7)
C4-C5	1.384(11)	C5-C6	1.364(12)
C9-C13	1.425(7)	C9-C10	1.426(7)
C10-C11	1.415(8)	C11-C12	1.414(7)
C12-C13	1.431(7)	C15-C16	1.412(7)
C15-C27	1.459(7)	C16-C17	1.365(8)
C32-C33	1.396(13)	C30-C31	1.357(8)
C45-C56	1.498(8)	C46-C50	1.398(9)
C46-C47	1.416(10)	C47-C48	1.423(10)
C57-C69	1.471(8)	C57-C58	1.388(8)
C59-C70	1.501(8)	C58-C59	1.385(9)
C60-C61	1.396(15)	C60-C64	1.370(15)
C62-C63	1.368(15)	C61-C62	1.399(15)
C65-C66	1.419(9)	C63-C64	1.372(15)
C66-C67	1.413(10)	C65-C69	1.425(8)
C68-C69	1.418(8)	C67-C68	1.412(8)
C73-C84	1.506(7)	C72-C73	1.364(8)

Angles (°)

B1-Fe1-N1	176.6(2)	B2-Fe5-N2	172.1(2)
N1-Fe1-N5	127.44(16)	N1-Fe1-N3	124.11(16)
N5-Fe1-N3	89.01(15)	N1-Fe1-N7	121.65(17)
N5-Fe1-N7	91.25(15)	N3-Fe1-N7	93.47(16)
N2-Fe5-N9	116.61(17)	N2-Fe5-N11	128.88(17)
N2-Fe5-N13	126.10(17)	N11-Fe5-N9	92.85(16)
N9-Fe5-N13	92.43(17)	N11-Fe5-N13	90.26(16)
N8-B1-N4	108.9(4)	N8-B1-N6	109.5(4)
N4-B1-N6	109.8(4)	N14-B2-N12	110.3(4)
N14-B2-N10	108.9(4)	N12-B2-N10	109.4(4)
C1-N3-N4	106.7(4)	C1-N3-Fe1	138.9(3)
C3-N4-B1	130.6(4)	N3-N4-B1	120.1(4)
C15-N5-N6	107.2(4)	C15-N5-Fe1	138.4(3)
C17-N6-B1	130.2(4)	N5-N6-B1	119.6(4)
C29-N7-N8	107.1(4)	C29-N7-Fe1	139.3(3)
C31-N8-B1	130.3(4)	N7-N8-B1	120.7(4)
C43-N9-N10	106.5(4)	C43-N9-Fe5	138.8(3)
C45-N10-B2	130.8(4)	N9-N10-B2	119.8(4)
C73-N12-B2	130.9(4)	N11-N12-B2	120.6(4)
C57-N13-N14	106.5(4)	C57-N13-Fe5	141.0(4)
C59-N14-B2	129.6(5)	N13-N14-B2	120.7(4)
N3-C1-C2	109.7(4)	N3-C1-C13	121.9(4)
C2-C1-C13	128.4(5)	C3-C2-C1	106.6(5)
N4-C3-C2	107.8(4)	N4-C3-C14	123.3(5)
C2-C3-C14	128.9(5)	C9-C13-C1	127.6(5)
C6-C5-C4	108.2(7)	N5-C15-C27	122.5(4)
C13-C9-C10	107.9(5)	C17-C16-C15	107.3(5)
C12-C11-C10	108.2(5)	N6-C17-C28	123.5(5)
C9-C13-C12	107.4(4)	C19-C18-C22	107.5(7)
C12-C13-C1	125.0(5)	C23-C27-C15	128.5(5)
N5-C15-C16	108.3(5)	N7-C29-C41	122.6(5)
C16-C15-C27	129.2(5)	C31-C30-C29	106.6(5)
N6-C17-C16	107.2(4)	C30-C31-C42	129.0(5)
C16-C17-C28	129.3(5)	C36-C32-C33	108.2(8)
C18-C19-C20	108.1(6)	C37-C41-C29	129.9(5)
C20-C21-C22	107.8(6)	N9-C43-C55	122.7(4)
C27-C23-C24	108.3(5)	C45-C44-C43	106.8(5)
C24-C25-C26	107.5(5)	C44-C45-C56	129.9(5)

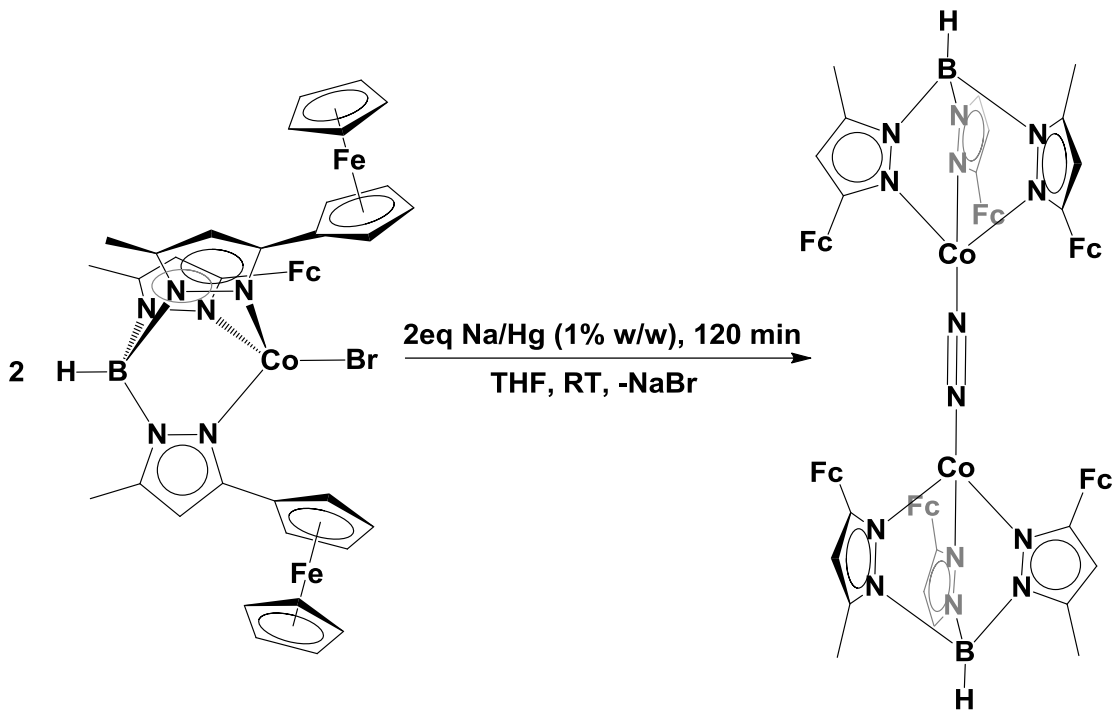
C23-C27-C26	107.2(5)	C50-C46-C47	106.8(6)
C26-C27-C15	124.2(5)	N13-C57-C69	122.3(5)
N7-C29-C30	109.1(5)	C59-C58-C57	106.2(5)
C30-C29-C41	128.3(5)	N14-C59-C70	123.2(6)
C30-C31-N8	108.3(5)	C64-C60-C61	106.5(12)
N8-C31-C42	122.6(5)	C68-C69-C57	128.8(5)
C38-C37-C41	108.3(7)	N12-C73-C84	121.8(5)
C38-C39-C40	109.6(7)	N14-C59-C58	107.8(5)
C37-C41-C40	106.1(6)	C58-C59-C70	129.0(6)
C40-C41-C29	123.9(6)	C60-C61-C62	107.1(11)
N9-C43-C44	109.1(4)	C62-C63-C64	106.6(12)
C44-C45-N10	108.3(5)	C66-C65-C69	108.5(6)
C46-C47-C48	107.7(6)	C68-C67-C66	108.5(6)
C52-C53-C54	108.4(5)	C68-C69-C65	107.0(5)
N13-C57-C58	109.9(5)	C65-C69-C57	124.1(6)
C58-C57-C69	127.7(5)	N12-C73-C72	108.6(5)
C72-C73-C84	129.6(5)		

Following the successful synthesis of **9**, we used the same methodology to produce $[\text{Tp}^{\text{Fc,Me}}\text{Co}]_2(\mu\text{-}\eta^1\text{:}\eta^1\text{-N}_2)$ (**10**). The process started by acquiring a cyclic voltammogram, shown in **Figure 1.17**, which displayed a quasi-reversible reduction event at -1.44 V vs SHE, presumed to be the reduction of the NNN ligated cobalt center. The voltammogram also displayed accompanying redox events at more negative potentials, indicative of ligand decomposition. Because of these features a similar reaction protocol with the same reductant was used. Reduction of **4** with 1.5 equivalents of 1% w/w Na/Hg amalgam over the course of 2 hours resulted in a stark color change from green to dark orange. Treatment of the mixture by filtration through celite and removal of solvent in vacuo results in an orange residue, which is then triturated with ether to remove over-reduction products. The remaining orange residue was dissolved in THF, layered with pentanes, and cooled to -35 °C. This produced crystals of the desired complex **10**, but with an extraordinary amount of solvent

present in the lattice, so much so that the crystals will lose crystallinity and be reduced to a powder after only as much as 10 minutes in a glove box environment.

Nonetheless, this material was used to acquire a crystal structure, shown in **Figure 1.18**, containing 10 molecules of THF per asymmetric unit. The remaining material that dissolved with trituration in ether was also layered with pentanes; after sitting for 24 hours dark orange crystals of **10** grew and were collected with filtration, with only 1 molecule of n-pentane per asymmetric unit, as determined by X-ray crystallography. Both methods produce analytically pure samples of **10**, with total yields in excess of 60%. The magnetic moment observed for **10** was surprisingly high, at $4.9(1) \mu_B$ (298 K), indicating that it behaves similarly to complex **9**, appearing to be a strongly ferrimagnetically coupled $\text{Co}^{\text{II}}\text{-N}_2^{2-}\text{-Co}^{\text{II}}$ core, or two high spin Co^{I} complexes that do not communicate electronically. The latter seems most consistent with the observed structural characteristics of the complex, showing an only marginally activated bond. We have not performed a variable temperature collection of the complex magnetic moment to determine with certainty if the two metal centers are magnetically coupled.

Both structures acquired for **10** lack an inversion center, similar to its iron analogue, and the relative structural parameters (bond lengths and angles) are the same to within error. The structure of **10** is further asymmetric in that it has a significant torsion angle, between the two Co centers and the bridging dinitrogen, of 50.2° . This lack of symmetry about the N_2 moiety results in an IR stretching frequency being present at 2070 cm^{-1} . This IR frequency matches the N_2 bond length of 1.138 \AA in good agreement for an only marginally activated N-N bond.¹⁷



Scheme 1.10: Synthesis of $[\text{Tp}^{\text{Fc,Me}}\text{Co}]_2(\mu\text{-}\eta^1\text{:}\eta^1\text{-N}_2)$ (10).

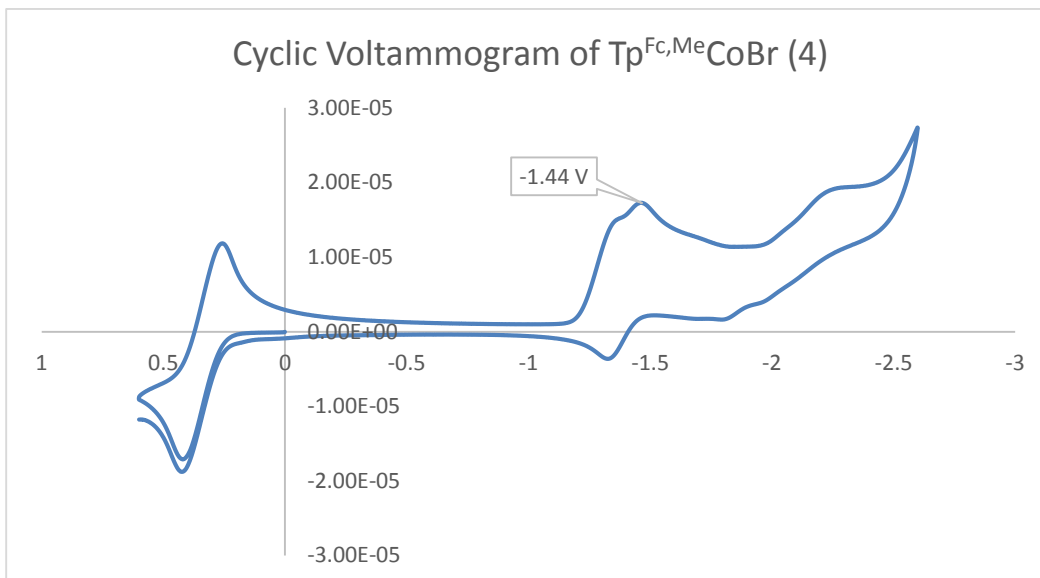


Figure 1.17: Cyclic voltammogram of compound (4), in 0.1 M solution of $[\text{N}^{\text{n}}\text{Bu}_4]\text{ClO}_4$ and $(\text{Cp}^*)_2\text{Fe}$ (0.14 V) (used to reference voltages to SHE = 0 V) in THF, (working electrode = GC, reference electrode = Ag/Ag⁺, Counter electrode = Pt)

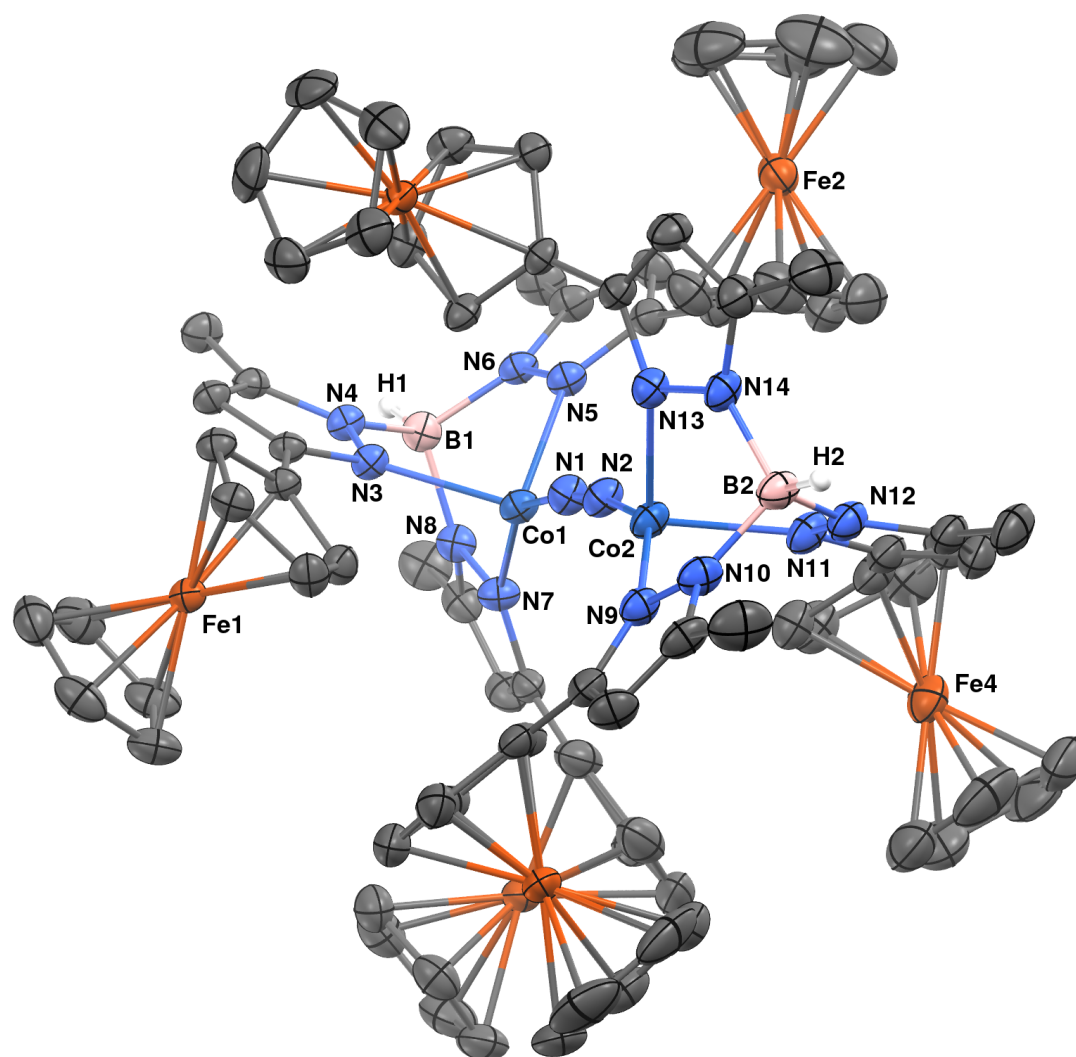


Figure 1.18: Molecular structure of $[\text{Tp}^{\text{Fc,Me}}\text{Co}]_2(\mu\text{-}\eta^1:\eta^1\text{-N}_2)$ (10) represented as 50% probability thermal ellipsoids. Hydrogen atoms (with the exception of the hydrogens attached to boron, H1 and H2), and 10 molecules of THF have been omitted for clarity.

Table 1.11: Selected interatomic distances (Å) and angles (°) for [Tp^{Fc,Me}Co]₂(μ-**η¹:η¹-N₂) (10)****Distances (Å)**

Co1-N1	1.815(3)	Co1-N7	2.025(3)
Co1-N3	2.048(3)	Co1-N5	2.073(3)
Co2-N2	1.813(3)	Co2-N9	2.006(3)
Co2-N13	2.062(3)	Co2-N11	2.077(3)
B1-N8	1.545(4)	B1-N6	1.547(4)
B1-N4	1.553(4)	B2-N14	1.535(5)
B2-N10	1.543(5)	B2-N12	1.540(5)
N1-N2	1.138(4)	N3-C1	1.337(4)
N3-N4	1.377(3)	N4-C3	1.349(4)
N7-N8	1.378(4)	N5-N6	1.373(3)
N11-N12	1.378(4)	N8-C31	1.350(4)
N12-C45	1.346(4)	N9-N10	1.374(4)
N13-N14	1.379(4)		

Angles (°)

B1-Co1-N1	156.1(1)	B2-Co2-N2	155.5(1)
N1-Co1-N7	148.41(12)	N1-Co1-N3	111.77(11)
N7-Co1-N3	89.29(10)	N1-Co1-N5	107.08(11)
N7-Co1-N5	95.10(10)	N3-Co1-N5	91.52(10)
N2-Co2-N9	146.45(12)	N2-Co2-N13	111.27(12)
N9-Co2-N13	91.85(11)	N2-Co2-N11	111.04(12)
N9-Co2-N11	90.63(11)	N13-Co2-N11	93.31(11)
N8-B1-N6	107.3(3)	N8-B1-N4	110.2(3)
N6-B1-N4	110.1(2)	N14-B2-N10	110.1(3)
N14-B2-N12	109.4(3)	N10-B2-N12	108.7(3)
N2-N1-Co1	172.8(3)	N1-N2-Co2	171.3(3)
N4-N3-Co1	112.46(18)	N3-N4-B1	120.4(2)
N6-N5-Co1	112.89(19)	N5-N6-B1	119.1(2)
N8-N7-Co1	114.26(19)	N7-N8-B1	119.3(2)
N10-N9-Co2	115.2(2)	N9-N10-B2	118.4(3)
N12-N11-Co2	112.4(2)	N11-N12-B2	120.1(3)
N14-N13-Co2	111.87(19)	N13-N14-B2	120.7(3)

Contrasting the two dinitrogen bearing compounds, **9** and **10**, by looking at just the core of heteroatoms about their respective metal centers, see **Figure 1.20** and **Table 1.12**, we see that the apparent decrease in symmetry for the Co compound, due to a pronounced α -angle of 23.3° and also its increased torsion angle about the N_2 moiety.¹² This difference in symmetry has an effect on the IR spectroscopy of the two compounds. Because the ligands are nearly perfectly isostructural, most of the resonances of the complexes are the same to within four wavenumbers between the two spectra and have very similar intensities, **Figure 1.19**. The most notable exceptions to this are the B-H and N_2 stretching frequency, the latter of which is more pronounced in **10** than in **9**.

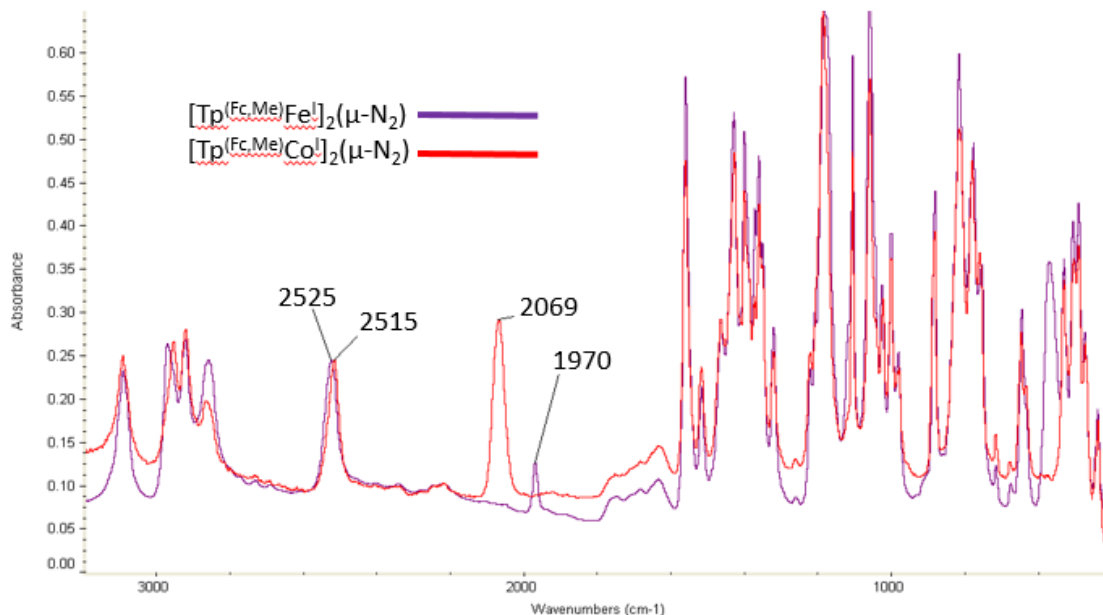


Figure 1.19: IR spectroscopy of compounds **9** (blue, $\nu_{NN} = 1970$) and **10** (red, $\nu_{NN} = 2069$ cm⁻¹), with their B-H and N-N stretching frequencies annotated

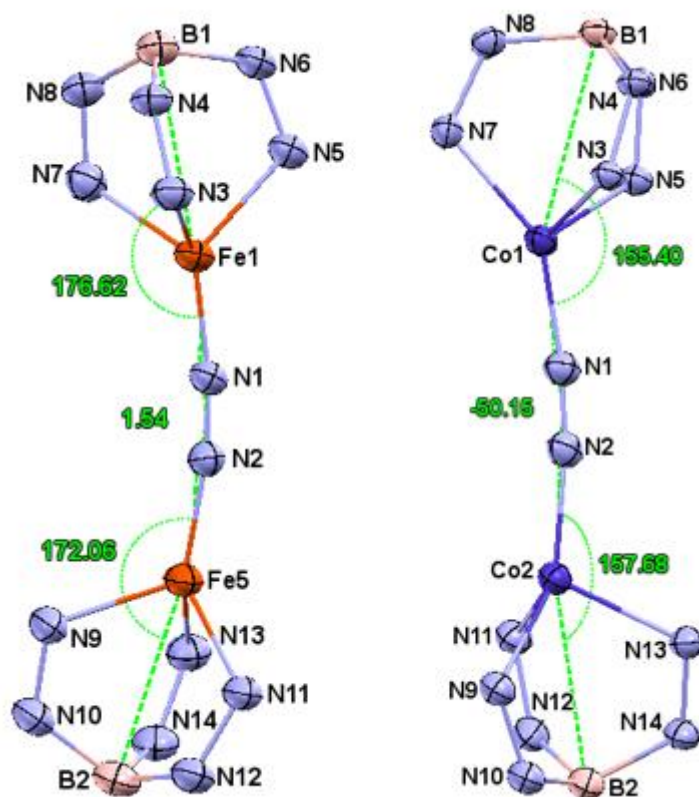


Figure 1.20: Comparison of α -angles and M-N₂-M torsions of compounds (9) and (10), atoms displayed as 50% thermal ellipsoids, all other atoms omitted for clarity

Table 1.12: Alpha angles and M-N₂-M torsions of (9) and (10), and their respective ν_{NN} stretching frequencies

	α ($^{\circ}$)	M-N ₂ -M torsion ($^{\circ}$)	ν_{NN} (cm^{-1})
$[Tp^{Fc,Me}Fe]_2(\mu-\eta^1:\eta^1-N_2)$ (9)	176.6(2), 172.1(2)	2(4)	1969.63
$[Tp^{Fc,Me}Co]_2(\mu-\eta^1:\eta^1-N_2)$ (10)	157.7(1), 155.4(1)	50(4)	2068.89

The N₂ bond lengths mentioned earlier and these IR stretching frequencies are in good agreement with other Fe and Co dinitrogen complexes supported by tris(pyrazolyl)borato ligands, as seen in **Table 1.13**. The degree to which the N₂ moiety is activated, when examined by comparing their N₂ bond length, appears to increase with decreasing Co-N_{pz} bond lengths, but for the Fe complex the trend is reversed, with decreasing N-N bond length coinciding with decreasing Fe-N_{pz} bond lengths. Although the values for these bond lengths are sequentially the same to within error, the extremes are not, indicating this trend is genuine and not an artifact resulting from measurement error. It must also be noted that the value for Tp^{tBu}Co(η¹-N₂) is distorted as a result of libration.^{7,20} ¹H-NMR spectra taken of **9** and **10** under N₂ gas and also after multiple FPT cycles reveal no significant changes that could be interpreted as an equilibrium between monomer and dimer states, see **Figures 1.21** and **1.22** below. The preference for bridging N₂ complexes is observed with most TpM dinitrogen complexes. Notable exceptions include the Tp^{tBu,Me}Co(η¹-N₂) complex, which is a terminal N₂ complex, and the Tp^{tBu,Me}Fe(N₂) complex which participates in an equilibrium between a terminal and dinuclear bridging N₂ configuration.^{6,20}

Table 1.13: Comparison of N₂ activation and select structural parameters of [Tp^{R,R'}M]_xN₂ complexes (R= tBu, Fc, Np, iPr, Ph, or Ad; R'= Me or H; M=Co or Fe; X= 1 or 2)

<i>TpCo</i>				
	NN (Å)	B-M-N (°)	M-N _{pz} (Å) avg	IR (cm ⁻¹)
<i>Tp</i> ^{tBu} Co(η^1 -N ₂) ²⁰	.956(10)*	171	2.062 (5)	2046
[<i>Tp</i> ^{Fc,Me} Co] ₂ (μ - η^1 : η^1 -N ₂) (10)	1.138(4)	157.7(1), 155.4(1)	2.049 (3)	2069
[<i>Tp</i> ^{Np} Co] ₂ (μ - η^1 : η^1 -N ₂) ¹⁹	1.141(30)	145.3, 142.1	2.032 (22)	2056
[<i>Tp</i> ^{iPr,Me} Co] ₂ (μ - η^1 : η^1 -N ₂) ⁷	1.154(9)	156.0(3)	2.024 (7)	-
<i>TpFe</i>				
	NN	B-M-N	M-N _{pz} (Å) avg	IR (cm ⁻¹)
[<i>Tp</i> ^{tBu,Me} Fe] ₂ (μ - η^1 : η^1 -N ₂) ⁶	1.183(5)	177.3(2)	2.135(4)	1967
[<i>Tp</i> ^{Ph,Me} Fe] ₂ (μ - η^1 : η^1 -N ₂) ²¹	1.181(1)	178.17(4)	2.085(1)	1779
[<i>Tp</i> ^{Fc,Me} Fe] ₂ (μ - η^1 : η^1 -N ₂) (9)	1.171(5)	176.6(2), 172.1(2)	2.074(4)	1970
<i>Tp</i> ^{Ad,Me} Fe(η^1 -N ₂) ²¹	1.119(2)	178.58(5)	2.061(1)	1959

*Value shortened by libration, see text^{7,20}

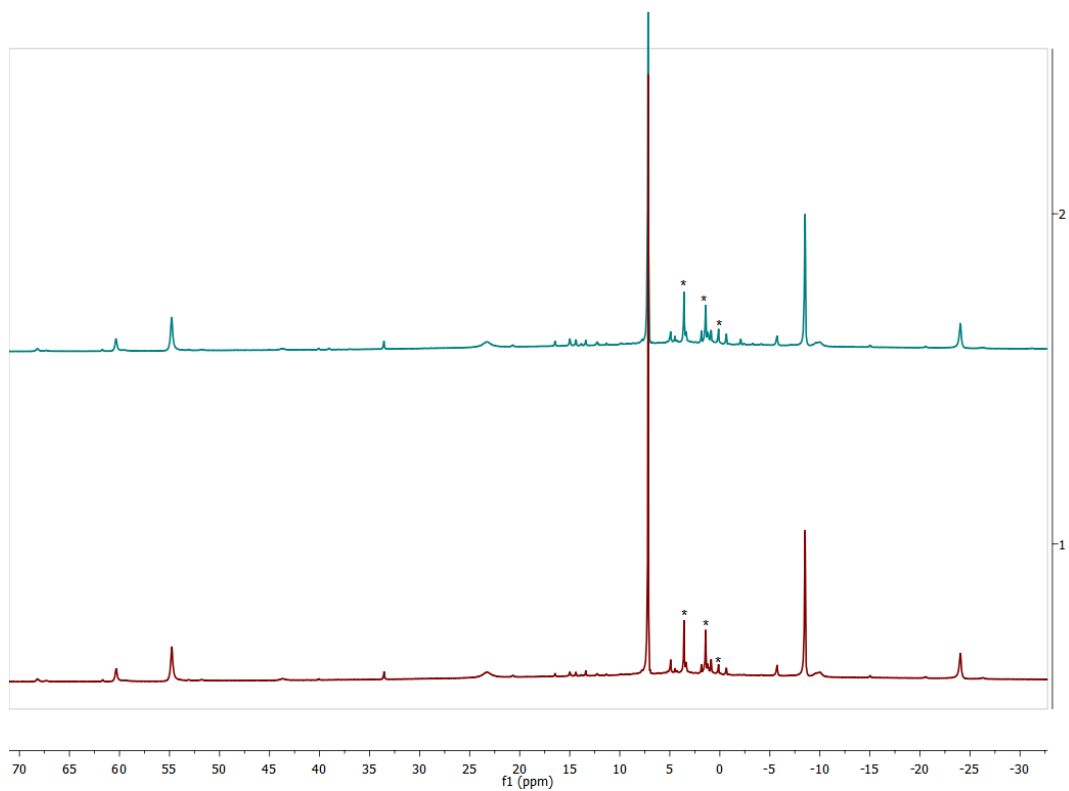


Figure 1.21: $^1\text{H-NMR}$ of crystals of 9 taken in C_6D_6 under vacuum, co-crystallized with $^*\text{THF}$ /pentanes, with some impurities from oxidation (bottom), and that sample when placed under an N_2 atmosphere for 10 minutes (top)

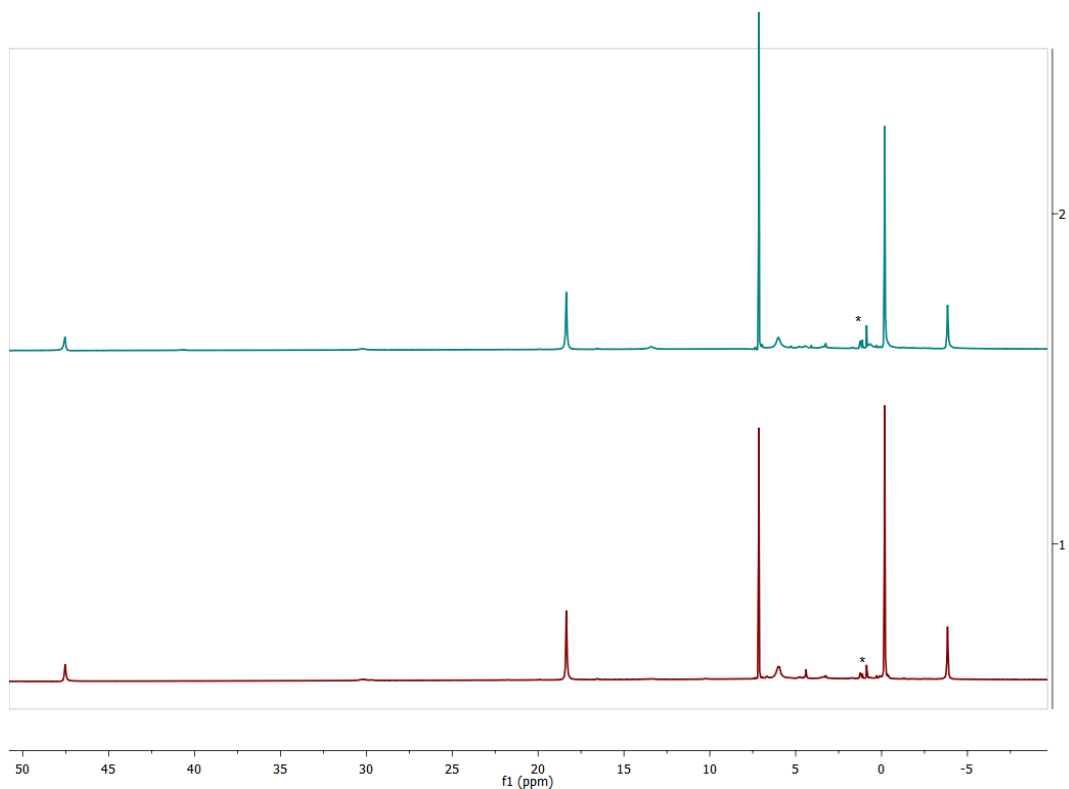


Figure 1.22: ^1H -NMR of crystals of **10 in C_6D_6 under vacuum, co-crystallized with pentanes*, with some impurities from oxidation (bottom), and that sample when placed under an N_2 atmosphere for 10 minutes (top)**

Attempts to reduce **9** and **10**, in an effort to further activate and possibly split the N_2 moiety, were unsuccessful. Cyclic voltammetry experiments performed on samples of **9** revealed no additional reduction events other than those observed for compounds **1**, **2**, and **3** at or above -2.15 V vs SHE, see **Figure 1.23**. **10** displayed 2 reversible reductions, see **Figure 1.24**, but attempts to isolate compounds through chemical reduction with KC_8 resulted in only the isolation of byproducts observed during the synthesis of **10**. One of those byproducts being a bis-ligand complex, $[\text{Tp}^{\text{Fc,Me}}]_2\text{Co}$ (**A1.2**), which can also be created by refluxing a mixture of **10** in THF for

7 days. This also produced the compound $\text{Tp}^{\text{Fc,Me}}\text{Co}(\text{PzH}^{\text{Fc,Me}})(\text{Pz}^{\text{Fc,Me}})$ (**A1.3**), likely through a mechanistic pathway of ligand decomposition at the B-N bonds of the ligand.

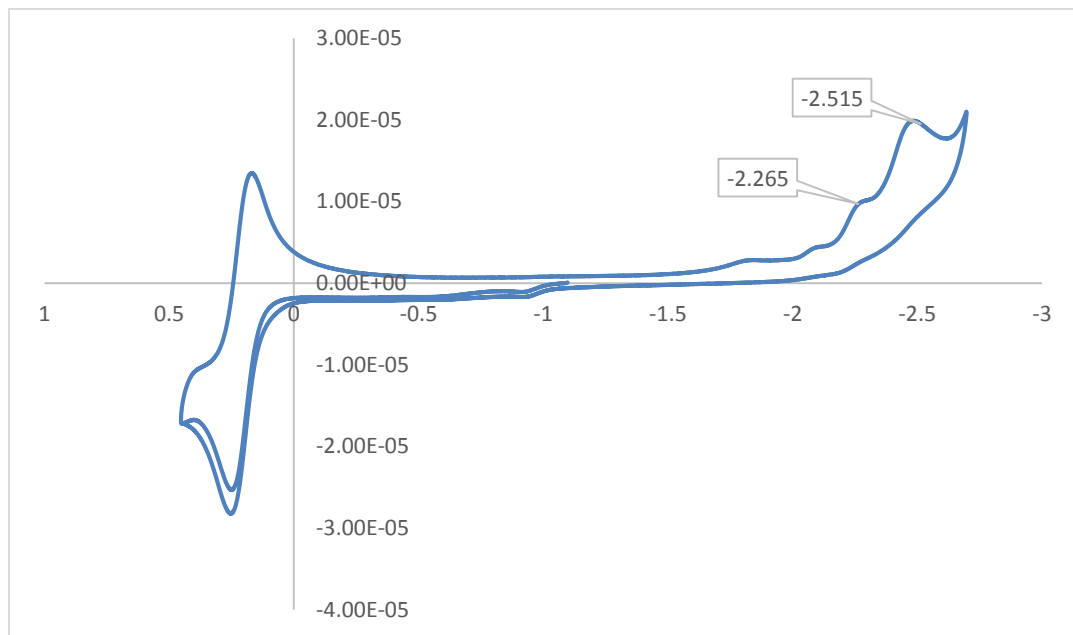


Figure 1.23: Cyclic voltammogram of 9, in a solution of 0.1 M $[\text{N}^n\text{Bu}_4]\text{ClO}_4$ and 0.1 M $(\text{Cp}^*)_2\text{Fe}$ (0.14 V) (used to reference voltages to SHE = 0 V) in THF, (working electrode = GC, reference electrode = Ag/Ag⁺, counter electrode = Pt)

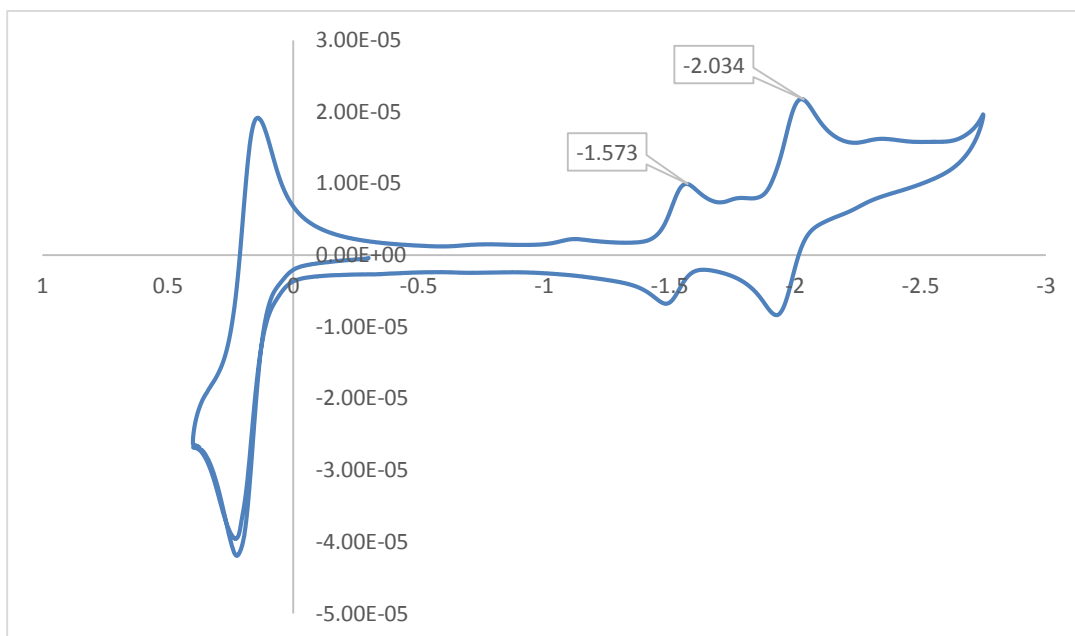
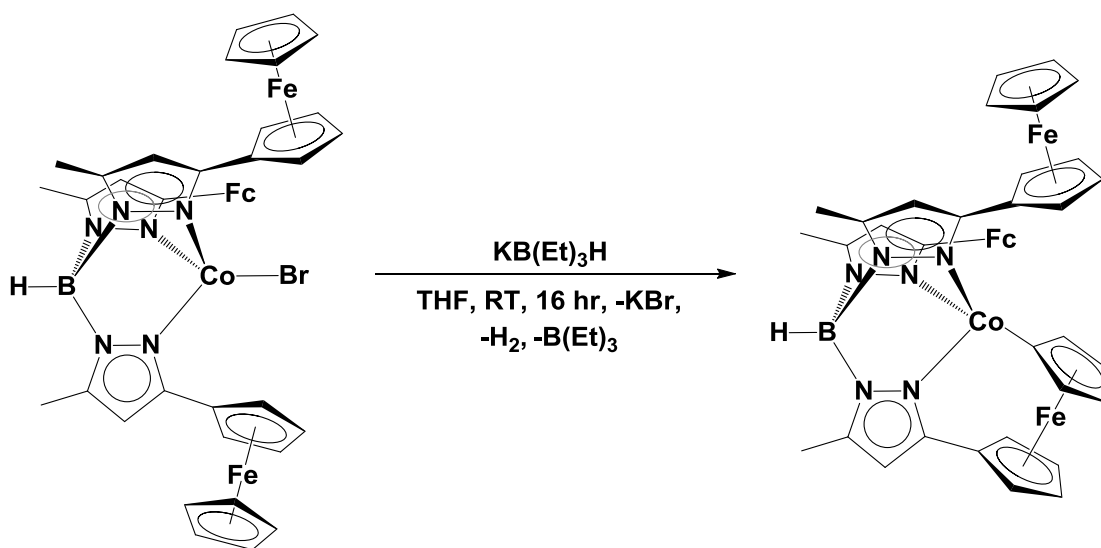


Figure 1.24: Cyclic voltammogram of 9, in a solution of 0.1 M [NⁿBu₄]ClO₄ and 0.1 M (Cp*)₂Fe (0.14 V) (used to reference voltages to SHE = 0 V) in THF, (working electrode = GC, reference electrode = Ag/Ag⁺, counter electrode = Pt).

Activation of ferrocenyl moiety by way of supposed hydride intermediate.

It was found previously by members of our group that metal hydrides can be used in the examination of oxygen activation, especially when cobalt is the metal center being used.⁵ To this end we set about trying to synthesize Tp^{Fc,Me}CoH, using LiBH₄ and later LiB(Et)₃H as potential sources of hydride. Unfortunately, in every attempt we found that the lithium metathesized with the NNN ligated cobalt, producing Tp^{Fc,Me} lithium salt. Given the use of potassium salts in chemistry published by Holland,²² and the consistency of lithiation when reacting either **3** or **4** with other lithium salts, we shifted our focus to the use of reagents with potassium counter ions. Although the use of a potassium reagent (KB(Et)₃H) prevented transmetallation of the ancillary ligand, the isolable product was not the intended hydride, see **Scheme 1.11**. Instead the product of

a σ bond metathesis involving a Fc-H bond of one of the pyrazole arms, $\text{Bp}^{\text{Fc,Me}}(\text{Me-pz-CpFe}(\text{C}_5\text{H}_4))\text{Co}$ (**11**), was the only product that is observed, see **Scheme 1.11**. The reaction was done in THF with 1 equiv. of 2 M $\text{KB}(\text{Et})_3\text{H}$ in THF, which resulted in a subtle change in color from the forest green of the halide starting material to a darker shade of green over the course of 2 hours. The resulting solution was filtered, and layered with ether and then pentanes, and after sitting at room temperature for 8 days small blocky crystals of **11** formed which were pure enough for further use. Analytically pure samples required an additional recrystallization using the same method. The effective magnetic moment of the compound was found to be $3.7(1) \mu_{\text{B}}$ when measured at room temperature, which is slightly lower than that associated with a high spin Co^{II} d^7 metal center. The complex displayed C_s symmetry by NMR, with 12 peaks being clearly observed, 1 of the peaks corresponding to the activated ferrocene could not be located, **Figure 1.26**.



Scheme 1.11: Synthesis of $\text{Bp}^{\text{Fc,Me}}(\text{Me-pz-CpFe}(\text{C}_5\text{H}_4))\text{Co}$ (11**)**

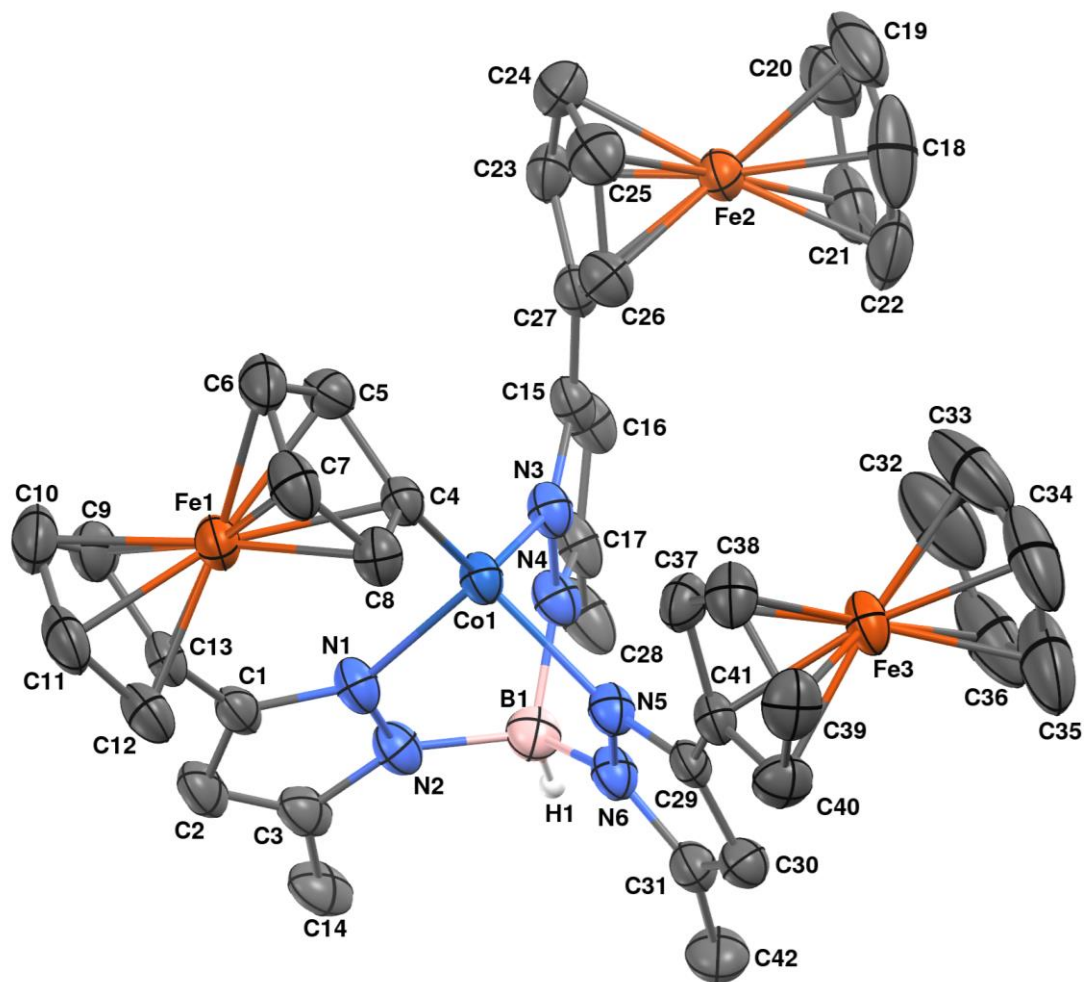


Figure 1.25: Molecular structure of $Bp^{Fc,Me}(Me-pz-CpFe(C_5H_4))Co$ (11) represented as 50% probability thermal ellipsoids. Hydrogen atoms (with the exception of the hydrogen attached to boron, H1), and one molecule of n-pentane have been omitted for clarity.

Table 1.14: Selected interatomic distances (Å) and angles (°) for Bp^{Fe,Me}(Me-pz-**CpFe(C₅H₄))Co (11)**

Distances (Å)			
Co1-C4	1.986(4)	Co1-N1	2.025(3)
Co1-N5	2.033(3)	Co1-N3	2.049(3)
Fe1-C10	2.032(4)	Fe1-C12	2.039(4)
Fe1-C7	2.040(4)	Fe1-C6	2.043(4)
Fe1-C11	2.048(4)	Fe1-C13	2.052(4)
Fe1-C8	2.043(4)	Fe1-C9	2.050(4)
Fe1-C5	2.062(4)	Fe1-C4	2.103(3)
Fe2-C21	2.026(4)	Fe2-C23	2.032(4)
Fe2-C24	2.033(4)	Fe2-C20	2.033(5)
Fe2-C22	2.037(4)	Fe2-C18	2.038(5)
Fe2-C25	2.043(4)	Fe2-C19	2.038(5)
Fe2-C26	2.052(4)	Fe2-C27	2.056(3)
Fe3-C32	2.023(6)	Fe3-C39	2.027(4)
Fe3-C33	2.028(5)	Fe3-C38	2.031(4)
Fe3-C40	2.029(4)	Fe3-C34	2.031(5)
Fe3-C35	2.033(6)	Fe3-C37	2.035(4)
Fe3-C36	2.034(5)	Fe3-C41	2.041(3)
B1-N4	1.544(5)	B1-N2	1.557(5)
B1-N6	1.558(5)	N1-C1	1.346(5)
N1-N2	1.359(4)	N2-C3	1.359(4)
N3-C15	1.339(4)	N3-N4	1.382(4)
N4-C17	1.356(5)	N5-C29	1.335(4)
N5-N6	1.382(4)	N6-C31	1.356(5)
C1-C2	1.397(5)	C1-C13	1.479(5)
C2-C3	1.378(6)	C3-C14	1.499(5)
C4-C5	1.430(5)	C4-C8	1.442(5)
C5-C6	1.422(5)	C6-C7	1.416(6)
C7-C8	1.417(5)	C9-C10	1.409(6)
C9-C13	1.421(5)	C10-C11	1.418(7)
C11-C12	1.415(6)	C12-C13	1.421(6)
C15-C16	1.399(5)	C15-C27	1.463(5)
C16-C17	1.375(5)	C17-C28	1.495(5)
C18-C19	1.366(8)	C18-C22	1.412(8)
C19-C20	1.390(8)	C20-C21	1.380(7)
C21-C22	1.397(7)	C23-C24	1.420(6)

C23-C27	1.431(5)	C24-C25	1.408(6)
C25-C26	1.418(5)	C26-C27	1.413(5)
C29-C30	1.396(5)	C29-C41	1.463(5)
C30-C31	1.372(5)	C31-C42	1.496(5)
C32-C36	1.408(9)	C32-C33	1.424(8)
C33-C34	1.373(9)	C34-C35	1.400(8)
C35-C36	1.370(9)	C37-C38	1.413(5)
C37-C41	1.428(5)	C38-C39	1.399(6)
C39-C40	1.417(5)	C40-C41	1.419(5)

Angles (°)

C4-Co1-N5	127.84(13)	B1-Co1-C4	163.7(1)
C4-Co1-N3	132.91(13)	C4-Co1-N1	108.19(13)
N5-Co1-N3	89.85(12)	N1-Co1-N5	93.50(12)
Co1-C4-Fe1	115.60(16)	N1-Co1-N3	94.33(12)
N4-B1-N2	108.1(3)	N4-B1-N6	110.0(3)
N2-B1-N6	108.8(3)	C1-N1-N2	107.5(3)
C1-N1-Co1	136.6(3)	N2-N1-Co1	115.9(2)
C3-N2-N1	110.0(3)	C3-N2-B1	132.3(3)
N1-N2-B1	117.7(3)	C15-N3-N4	106.9(3)
C15-N3-Co1	140.2(2)	N4-N3-Co1	111.6(2)
C17-N4-N3	109.2(3)	C17-N4-B1	129.7(3)
N3-N4-B1	121.0(3)	C29-N5-N6	106.7(3)
C29-N5-Co1	140.8(2)	N6-N5-Co1	112.1(2)
C31-N6-N5	109.1(3)	C31-N6-B1	130.0(3)
N5-N6-B1	120.9(3)	N1-C1-C2	108.7(3)
N1-C1-C13	121.6(3)	C2-C1-C13	129.7(3)
C3-C2-C1	106.8(3)	N2-C3-C2	107.1(3)
N2-C3-C14	122.5(4)	C2-C3-C14	130.4(4)
C5-C4-C8	104.1(3)	C5-C4-Co1	126.8(3)
C8-C4-Co1	127.1(3)	C7-C6-C5	107.6(3)
C6-C5-C4	110.5(3)	C7-C8-C4	110.6(4)
C6-C7-C8	107.3(4)	C11-C10-C9	108.3(4)
C10-C9-C13	108.5(4)	C13-C12-C11	108.9(4)
C10-C11-C12	107.3(4)	C12-C13-C1	126.3(4)
C12-C13-C9	106.9(4)	N3-C15-C27	120.8(3)
C9-C13-C1	126.6(4)	C17-C16-C15	106.2(3)
N3-C15-C16	109.6(3)	N4-C17-C28	121.9(4)
C16-C15-C27	129.7(3)	C19-C18-C22	107.5(5)
N4-C17-C16	108.0(3)	C21-C20-C19	107.9(5)

C16-C17-C28	130.1(4)	C21-C22-C18	107.3(5)
C18-C19-C20	109.2(5)	C25-C24-C23	108.3(4)
C20-C21-C22	108.1(4)	C27-C26-C25	108.3(4)
C24-C23-C27	107.6(4)	C26-C27-C15	126.9(3)
C24-C25-C26	108.2(4)	N5-C29-C41	122.1(3)
C26-C27-C23	107.6(3)	C31-C30-C29	106.0(3)
C23-C27-C15	125.5(3)	N6-C31-C42	123.1(3)
N5-C29-C30	109.9(3)	C36-C32-C33	106.0(7)
C30-C29-C41	127.9(3)	C33-C34-C35	108.7(6)
N6-C31-C30	108.2(3)	C35-C36-C32	109.2(6)
C30-C31-C42	128.7(4)	C39-C38-C37	108.2(3)
C34-C33-C32	108.1(7)	C39-C40-C41	108.2(3)
C36-C35-C34	107.9(7)	C40-C41-C29	125.3(3)
C38-C37-C41	108.3(3)	C40-C41-C37	106.9(3)
C38-C39-C40	108.4(3)	C37-C41-C29	127.7(3)

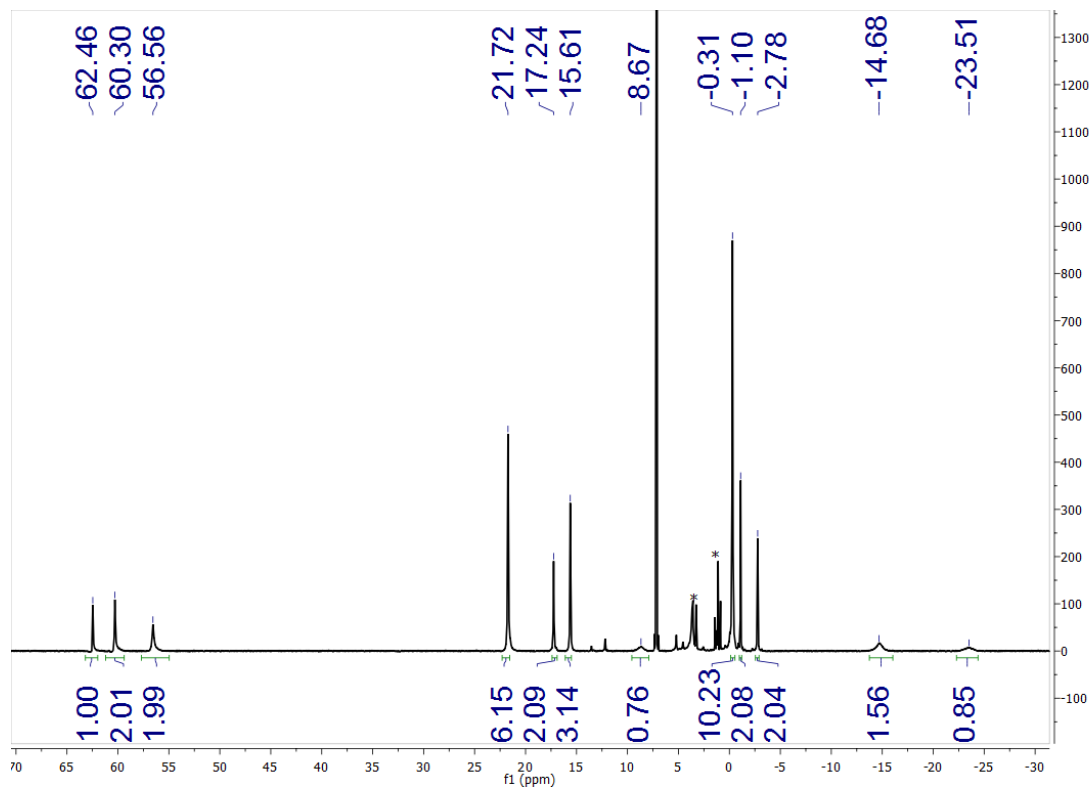
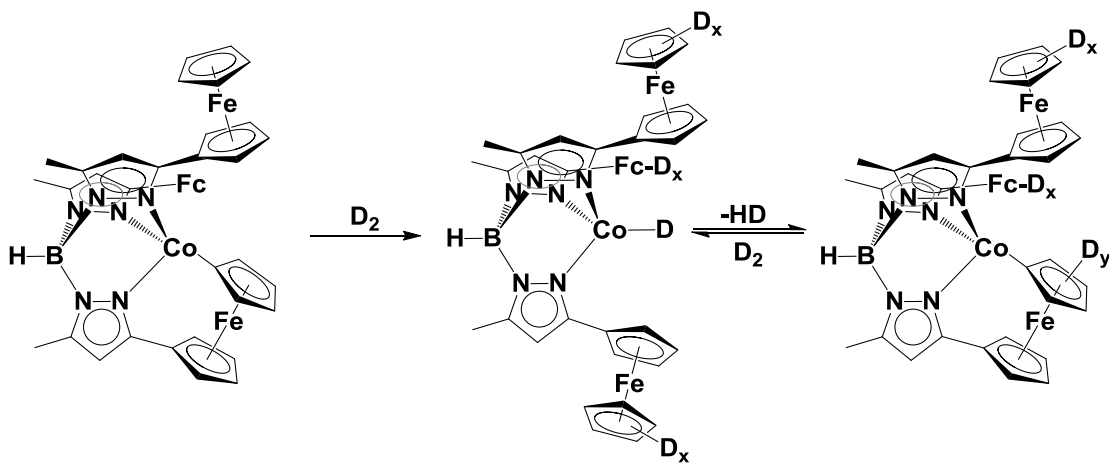


Figure 1.26: ^1H -NMR spectrum of $\text{Bp}^{\text{Fc,Me}}(\text{Me-pz-CpFe}(\text{C}_5\text{H}_4))\text{Co}$ (11**) recorded in C_6D_6 at 400MHz, with some *THF/Ether/Pentanes present in crystals used for collection.**

Our interpretation of **11** was that it likely comes from the elimination of H_2 gas from the originally intended target cobalt hydride, $\text{Tp}^{\text{Fc,Me}}\text{CoH}$. This would mean the desired compound is created as an intermediate, and were this the case an equilibrium between that hydride and **11** might be established in the presence of H_2 gas. When **11** was put under an atmosphere of H_2 at 300 K no appreciable change was observed when monitored by ^1H -NMR. However, upon addition of D_2 gas and mild heating at 45°C for 16 hours, the resonances at 56.6 and -0.3 ppm were seen to diminish significantly in their integrations relative to the rest of the chemical shifts. This

indicates incorporation of deuterium into the system. This is further supported by the appearance of additional chemical shifts corresponding to H₂ and HD gas dissolved in the NMR solvent, see **Figures 1.27** and **Scheme 1.12**. The assignment of the peaks as HD comes from their $J_{\text{HD}} = 42$ Hz, and chemical shift at ~ 4.5 ppm, both consistent with literature precedent.²³ Furthermore, when the sample is observed by ²H-NMR, it displays resonances at the same chemical shifts seen to dissipate in the ¹H-NMR, 56.2 and -0.3, giving an additional positive indication of the incorporation of deuterium into the complex, as seen in **Figure 1.28**. **Figure 1.28** also shows a resonance at 5.17 ppm, which may correspond to the two hydrogens on the metallated Cp that could not be located in the ¹H-NMR of **11**, as well as a small peak at 2.6 ppm which may be the result of some of the ferrocene moieties being only partially deuterated.



Scheme 1.12: Incorporation of deuterium into the ferrocene moieties of 11, elimination of HD and equilibrium under deuterium atmosphere

($x = 0$ to 5, $y = 0$ to 4).

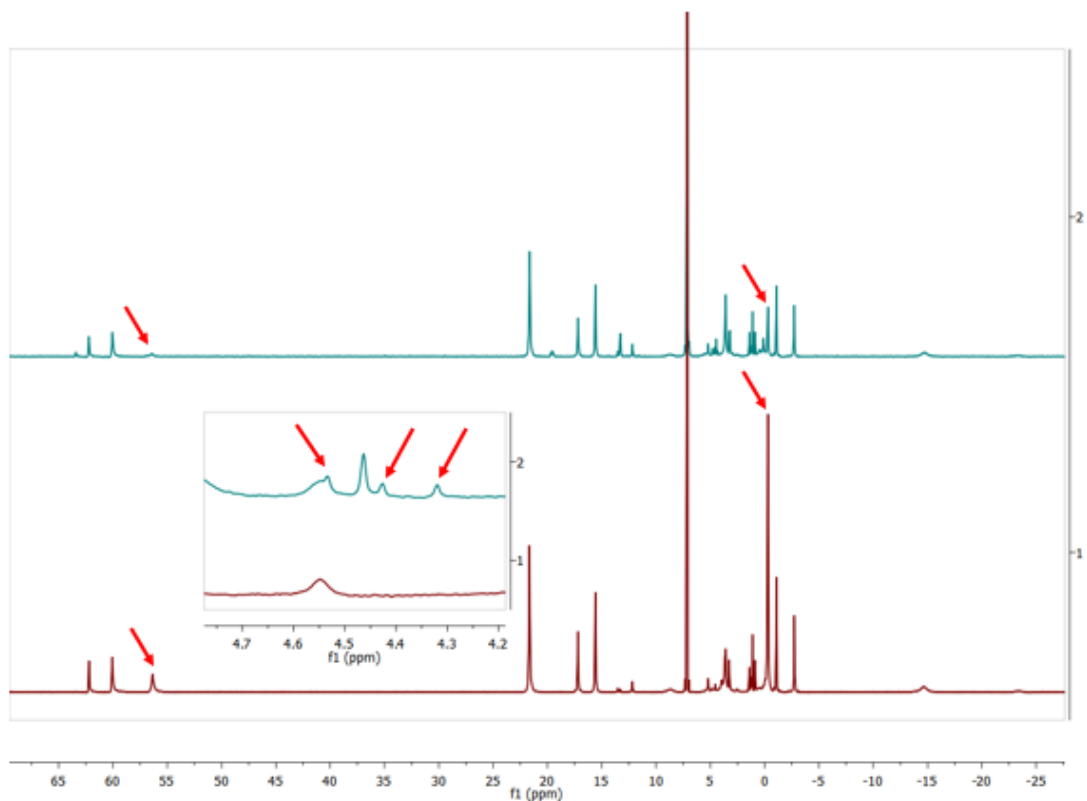


Figure 1.27: ^1H -NMR spectrum of $\text{Bp}^{\text{Fc,Me}}(\text{Me-pz-CpFe}(\text{C}_5\text{H}_4))\text{Co}$ (11) recorded in C_6D_6 (bottom), the same sample with 1 atm of D_2 gas added and heated at 45 °C for 16 hours (top), Cp rings effected by deuterium incorporation highlighted with red arrows, (inset: HD resonances highlighted with red arrows)

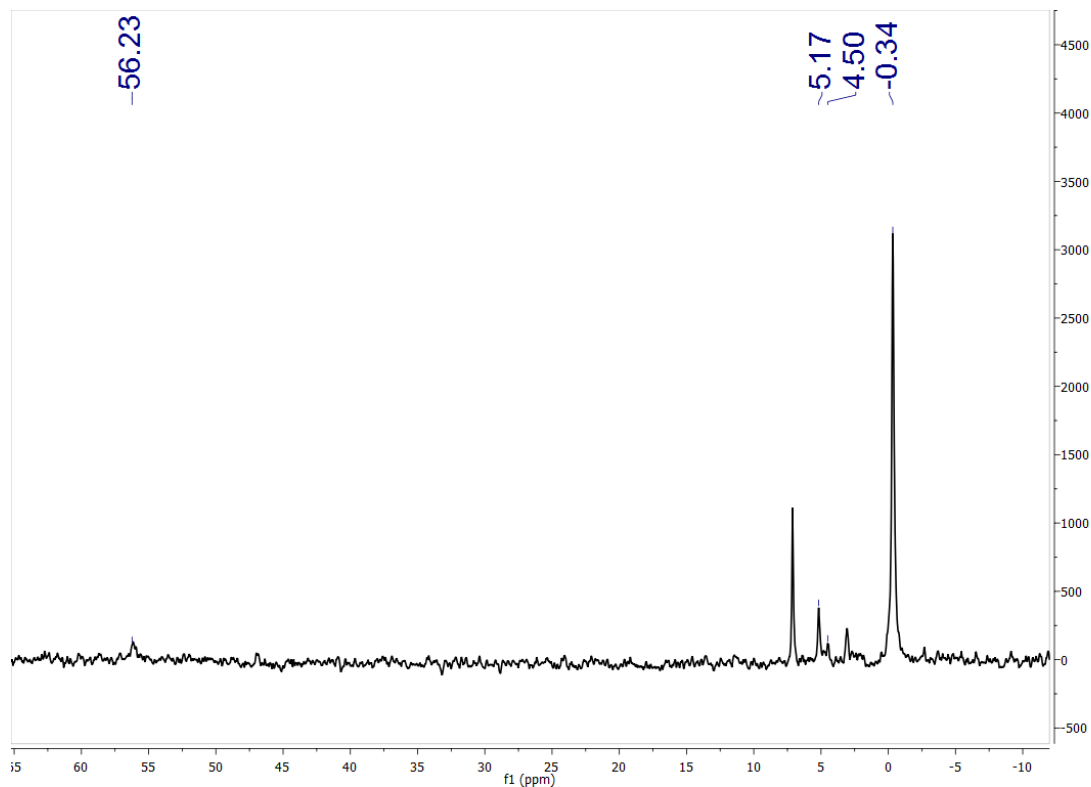
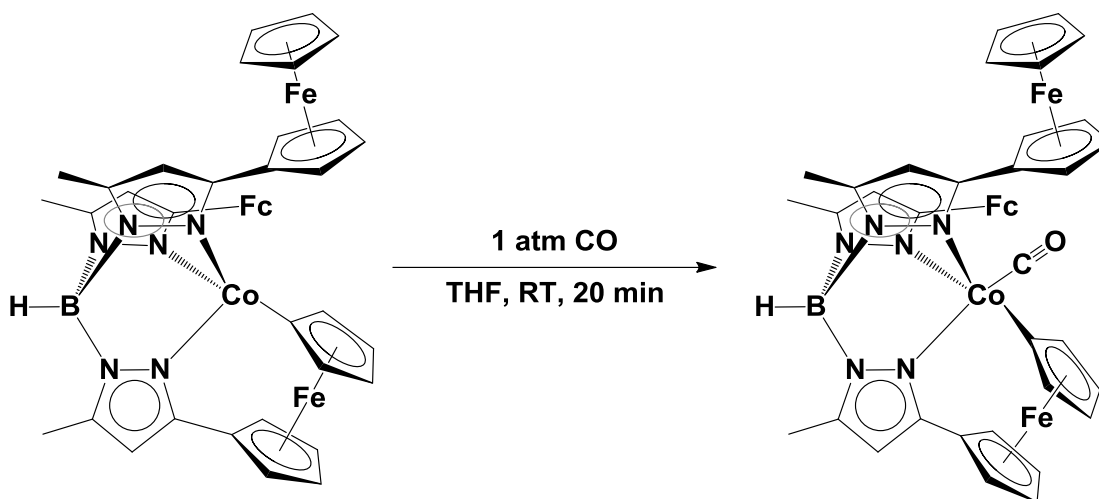


Figure 1.28: ^2H -NMR spectrum of $\text{Bp}^{\text{Fc,Me}}(\text{Me-pz-CpFe}(\text{C}_5\text{H}_4))\text{Co}$ (11**) after heating at 45 °C under 1 atm of D_2 , recorded in C_6H_6 , with residual C_6D_6 visible at 7.16 ppm, D_2 still present at 4.5 ppm**

I sought to better understand the reactivity of **11** and the unusual strength of its cobalt cyclopentadienyl bond. To that end I placed a sample of twice recrystallized **11** dissolved in degassed THF under ~ 0.9 atm of CO gas, in an effort to insert a carbonyl into the ferrocenyl-cobalt bond. This mixture was stirred for several minutes, resulting in a rapid color change from green to orange. The mixture was then degassed and the solvent removed in vacuo. The orange residue was dissolved in ether and filtered through celite, then layered with pentanes to afford a novel terminal metal carbonyl complex, $\text{Bp}^{\text{Fc,Me}}(\text{Me-pz-CpFe}(\text{C}_5\text{H}_4))\text{Co}(\text{CO})$ (**12**), having a $\nu_{\text{CO}} = 2021 \text{ cm}^{-1}$

observable in its IR spectrum, in yields ranging from 70 to 90%. The identity of the complex was confirmed by X-ray diffraction analysis, see **Figure 1.29** and **Scheme 1.14**. The structure shows a nearly square pyramidal ($\tau_5 = .063$) coordination geometry about the metal center,²⁴ while remaining a mono-carbonyl, presumably due to the cobalt having a total valence electron count of 17. Of note in the crystal structure is the long Co1-N3 bond, corresponding to the apically bound pyrazole arm. The ¹H-NMR of the complex displays broad chemical shifts between -1 and 23 ppm, indicating the compound is still paramagnetic. The effective magnetic moment was found to be 2.0(1) μ_B when measured at room temperature, consistent with the assignment of the metal center as a low spin d^7 Co^{II}. The lack of insertion of the carbonyl into the Co-C bond is indicative of its being an especially strong metal to carbon bond.



Scheme 1.14: Synthesis of $Bp^{Fc,Me}(Me-pz-CpFe(C_5H_4))Co(CO)$ (12).

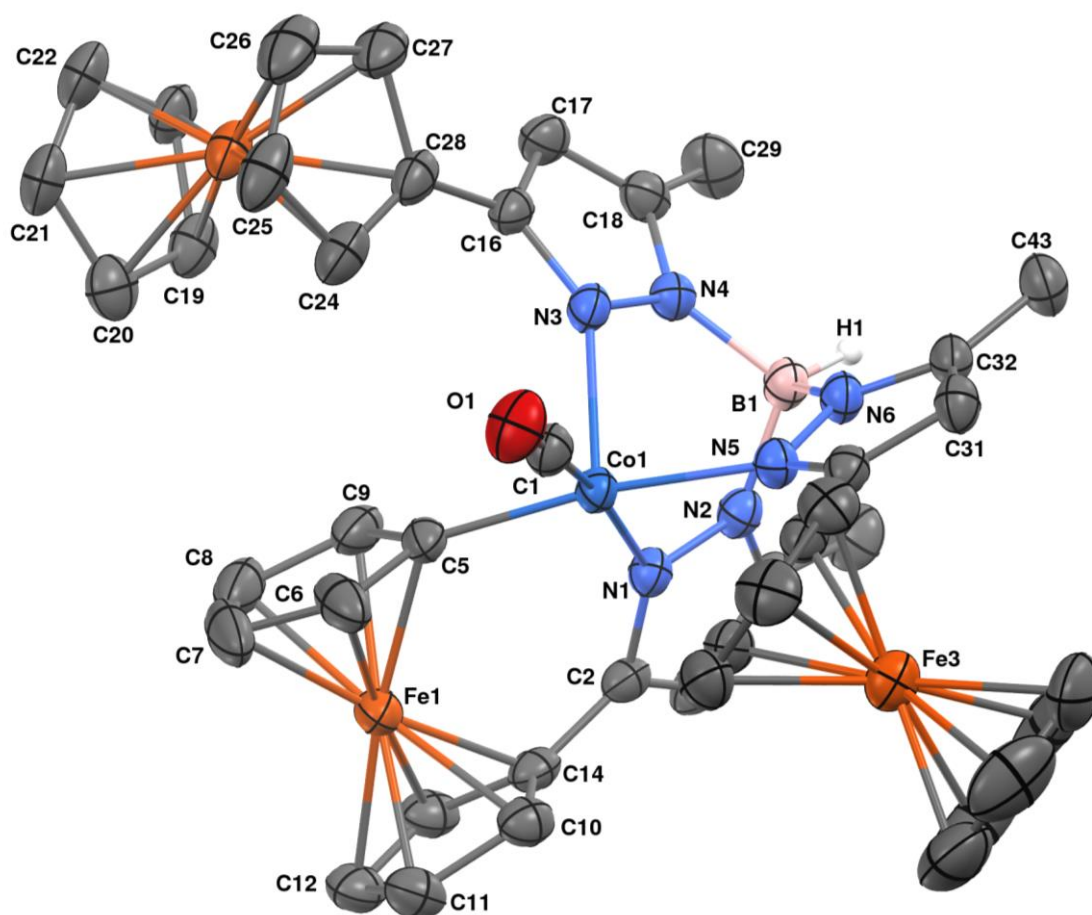


Figure 1.29: Molecular structure of $\text{Bp}^{\text{Fc,Me}}(\text{Me-pz-CpFe}(\text{C}_5\text{H}_4))\text{Co}(\text{CO})$ (**12**) represented as 50% probability thermal ellipsoids. Hydrogen atoms (with the exception of the hydrogen attached to boron, H1) have been omitted for clarity.

Table 1.15: Selected interatomic distances (Å) and angles (°) for



Distances (Å)

Co1-C1	1.766(2)	Co1-C5	1.946(2)
Co1-N5	1.9890(18)	Co1-N1	1.9989(18)
Co1-N3	2.1618(19)	Fe1-C14	2.000(2)
Fe1-C10	2.020(2)	Fe1-C6	2.033(3)

Fe1-C5	2.038(2)	Fe1-C7	2.041(3)
Fe1-C9	2.042(3)	Fe1-C13	2.042(3)
Fe1-C8	2.043(3)	Fe1-C11	2.048(3)
Fe1-C12	2.063(2)	N1-N2	1.374(3)
N1-C2	1.350(3)	N2-B1	1.542(3)
N2-C4	1.352(3)	N3-N4	1.375(3)
N3-C16	1.341(3)	N4-B1	1.542(3)
N4-C18	1.351(3)	N5-N6	1.370(3)
N5-C30	1.342(3)	N6-B1	1.545(3)
N6-C32	1.357(3)	O1-C1	1.137(3)
C2-C3	1.389(3)	C2-C14	1.466(3)
C3-C4	1.373(4)	C5-C6	1.434(3)
C4-C15	1.491(3)	C6-C7	1.430(5)
C5-C9	1.442(4)	C7-C8	1.408(6)
C10-C11	1.420(4)	C8-C9	1.421(4)
C10-C14	1.427(3)	C13-C14	1.432(3)
C11-C12	1.417(4)	C16-C28	1.471(3)
C12-C13	1.417(4)	C24-C28	1.426(4)
C19-C20	1.413(10)	C19-C23	1.440(15)
C20-C21	1.427(15)	C21-C22	1.348(16)
C22-C23	1.397(15)	C30-C31	1.399(3)
C16-C17	1.396(3)	C31-C32	1.375(3)
C17-C18	1.367(4)	C32-C43	1.498(3)
C18-C29	1.498(4)	C33-C34	1.447(8)
C24-C25	1.429(4)	C34-C35	1.357(7)
C25-C26	1.402(5)	C35-C36	1.331(6)
C26-C27	1.415(4)	C36-C37	1.334(6)
C27-C28	1.437(3)	C38-C42	1.427(3)
C30-C42	1.461(3)	C39-C40	1.420(4)
C33-C37	1.378(8)	C38-C39	1.411(4)
C40-C41	1.422(4)	C41-C42	1.427(3)

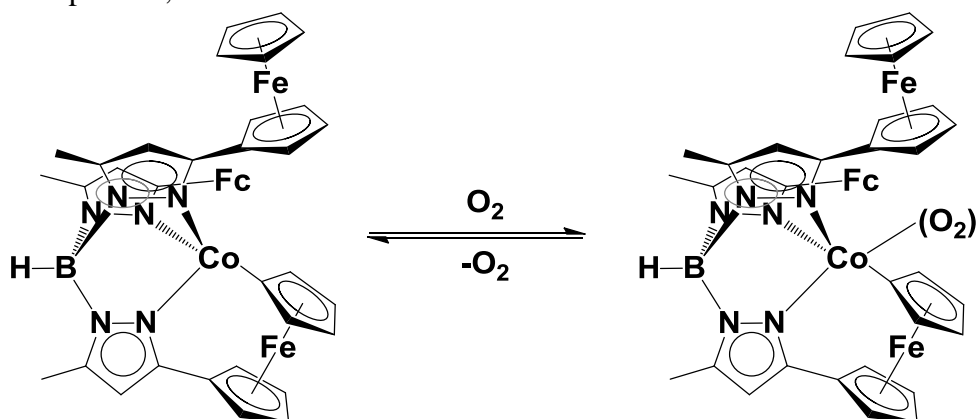
Angles (°)

C1-Co1-C5	84.76(10)	C1-Co1-N5	94.36(9)
C5-Co1-N5	171.72(9)	C1-Co1-N1	167.89(10)
C5-Co1-N1	92.88(9)	N5-Co1-N1	86.27(7)
C1-Co1-N3	98.94(9)	C5-Co1-N3	99.39(9)
N5-Co1-N3	88.88(7)	N1-Co1-N3	93.16(7)
O1-C1-Co1	177.8(2)	C14-Fe1-C6	133.93(10)
C14-Fe1-C10	41.58(10)	C14-Fe1-C5	103.56(9)

C10-Fe1-C6	108.78(12)	C6-Fe1-C5	41.25(10)
C10-Fe1-C5	105.61(10)	C10-Fe1-C7	139.92(16)
C14-Fe1-C7	173.19(11)	C5-Fe1-C7	69.70(11)
C6-Fe1-C7	41.11(13)	C10-Fe1-C9	134.71(10)
C14-Fe1-C9	106.03(11)	C5-Fe1-C9	41.41(10)
C6-Fe1-C9	68.62(13)	C14-Fe1-C8	137.33(15)
C7-Fe1-C9	68.41(14)	C6-Fe1-C8	68.51(15)
C10-Fe1-C8	175.04(11)	C7-Fe1-C8	40.32(16)
C5-Fe1-C8	69.56(11)	C10-Fe1-C11	40.86(10)
C9-Fe1-C8	40.72(12)	C5-Fe1-C11	137.17(10)
C14-Fe1-C11	69.51(10)	C9-Fe1-C11	175.32(11)
C6-Fe1-C11	113.21(12)	C8-Fe1-C11	143.77(13)
C7-Fe1-C11	115.92(14)	C10-Fe1-C12	68.46(10)
C14-Fe1-C12	69.24(10)	C5-Fe1-C12	172.72(10)
C6-Fe1-C12	143.65(11)	C9-Fe1-C12	140.23(11)
C7-Fe1-C12	117.51(12)	C8-Fe1-C12	116.26(11)
C11-Fe1-C12	40.33(10)	C2-N1-Co1	136.42(16)
C2-N1-N2	106.18(18)	N1-N2-B1	119.07(18)
N2-N1-Co1	117.31(14)	C16-N3-Co1	140.03(16)
C16-N3-N4	105.68(18)	C18-N4-N3	110.56(18)
N4-N3-Co1	111.83(13)	N3-N4-B1	119.33(18)
C18-N4-B1	129.7(2)	C32-N6-N5	109.38(19)
N6-N5-Co1	116.98(14)	N5-N6-B1	118.29(17)
C32-N6-B1	132.27(19)	N2-B1-N6	107.92(19)
N2-B1-N4	107.70(18)	C6-C5-Co1	129.5(2)
N4-B1-N6	109.50(19)	C6-C5-Fe1	69.19(14)
N1-C2-C14	122.4(2)	Co1-C5-Fe1	121.54(11)
C6-C5-C9	106.0(2)	C7-C6-Fe1	69.75(17)
C9-C5-Co1	124.27(19)	C8-C7-Fe1	69.92(18)
C7-C6-C5	108.9(3)	C7-C8-Fe1	69.76(19)
C8-C7-C6	107.9(3)	C8-C9-Fe1	69.70(18)
C7-C8-C9	108.5(3)	C11-C10-Fe1	70.61(15)
C8-C9-C5	108.8(3)	C12-C11-Fe1	70.39(15)
C11-C10-C14	108.3(2)	C11-C12-Fe1	69.28(14)
C12-C11-C10	108.1(2)	C10-C14-C2	127.8(2)
N3-C16-C17	110.0(2)	C10-C14-Fe1	69.97(14)
C17-C16-C28	124.9(2)	C2-C14-Fe1	120.70(15)
N4-C18-C17	107.4(2)	N3-C16-C28	124.8(2)
C17-C18-C29	129.5(2)	C18-C17-C16	106.4(2)

C24-C28-C16	130.7(2)	N4-C18-C29	123.0(2)
N6-C32-C43	122.4(2)	C24-C28-C27	107.4(2)
C19-C20-C21	104.8(8)	C27-C28-C16	122.0(2)
C22-C21-C20	112.6(10)	N6-C32-C31	108.0(2)
C31-C32-C43	129.6(2)		

Reactions of **11** with oxygen were also carried out, with the reasoning that an additional open coordination site and the potential to oxidize the metal center to a Co^{III} may result in the formation of a new superoxo complex. There was a clear reaction when 1 atm of oxygen gas was added to a mixture of **11** in THF, given both a color change from green to orange as well as a distinct change in the ^1H -NMR with none of the starting **11** remaining. Although the solution remained orange during efforts to isolate a product, the only compound isolated as a crystal was the starting material **11**, seeming to indicate that oxygen binding to the complex is reversible. After this initial observation, an NMR tube containing singly re-crystallized **11** dissolved in C_6D_6 was charged with O_2 gas and then freeze pump thaw degassed multiple times, and its ^1H -NMR spectrum recorded after each manipulation resulting in the reformation of **11**, see **Figure 1.30**. This verifies that oxygen binds to the complex in a reversible manner, but does not give any indication as to the fate of the oxygen moiety once it is incorporated, see **Scheme 1.14**.



Scheme 1.13: reversible binding of O_2 to $\text{Bp}^{\text{Fc,Me}}(\text{Me-pz-CpFe}(\text{C}_5\text{H}_4))\text{Co}$ (**11**).

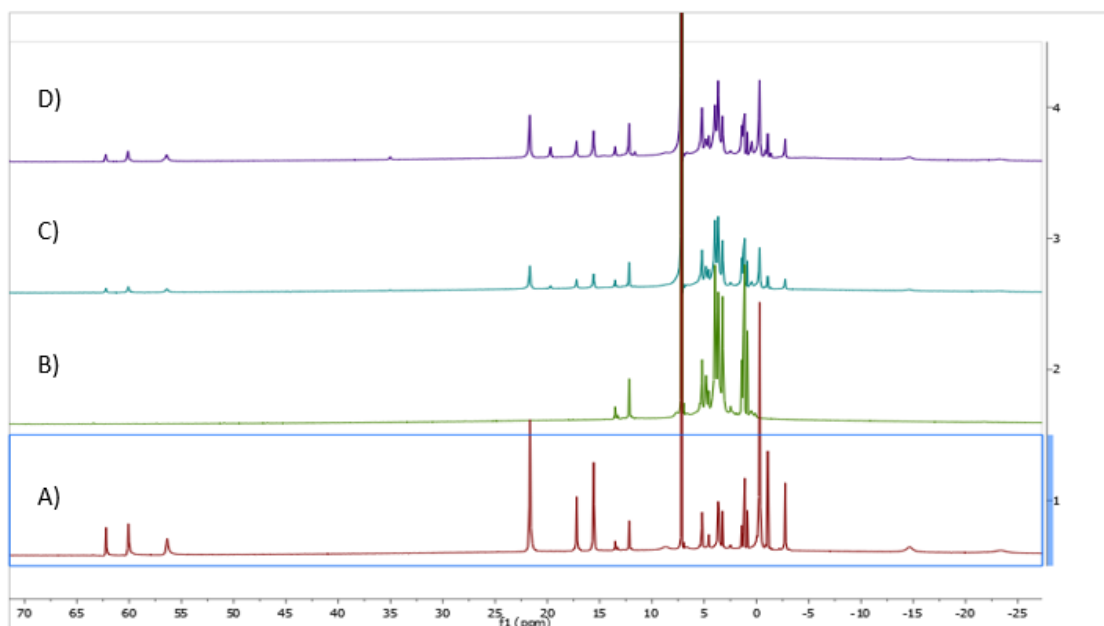


Figure 1.30: ^1H -NMR spectrum of $\text{Bp}^{\text{Fc,Me}}(\text{Me-pz-CpFe}(\text{C}_5\text{H}_4))\text{Co}$ (11) recorded in C_6D_6 (spectrum A), the same sample with 1 atm of O_2 gas added (spectrum B), the same sample after 1 FPT degas cycle (spectrum C), the same sample after a second FPT degas cycle (spectrum D).

Conclusions

The synthesis and characterization of $\text{Tp}^{\text{Fc,Me}}\text{MX}$ complexes ($\text{M}=\text{Fe}$ or Co ; $\text{X}=\text{Cl}$, Br , or I) has been accomplished through a mixture of solid state and solution state syntheses. $\text{Tp}^{\text{Fc,Me}}\text{FeCl}$ and $\text{Tp}^{\text{Fc,Me}}\text{FeBr}$ are both susceptible to borotropic rearrangement in solution, making them unacceptable as starting materials for any syntheses that require a reaction time of longer than 24 hours; however $\text{Tp}^{\text{Fc,Me}}\text{FeI}$ resistance to isomerization makes it amenable to chemical manipulations over long time periods. Alkyl complexes of iron supported by the $\text{Tp}^{\text{Fc,Me}}$ ligand system have been prepared and found to be similar in their spectroscopic and physical characteristics to those previously reported in the $\text{Tp}^{\text{tBu,Me}}$ ligand system. A mono-

carbonyl complex on iron supported by the $\text{Tp}^{\text{Fc,Me}}$ ligand system has been isolated, and found to have the same IR stretching frequency as that of the $\text{Tp}^{\text{tBu,Me}}\text{FeCO}$ complex,⁶ to within the error of the measurement device. The iodide complex on iron and the bromide complex on cobalt were used to produce univalent di-nitrogen complexes of their respective metals, the reactivity of which will be discussed in **Chapter 3**. Attempts to produce a terminal hydride complex on cobalt supported by the $\text{Tp}^{\text{Fc,Me}}$ ligand system were ultimately unsuccessful, with the suggestion being that such a compound will always eliminate H_2 gas with the formation of **11**. All complexes discussed above and whose structures were characterized by X-ray diffraction were found to be κ^3 with respect to the Tp ligand. With the exception of complexes **11** and **12**, all compounds characterized herein were found to display C_{3v} symmetry in solution when examined by NMR.

Experimental Section

All reactions were run under a nitrogen atmosphere using standard glovebox and Schlenk techniques, unless otherwise stated. Diethyl ether, pentane, tetrahydrofuran (THF), and toluene were distilled over Na using benzophenone ketyl as an indicator while under a nitrogen atmosphere, or by passing the solvent through activated alumina columns followed by a nitrogen purge to remove dissolved oxygen.²⁵ Organic chemicals were bought from Fischer, Aldrich, or Acros and all inorganic chemicals were purchased from Strem. Carbon monoxide gas was purchased from Matheson. NMR spectra were obtained on Bruker AVIII-400 or AV-600 spectrometers and were referenced to the residual protons of the solvent (C_6D_6 , 7.16 ppm; THF- D_8 , 3.76, 1.85 ppm). FT-IR spectra were recorded on a Nicolet Magna-IR

560 spectrometer with a resolution of 4 cm^{-1} . Mass spectra (LIFDI-MS) were obtained in the University of Delaware Mass Spectrometry Laboratory, using a Waters GCT Premier high resolution time-of-flight mass spectrometer. X-ray crystallographic studies were conducted in the University of Delaware X-ray crystallographic facility. Molar magnetic susceptibilities (χ_m) were acquired in the solid state at room temperature using a Johnson Matthey magnetic susceptibility balance, and corrected for diamagnetism using Pascal constants to give effective magnetic moments (μ_{eff}).²⁶ Elemental analyses were obtained from Robertson Microlit, Ledgewood, NJ 07852. $\text{Tp}^{\text{Fc,Me}}\text{Ti}$ was prepared by the literature procedure.⁹

General considerations for X-ray diffraction studies: Single crystal X-ray diffraction studies were performed under the conditions listed here. Crystals were selected, sectioned as necessary, and mounted on MiTeGenTM plastic mesh with viscous oil, then flash-cooled to the data collection temperature (200 K). Diffraction data were collected on a Bruker-AXS CCD diffractometer with graphite-monochromated Mo-K α radiation ($\lambda = 0.71073 \text{ \AA}$). The data-sets were treated with absorption corrections based on redundant multi-scan data.²⁷ The structures were solved using direct methods and refined with full-matrix, least-squares procedures on F^2 . Unit cell parameters were determined by sampling three different sections of the Ewald sphere. Non-hydrogen atoms were refined with anisotropic displacement parameters. Hydrogen atoms were treated as idealized contributions with geometrically calculated positions and with U_{iso} equal to 1.2, or 1.5 for methyl, U_{eq} of the attached atom. Structure factors and anomalous dispersion coefficients are contained in the SHELXTL program library.²⁸

Tp^{Fc,Me}FeCl (1): 1.500 g (1.484 mmol) of Tp^{Fc,Me}Tl and .200 g (1.577 mmol, 1.06 equiv.) of FeCl₂ were placed in an agate mortar and ground to homogeneity for 2 hours. A color change is observed, to dark orange, with the formation of TlCl as a fine colorless salt. The mixture was dissolved in THF and filtered through Celite. The material was then immediately dried in vacuo, to afford an orange solid. The solid residue was collected and washed 3 times with di-ethyl ether to remove borotropically rearranged products. The remaining orange residue was collected, giving a yield of .85 g (0.947 mmol, 64 %) of Tp^{Fc,Me}FeCl. ¹H-NMR (400 MHz, THF-d₈): -2.6 (br, 6 H), -1.2 (br, 15 H), 2.5 (br, 6 H), 33.3 (br, 9 H), 58.6 (br, 3 H) δ; IR (KBr): 3094 (m), 2964 (m), 2924 (m), 2858 (m), 2533 (m, B-H), 1554 (s), 1472 (m), 1430 (m), 1403 (s), 1360 (m), 1184 (s), 1060 (s), 1030 (m), 996 (m), 884 (s), 815 (s), 784 (s), 754 (m), 717 (w), 669 (w), 642 (m), 502 (s), 490 (w), 472 (s) cm⁻¹; m.p. 180 – 182 °C; μ_{eff} = 4.9(1) μ_B (295 K); MS (LIFDI, THF): m/z 898.0522 [M⁺]. Calcd.: 898.0506 [M⁺];

Tp^{Fc,Me}FeBr (2): 1.000 g (0.989 mmol) of Tp^{Fc,Me}Tl and .235 g (1.577 mmol, 1.59 equiv.) of FeBr₂ were added to an agate mortar and ground to homogeneity for 2 hours. A color change is observed, to dark orange, with the formation of TlBr as a fine colorless salt. The mixture was dissolved in THF and filtered through celite. The material was then immediately dried in vacuo, to afford an orange solid. The solid residue was collected and washed 3 times with di-ethyl ether to remove borotropically rearranged products. The remaining orange residue was collected, and orange crystals of Tp^{Fc,Me}FeBr were grown from a solution of THF layered with pentane, giving a yield of .700 g (0.742 mmol, 75 %). ¹H-NMR (400 MHz, THF-d₈): 3.0 (br, 15 H), 3.3

(br, 6 H), 3.8 (br, 6 H), 27.8 (br, 9 H), 59.8 (br, 3 H) δ ; IR (KBr): 3097 (m), 2962 (m), 2922 (m), 2858 (m), 2536 (m, B-H), 1557 (s), 1514 (w), 1474 (m), 1431 (s), 1400 (s), 1361 (m), 1321 (w), 1260 (w), 1186 (s), 1107 (s), 1058 (s), 1030 (w), 1002 (m), 981 (w), 880 (m), 822 (s), 785 (m), 757 (m), 715 (w), 650 (m), 537 (m), 506 (s), 473 (w) cm^{-1} ; m.p. 184 – 187 $^{\circ}\text{C}$; $\mu_{\text{eff}} = 5.0(1) \mu_{\text{B}}$ (297 K); MS (LIFDI, THF): m/z 945.0001, 947.0026 [M^+]. Calcd.: 944.9985, 946.9969 [M^+]; Anal. Calcd for $\text{C}_{42}\text{H}_{40}\text{N}_6\text{B}_1\text{Fe}_4\text{Br}_1$ and one THF: C, 54.43; H, 4.77; N, 8.28. Found C, 54.34; H, 5.17; N, 7.88.

$\text{Tp}^{\text{Fc,Me}}\text{FeBr}$ (2) (alternate synthesis): 4.000 g (3.957 mmol) of $\text{Tp}^{\text{Fc,Me}}\text{Ti}$ and 1.000 g (4.637 mmol) of FeBr_2 were placed in a round bottom flask, to which 150 ml of THF was added. The mixture was left to stir for 90 minutes. It was then filtered through Celite to remove the TiBr salt, and all volatile material was then removed in vacuo. The orange residue was collected and washed three times with 30ml portions of ether, to removed borotropically rearranged products. The remaining orange solid was collected, and orange crystals of $\text{Tp}^{\text{Fc,Me}}\text{FeBr}$ were grown from a solution of THF layered with pentane and left at -35°C , giving a yield of 2.530 g (2.690 mmol, 68 %).

$\text{Tp}^{\text{Fc,Me}}\text{FeI}$ (3): 4.000 g (3.957 mmol) of $\text{Tp}^{\text{Fc,Me}}\text{Ti}$ and 1.358 g (4.381 mmol, 1.1 equiv.) of FeI_2 , which had been left for 10 hours in high vacuum to remove any I_2 impurity, were placed in a round bottom flask containing 100 ml of THF. The mixture was left to stir for 50 minutes, then the mixture was filtered through Celite to remove the TiI salt, and the solvent was then removed in vacuo. The orange residue was stirred in 70 ml of ether and the solid residue collected by filtration to removed borotropically rearranged products. The residue was added to THF and layered with

pentanes before being placed in a freezer at -35 °C. Orange crystals of $\text{Tp}^{\text{Fc,Me}}\text{FeI}$ grew after several days, giving a yield of 2.620 g (2.650 mmol, 67 %). $^1\text{H-NMR}$ (400 MHz, C_6D_6) 64.1 (br, 3H), 27.2 (br, 9H), 11.7 (br, 6H), 9.5 (br, 15H), 5.5 (br, 6H), -23.13 (br, 1H) δ ; IR (KBr): 3099 (m), 2974 (m), 2922 (m), 2864 (w), 2537 (m, B-H), 1557 (s), 1516 (w), 1470 (m), 1426 (s), 1402 (s), 1364 (m), 1349 (m), 1322 (w), 1261 (w), 1222 (w), 1209 (sh), 1184 (s), 1107 (s), 1058 (s), 1030 (s), 1002 (s), 983 (m), 885 (s), 859 (vw), 815 (s), 798 (sh), 788 (s), 758 (s), 715 (w), 673 (w), 648 (m), 639 (sh), 594 (w), 532 (s), 504 (s), 488 (s), 470 (s), 437 (s) cm^{-1} ; m.p. 181 – 183 °C; $\mu_{\text{eff}} = 5.0(1) \mu_{\text{B}}$ (298 K); MS (LIFDI, THF): m/z 989.9854 [M^+]. Calcd.: 989.9861 [M^+]; Anal. Calcd for $\text{C}_{42}\text{H}_{40}\text{B}_1\text{N}_6\text{Fe}_4\text{I}$: C, 50.96; H, 4.07; N, 8.49. Found C, 50.89; H, 4.12; N, 8.27.

$\text{Tp}^{\text{Fc,Me}}\text{CoBr}$ (4): 5.000 g (4.947 mmol) of $\text{Tp}^{\text{Fc,Me}}\text{Ti}$, 1.600 g (7.420 mmol, 1.5 equiv.) of CoBr_2 , and 400 ml of dry dichloromethane was added to a flame dried 1 L round bottom flask, and the mixture refluxed with stirring for 1 hour. The solution color changed from dark orange to bright green, signaling completion of the reaction. The solution was filtered twice through Celite to remove Ti salts, and then concentrated to ~150ml in vacuo. 300ml of dry diethyl ether was then added. Upon cooling to -35 °C for 30 hours the desired $\text{Tp}^{\text{Fc,Me}}\text{CoBr}$ crystallized out of the mixture as forest green crystals, with a yield of 3.405 g (3.597 mmol, 72.7 %). $^1\text{H-NMR}$ (400 MHz, THF-d_8) 74.0 (3H, br), 14.5 (9H, br), 13.2 (6H, br), 10.3 (6H, br), 5.0 (15H, br), -23.8 (1H, br) δ ; IR (KBr): 3097 (m), 2963 (w), 2923 (m), 2859 (w), 2539 (m, B-H), 1555 (vs), 1518 (w), 1470 (m), 1428 (s), 1402 (vs), 1371 (m), 1363 (m), 1349 (m), 1322 (w), 1263 (w), 1211 (w), 1183 (vs), 1106 (vs), 1058 (vs), 1031 (s), 1001 (s), 985 (m), 885 (m), 818 (s), 788 (s), 756 (m), 713 (w), 673 (w), 646 (sh), 648 (m), 534 (m), 505 (s), 490

(m), 472 (s), 438 (w) cm^{-1} ; m.p. 243 – 246 $^{\circ}\text{C}$; $\mu_{\text{eff}} = 3.9(1) \mu_{\text{B}}$ (293.15 K); MS (LIFDI, THF): m/z 945.0007, 946.9959 [M^+]. Calcd.: 944.9985, 946.9969 [M^+]; Anal. Calcd for $\text{C}_{42}\text{H}_{40}\text{B}_1\text{N}_6\text{Fe}_3\text{Co}_1\text{Br}_1$: C, 52.55; H, 4.2; N, 8.88. Found C, 52.02; H, 4.19; N, 8.53. Uv/Vis (λ_{max} (THF), ϵ): 330, 1747.7; 445, 792.7; 650, 482.5 (nm , $\text{cm}^{-1} \text{M}^{-1}$).

$\text{Tp}^{\text{Fc,Me}}\text{FeBn}$ (5): 1.000 g (1.061 mmol) of $\text{Tp}^{\text{Fc,Me}}\text{FeBr}$ was dissolved in 70 ml of 1,4-Dioxane, and stirred for 10 minutes. 1.14 ml of 2 M BnMgBr (2.280 mmol, 2.15 equiv.) in THF was added drop wise over 15 minutes. The solution was left to stir at room temperature for an additional 210 minutes, during which time a color change was observed to dark brown. The solution was then filtered through Celite, and all volatiles removed in vacuo. The remaining brown residue was dissolved in toluene, and filtered through Celite to remove any remaining magnesium salts. Dark orange crystals of the desired $\text{Tp}^{\text{Fc,Me}}\text{FeBn}$ were grown from a solution of toluene layered with pentane, giving a yield of 0.690 g (0.722 mmol, 68 %). $^1\text{H-NMR}$ (400 MHz, C_6D_6) -29.6 (br, 2H), -24.5 (br, 6H), -3.5 (br, 15H), 35.1 (br, 2H), 38.7 (br, 9H), 50.0 (br, 3H) δ ; IR (KBr): 3085 (m), 3061 (w), 3026 (m), 2924 (m), 2857 (w), 2535 (m, B-H), 1705 (m), 1601 (w), 1558 (s), 1495 (m), 1453 (s), 1425 (s), 1401 (s), 1363 (s), 1319 (m), 1262 (w), 1190 (br, s), 1106 (s), 1065 (s), 1029 (s), 1001 (s), 981 (w), 884 (m), 815 (s), 787 (s), 755 (s), 699 (s), 647 (m), 583 (w), 524 (m), 503.99 (s), 490.66 (s), 470.45 (m) cm^{-1} ; m.p. 184 – 186 $^{\circ}\text{C}$; $\mu_{\text{eff}} = 3.9(1) \mu_{\text{B}}$ (295 K); MS (LIFDI, THF): m/z 954.1367 [M^+]. Calcd.: 954.1407 [M^+]; Anal. Calcd for $\text{C}_{49.84}\text{H}_{47.96}\text{N}_6\text{B}_1\text{Fe}_4$ (toluene is observed in the crystal asymmetric unit, but partially de-solvates under vacuum): C, 62.02; H, 5.01; N, 8.71. Found C, 61.66; H, 5.21; N, 8.21.

Tp^{Fc,Me}FeEt (6): 0.500 g (0.506 mmol) Tp^{Fc,Me}FeI was put in a flask with 60 ml of 1,4-dioxane, and stirred for 30 minutes. To this solution was added 0.53 ml of 2 M EtMgCl in THF (1.060 mmol, 2.1 eq), added in two increments, the first of which being 1.1 eq over the course of 5 minutes, the second being 1 eq added dropwise 30 minutes later. After 2.5 hours the reaction was ended by removal of solvent in vacuo. The orange residue was dissolved in toluene and then filtered through celite to remove magnesium salts. The toluene was removed in vacuo and the resulting orange solid was pure enough to use without further work up, but analytical samples could be prepared by recrystallization from THF/pentanes solution, with a yield of 0.392 g (0.440 mmol, 87 %). ¹H-NMR (400 MHz, C₆D₆) 45.5 (br, 3H), 43.3 (br, 9H), 1.24 (br, 6H), -8.21 (br, 15H), -28.9 (br, 6H) δ; IR (KBr): 3098 (m), 2953 (m), 2922 (m), 2883 (sh), 2854 (m), 2524 (m, B-H), 1635 (w), 1560 (st), 1515 (m), 1468 (m), 1428 (st), 1401 (st), 1370 (sh), 1362 (st), 1349 (st), 1323 (m), 1224 (w), 1207 (sh), 1184 (s, br), 1107 (st), 1058 (st), 1026 (st), 1001 (st), 981 (m), 886 (st), 812 (st), 799 (sh), 784 (st), 760 (st), 718 (w), 675 (w), 649 (m), 637 (m), 530 (st), 504 (st), 491 (st), 472 (st), 442 (m) cm⁻¹; m.p. >315 °C; μ_{eff} = 4.0(1) μ_B (293.15 K); MS (LIFDI, THF): m/z 892.1265 [M⁺]. Calcd.: 892.1208 [M⁺]; Anal. Calcd for C₄₄H₄₅B₁N₆Fe₄Mg_{0.5}Cl₁: C, 56.24; H, 4.83; N, 8.94. Found C, 56.77; H, 5.1; N, 8.97.

Tp^{Fc,Me}Fe(CO) (7): 0.500 g (0.524 mmol) of Tp^{Fc,Me}FeBn was dissolved in toluene and added to a Schlenk tube. The mixture was thoroughly degassed and then frozen. 1 atm of CO gas was added over the frozen mixture, which was then allowed to warm to room temperature with stirring. A color change was observed from dark orange to bright yellow. All volatiles were removed in vacuo with stirring, to afford a

yellow/orange solid residue. The residue was washed with a minimal amount of THF to remove any starting material or impurities present in the starting material, and collected by filtration. Crystals of the desired $\text{Tp}^{\text{Fc,Me}}\text{FeCO}$ complex were grown from a solution of THF layered with pentane, giving a yield of 0.390 g (0.441 mmol, 84 %). $^1\text{H-NMR}$ (400 MHz, THF-d_8) 39.5 (br, 9H), 7.0 (br, 15H), -11.2 (br, 3H) δ ; IR (KBr): 3097 (m), 2961 (m), 2922 (m), 2860 (m), 2533 (m, B-H), 1891 (vs, C-O), 1560 (s), 1517 (w), 1466 (m), 1424 (m), 1396 (m), 1322 (w), 1182 (s), 1108 (sharp), 1062 (s), 1034 (w), 1003 (m), 984 (w), 890 (m), 820 (m), 785 (m), 762 (m), 641 (m), 532 (w), 505 (m), 485 (w), 470 (w) cm^{-1} ; m.p. 291 – 294 °C dec; $\mu_{\text{eff}} = 4.0(1) \mu_{\text{B}}$ (295 K);

$\text{Tp}^{\text{Fc,Me}}\text{Fe}(\text{PzH}^{\text{Fc,Me}})(\text{Pz}^{\text{Fc,Me}})$ (8): 0.300 g (0.303 mmol) of $\text{Tp}^{\text{Fc,Me}}\text{FeI}$ was added to a stirring solution of THF, along with 92 mg of $\text{Kpz}^{\text{Fc,Me}}$ (0.303 mmol, 1 equiv.) and 81 mg of $\text{Hpz}^{\text{Fc,Me}}$ (0.303 mmol, 1 equiv.). After stirring for 1 hour the solution became increasingly dark in color and opaque with the formation of potassium salt. The mixture was left to stir for 24 hours, then filtered to remove potassium salts. The solution was concentrated in vacuo and layered with pentanes to afford the desired complex as orange blocks, with a yield of 0.130 g (0.093 mmol, 31 %) $^1\text{H-NMR}$ (400 MHz, C_6D_6) 52.8 (br, 2H), 44.4 (br, 6H), 32.3 (br, 3H), 16.6 (br, 9H), 6.6 (br, 10H), 4.7 (br, 4H), 1.9 (br, 15H), -3.9 (br, 6H), -39.43 (4, br) δ ; IR (KBr): 3308 (m, N-H), 3089 (m), 2968 (m), 2922 (m), 2864 (m), 2555 (m, B-H), 1594 (w), 1558 (s), 1515 (w), 1485 (m), 1470 (m), 1429 (s), 1403 (s), 1365 (s), 1350 (m), 1319 (w), 1276 (w), 1227 (w), 1204 (sh), 1178 (s), 1117 (sh), 1108 (s), 1084 (m), 1071 (s), 1048 (s), 1037 (s), 1023 (s), 1001 (s), 985 (m), 887 (s), 874 (sh), 814 (s), 787 (s), 760 (m), 708 (m), 674 (w), 648 (m), 635 (m), 586 (w), 521 (w), 499 (s), 468 (m), 436 (w) cm^{-1} ; m.p. 205

– 207 °C dec.; $\mu_{\text{eff}} = 4.9(1) \mu_{\text{B}}$ (296 K); MS (LIFDI, THF): m/z 1128.1191 [M^+].
Calcd.: 1128.1251 [$\text{M}^+ - \text{C}_{14}\text{H}_{14}\text{N}_2\text{Fe}_1$]; Anal. Calcd for $\text{C}_{70}\text{H}_{67}\text{B}_1\text{N}_{10}\text{Fe}_6\text{O}_2$ (This complex is extremely sensitive to oxygen gas, the elemental analysis matches the incorporation of O_2): C, 58.95; H, 4.73; N, 9.82. Found C, 58.98; H, 4.83; N, 9.60

[Tp^{Fc,Me}Fe^I]₂(μ_2 - η^1 : η^1 -N₂) (9): 186 mg of sodium metal (80.90 mmol) were added to 15.5 g of mercury, to create a 1.2 % w/w Na/Hg amalgam, which was then added to 100 ml of THF with stirring and left for 10 minutes. To this solution, 2.000 g (2.022 mmol) of Tp^{Fc,Me}FeI was added. The mixture was stirred vigorously for 160 hours, over which time a color change from orange to red was observed. The solution was filtered to remove NaI salt and Hg, and all volatiles removed in vacuo. The red/orange solid was extracted with ether and filtered to remove all remaining starting material as well as any NaI that remained dissolved in the THF solution. The ether solvent was removed in vacuo and the resulting red residue was dissolved in THF. The solution was concentrated, pentane was added as a layer, and the combined solution cooled to -35 °C to afford [Tp^{Fc,Me}Fe^I]₂(μ_2 - η^1 : η^1 -N₂) as blood red blocks, with a yield of 1.380 g (0.789 mmol, 78 %). ¹H-NMR (400 MHz, C₆D₆) -23.1 (br, 6H), -8.1 (br, 15H), 22.8 (br, 6H), 53.3 (br, 9H), 59.0 (br, 3H) δ ; IR (KBr): 3093 (m), 2971 (m), 2923 (m), 2861 (m), 2525 (m, B-H), 1970 (w, N=N), 1560 (s), 1517 (w), 1465 (m), 1429 (s), 1400 (s), 1372 (s), 1361 (s), 1349 (sh), 1321 (m), 1262 (vw), 1208 (sh), 1182 (s, br), 1106 (s), 1059 (s), 1025 (m), 1000 (s), 980 (m), 882 (s), 815 (s), 776 (s), 754 (m), 715 (w), 675 (w), 644 (m), 569 (s, br), 530 (s), 505 (s), 490 (s), 472 (m), 438 (m) cm^{-1} ; m.p. 255 – 257 °C dec; $\mu_{\text{eff}} = 5.9(1) \mu_{\text{B}}$ (293 K); Anal. Calcd for $\text{C}_{42}\text{H}_{40}\text{B}_1\text{N}_7\text{Fe}_4$: C, 57.51; H, 4.60; N, 11.18. Found C, 56.91; H, 4.95; N, 9.53. Found C, 57.01; H, 4.20; N, 9.26.

Found C, 57.82; H, 4.81; N, 9.71. This compound is highly sensitive to oxygen and moisture, and prone to decomposition by loss of N₂, after submitting the sample for three separate analyses, it was deemed too fragile for elemental analysis.

[Tp^{Fc,Me}Co^I]₂(μ₂-η¹:η¹-N₂) (10): 77 mg (3.043 mmol) of sodium metal was added to 7.800 g of Hg, to create a 1.0 % w/w Na/Hg amalgam, which was then added to 100 ml of THF with stirring and left for 10 minutes. To this solution, 2.000 g (2.116 mmol) of Tp^{Fc,Me}CoBr was added. The mixture was stirred vigorously for 130 minutes at which time a color change from green to dark orange was observed. The solution was filtered to remove NaBr salt and Hg, and all volatiles were then removed in vacuo. The orange solid was triturated with 80ml of ether and the suspension filtered. The remaining solid was re-dissolved in THF and crystallized with the addition of pentanes at -35 °C to produce [Tp^{Fc,Me}Co^I]₂(μ₂-η¹:η¹-N₂) as dark orange crystals having 10 molecules of THF per asymmetric unit. The ether used for trituration was concentrated and pentane was added as a layer to afford additional [Tp^{Fc,Me}Co^I]₂(μ₂-η¹:η¹-N₂) as dark orange crystals, the combined yield of both portions being 1.280 g (0.073 mmol, 68.8 %). ¹H-NMR (400 MHz, C₆D₆) 47.8 (br, 3H), 30.4 (br, 1H, B-H), 18.4 (br, 9H), 5.9 (br, 6H), -0.2 (br, 15H), -3.9 (br, 6H) δ; IR (KBr): 3093 (m), 2955 (m), 2921 (m), 2868 (w), 2517 (m, B-H), 2070 (m, N=N), 1561 (s), 1517 (m), 1465 (m), 1428 (s), 1395 (s), 1373 (m), 1360 (s), 1321 (m), 1262 (vw), 1221 (m), 1185 (vs), 1106 (s), 1059 (vs), 1023 (m), 1000 (s), 980 (m), 882 (s), 815 (s), 780 (s), 759 (s), 716 (w), 646 (m), 673 (sh), 530 (m), 503 (s), 490 (s), 471 (m), 437 (m) cm⁻¹; m.p. 226 – 228 °C dec; μ_{eff} = 4.9(1) μ_B (298 K); Anal. Calcd for C₄₆H₄₈B₁N₇Fe₃Co₁O₁ (Crystals grown from ether were used, they contained 1 ether molecule per molecule of

[Tp^{Fc,Me}Co^I]₂(μ₂-η¹:η¹-N₂): C, 57.90; H, 5.28; N, 10.28. Found C, 58.14; H, 5.14; N, 10.13. Uv/Vis (λ_{max}(THF), ε): 280, 6960.0; 450, 105.5 (nm, cm⁻¹ M⁻¹).

Bp^{Fc,Me}(Me-pz-CpFe(C₅H₄))Co (11): 0.500 g (0.053 mmol) of Tp^{Fc,Me}CoBr was dissolved with stirring in 18 ml of THF, to this was added dropwise over 4 minutes 0.55 ml of a 1 M solution of KB(Et)₃H in THF (0.550 mmol, 1 equiv.). The solution was left to stir for 16 hours, during which time the color of the solution changed from forest green to olive green. The solution was filtered through a plug of Celite to remove potassium salts, and the volatiles removed in vacuo. The resulting green residue was washed with 5 ml of ether three times to remove impurities, and the remaining green solid re-dissolved in 8 ml of THF and then filtered through Celite a second time. The resulting green THF solution was then layered with 6 ml of diethyl ether and 4 ml of pentane, which left at room temperature for 3 to 6 days give the product in the form of small green blockish crystals, with a yield of 0.248 g, (0.029 mmol, 54 %). ¹H-NMR (400 MHz, C₆D₆) 62.5 (br, 1H), 60.3 (br, 2H), 56.6 (br, 2H), 21.7 (br, 6H), 17.3 (br, 2H), 15.6 (br, 3H), 5.2 (br, 2H), -0.3 (br, 10H), -1.1 (br, 2H), -2.8 (br, 2H), -14.8 (br, 2H), -23.4 (br, 2H) δ; IR (KBr): 3101 (m), 2973 (m), 2918 (m), 2868 (m), 2560 (m, B-H), 1561 (s), 1517 (w), 1469 (m), 1431 (m), 1402 (m), 1373 (sh), 1358 (m), 1325 (w), 1175 (s), 1106 (s), 1063 (s), 1029 (s), 1029 (m), 1001 (m), 985 (m), 888 (m), 820 (m), 796 (m), 757 (m), 716 (w), 676 (w), 645 (m), 534 (m), 501 (s), 473 (s), 438 (m) cm⁻¹; m.p. >315 °C; μ_{eff} = 3.7(1) μ_B (298 K); MS (LIFDI, THF): m/z 865.0700 [M]. Calcd.: 865.0720 [M]; Anal. Calcd for C₄₄H₄₃B₁N₆Fe₃Co₁O₅ (Ether was present in the crystals sent for elemental analysis, in a ratio of 1:2 ether to

$\text{Bp}^{\text{Fc,Me}}(\text{Me-pz-CpFe}(\text{C}_5\text{H}_4))\text{Co}$: C, 58.54; H, 4.92; N, 9.32. Found C, 58.36; H, 5.07; N, 9.05. Uv/Vis ($\lambda_{\text{max}}(\text{THF}), \epsilon$): 450, 907.5; 715, 640.2 (nm, $\text{cm}^{-1} \text{M}^{-1}$).

$\text{Bp}^{\text{Fc,Me}}(\text{Me-pz-CpFe}(\text{C}_5\text{H}_4))\text{Co}(\text{CO})$ (12): 0.400 g (0.046 mmol) of $\text{Bp}^{\text{Fc,Me}}(\text{Me-pz-CpFe}(\text{C}_5\text{H}_4))\text{Co}$ was dissolved in 20 ml of THF in a schlenk tube that was charged with a magnetic stir bar. The mixture was thoroughly degassed and then .9 atm of carbon monoxide gas were introduced at room temperature, while the mixture was stirred. The solution rapidly changed color from green to dark orange, and after 20 minutes was freeze pump thaw degassed in three cycles to remove the remaining carbon monoxide. The mixture was then brought into a glove box and the solvents removed in vacuo. The remaining orange residue was re-dissolved in ether, filtered, and then layered with pentanes to afford crystals of the desired $\text{Bp}^{\text{Fc,Me}}(\text{Me-pz-CpFe}(\text{C}_5\text{H}_4))\text{Co}(\text{CO})$ complex, with a yield of 0.297g (0.033 mmol, 72 %). $^1\text{H-NMR}$ (400 MHz, C_6D_6) 21.5 (br, 1H), 10.6 (br, 2H), 4.1 (br, 4H), 3.5 (br, 4H), 3.1 (br, 10H), 1.1 (br, 2H), 0.87 (br, 6H), -0.29 (br, 2H) δ ; IR (KBr): 3080 (m), 2963 (m), 2922 (m), 2852 (m), 2517 (m, B-H), 2021 (vs, C=O), 1558 (s), 1514 (m), 1466 (m), 1425 (s), 1399 (s), 1372 (s), 1350 (s), 1317 (m), 1223 (w), 1185 (vs, br), 1106 (s), 1059 (s), 1021 (m), 1001 (m), 977 (w), 891 (m), 882 (m), 864 (w), 808 (s), 790 (s), 717 (w), 677 (w), 644 (s), 550 (w), 527 (w), 491 (s), 471 (s), 444 (w) cm^{-1} ; m.p. 307 – 309 °C; $\mu_{\text{eff}} = 2.0(1) \mu_{\text{B}}$ (293 K); MS (LIFDI, THF): m/z 865.0822 [M - CO]. Calcd.: 865.0720 [M - CO]; Anal. Calcd for $\text{C}_{43}\text{H}_{39}\text{B}_1\text{N}_6\text{Fe}_3\text{Co}_1\text{O}_1$: C, 57.87; H, 4.40; N, 9.41. Found C, 57.94; H, 4.45; N, 9.18. Uv/Vis ($\lambda_{\text{max}}(\text{THF}), \epsilon$): 320, 3229.3; 414.9, 1002.6 (nm, $\text{cm}^{-1} \text{M}^{-1}$).

REFERENCES

1. a) Egan, J. W.; Haggerty, B. S.; Rheingold, A. L.; Sendlinger, S. C.; Theopold, K. H. *J. Am. Chem. Soc.*, **1990**, *112*, p. 2445 – 2446; b) Hagadorn, J. R.; Arnold, J. J. *J. Am. Chem. Soc.*, **1996**, *118*, p. 893 – 894; c) Teller, D. M.; Bergman, R. G., *J. Am. Chem. Soc.*, **2000**, *122*, p. 954 – 955; d) Thyagarajan, S.; Incarvito, C. D.; Rheingold, A. L.; Theopold, K. H., *Inorganica Chimica Acta*, **2003**, *345*, p. 333 – 339; e) Monillas, W. H.; Yap, G. P. A.; MacAdams, L. A.; Theopold, K. H., *J. Am. Chem. Soc.*, **2007**, *129*, p. 8090 – 8091; f) Yao, S.; Herwig, C.; Xiong, Y.; Company, A.; Bill, E.; Limberg, C.; Driess, M., *Angew. Chem. Int. Ed.*, **2010**, *49*, p. 7054 – 7058; g) Milsmann, C.; Turner, Z. R.; Semproni, S. P.; Chirik, P. J., *Angew. Chem. Int. Ed.*, **2012**, *51*, p. 5386 – 5390.
2. a) Teller, D. M.; Bergman, R. G., *J. Am. Chem. Soc.*, **2000**, *122*, p. 954 – 955; b) Monillas, W. H.; Yap, G. P. A.; MacAdams, L. A.; Theopold, K. H., *J. Am. Chem. Soc.*, **2007**, *129*, p. 8090 – 8091.
3. a) Akturk, E. S.; Yap, G. P. A.; Theopold, K. H., *Chem. Comm.*, **2015**, *51*, p. 15402 – 15405; b) E. S. Akturk, Ph. D. Thesis, University of Delaware, (Newark, DE), USA, **2016**.
4. E. R. Sirianni, Ph. D. thesis, University of Delaware (Newark, DE), USA, **2014**.
5. Thyagarajan, S.; Incarvito, C. D.; Rheingold, A. L.; Theopold, K. H., *Chem. Commun.*, **2001**, p. 2198 – 2199.
6. F. A. Jove, Ph. D. thesis, University of Delaware (Newark, DE), **2008**
7. J. D. Detrich, Ph. D. thesis, University of Delaware (Newark, DE), **1996**
8. J. D. Jewson, L. M. Liable-Sands, G. P. A. Yap, A. L. Rheingold and K. H. Theopold, *Organometallics*, **1999**, *18*, p. 300.
9. Sirianni, E. R.; Yap, G. P. A.; Theopold, K. H., *Inorg. Chem.*, **2014**, *53*, p. 9424 – 9430.

10. Kolotilov, S. V.; Addison, A. W.; Trofimenko, S.; Dougherty, W.; Pavlishchuk, V. V., *Inorg. Chem. Commun.*, **2004**, 7, p. 485 – 488.
11. DuPont, J. A.; Coxey, M. B.; Schebler, P. J.; Incarvito, C. D.; Dougherty, W. G.; Yap, G. P. A.; Rheingold, A. L.; Riordan, C. G., *Organometallics*, **2007**, 26, p. 971.
12. Detrich, J. L.; Konečný, R.; Vetter, W. M.; Doren, D.; Rheingold, A. L.; Theopold, K. H., *J. Am. Chem. Soc.*, **1996**, 118, 1703-1712
13. Langer, J.; Krieck, S.; Fischer, R.; Görls, H.; Walther, D.; Westerhausen, M., *Organometallics*, **2009**, 28, p. 5814.
14. Kisko, J. L.; Hascall, T.; Parkin, G., *J. Am. Chem. Soc.*, **1998**, 120 (40), p. 10561 – 10562.
15. Huheey, James E.; Keiter, Ellan A.; Keiter, Richard L.; *Inorganic Chemistry: Principles of Structure and Reactivity*, 4th Ed., Harper Collins College, Appendix A-28, ISBN: 0-06-042995-x
16. Mussini, T.; Longhi, P.; Rondini, S., *Pure & Appl. Chem.*, **1985**, 57, No. 1, p. 169 – 179.
17. Laplaza, C. E.; Johnson, M. J. A.; Peters, J. C.; Odom, A. L.; Kim E.; Cummins, C. C.; George, G. N.; Pickering, I. J., *J. Am. Chem. Soc.*, **1996**, Vol. 118, No. 36, p. 8623 – 8638.
18. S. A. Stoian, J. Vela, J. M. Smith, A. R. Sadique, P. L. Holland, E. Munck, E. L. Bominaar, *J. Am. Chem. Soc.*, **2006**, 128, p. 10181 – 10192.
19. Calabrese, J. C.; Trofimenko, S., *Inorg. Chem.*, **1992**, 31, p. 4810 – 4814.
20. Cummins, D. C.; Yap, G. P. A.; Theopold, K. H., *Euro. J. Inor. Chem.*, **2016**, (15-16), 2349 – 2356.
21. McSkimming, A.; Harman, W. H., *J. Am. Chem. Soc.*, **2015**, 137, p. 8940 – 8943.
22. Addison, A. W.; Rao, N. T.; Reedijk, J.; van Rijn, J.; Verschoor, G. C., *J. Chem. Soc., Dalton Tans.*, **1984**, 0, p. 1349 – 1356.
23. a) Neronov, Y. I.; Karshenboim, S. G., *Phys. Lett. A*, **2003**, 318, p. 126 – 132; b) Chen, J. Y.-C.; Martí, A. A.; Turro, N. J.; Komatsu, K.; Murata, Y.; Lawler, R. G., *J. Phys. Chem. B*, **2010**, 114, p. 14689 – 14695.

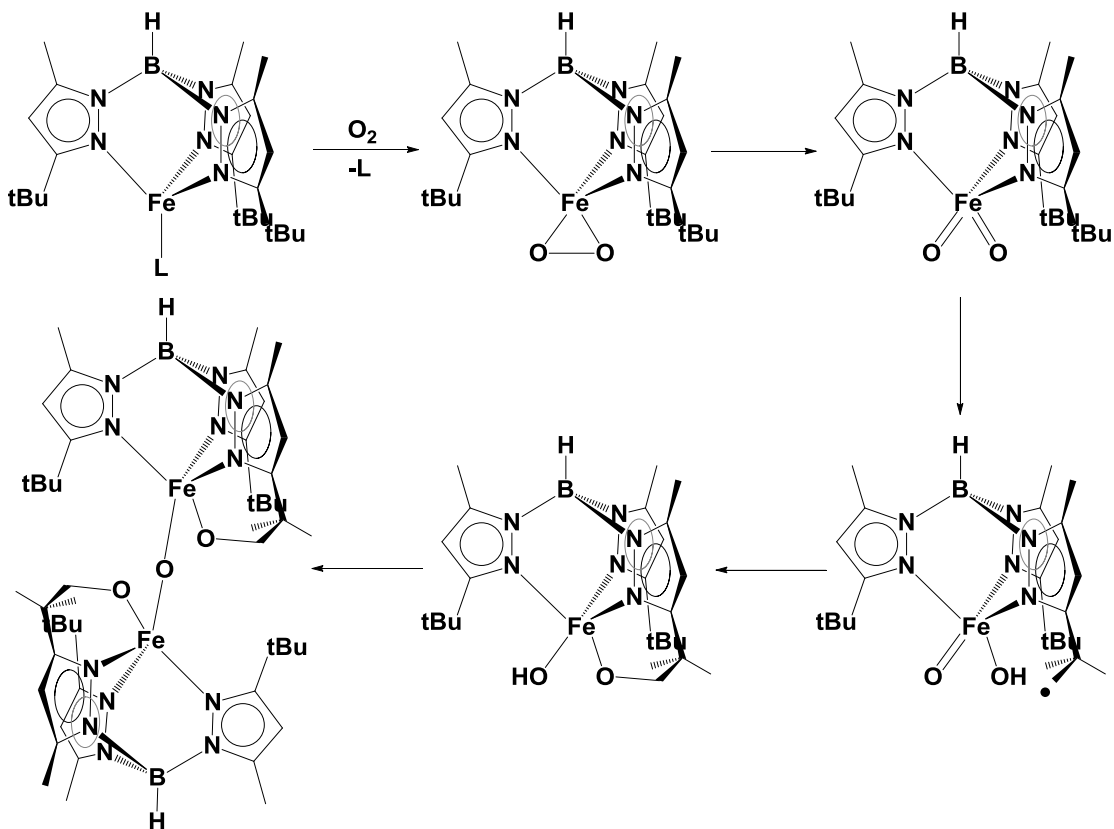
24. a) Smith, J. S.; Lachicotte, R. J.; Holland, P. L., *J. Am. Chem. Soc.*, **2003**, 125 (51), p. 15752 – 15753; b) Vela, J.; Smith, J. M.; Yu, Y.; Ketterer, N. A.; Flaschenriem, C. J.; Lachicotte, R. J.; Holland, P. L., *J. Am. Chem. Soc.*, **2005**, 127 (21), p. 7857 – 7870.
25. Pangborn, A. B.; Giardello, M. A.; Grubbs, R. H.; Rosen, R. K.; Timmers, F. J., *Organometallic*, **1996**, 15, p. 1518 – 1520.
26. Bain, G. A.; Berry, J. F., *J. Chem. Educ.*, **2008**, 85, No. 4, p. 532 – 536.
27. Apex2, Bruker-AXS Inc, Madison, WI, p. 2007.
28. Sheldrick, G.M., *Acta Cryst.*, **2008**, A64, p. 112.

Chapter 3

REACTIONS OF LOW VALENT IRON AND COBALT COMPLEXES SUPPORTED BY HYDROTRIS(3-FERROCENYL-5-METHYL)PYRAZOLYL BORATO LIGANDS WITH OXO AND IMIDO TRANSFER REAGENTS

INTRODUCTION

The activation of dioxygen has gained significant interest to both academia and industry. The use of first row transition metals to activate O₂ and then transfer single oxygen atoms to substrates and thus create more valuable compounds has driven a significant fraction of research in this area.¹ In the service of furthering knowledge of oxygen activation, we set about attempting to produce additional novel oxo complexes on both iron and cobalt, building on work previously done in this laboratory. With regard to cobalt and iron, previous members of the Theopold Lab have found that oxo species of these late transition metals are too reactive to be supported by many of the Tp ligands we have previously used.² The most persistent issue is C-H bond activation of the ligand. The use of a more robust ligand bearing ferrocenyl substituents at the 3rd position of the pyrazole moiety may overcome this problem which was observed with O₂ activation on iron by Dr. Fernando Jove, see **Scheme 2.1**.³ The first aim of this chapter is to examine the reactivity of compounds introduced in **Chapter 2** with oxygen gas, explore various means to produce novel metal oxo complexes, and to study the properties of such compounds.



Scheme 2.1: Suggested mechanism for the formation of an Fe^{III}/Fe^{III} bridging oxo species supported by Tp^{tBu,Me}, taken from the thesis of Dr. Fernando Jove.

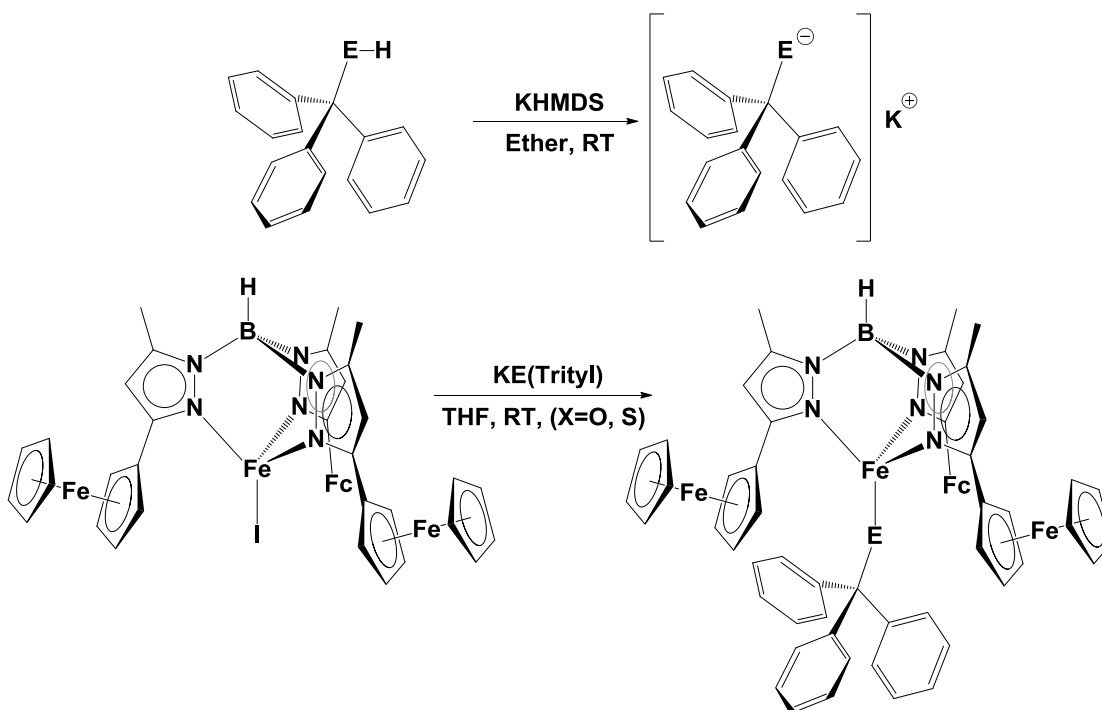
(L = CO, N₂, or C₂H₄).³

Of similar interest to terminal oxo complexes are metal imides. Being isoelectronic to terminal oxo species, they provide an often more easily accessed route to studying the chemistry of these moieties.⁴ Terminal imides are also the intermediates of aziridine synthesis done with transition metal catalysts.⁵ The second aim of this chapter is to explore methods of terminal imide production on iron and cobalt centers supported by the Tp^{Fc,Me} ligand system.

RESULTS AND DISCUSSION

Synthesis of triphenylmethyl chalcogenide iron complexes supported by $\text{Tp}^{\text{Fc,Me}}$ and reaction to form novel bridging sulfide complex. In an effort that ran concurrent to the production of low valent complexes of iron supported by the $\text{Tp}^{\text{Fc,Me}}$ ligand system, I set about producing Fe^{II} chalcogenide complexes. This was inspired by work done in the Hayton group, wherein they used a reductive deprotection of a Ni^{II} trityl sulfide to produce a formally Ni^{II} terminal sulfide complex supported by the $[2,6\text{-}^i\text{Pr}_2\text{C}_6\text{H}_3\text{NC}(\text{Me})_2\text{CH}(\text{NacNac})]$ ligand. In that work a $(\text{NacNac})\text{NiS}(\text{CPh}_3)$ complex is reacted with a K containing reducing agent in the presence of either 18-crown-6, 2,2,2-cryptand, or other encapsulating ligands, to form the anionic Ni^{II} terminal sulfide.⁶ Hoping to find similar results on iron, I synthesized both $\text{Tp}^{\text{Fc,Me}}\text{FeO}(\text{CPh}_3)$ (**13**) and $\text{Tp}^{\text{Fc,Me}}\text{FeS}(\text{CPh}_3)$ (**14**), by a route shown in **Scheme 2.2**. **13** is produced in modest yields, by reaction of the potassium salt of triphenylmethoxide with either $\text{Tp}^{\text{Fc,Me}}\text{FeBr}$ (**2**) or $\text{Tp}^{\text{Fc,Me}}\text{FeI}$ (**3**) in THF. After 30 minutes the solution color had changed between shades of orange and the mixture was filtered, then all volatile material was removed in vacuo before the complex was extracted with ether and then layered with pentanes to afford **13** as dark orange blocks. The structure of that complex was determined by X-ray crystallography and found to contain 2 molecules of **13** per asymmetric unit having bond lengths and angles that are the same to within error. The complex was tetrahedral, with geometry index values for **13** where $\tau_4 = 0.743$ and $\tau_4' = 0.700$,⁷ see **Figure 2.1** and **Table 2.1**. The procedure for synthesizing **14** was the same as that for **13**, but layering with pentanes was not necessary to afford X-ray quality crystals, which instead grew from concentrated ether solutions. The structure of **14** was determined by X-ray crystallography, and was

found to have a considerably different unit cell from that of **13**, see **Table B.1** and **Table B.2**, which may account for the difference in solubility and propensity for crystallization from ether. Similar to **13**, **14** was tetrahedral with the Tp ligand binding in a κ^3 manner, with geometry index values of $\tau_4 = 0.730$ and $\tau_4' = 0.681$,⁷ see **Figure 2.2** and **Table 2.2**. The structural differences between **13** and **14** was apparent in the Fe-E-CPh₃ bond angles, being 157.4(2)^o and 108.4(1)^o for **13** and **14** respectively. The most unexpected aspect of **13** and **14** were their low effective magnetic moments, with **13** having a μ_{eff} of 2.4(1) μ_{B} (296 K), and complex **14** displaying a μ_{eff} of 4.6(1) μ_{B} (295 K).



Scheme 2.2: Synthesis of KE(CPh₃) (E = O, S) and their reaction with **3**, synthesis of Tp^{Fc,Me}FeE(CPh₃), E = O (**13**), E = S (**14**).

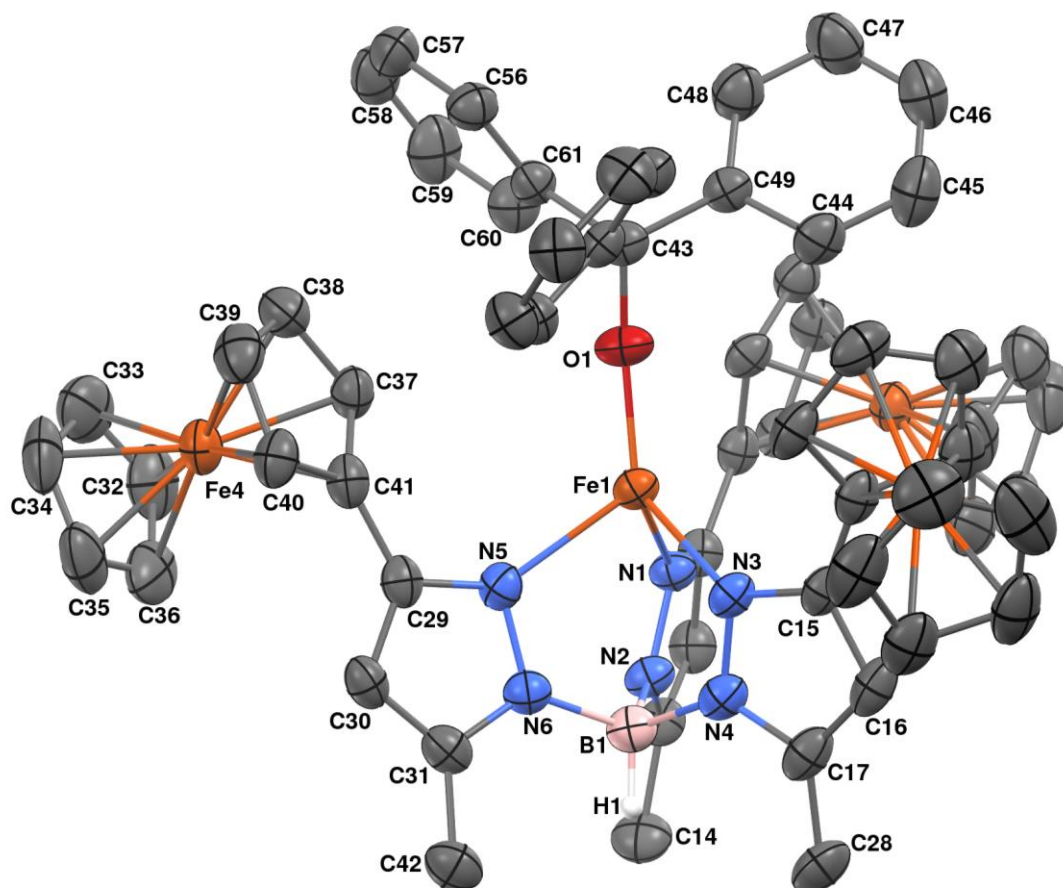


Figure 2.1: Molecular structure of $\text{Tp}^{\text{Fc,Me}}\text{FeO}(\text{CPh}_3)$ (13) represented as 50% probability thermal ellipsoids. Hydrogen atoms (with the exception of the hydrogens attached to boron, H1), and a second molecule of 13 present in the asymmetric unit have been omitted for clarity.

Table 2.1: Selected interatomic distances (\AA) and angles ($^\circ$) for $\text{Tp}^{\text{Fc,Me}}\text{FeO}(\text{CPh}_3)$ (13).

Distances (\AA)			
Fe1-O1	1.826(2)	Fe1-N3	2.115(2)
Fe1-N1	2.133(2)	Fe1-N5	2.144(2)
N1-C1	1.352(3)	N1-N2	1.376(3)
N3-C15	1.351(4)	N2-B1	1.547(4)

N4-C17	1.346(4)	N3-N4	1.377(3)
N5-C29	1.346(3)	N4-B1	1.544(4)
N6-C31	1.355(3)	N5-N6	1.381(3)
O1-C43	1.393(3)	N6-B1	1.539(4)
C29-C30	1.392(4)	C15-C16	1.386(4)
C30-C31	1.373(4)	C16-C17	1.383(4)
C31-C42	1.496(4)	C17-C28	1.492(4)
C32-C33	1.401(5)	C29-C41	1.463(4)
C33-C34	1.412(5)	C32-C36	1.392(5)
C34-C35	1.395(5)	C37-C41	1.421(4)
C35-C36	1.396(5)	C43-C49	1.539(4)
C37-C38	1.421(4)	C44-C49	1.390(4)
C38-C39	1.412(4)	C45-C46	1.374(5)
C39-C40	1.406(4)	C46-C47	1.367(5)
C40-C41	1.424(4)	C47-C48	1.386(4)
C43-C61	1.544(4)	C48-C49	1.378(4)
C44-C45	1.380(4)	C57-C58	1.367(5)
C59-C60	1.382(4)	C58-C59	1.364(5)
C60-C61	1.388(4)		

Angles (°)

B1-Fe1-O1	170.5(2)	Fe1-O1-C43	157.4(2)
O1-Fe1-N3	134.51(10)	O1-Fe1-N1	119.30(9)
N3-Fe1-N1	88.90(9)	N1-N2-B1	120.2(2)
N3-Fe1-N5	91.50(9)	C17-N4-N3	110.2(3)
C15-N3-N4	106.5(2)	N3-N4-B1	121.3(2)
C17-N4-B1	128.2(3)	C31-N6-N5	109.7(2)
C29-N5-N6	106.0(2)	N5-N6-B1	120.8(2)
C31-N6-B1	129.4(3)	N6-B1-N4	109.7(2)
N6-B1-N2	110.4(3)	N3-C15-C16	109.2(3)
N2-B1-N4	107.7(2)	N4-C17-C16	107.2(3)
C17-C16-C15	106.9(3)	C16-C17-C28	130.4(3)
N4-C17-C28	122.4(3)	N5-C29-C41	121.9(3)
N5-C29-C30	110.1(3)	C31-C30-C29	106.1(3)
C30-C29-C41	128.0(3)	N6-C31-C42	122.2(3)
N6-C31-C30	108.0(3)	C36-C32-C33	107.8(4)
C30-C31-C42	129.8(3)	C32-C33-C34	107.6(4)
C37-C41-C29	128.3(3)	C35-C34-C33	108.1(4)
O1-C43-C61	108.4(2)	C36-C35-C34	107.6(4)
C46-C45-C44	120.1(3)	C32-C36-C35	108.9(4)

C46-C47-C48	120.3(4)	C41-C37-C38	108.2(3)
C48-C49-C44	117.2(3)	C39-C38-C37	107.5(3)
C44-C49-C43	119.2(3)	C40-C39-C38	108.8(3)
C58-C59-C60	120.8(3)	C39-C40-C41	108.0(3)
C60-C61-C43	118.4(3)	C37-C41-C40	107.4(3)
C59-C58-C57	120.0(3)	C40-C41-C29	124.3(3)
C59-C60-C61	120.2(3)	O1-C43-C49	109.7(2)
C47-C46-C45	119.4(3)	C49-C43-C61	109.5(2)
C47-C48-C49	121.5(3)	C45-C44-C49	121.5(3)
C48-C49-C43	123.6(3)		

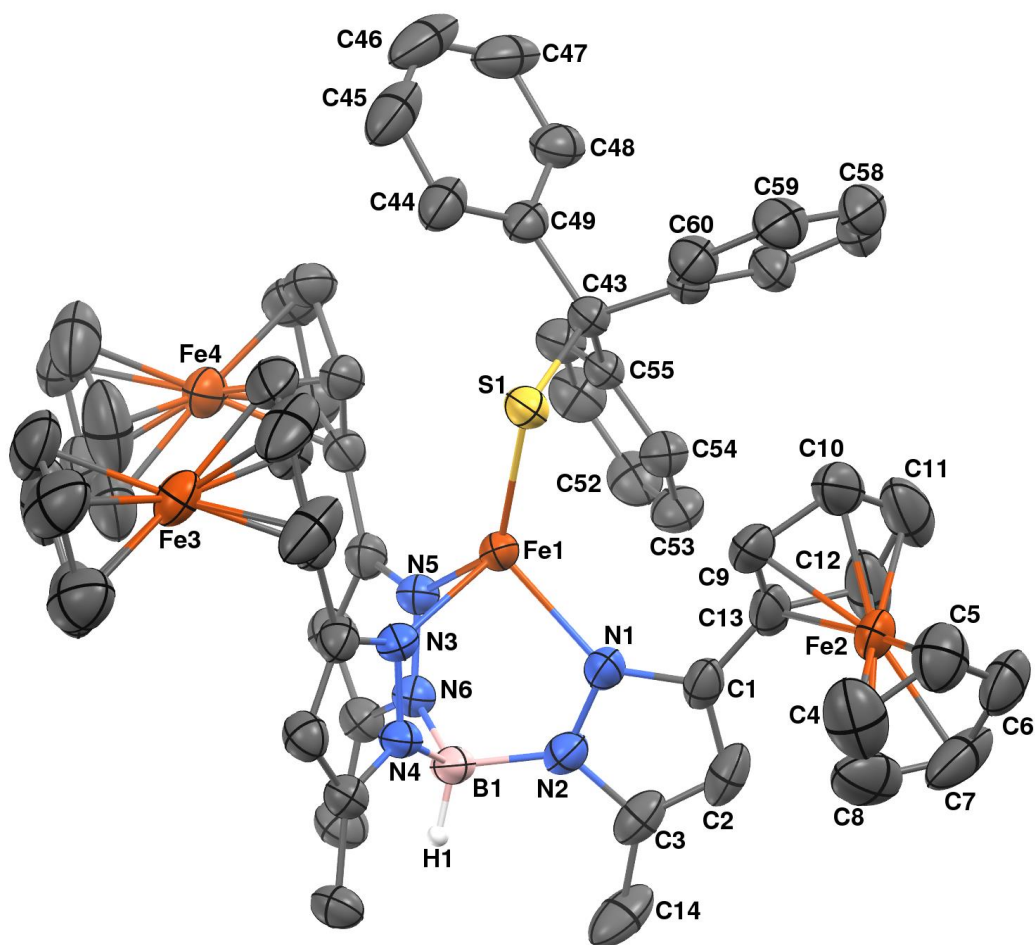


Figure 2.2: Molecular structure of $\text{Tp}^{\text{Fc,Me}}\text{FeS}(\text{CPh}_3)$ (14) represented as 50% probability thermal ellipsoids. Hydrogen atoms (with the exception of the hydrogens attached to boron, H1) have been omitted for clarity.

Table 2.2: Selected interatomic distances (\AA) and angles ($^\circ$) for $\text{Tp}^{\text{Fc,Me}}\text{FeS}(\text{CPh}_3)$ (14).

Distances (\AA)			
Fe1-N5	2.090(3)	Fe1-N3	2.114(3)
Fe1-N1	2.127(3)	Fe1-S1	2.2798(9)
N1-C1	1.354(4)	N1-N2	1.381(4)
N2-C3	1.354(4)	N2-B1	1.543(4)

N3-C15	1.335(4)	N3-N4	1.370(3)
N4-C17	1.345(4)	N4-B1	1.552(4)
N5-C29	1.346(4)	N5-N6	1.378(4)
N6-C31	1.354(4)	N6-B1	1.546(4)
S1-C43	1.887(3)	C1-C13	1.467(5)
C1-C2	1.383(5)	C4-C8	1.365(9)
C2-C3	1.379(6)	C9-C10	1.425(6)
C3-C14	1.485(6)	C43-C55	1.532(4)
C4-C5	1.409(8)	C43-C49	1.543(4)
C5-C6	1.384(7)	C44-C45	1.394(6)
C6-C7	1.407(7)	C45-C46	1.359(8)
C7-C8	1.393(9)	C46-C47	1.378(8)
C9-C13	1.430(7)	C47-C48	1.392(5)
C10-C11	1.378(9)	C48-C49	1.389(5)
C11-C12	1.410(8)	C50-C55	1.384(4)
C12-C13	1.434(5)	C56-C57	1.394(5)
C43-C61	1.542(4)	C57-C58	1.372(6)
C44-C49	1.389(5)	C58-C59	1.369(6)
C52-C53	1.379(6)	C59-C60	1.387(5)
C53-C54	1.392(5)	C60-C61	1.385(5)
C54-C55	1.394(4)	C56-C61	1.392(5)

Angles (°)

B1-Fe1-S1	163.57(7)	Fe1-S1-C43	108.39(10)
N5-Fe1-N3	84.01(10)	N5-Fe1-N1	99.40(11)
N3-Fe1-N1	89.57(10)	N5-Fe1-S1	136.32(7)
N3-Fe1-S1	110.60(7)	N1-Fe1-S1	120.81(8)
C1-N1-Fe1	140.6(2)	C1-N1-N2	106.3(3)
C3-N2-N1	110.0(3)	N2-N1-Fe1	110.41(18)
N1-N2-B1	120.8(2)	C3-N2-B1	129.1(3)
C15-N3-Fe1	140.3(2)	C15-N3-N4	106.6(2)
C17-N4-N3	110.5(2)	N4-N3-Fe1	112.37(18)
N3-N4-B1	119.6(2)	C17-N4-B1	129.6(3)
C29-N5-Fe1	141.4(2)	C29-N5-N6	106.2(2)
C31-N6-N5	110.0(3)	N6-N5-Fe1	112.45(18)
N5-N6-B1	120.7(2)	C31-N6-B1	128.8(3)
N2-B1-N6	110.9(3)	N2-B1-N4	108.8(3)
N6-B1-N4	109.1(2)	C3-C2-C1	107.2(3)
N1-C1-C13	122.1(3)	N2-C3-C14	122.6(3)
N1-C1-C2	109.3(3)	C8-C4-C5	109.6(5)

C2-C1-C13	128.6(3)	C6-C5-C4	107.1(5)
N2-C3-C2	107.1(3)	C5-C6-C7	107.4(5)
C2-C3-C14	130.3(3)	C8-C7-C6	108.6(5)
N4-C17-C28	123.5(3)	C4-C8-C7	107.3(5)
C55-C43-C49	113.8(3)	C10-C9-C13	107.2(5)
C55-C43-S1	107.3(2)	C11-C10-C9	109.0(5)
C49-C43-S1	109.4(2)	C10-C11-C12	109.0(4)
C46-C45-C44	120.8(5)	C11-C12-C13	107.7(5)
C46-C47-C48	119.5(5)	C9-C13-C12	107.0(4)
C44-C49-C48	117.6(3)	C12-C13-C1	124.8(4)
C48-C49-C43	118.8(3)	N3-C15-C16	109.3(3)
C52-C51-C50	121.2(4)	C55-C43-C61	111.8(2)
C52-C53-C54	120.2(3)	C61-C43-C49	105.8(2)
C50-C55-C54	117.7(3)	C61-C43-S1	108.7(2)
C54-C55-C43	117.7(3)	C49-C44-C45	120.6(4)
C58-C57-C56	120.4(4)	C45-C46-C47	119.9(4)
C58-C59-C60	120.2(4)	C44-C49-C43	123.4(3)
C60-C61-C56	118.0(3)	C55-C50-C51	120.6(3)
C56-C61-C43	121.4(3)	C51-C52-C53	118.9(3)
C50-C55-C43	124.6(3)	C53-C54-C55	121.3(3)
C61-C56-C57	120.4(4)	C60-C61-C43	120.3(3)
C59-C58-C57	119.8(3)	C61-C60-C59	121.2(4)

Comparing the bond lengths and angles of compounds **13** and **14** with other similar alkyl chalcogenides, several trends emerge. Other alkyl chalcogenides on $\text{Tp}^{\text{tBu,Me}}\text{Fe}$ and $\text{Tp}^{\text{iPr,iPr}}\text{Fe}$ systems have previously been described, see **Table 2.3**.^{8,9} For these compounds the Fe-O bond length decreases with increasing O-R bond lengths, but this trend doesn't follow a pattern in conjunction with changing steric bulk of the ligand, but does appear to follow a trend with the relative electronegativity of the R group. The fluorinated R group has the shortest O-R bond distance and the CPh_3 has the longest. This is mirrored in the sulfur analogues of the complexes as well, **Table 2.3**. Oddly, the complex most consistent with both **13** and **14** in terms of Fe-E-C and α angle were two tris(3-mesityl-pyrrolide) ethane (tpe) complexes, being more sterically similar to the $\text{Tp}^{\text{Fc,Me}}$ ligand but with an Fe^{III} , making them distinct

electronically.¹⁰ Given this, it appears that the factor that governs the Fe-E-C and α angle is the steric profile of the ligand, as electronic factors do not appear to play a role.

(NNN)FeOR	Fe-N(avg) (Å)	Fe-O (Å)	O-R (Å)	Fe-O-R (°)	α angle (°)
13	2.131(2)	1.827(2)	1.393(4)	157.4(2)	170.3(1)
<i>Tp</i> ^{tBu,Me} FeOMe ⁸	2.095(3)	1.830(3)	1.377(6)	138.9(3)	164.4(1)
<i>Tp</i> ^{iPr,iPr} FeO(C ₆ F ₅) ⁹	2.059(5)	1.875(5)	1.297(9)	133.2(5)	169.6(2)
(<i>tpe</i>)FeOC(CH ₃) ₂ (Ph) ¹⁰	1.976(3)	1.781(3)	1.397(5)	153.9(2)	174.4(1)
(NNN)FeSR	Fe-N(avg) (Å)	Fe-S (Å)	S-R (Å)	Fe-S-R (°)	α angle (°)
14	2.110(3)	2.2798(9)	1.887(4)	108.4(1)	167.57(7)
<i>Tp</i> ^{tBu,Me} FeSMe ⁸	2.093(4)	2.264(2)	1.813(4)	113.8(2)	174.4(1)
<i>Tp</i> ^{iPr,iPr} FeS(C ₆ F ₅) ⁹	2.057(4)	2.288(2)	1.749(5)	107.4(2)	162.7(1)
(<i>tpe</i>)FeSBn ¹⁰	1.969(3)	2.238(1)	1.835(4)	102.8(1)	177.64(8)

Table 2.3: Comparison of relevant structural features of (NNN)FeER complexes, (E = S or O, R = CPh₃, C₆F₅, C(CH₃)₂Ph or Benzyl)

With both **13** and **14** available, I set about reducing them with KH, hoping that the resulting triphenyl methane would be easily separated from the resulting salt. This was decided after initial attempts at directly reducing the complex with KC₈ produced an inseparable mixture of products. We also tested the reactivity of both **13** and **14** with dihydroanthracene in an attempt to produce metal hydroxo and hydrogen sulfide compounds. **13** was found to be entirely unreactive with dihydroanthracene as well as KH in the presence of 18-crown-6, even when heated in excess of 80 °C for several hours. In contrast, **14** did react with potassium hydride in the presence of 18-crown-6 at room temperature, producing a bridging sulfide instead of the expected [Tp^{Fc,Me}FeS][K(18-crown-6)] compound. The aforementioned bridging sulfide complex, [Tp^{Fc,Me}Fe]₂(μ - η^1 : η^1 -S) (**15**), was immediately identifiable from its LIFDI-

MS, see **Figure 2.3**, having a mass of 1758.0967 daltons, vs the model of 1758.1375 daltons for the most abundant distribution of isotopes for each element. **15** could be isolated by re-crystallization, with the reaction mixture being filtered, concentrated, and then layered with pentanes to afford the bridging sulfide as dark orange, almost black, blocks in a triclinic unit cell, seen in **Figure A2.3**. The Fe-S-Fe bond angle was $133.6(1)^\circ$, with α angles of $173.9(1)^\circ$ and $174.9(1)^\circ$ for either respective B-Fe-S, see **Table 2.4**. Both Tp ligands remained bound in a κ^3 manner, leaving both iron atoms in a tetrahedral coordination sphere, see **Figure 2.4**.

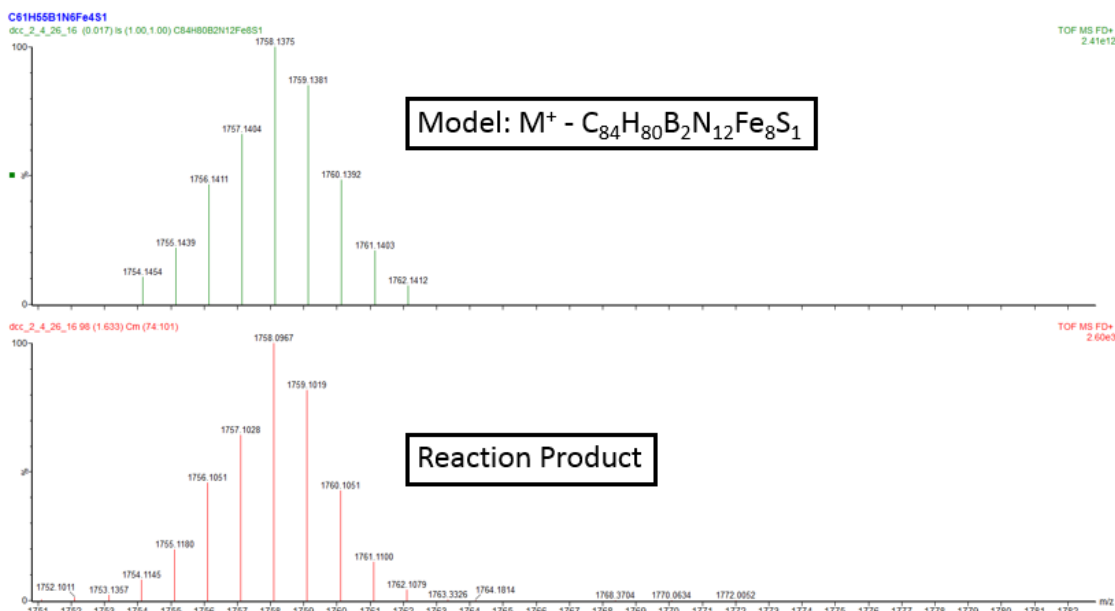


Figure 2.3: Predicted isotope model for the molecular ion of [Tp^{Fe,Me}Fe]₂(μ - η^1 : η^1 -S) (15**) [M⁺: 1758.1375]LIFDI-MS, and a sample taken from the crystallization mother liquor used to produce crystals of **15**.**

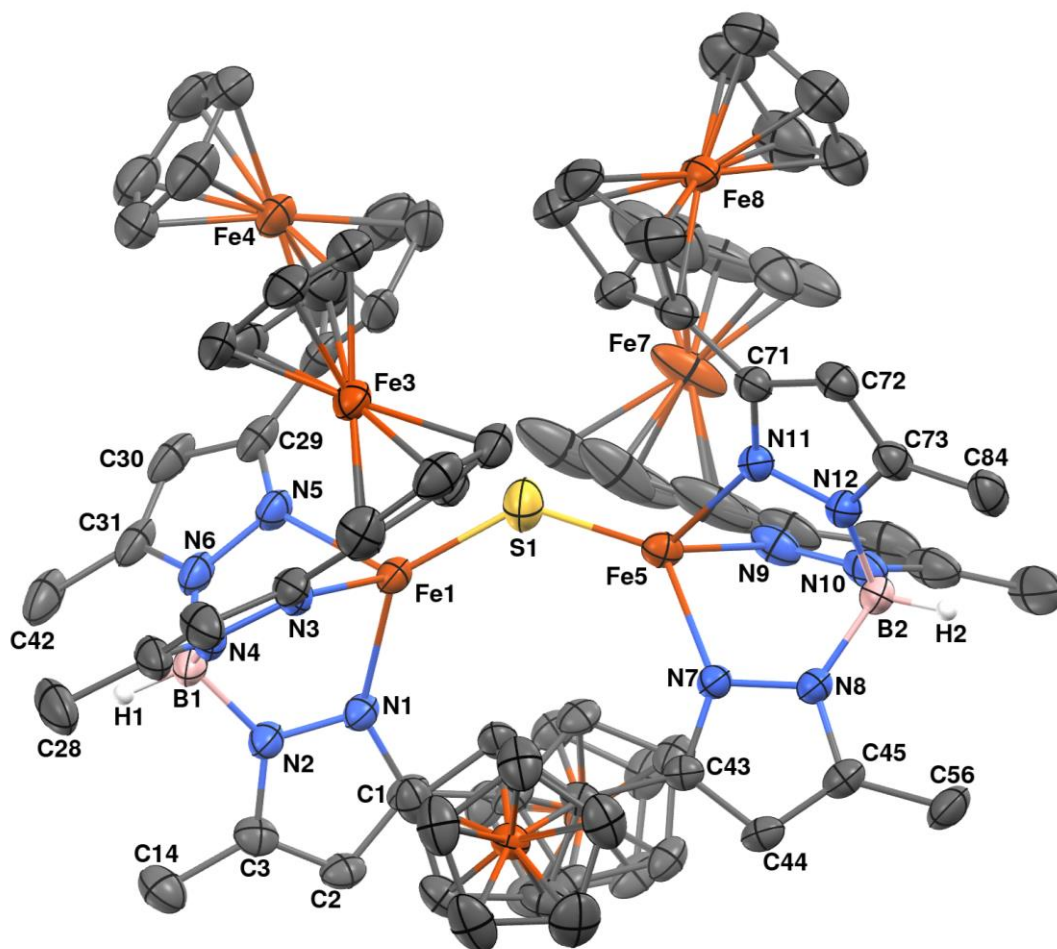


Figure 2.4: Molecular structure of $[\text{Tp}^{\text{Fc,Me}}\text{Fe}]_2(\mu\text{-}\eta^1:\eta^1\text{-S})$ (15) represented as 30% probability thermal ellipsoids. Hydrogen atoms (with the exception of the hydrogens attached to borons, H1 and H2), and one molecule of ether have been omitted for clarity.

Table 2.4: Selected interatomic distances (Å) and angles (°) for [Tp^{Fe,Me}Fe]₂(μ-η¹:η¹-S) (15)

Distances (Å)			
Fe1-S1	2.0366(18)	Fe5-S1	2.0413(17)
Fe1-N1	2.143(4)	Fe1-N5	2.131(4)
Fe5-N7	2.139(3)	Fe1-N3	2.148(4)
Fe5-N11	2.135(4)	Fe5-N9	2.113(4)
N1-C1	1.348(5)	N1-N2	1.374(5)
N2-C3	1.355(6)	N2-B1	1.543(7)
N3-C15	1.344(6)	N3-N4	1.378(5)
N4-C17	1.360(7)	N4-B1	1.550(8)
N5-C29	1.337(7)	N5-N6	1.380(6)
N6-C31	1.358(7)	N6-B1	1.534(9)
N7-C43	1.346(5)	N7-N8	1.377(5)
N8-C45	1.353(6)	N8-B2	1.546(7)
N9-C57	1.352(7)	N9-N10	1.379(7)
N10-C59	1.354(7)	N10-B2	1.551(8)
N11-C71	1.349(6)	N11-N12	1.379(5)
N12-C73	1.353(6)	N12-B2	1.545(7)
C1-C2	1.402(7)	C1-C13	1.463(7)
C2-C3	1.354(7)	C15-C16	1.411(7)
C3-C14	1.502(8)	C16-C17	1.357(9)
C15-C27	1.469(7)	C17-C28	1.495(8)
C29-C30	1.405(8)	C29-C41	1.442(8)
C30-C31	1.357(9)	C32-C36	1.370(12)
C31-C42	1.507(9)	C43-C44	1.384(6)
C43-C55	1.457(6)	C44-C45	1.359(7)
Angles (°)			
B1-Fe1-S1	174.9(1)	B2-Fe5-S1	173.9(1)
S1-Fe1-N5	121.43(14)	S1-Fe1-N1	130.29(12)
N5-Fe1-N1	90.31(15)	S1-Fe1-N3	122.52(12)
N5-Fe1-N3	86.03(16)	N1-Fe1-N3	94.35(15)
S1-Fe5-N11	119.63(12)	S1-Fe5-N9	124.41(15)
S1-Fe5-N7	129.87(11)	N9-Fe5-N11	85.54(16)
N11-Fe5-N7	92.24(14)	N9-Fe5-N7	93.24(16)
Fe1-S1-Fe5	133.64(11)	C1-N1-N2	106.0(4)
C1-N1-Fe1	138.9(3)	N2-N1-Fe1	112.3(3)

C3-N2-N1	109.8(4)	C3-N2-B1	130.0(4)
N1-N2-B1	120.2(4)	C15-N3-N4	106.8(4)
C15-N3-Fe1	140.9(3)	N4-N3-Fe1	112.2(3)
C17-N4-N3	109.7(4)	C17-N4-B1	128.9(4)
N3-N4-B1	121.4(4)	C29-N5-N6	106.7(4)
C29-N5-Fe1	138.5(4)	N6-N5-Fe1	111.4(3)
C31-N6-N5	109.5(5)	C31-N6-B1	129.0(5)
N5-N6-B1	121.5(4)	C43-N7-N8	105.8(3)
C43-N7-Fe5	139.8(3)	N8-N7-Fe5	112.0(2)
C45-N8-N7	109.9(4)	C45-N8-B2	128.8(4)
N7-N8-B2	121.2(4)	C57-N9-N10	106.4(5)
C57-N9-Fe5	140.4(5)	N10-N9-Fe5	113.2(3)
C59-N10-N9	110.1(6)	C59-N10-B2	128.8(6)
N9-N10-B2	121.0(4)	C71-N11-N12	106.3(4)
C71-N11-Fe5	140.2(3)	N12-N11-Fe5	112.3(3)
C73-N12-N11	110.4(4)	C73-N12-B2	129.2(4)
N11-N12-B2	119.9(4)	N6-B1-N2	109.8(5)
N6-B1-N4	110.1(4)	N2-B1-N4	109.2(4)
N12-B2-N10	109.7(4)	N8-B2-N12	110.3(4)
N8-B2-N10	108.8(4)	N1-C1-C2	109.6(4)
N1-C1-C13	123.7(4)	C2-C1-C13	126.5(4)
C3-C2-C1	106.2(4)	N2-C3-C2	108.4(4)
N2-C3-C14	121.9(5)	C2-C3-C14	129.5(5)
N3-C15-C16	108.7(5)	C17-C16-C15	107.0(5)
C16-C15-C27	125.5(5)	C16-C17-C28	127.8(6)
C16-C17-N4	107.8(5)	N5-C29-C30	109.1(6)
N4-C17-C28	124.4(6)	C30-C29-C41	128.1(5)
N5-C29-C41	122.8(5)	C30-C31-N6	107.9(5)
C31-C30-C29	106.8(5)	N6-C31-C42	122.8(7)
C30-C31-C42	129.3(6)	N7-C43-C55	123.3(4)
N7-C43-C44	109.8(4)	C45-C44-C43	106.8(4)
C44-C43-C55	126.9(4)	N8-C45-C56	122.7(5)
N8-C45-C44	107.7(4)	N11-C71-C83	122.7(4)
C44-C45-C56	129.6(5)	C73-C72-C71	107.1(4)
C51-C55-C43	130.0(4)		

The reaction of **14** with dihydroanthracene produced a somewhat ambiguous result. The progress of the reaction was made obvious by a change in color to light orange and the $^1\text{H-NMR}$ spectrum no longer demonstrating the chemical shifts associated with the starting material. Despite this, no pure compound could be isolated from the reaction mixture, even as the LIFDI-MS data was consistent with the expected hydrogen sulfide complex, shown in **Figure 2.5**. The aspect the data which remains unclear is the apparent presence of two additional compounds, having masses ± 2 daltons, which we were unable to separate.

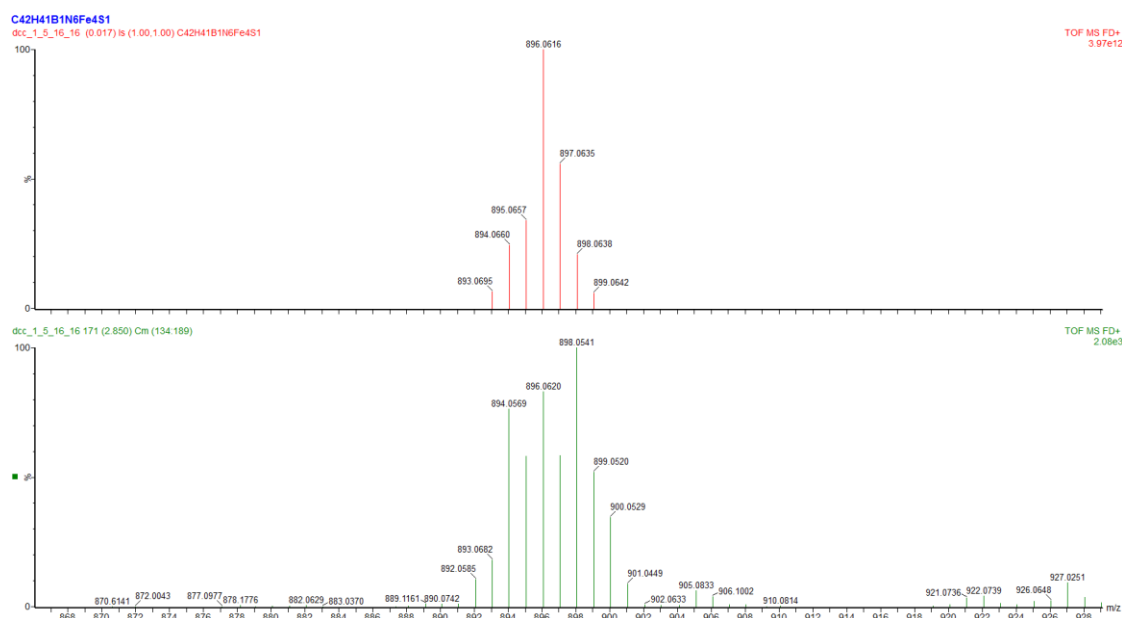
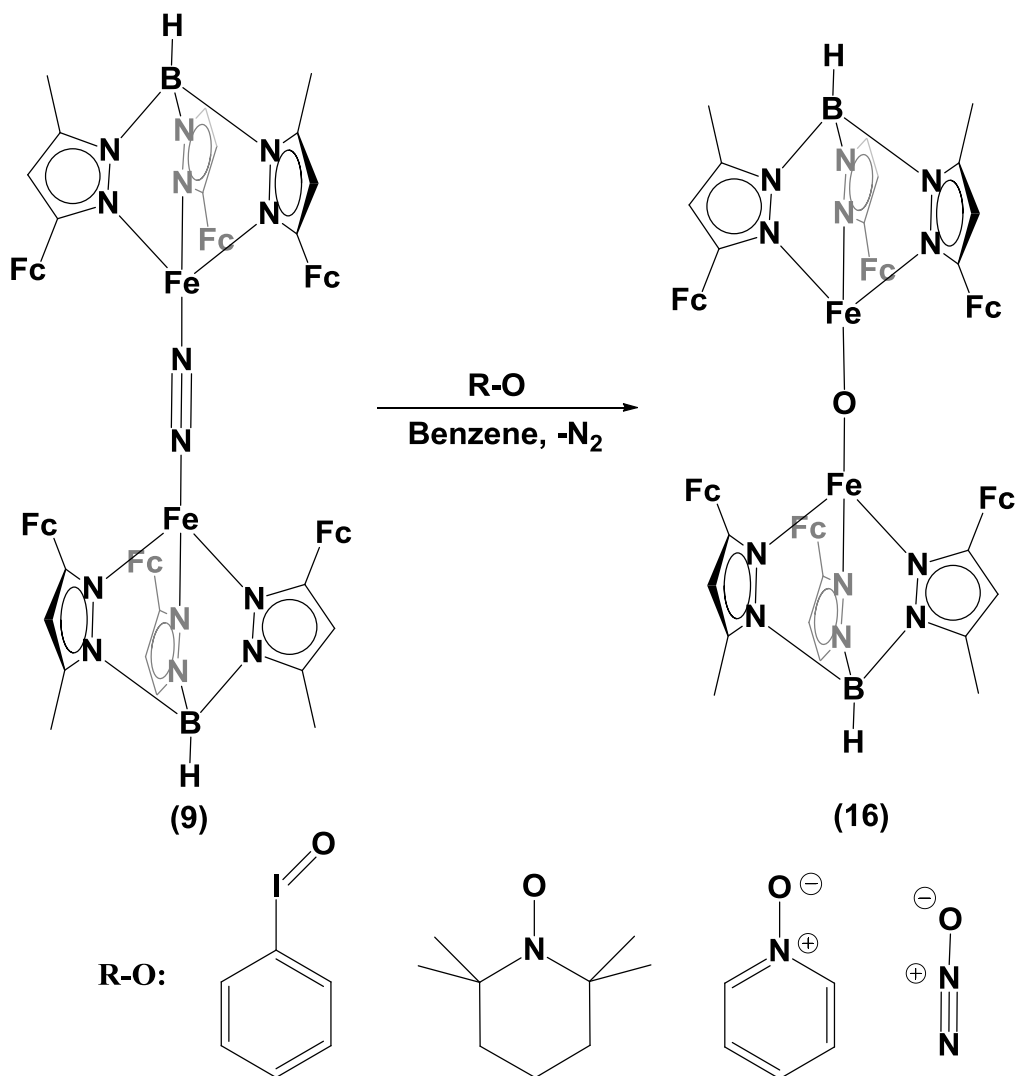


Figure 2.5: LIFDI-MS of the result of reaction of **14 with DHA (bottom), the calculated isotope pattern of the desired $\text{Tp}^{\text{Fc,Me}}\text{FeSH}$ complex (top).**

Reactions of single atom oxygen transfer reagents with $[\text{Tp}^{\text{Fc,Me}}\text{Fe}]_2(\mu\text{-}\eta^1:\eta^1\text{-N}_2)$ (9**).** With the setbacks encountered in using trityl chalcogenide complexes to access terminal oxo or other chemically relevant oxo species, I shifted focus to

producing novel oxo complexes from $[\text{Tp}^{\text{Fc,Me}}\text{Fe}]_2(\mu\text{-}\eta^1\text{:}\eta^1\text{-N}_2)$ (**9**), introduced in **Chapter 2**. Attempting first to use single oxygen atom transfer reagents to produce terminal oxo complexes, I started with iodosobenzene, TEMPO,¹¹ pyridine-N-oxide, and N_2O as oxygen atom transfer reagents, shown in **Scheme 2.3**. All of these reagents reacted with **9** in benzene produce a quantity of pyrazole pyrazolate, $\text{Tp}^{\text{Fc,Me}}\text{Fe}(\text{PzH}^{\text{Fc,Me}})(\text{Pz}^{\text{Fc,Me}})$ (**8**), as well as the bridging oxo compound $[\text{Tp}^{\text{Fc,Me}}\text{Fe}]_2(\mu\text{-}\eta^1\text{:}\eta^1\text{-O})$ (**16**) in yields varying from 60 to 85 %. Once **16** is produced, it can be purified by crystallization from mixtures of THF and pentane or layering pentanes onto a solution of **16** in benzene. The Fe-O-Fe angle was $143.6(1)^\circ$, with Fe-O bond lengths being the same to within error at $1.796(2)$ and $1.798(2)$ Å, see **Table 2.5**. As with **15**, both Tp ligands are bound κ^3 to the metal centers in **16**, see **Figure 2.6**.

16 has only one precedent, in the form of a $((\text{NacNac})\text{Fe}^{\text{II}})_2(\mu\text{-}\eta^1\text{:}\eta^1\text{-O})$ complex, prepared in the lab of Patrick Holland.¹² In solution, **16** displays apparent C_{3v} symmetry in solution, with 4 resonances between -2 and 18 ppm corresponding to the hydrogens on the $\text{Tp}^{\text{Fc,Me}}$ ligand, with 1 additional resonance being assigned to the hydrogen on the boron, shown in **Figure 2.7**. The 5th resonance corresponding to hydrogens on one of either the 2nd and 5th or 3rd and 4th positions of the Cp rings on the $\text{Tp}^{\text{Fc,Me}}$ ligand was not observed, presumably being too broad due to the paramagnetism of the complex. The effective magnetic moment of **16** was found to be $2.9(1) \mu_{\text{B}}$ when measured at 298 K in the solid state.



Scheme 2.3: Reaction of [Tp^{Fc,Me}Fe]₂(μ-η¹:η¹-N₂) (9) with various single oxygen atom transfer reagents, synthesis of [Tp^{Fc,Me}Fe]₂(μ-η¹:η¹-O) (16).

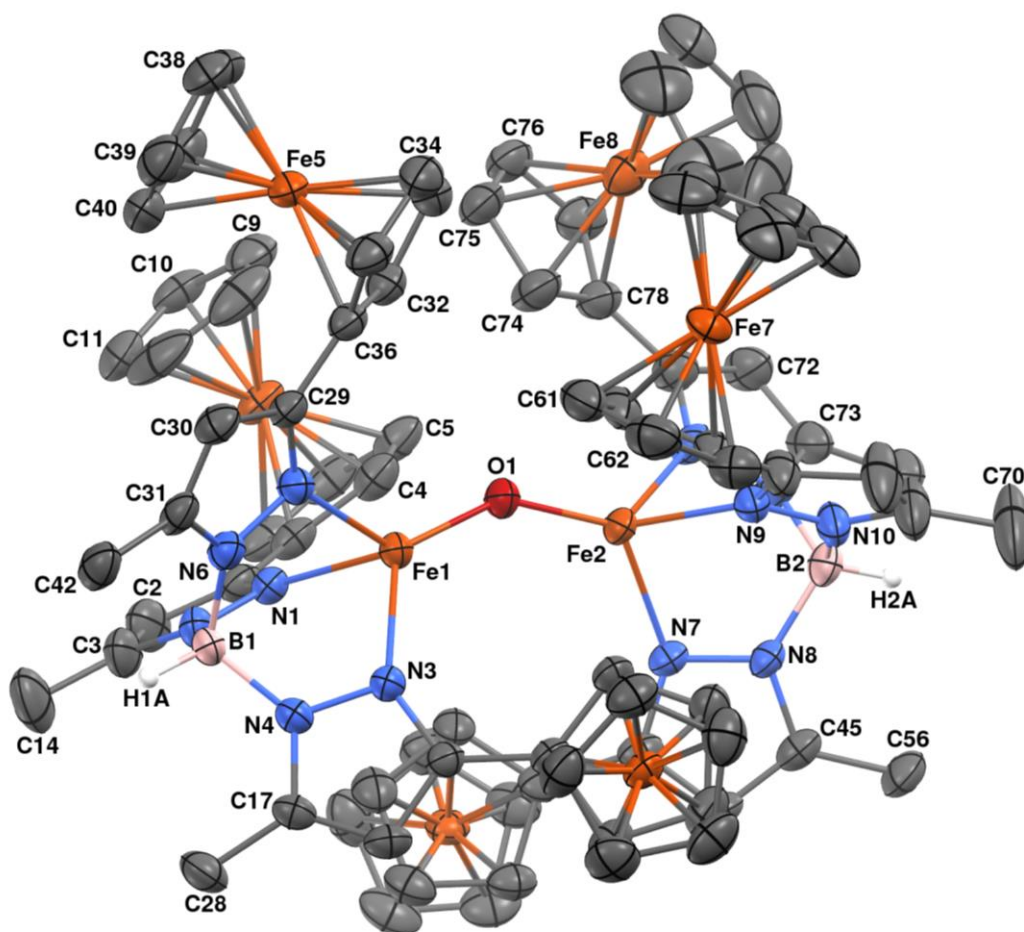


Figure 2.6: Molecular structure of $[\text{Tp}^{\text{Fc,Me}}\text{Fe}]_2(\mu\text{-}\eta^1:\eta^1\text{-O})$ (**16**) represented as 50% probability thermal ellipsoids. Hydrogen atoms (with the exception of the hydrogens attached to boron, H1A and H2A), and 2 molecules of THF have been omitted for clarity.

Table 2.5: Selected interatomic distances (Å) and angles (°)

for $[\text{Tp}^{\text{Fc,Me}}\text{Fe}]_2(\mu\text{-}\eta^1:\eta^1\text{-O})$ (**16**)

Distances (Å)

Fe1-O1	1.796(2)	Fe2-O1	1.798(2)
Fe1-N3	2.156(3)	Fe1-N1	2.183(3)
Fe2-N9	2.145(3)	Fe2-N7	2.137(3)

B1-N6	1.539(5)	B1-N4	1.540(5)
B2-N8	1.537(5)	B2-N10	1.542(6)
N3-N4	1.371(4)	N3-C15	1.340(4)
N6-C31	1.359(4)	N4-C17	1.354(4)
N7-N8	1.381(4)	N7-C43	1.340(4)
N9-C57	1.330(5)	N8-C45	1.349(4)
N10-C59	1.347(5)	N9-N10	1.370(4)
C2-C3	1.358(6)	C4-C5	1.418(5)
C3-C14	1.503(6)	C9-C10	1.392(6)
C4-C8	1.433(5)	C10-C11	1.407(6)
C5-C6	1.413(6)	C11-C12	1.433(7)
C6-C7	1.422(6)	C12-C13	1.394(8)
C7-C8	1.438(5)	C15-C16	1.399(5)
C9-C13	1.388(7)	C16-C17	1.365(5)
C29-C30	1.393(5)	C17-C28	1.499(5)
C30-C31	1.368(5)	C18-C19	1.421(5)
C31-C42	1.494(5)	C29-C36	1.469(5)
C57-C64	1.461(6)	C32-C36	1.417(5)
C43-C50	1.459(5)	C38-C39	1.400(6)
C57-C58	1.399(6)	C39-C40	1.395(6)
C58-C59	1.365(7)	C60-C61	1.424(6)
C59-C70	1.502(6)	C65-C69	1.412(7)
C60-C64	1.427(5)	C66-C67	1.400(7)
C61-C62	1.407(6)	C67-C68	1.431(7)
C62-C63	1.420(6)	C68-C69	1.400(7)
C63-C64	1.420(6)	C71-C72	1.401(5)
C65-C66	1.406(7)	C72-C73	1.358(6)
C79-C80	1.414(9)	C73-C84	1.493(5)
C71-C78	1.460(5)	C74-C75	1.423(5)
C74-C78	1.416(5)	C75-C76	1.397(6)
C79-C83	1.420(9)	C76-C77	1.418(6)
C80-C81	1.447(9)	C77-C78	1.428(5)
C81-C82	1.372(10)	C82-C83	1.412(11)

Angles (°)

Fe1-O1-Fe2	143.59(14)	O1-Fe1-N3	126.91(10)
O1-Fe2-N7	128.03(11)	O1-Fe1-N1	120.71(11)
O1-Fe2-N9	123.92(11)	N3-Fe1-N1	93.28(10)
N7-Fe2-N9	93.70(11)	C17-N4-N3	109.6(3)
N6-B1-N4	110.5(3)	N3-N4-B1	121.0(3)

N8-B2-N10	110.2(3)	N4-N3-Fe1	111.49(19)
C1-N1-Fe1	140.4(2)	C17-N4-B1	129.4(3)
C43-N7-Fe2	139.7(2)	C31-N6-B1	128.9(3)
N7-N8-B2	121.0(3)	C43-N7-N8	105.6(3)
C57-N9-Fe2	139.3(2)	N8-N7-Fe2	112.0(2)
C59-N10-N9	109.6(3)	C57-N9-N10	106.9(3)
N9-N10-B2	120.5(3)	N10-N9-Fe2	113.7(2)
C59-N10-B2	129.8(3)	C4-C8-C1	127.6(3)
N1-C1-C2	109.1(3)	N4-C17-C28	122.9(3)
C2-C1-C8	126.5(4)	C30-C29-C36	127.0(3)
N1-C1-C8	124.3(3)	N6-C31-C30	107.8(3)
C3-C2-C1	107.0(4)	C30-C31-C42	129.5(3)
C2-C3-C14	130.0(4)	C32-C36-C29	128.0(3)
C5-C4-C8	108.5(4)	N7-C43-C50	123.8(3)
C6-C5-C4	108.3(4)	N9-C57-C58	109.4(4)
C5-C6-C7	108.2(4)	C58-C57-C64	126.9(4)
C6-C7-C8	108.2(4)	N10-C59-C58	108.0(4)
C4-C8-C7	106.7(3)	C58-C59-C70	129.7(5)
C7-C8-C1	125.3(4)	C63-C64-C57	124.0(4)
C13-C9-C10	108.8(5)	C73-C72-C71	106.7(3)
C9-C10-C11	108.8(4)	C72-C73-C84	129.9(4)
C10-C11-C12	106.0(4)	C78-C74-C75	108.2(3)
C13-C12-C11	108.4(4)	C76-C75-C74	108.2(4)
C9-C13-C12	108.0(5)	C75-C76-C77	108.4(3)
C31-C30-C29	106.1(3)	C76-C77-C78	107.9(4)
N6-C31-C42	122.8(3)	C74-C78-C77	107.3(3)
C40-C39-C38	108.0(4)	C77-C78-C71	124.5(4)
N9-C57-C64	123.5(3)	C80-C79-C83	109.5(6)
C59-C58-C57	106.1(4)	C79-C80-C81	106.3(6)
N10-C59-C70	122.3(4)	C82-C81-C80	107.5(7)
C61-C60-C64	107.5(4)	C81-C82-C83	111.0(7)
C62-C61-C60	108.3(4)	C82-C83-C79	105.7(7)
C61-C62-C63	108.3(4)	C66-C67-C68	107.4(5)
C62-C63-C64	107.9(4)	C69-C68-C67	108.2(5)
C63-C64-C60	107.9(4)	C68-C69-C65	107.7(5)
C60-C64-C57	128.1(4)	C72-C71-C78	127.2(3)
C66-C65-C69	108.4(5)	C74-C78-C71	128.0(3)
C67-C66-C65	108.3(5)		

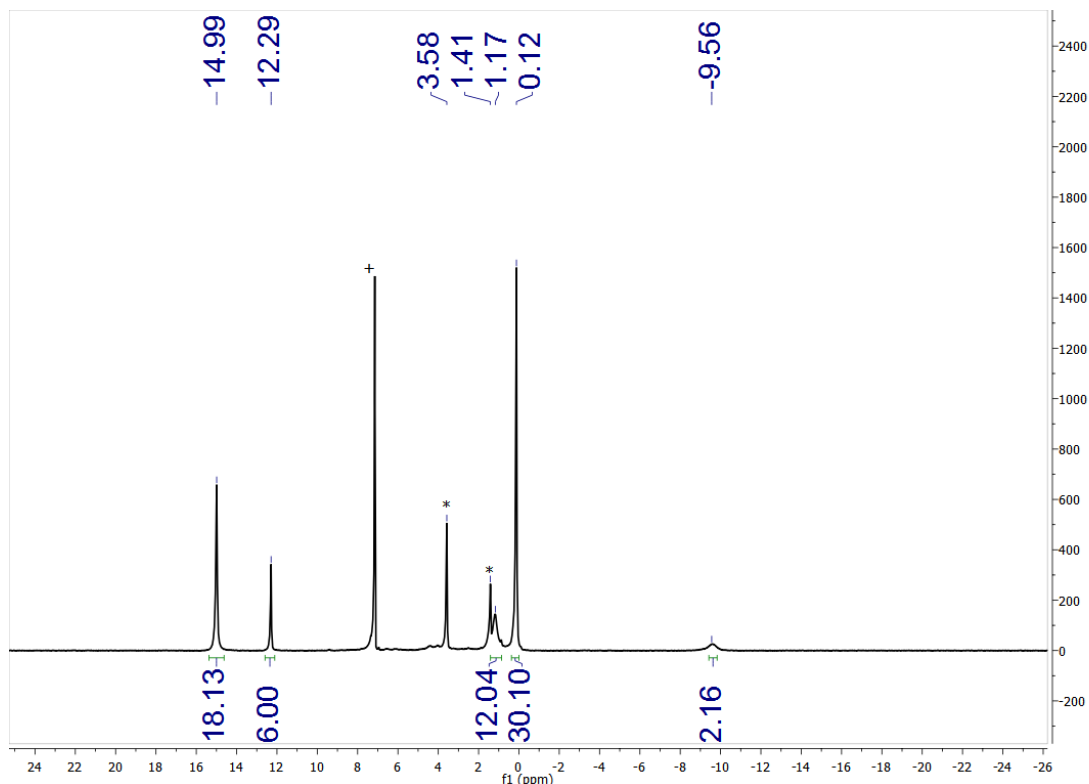


Figure 2.7: $^1\text{H-NMR}$ spectrum of $[\text{Tp}^{\text{Fc,Me}}\text{Fe}]_2(\mu\text{-}\eta^1\text{:}\eta^1\text{-O})$ (**16**) recorded in C_6D_6 (+) at 400 MHz, with THF (*) present in crystals used for collection.

Given the rarity of such bridging $\text{Fe}^{\text{II}}\text{-O-Fe}^{\text{II}}$ complexes,¹³ and the reactivity of similar complexes having an oxidation state of (III) for the iron centers found in enzymes,¹⁴ we set about investigating the reactivity of **16** with small molecules. The complex showed no reactivity with ethylene, carbon monoxide, or trimethyl phosphine. However, the complex did react with oxygen and to a lesser extent it reacts with moisture. The reaction of **16** with oxygen produces **8** and potentially a complex resulting from the activation of the ferrocenyl moiety on one of the pyrazole arms, as indicated by a LIFDI-MS of the reaction mixture, see **Figure 2.8**.

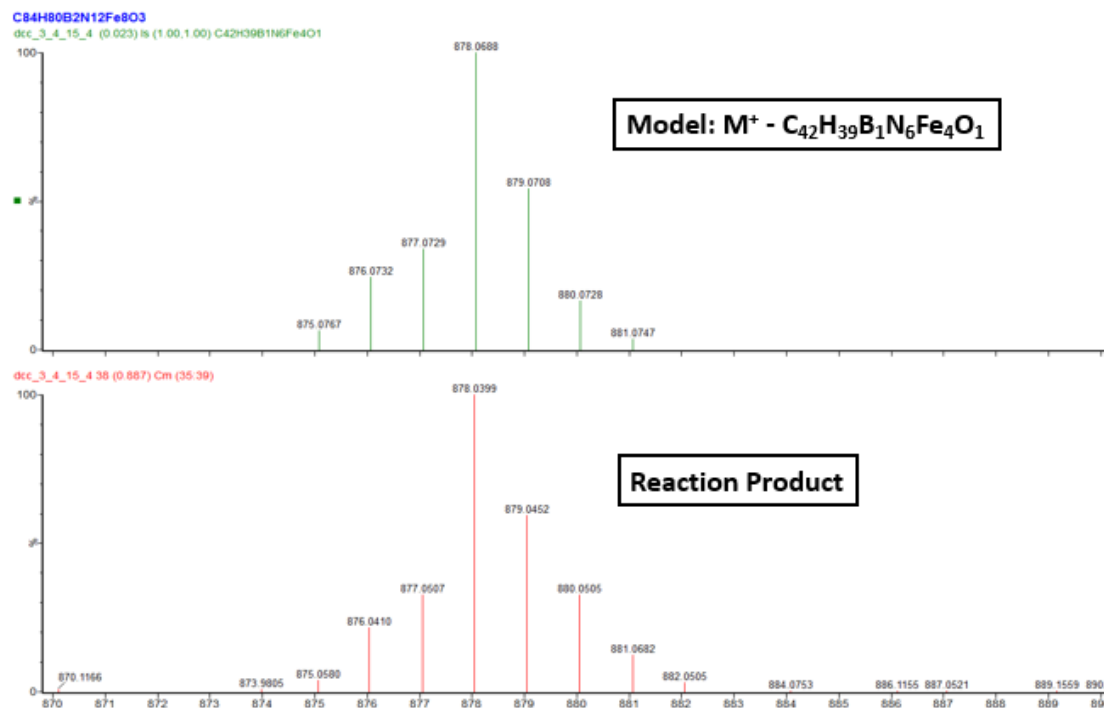


Figure 2.8: LIFDI-MS of the result from a reaction of **16 with oxygen gas (Bottom), calculated isotope pattern for $C_{42}H_{39}B_1N_6Fe_4O$, the apparent activation of the ferrocene arms of the ligand (top).**

Reactions of $[Tp^{Fc,Me}Fe]_2(\mu-\eta^1:\eta^1-N_2)$ (9**) with oxygen gas as an oxygen atom transfer reagent.** Following up on the formation of the bridging oxo complex, $[Tp^{Fc,Me}Fe]_2(\mu-\eta^1:\eta^1-O)$ (**16**), we set about testing the reactivity of **9** with oxygen gas. Iron complexes supported by the $Tp^{tBu,Me}$ ligand are able split dioxygen but produce bridging Fe^{III}/Fe^{III} complexes with activation of the ligand C-H bonds, see **Scheme 2.1**.³ Initial attempts at room temperature with excess oxygen resulted only in decomposition and the formation of **8**, and trace amounts of the insertion product discussed at the end of the previous section, as indicated by LIFDI-MS and illustrated by **Figure 2.8**. Reactions of **9** with single equivalents of O_2 produced mostly **8** and

accompanying insertion products, but also produced trace amounts of **16**. These compounds were observed when the reaction was monitored by $^1\text{H-NMR}$, seen in **Figure 2.9**. This suggests that **9** is capable of splitting oxygen, and that the resulting terminal complex then reacts with the remaining **9** to produce **16**, this suggested mechanism is shown in **Scheme 2.4**. This mechanism is similar to the one presented by the Smith group, for the thermolysis of an Fe^{II} TEMPO complex supported by a tris(3-mesityl)imidazole carbene ligand, which produces a terminal oxo that then either decomposes or reacts with other radicals present in solution.¹¹

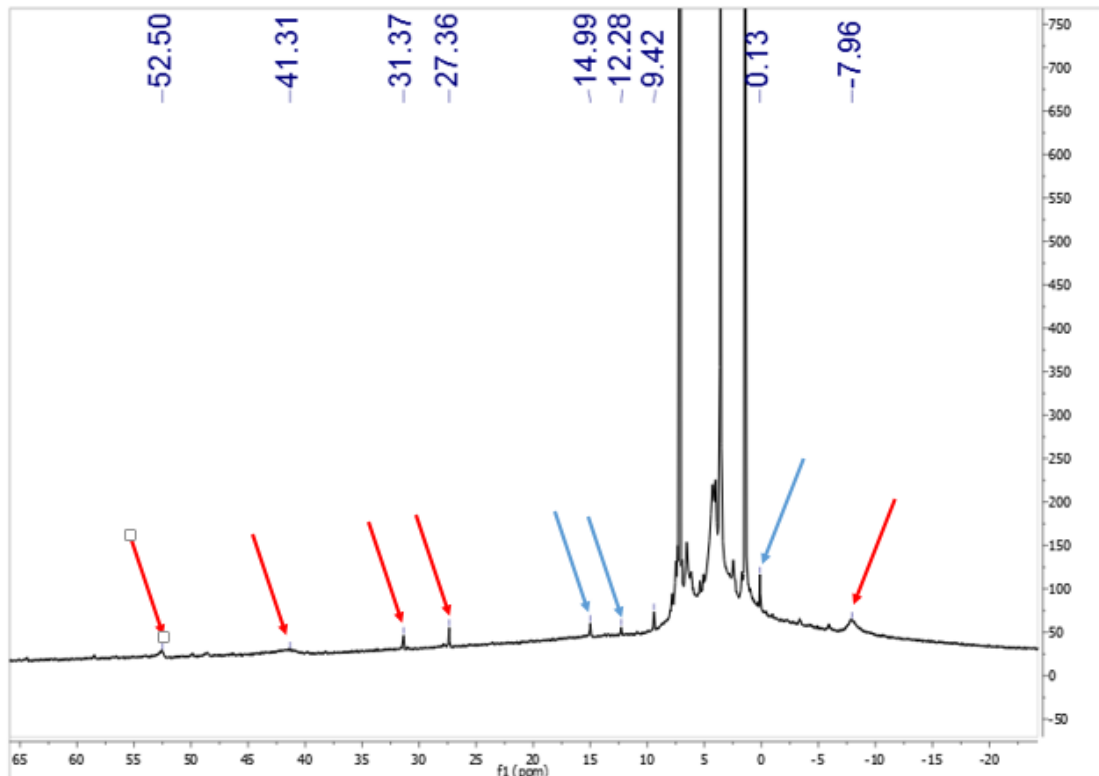
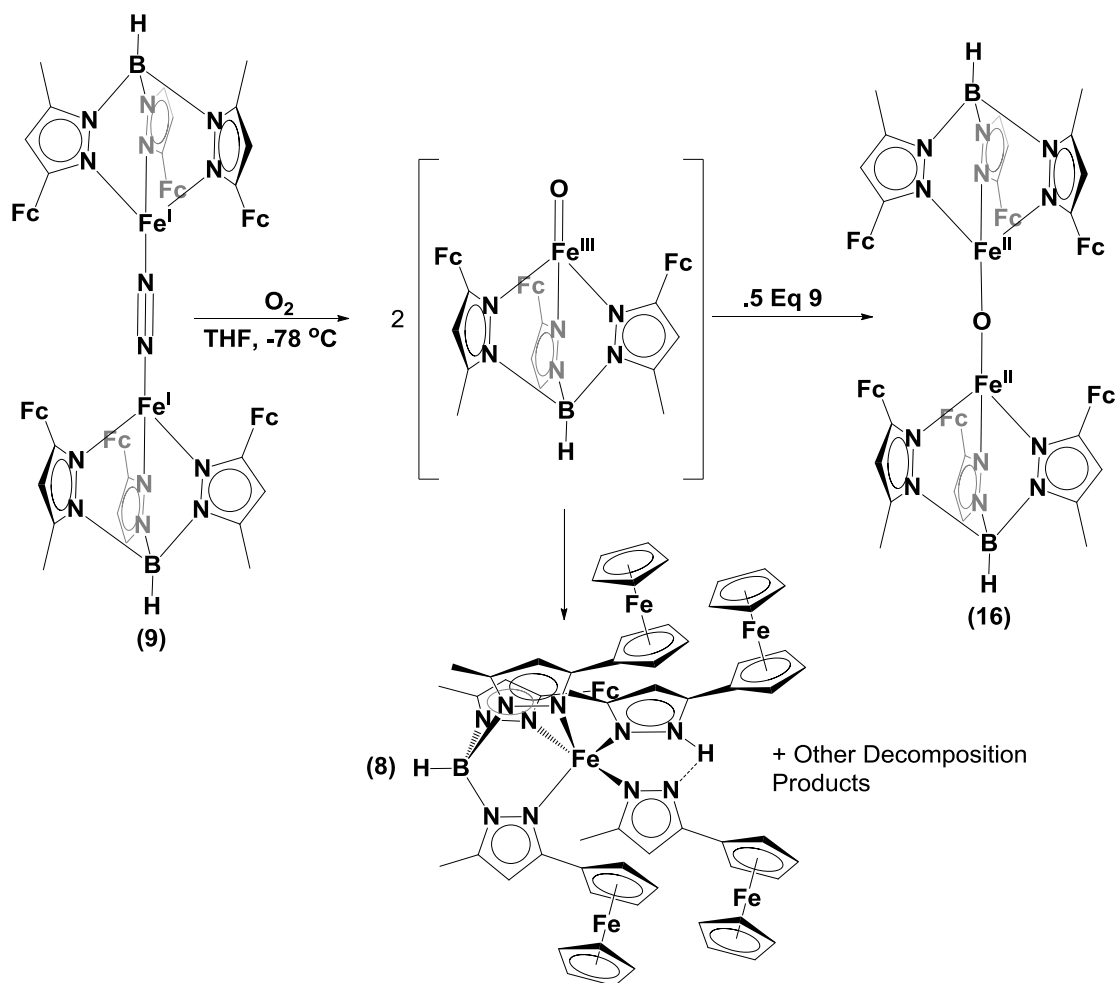


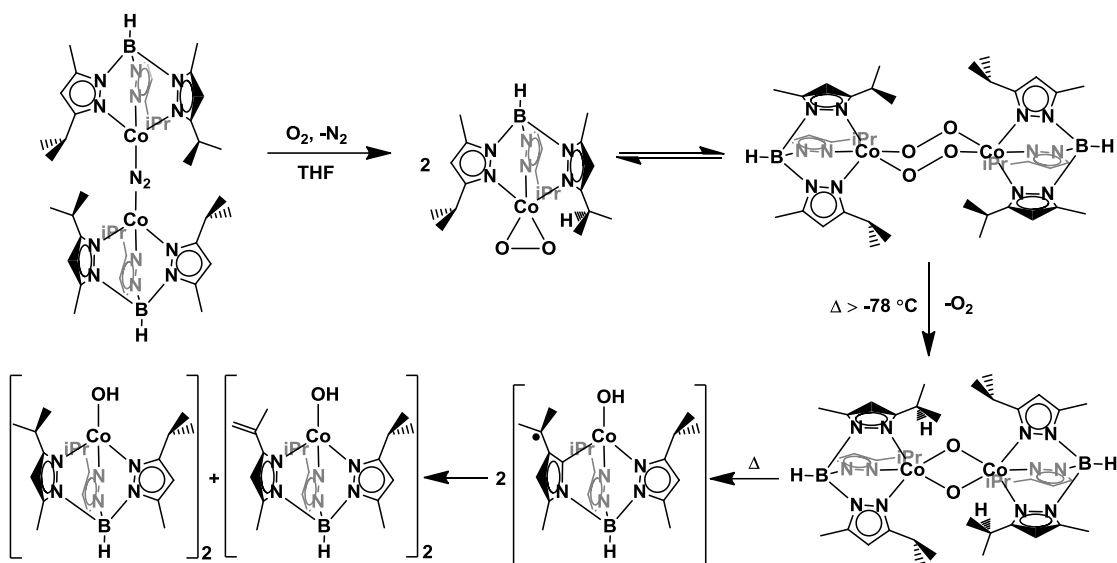
Figure 2.9: $^1\text{H-NMR}$ spectrum of THF extracts from a reaction of **9** with 1 Eq of O_2 at $-78\text{ }^\circ\text{C}$ in Ether, (**8** = red arrows), (**16** = blue arrows).



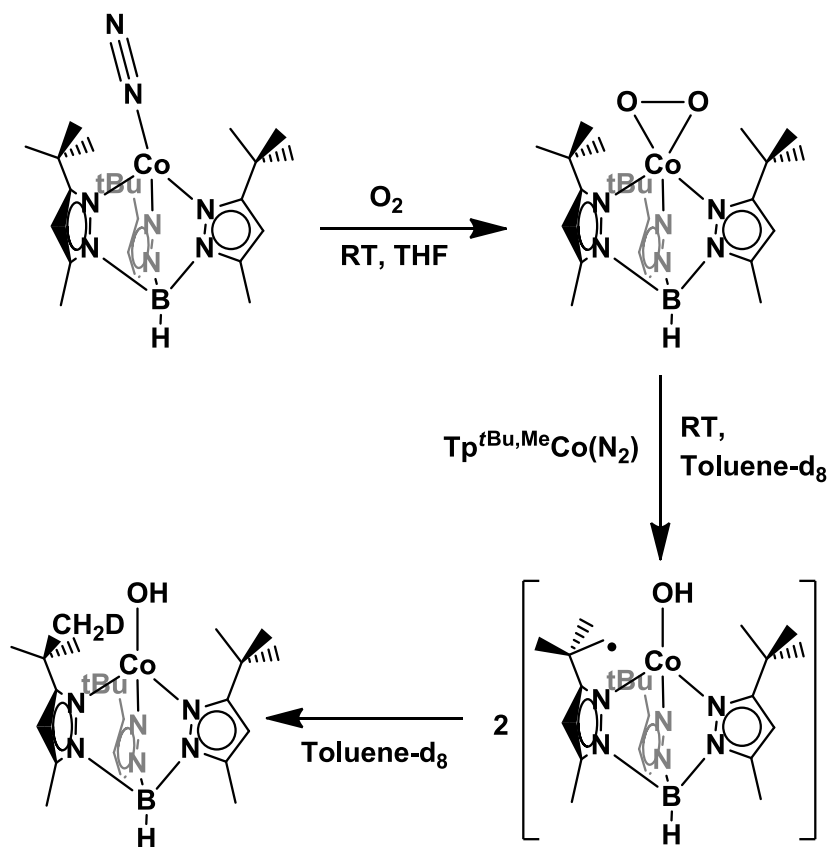
Scheme 2.4: Reaction of **9** with 1 Eq of oxygen gas at low temperature, synthesis of trace amounts of $[Tp^{Fc,Me}Fe]_2(\mu-\eta^1:\eta^1-O)$ (**16**).

Reaction of $[Tp^{Fc,Me}Co]_2(\mu-\eta^1:\eta^1-N_2)$ (10**) with O_2 and single oxygen atom transfer reagents.** It was previously observed that reactions of cobalt dinitrogen complexes supported by either $Tp^{tBu,Me}$ or $Tp^{iPr,Me}$ would produce hydroxo complexes by way of ligand C-H bond activation, shown in **Schemes 2.5**, and **2.6**.² As previously stated in the **Introduction**, the impetus for using the $Tp^{Fc,Me}$ as an ancillary ligand was to circumvent decomposition through C-H bond activation of the ligand. The reaction

of **10** with excess O₂ produced Tp^{Fc,Me}Co(O₂), as previously described by Sirianni.¹⁵ The ¹H-NMR taken of the reaction mixture from excess of O₂ with **10** clearly shows the resonances associated with Tp^{Fc,Me}Co(O₂) as the main product, but also shows some amount of Tp^{Fc,Me}CoOH having been formed, see **Figure 2.10**. This at first indicated ligand activation, as the source of the hydrogen was unknown. To investigate the possibility that this would occur through the mechanism shown in **Scheme 2.5**, pure samples of both Tp^{Fc,Me}Co(O₂) and **10** were placed in an NMR tube in C₆D₆ and stirred at room temperature, resulting in no apparent hydroxide formation. In an effort to force a reaction, a 2:1 molar quantity of Tp^{Fc,Me}Co(O₂) and **10** were then dissolved in THF and heated at 110 °C with stirring for 21 days, after which the superoxo starting material remained unconsumed, see **Figure 2.11**. All of the starting **10** had disproportionated into Co⁰ and Co^{II} bis-ligand complex **A1.3**, identified by the unit cell of crystals which grew from the reaction mixture upon cooling. No **A1.3** is present in **Figure 2.11**, as the compound is completely insoluble in THF. These results taken together indicate that the Tp^{Fc,Me}CoOH produced and visible in the **Figure 2.10** were the result of exogenous water reacting with the starting material, as **10** will react to even trace moisture from glove box atmosphere.



Scheme 2.5: Reaction of $[\text{Tp}^{\text{iPr,Me}}\text{Co}]_2(\mu\text{-}\eta^1\text{:}\eta^1\text{-N}_2)$ with oxygen gas.²



Scheme 2.6: Reaction of $\text{Tp}^{\text{tBu,Me}}\text{Co-N}_2$ with oxygen gas.²

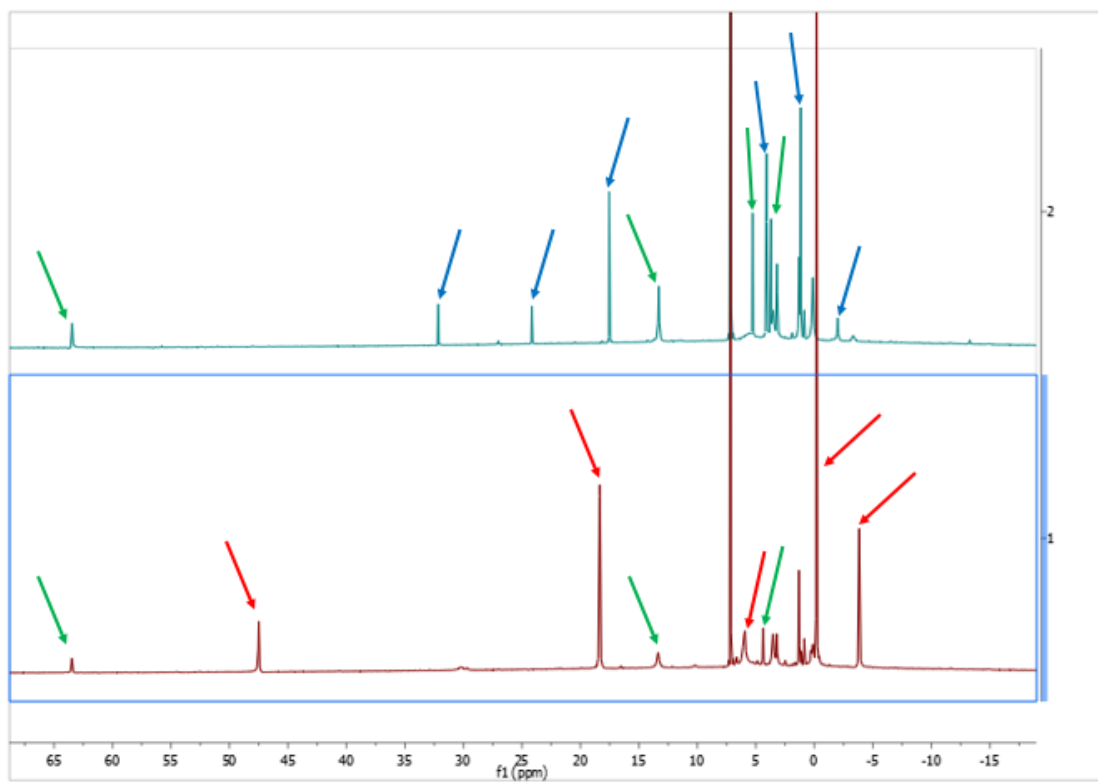


Figure 2.10: ¹H-NMR spectrum of the starting material, **10** (bottom), for the reaction with excess O₂ at RT in C₆D₆ (Top), ($\text{Tp}^{\text{Fc,Me}}\text{CoOH}$ = green arrows, **10** = red arrows, $\text{Tp}^{\text{Fc,Me}}\text{Co}(\text{O}_2)$ = blue arrows).

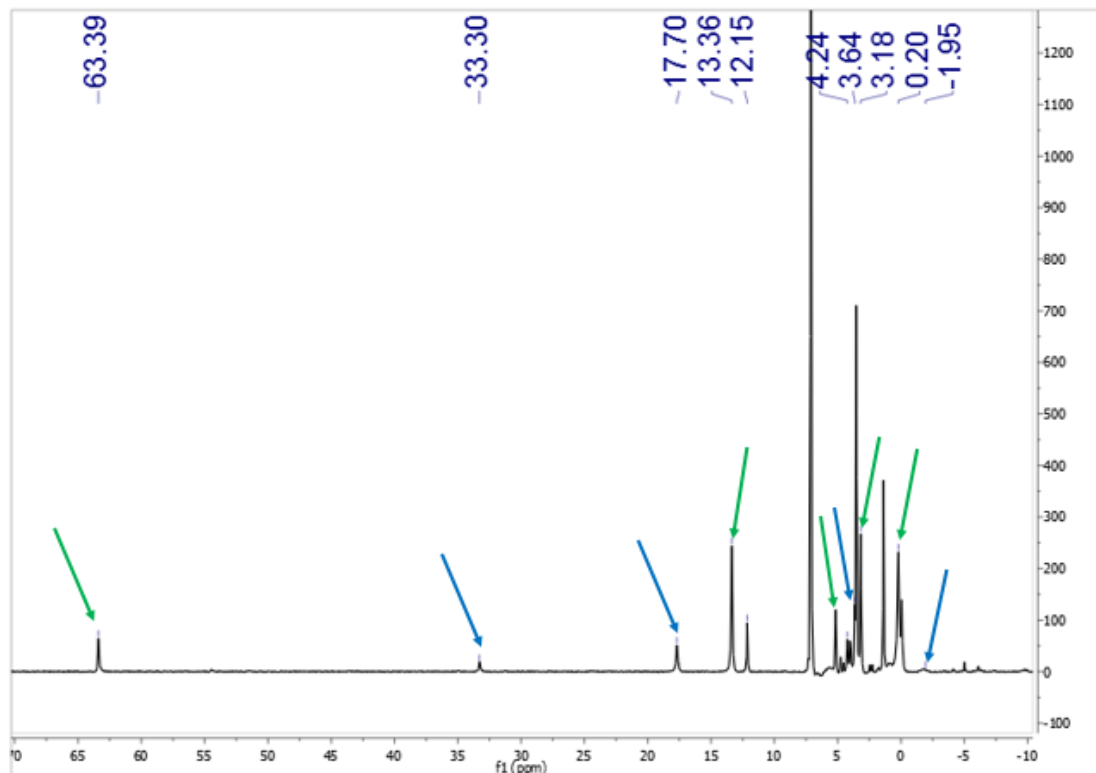
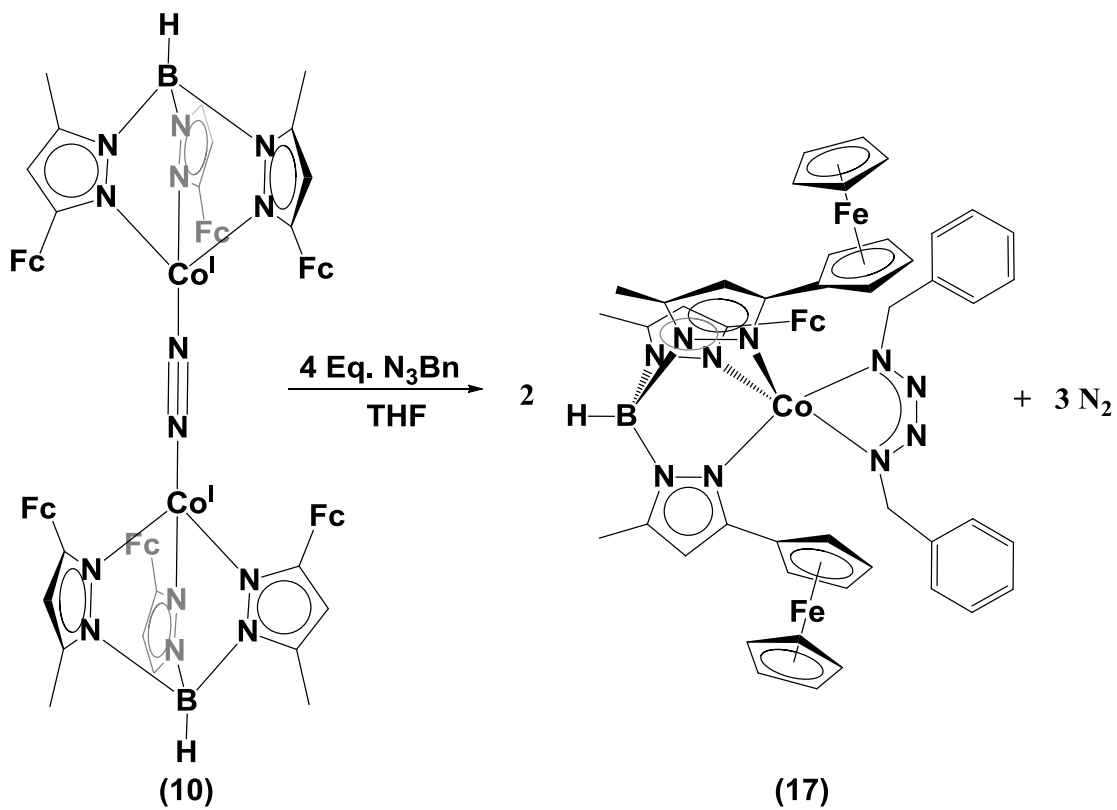


Figure 2.11: $^1\text{H-NMR}$ spectrum of an aliquot taken from the reaction of $\text{Tp}^{\text{Fc,Me}}\text{Co}(\text{O}_2)$ with $[\text{Tp}^{\text{Fc,Me}}\text{Co}]_2(\mu\text{-}\eta^1\text{:}\eta^1\text{-N}_2)$ (10**) at $60\text{ }^\circ\text{C}$ in THF for 21 days, ($\text{Tp}^{\text{Fc,Me}}\text{CoOH}$ = green arrows, $\text{Tp}^{\text{Fc,Me}}\text{Co}(\text{O}_2)$ = blue arrows).**

Reactions of $[\text{Tp}^{\text{Fc,Me}}\text{Fe}]_2(\mu\text{-}\eta^1\text{:}\eta^1\text{-N}_2)$ (9**) and $[\text{Tp}^{\text{Fc,Me}}\text{Co}]_2(\mu\text{-}\eta^1\text{:}\eta^1\text{-N}_2)$ (**10**) with organic azides, general considerations.** Given the inability to produce a stable terminal oxide complex that are not bridging between two metal centers using the $\text{Tp}^{\text{Fc,Me}}$ ligand, the focus was re-directed towards the synthesis of organic imides, which are isoelectronic to terminal oxo moieties and demonstrate similar reactivity.⁴ Reactions of either **9** or **10** with organic azides, in an attempt to produce novel aryl and alkyl imides, produced only a mixture of tetrazene and metal azide complexes. Reaction of even sub-stoichiometric quantities of BnN_3 with **10** in THF produced

$\text{Tp}^{\text{Fc,Me}}\text{Co}(\text{N}_4\text{Bn}_2)$ (**17**), and in good yields (~80%) relative to the amount of azide used, see **Scheme 2.7**. $^1\text{H-NMR}$ spectroscopy indicated that the compound was diamagnetic, exhibiting peaks between 7.5 and 2 ppm, see **Figure 2.12**. The complex is easily purified by extraction with diethyl ether and then layering with pentanes, producing **17** as dark orange blocks. Crystals generated this way were of sufficient quality to determine the structure of **17** by X-ray diffraction analysis. That structure showed that the $\text{Tp}^{\text{Fc,Me}}$ ligand binds to the cobalt metal center in a κ^3 manner, producing a roughly square pyramidal coordination sphere, having a $\tau_5 = 0.286$, see **Figure 2.13**.¹⁶ The crystals contained two molecules of the **17** per asymmetric unit, with the unit cell being triclinic. The N-N bond distances of the tetrazene were determined to be 1.308(4), 1.341(4), and 1.317(4) Å, which appears to indicate a distributed 1⁻ charge to the tetrazene ligand.



Scheme 2.7: Reaction of [Tp^{Fc,Me}Co]₂(μ-η¹:η¹-N₂) (10) with benzyl azide to make Tp^{Fc,Me}CoN₄Bn₂ (17) by elimination of N₂.

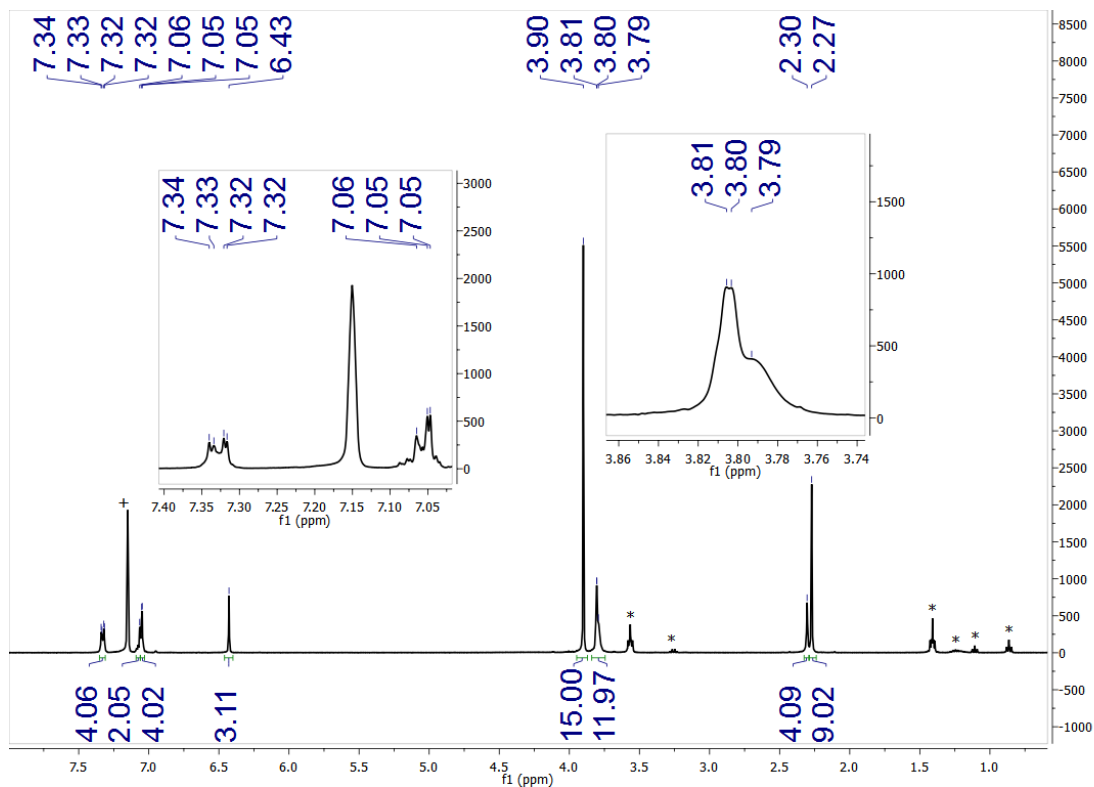


Figure 2.12: ¹H-NMR spectrum of $\text{Tp}^{\text{Fc,Me}}\text{CoN}_4\text{Bn}_2$ (17) recorded in C_6D_6 (7.16 ppm (+)) at 400 MHz, with some THF, ether, and pentane (*) present in the spectrum, (Inset - left: close up of resonances between 7 and 7.4 ppm; Inset - right: Close up of resonance between 3.74 and 3.86ppm)

Table 2.6: Selected interatomic distances (Å) and angles (°) for $\text{Tp}^{\text{Fc,Me}}\text{Co}(\text{N}_4\text{Bn}_2)$

(17).

Distances (Å)

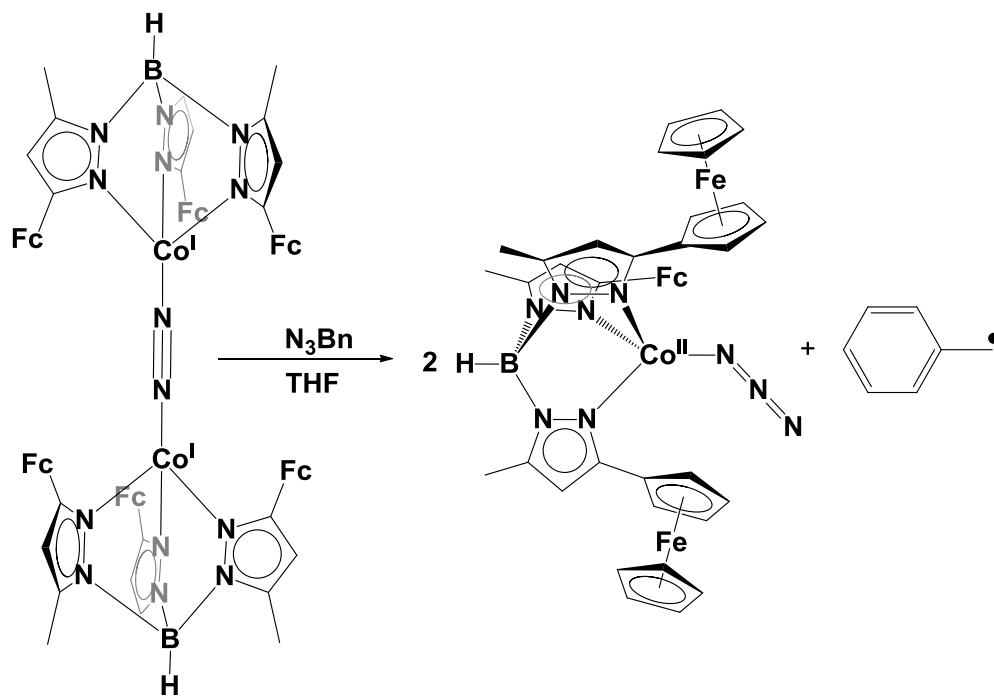
Co1-N4	1.835(3)	Co1-N1	1.846(3)
Co1-N7	2.002(3)	Co1-N9	2.027(3)
Co1-N5	2.056(3)	N1-C1	1.478(5)
N1-N2	1.308(4)	N3-N4	1.341(4)
N2-N3	1.317(4)	N5-C15	1.351(4)
N4-C8	1.482(4)	N6-C17	1.351(4)
N5-N6	1.381(4)	N7-C29	1.354(4)
N6-B1	1.515(5)	N8-C31	1.351(4)
N7-N8	1.376(4)	N9-C43	1.358(4)
N8-B1	1.537(5)	N10-C45	1.355(5)
N9-N10	1.381(4)	C2-C7	1.365(6)
N10-B1	1.531(5)	C9-C14	1.385(6)
C1-C7	1.498(5)	C9-C10	1.393(7)
C2-C3	1.391(7)	C10-C11	1.344(7)
C3-C4	1.389(9)	C11-C12	1.375(7)
C4-C5	1.350(8)	C12-C13	1.399(6)
C5-C6	1.376(7)	C13-C14	1.384(6)
C6-C7	1.387(6)	C15-C16	1.397(5)
C8-C14	1.506(5)		

Angles (°)

N4-Co1-N1	78.60(14)	N4-Co1-N7	148.23(13)
N1-Co1-N7	94.56(13)	N4-Co1-N9	99.09(13)
N1-Co1-N9	171.48(13)	N7-Co1-N9	83.09(12)
N4-Co1-N5	119.61(13)	N1-Co1-N5	94.26(13)
N7-Co1-N5	91.64(12)	N9-Co1-N5	94.00(12)
N2-N1-C1	114.5(3)	N2-N1-Co1	118.6(3)
C1-N1-Co1	126.4(2)	N1-N2-N3	112.7(3)
N2-N3-N4	112.3(3)	N3-N4-C8	109.2(3)
N3-N4-Co1	117.7(2)	C8-N4-Co1	132.9(3)
C15-N5-N6	105.7(3)	C15-N5-Co1	137.3(3)
N6-N5-Co1	115.5(2)	C17-N6-N5	110.1(3)
C17-N6-B1	131.7(3)	N5-N6-B1	118.2(3)
C29-N7-N8	106.4(3)	C29-N7-Co1	135.7(2)
N8-N7-Co1	117.1(2)	C31-N8-N7	109.8(3)

C31-N8-B1	131.7(3)	N7-N8-B1	118.1(3)
C43-N9-N10	105.9(3)	C43-N9-Co1	140.1(2)
N10-N9-Co1	113.8(2)	C45-N10-N9	110.4(3)
C45-N10-B1	127.8(3)	N9-N10-B1	118.1(3)
N12-N11-C57	108.7(3)	N13-N12-N11	111.8(3)
N12-N13-N14	112.9(3)	N6-B1-N8	108.5(3)
N6-B1-N10	110.5(3)	C2-C3-C4	119.0(6)
N10-B1-N8	108.0(3)	C4-C5-C6	120.1(7)
N16-B2-N18	108.8(3)	C2-C7-C6	119.0(4)
N18-B2-N20	108.4(3)	C6-C7-C1	119.0(4)
N1-C1-C7	115.7(3)	C11-C10-C9	119.6(6)
C7-C2-C3	120.7(5)	C11-C12-C13	119.7(6)
C5-C4-C3	120.6(6)	C13-C14-C9	118.1(4)
C5-C6-C7	120.7(5)	C9-C14-C8	119.0(4)
C2-C7-C1	122.0(4)	N5-C15-C27	123.6(3)
N4-C8-C14	115.5(3)	C17-C16-C15	106.1(4)
C14-C9-C10	121.4(5)	N6-C17-C28	121.8(4)
C10-C11-C12	121.0(6)	C14-C13-C12	120.2(5)

The reaction also produced a ~10% yield of another cobalt containing compound, which was suggested first by its IR to be a cobalt azide, having an extremely strong peak with a frequency of 2086 cm^{-1} . This is accomplished through the reduction of the organic fragment of the azide molecule by the Co^{I} species, making N_3^- and R^\bullet , with the N_3^- then binding to the metal center, see **Scheme 2.8**.¹⁷ The cobalt azide produced in the reaction of **10** with benzyl azide can be independently produced by a reaction of $\text{Tp}^{\text{Fc,Me}}\text{CoBr}$ (**4**) with an excess (8 equiv.) of KN_3 in THF, which produces $\text{Tp}^{\text{Fc,Me}}\text{CoN}_3$. More about the purification, reactivity, and the characteristics of this complex will be discussed in **Chapter 4**.



Scheme 2.8: Reaction of $[\text{Tp}^{\text{Fc,Me}}\text{Co}]_2(\mu\text{-}\eta^1\text{:}\eta^1\text{-N}_2)$ (**10**) with benzyl azide, the formation of $\text{Tp}^{\text{Fc,Me}}\text{Co}(\text{N}_3)$ by the formation of an organic radical.

The inability to produce terminal benzyl imide is likely due to its lacking sufficient steric bulk to prevent a second equivalent of azide from reacting with the metal center once an imide is formed, evident from the ability to produce terminal adamantyl imide either from **10** or reduction of a $\text{Tp}^{\text{Fc,Me}}\text{CoI}$ in the presence of AdN_3 .¹⁵

Following the work on cobalt, I set about exploring the reaction of **9** with adamantyl azide, but was unable to produce a terminal imide. In all cases, including those done at low temperature with a dearth of azide, the product mixture was found to contain none of the desired terminal $\text{Tp}^{\text{Fc,Me}}\text{FeNAd}$, but instead a mixture of other products $\text{Tp}^{\text{Fc,Me}}\text{FeN}_3$, and $\text{Pz}^{\text{Fc,Me}}\text{Bp}^{\text{Fc,Me}}\text{FeN}_4\text{Ad}$ (**A2.1**) being present in the product mixture. **A2.1** can be purified from repeated crystallization of the product mixture

using solutions of ether and pentane, see **Figure 2.14**. Given the low yields for the complex, only ~12%, further studies were forgone. The N-N bond lengths of the tetrazene ligand were 1.307(3), 1.327(3), and 1.314(3) Å, given the extreme similarity between the bond lengths it is likely that this ligand is mono-anionic. $\text{Tp}^{\text{Fc,Me}}\text{FeN}_3$ will be further discussed in **Chapter 4**.

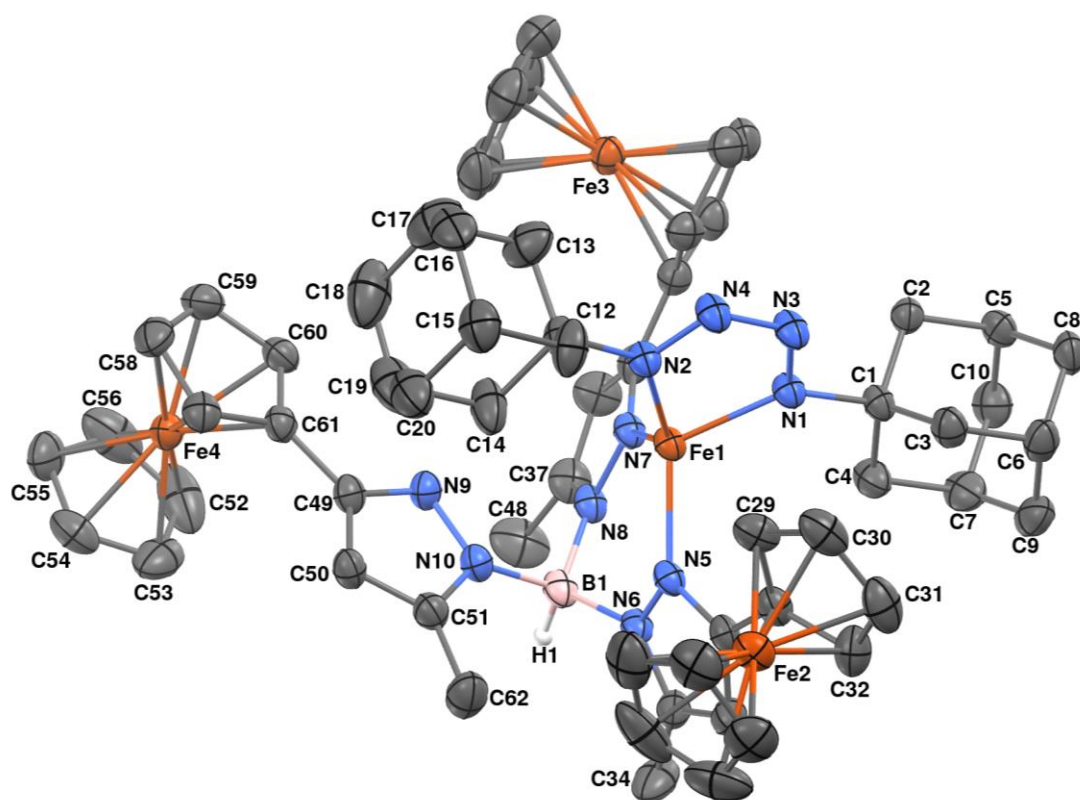


Figure 2.14: Molecular structure of $\text{Tp}^{\text{Fc,Me}}\text{Fe}(\text{N}_4\text{Ad}_2)$ (A2.1) represented as 50% probability thermal ellipsoids. Hydrogen atoms (with the exception of the hydrogen attached to boron, H1) omitted for clarity.

Table 2.7: Selected interatomic distances (Å) and angles (°) for $\text{Tp}^{\text{Fc,Me}}\text{Fe}(\text{N}_4\text{Ad}_2)$ **(A2.1)****Distances (Å)**

Fe1-N2	1.9646(18)	Fe1-N1	1.9743(19)
Fe1-N5	2.0090(19)	Fe1-N7	2.0166(19)
B1-N8	1.543(3)	B1-N10	1.543(3)
B1-N6	1.557(3)	N1-C1	1.490(3)
N1-N3	1.307(3)	N2-C11	1.487(3)
N2-N4	1.314(3)	N5-C21	1.345(3)
N3-N4	1.327(3)	N6-C23	1.350(3)
N5-N6	1.382(3)	N7-N8	1.379(3)
N7-C35	1.344(3)	N9-C49	1.328(3)
N8-C37	1.354(3)	N10-C51	1.359(3)
N9-N10	1.384(3)	C1-C3	1.530(3)
C1-C4	1.525(3)	C2-C5	1.529(3)
C1-C2	1.536(3)	C4-C7	1.543(3)
C3-C6	1.536(4)	C5-C10	1.530(4)
C5-C8	1.526(4)	C6-C9	1.527(4)
C6-C8	1.532(4)	C7-C9	1.525(4)
C7-C10	1.517(4)	C12-C15	1.547(6)
C12-C11	1.542(5)	C13-C17	1.556(7)
C13-C11	1.476(5)	C14-C19	1.591(7)
C14-C11	1.545(5)	C15-C16	1.537(7)
C15-C20	1.515(6)	C16-C17	1.546(9)
C17-C18	1.502(10)	C19-C20	1.475(9)
C18-C19	1.459(11)	C21-C22	1.388(3)
C21-C33	1.464(3)	C22-C23	1.374(4)
C24-C27	1.408(5)	C23-C34	1.499(4)
C29-C30	1.423(4)	C24-C25	1.405(5)
C37-C48	1.502(4)	C25-C26	1.395(4)
C49-C61	1.469(3)	C26-C28	1.402(5)
C52-C56	1.390(5)	C27-C28	1.402(6)
C57-C58	1.407(4)	C52-C53	1.400(5)
C29-C33	1.429(4)	C53-C54	1.395(5)
C30-C31	1.404(4)	C54-C55	1.395(4)
C31-C32	1.423(4)	C55-C56	1.400(5)
C32-C33	1.425(4)	C57-C61	1.427(3)
C49-C50	1.408(3)	C58-C59	1.419(4)

C50-C51	1.377(3)	C59-C60	1.411(4)
C51-C62	1.484(4)	C60-C61	1.421(3)

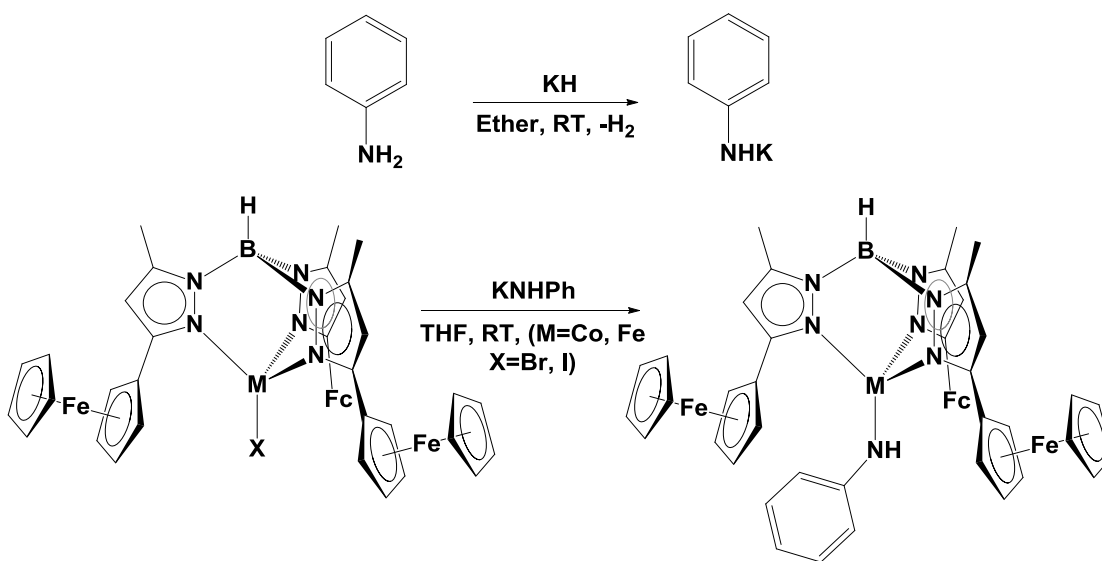
Angles (°)

N2-Fe1-N1	76.70(8)	N2-Fe1-N5	123.67(8)
N1-Fe1-N5	112.22(8)	N2-Fe1-N7	126.24(8)
N1-Fe1-N7	114.52(8)	N5-Fe1-N7	101.25(8)
N8-B1-N6	111.81(19)	N8-B1-N10	107.1(2)
N3-N1-Fe1	116.26(15)	N10-B1-N6	111.2(2)
N4-N2-C11	111.57(17)	N3-N1-C1	111.38(18)
C11-N2-Fe1	131.84(14)	C1-N1-Fe1	132.28(14)
N2-N4-N3	115.00(18)	N4-N2-Fe1	116.58(14)
C21-N5-Fe1	131.40(15)	N1-N3-N4	115.44(18)
C23-N6-N5	109.06(19)	C21-N5-N6	106.71(18)
N5-N6-B1	121.82(18)	N6-N5-Fe1	115.47(14)
C35-N7-Fe1	134.42(16)	C23-N6-B1	128.6(2)
C37-N8-N7	109.1(2)	C35-N7-N8	106.74(18)
N7-N8-B1	122.64(18)	N8-N7-Fe1	118.79(15)
C51-N10-N9	110.27(19)	C37-N8-B1	127.3(2)
N9-N10-B1	117.94(19)	C49-N9-N10	105.72(19)
N1-C1-C3	110.48(19)	C51-N10-B1	130.0(2)
N1-C1-C2	109.63(19)	N1-C1-C4	108.46(18)
C3-C1-C2	109.41(19)	C4-C1-C3	110.0(2)
C8-C5-C2	109.7(2)	C4-C1-C2	108.9(2)
C9-C6-C3	109.6(2)	C5-C2-C1	109.76(19)
C10-C7-C4	109.6(2)	C1-C3-C6	109.2(2)
C11-C12-C15	110.0(3)	C1-C4-C7	109.1(2)
C11-C13-C17	111.1(4)	C8-C5-C10	109.9(2)
C11-C14-C19	109.8(3)	C10-C5-C2	108.9(2)
C20-C15-C16	111.2(4)	C9-C6-C8	109.7(2)
C16-C15-C12	107.9(4)	C8-C6-C3	109.5(2)
C15-C16-C17	109.4(4)	C10-C7-C9	110.1(2)
C18-C17-C16	112.0(6)	C9-C7-C4	109.4(2)
C16-C17-C13	105.7(5)	C5-C8-C6	109.2(2)
C19-C18-C17	113.1(5)	C7-C9-C6	109.3(2)
C18-C19-C20	112.5(5)	C7-C10-C5	109.4(2)
C20-C19-C14	105.3(5)	C20-C15-C12	106.4(4)
C19-C20-C15	113.3(5)	C18-C17-C13	107.8(5)
C13-C11-N2	112.0(2)	C18-C19-C14	107.0(6)

N2-C11-C12	111.1(2)	C13-C11-C12	111.5(3)
N2-C11-C14	106.6(2)	C13-C11-C14	110.0(3)
N5-C21-C33	123.0(2)	C12-C11-C14	105.3(3)
C23-C22-C21	106.3(2)	N5-C21-C22	109.6(2)
N6-C23-C34	124.1(2)	C22-C21-C33	127.3(2)
C27-C24-C25	107.5(3)	N6-C23-C22	108.4(2)
C26-C25-C24	108.5(3)	C22-C23-C34	127.5(2)
C25-C26-C28	107.9(3)	C32-C33-C21	124.6(2)
C24-C27-C28	107.9(3)	N7-C35-C47	123.1(2)
C26-C28-C27	108.2(3)	C37-C36-C35	106.2(2)
C30-C29-C33	108.3(3)	N8-C37-C48	122.5(3)
C31-C30-C29	108.1(3)	N9-C49-C50	111.0(2)
C30-C31-C32	108.3(3)	C50-C49-C61	128.5(2)
C31-C32-C33	108.3(3)	N10-C51-C50	107.6(2)
C32-C33-C29	107.0(2)	C50-C51-C62	129.6(2)
C29-C33-C21	128.5(2)	C60-C61-C49	125.7(2)
N7-C35-C36	109.7(2)	C57-C58-C59	108.0(2)
C36-C35-C47	127.1(2)	C60-C59-C58	108.2(2)
N8-C37-C36	108.2(2)	C59-C60-C61	108.2(2)
C36-C37-C48	129.1(3)	C60-C61-C57	107.3(2)
N9-C49-C61	120.5(2)	C57-C61-C49	127.0(2)
C51-C50-C49	105.4(2)	C53-C54-C55	108.3(3)
N10-C51-C62	122.7(2)	C54-C55-C56	107.9(3)
C56-C52-C53	108.4(3)	C52-C56-C55	107.9(3)
C54-C53-C52	107.6(3)	C58-C57-C61	108.3(2)

Synthesis of $\text{Tp}^{\text{Fc,Me}}\text{MN}(\text{H})\text{Ph}$ complexes, general considerations, and reactions with hydrogen abstraction reagents. Given the difficulties encountered in producing terminal imides from compounds **9** and **10**, I attempted to produce imides using the method demonstrated by Smiths et. al.¹⁸ That pathway involves starting from amides which are then oxidized and deprotonated to form imides, or otherwise reacted with hydrogen atom abstraction reagents to produce the desired imide in a one-step reaction.¹⁸ Given the problem of lithium trans-metalation discussed in **Chapter 2**, I was limited to using potassium amides to produce the iron and cobalt amide starting

materials, meaning I was limited to using aryl substituents as the pKa of alkyl amines is such that they can not be deprotonated by KH.¹⁹ Reaction of either **3** or **4** with 1 equiv. of KN(H)Ph in THF yielded the desired $\text{Tp}^{\text{Fc,Me}}\text{FeNHPH}$ (**18**) or $\text{Tp}^{\text{Fc,Me}}\text{CoNHPH}$ (**19**) in yields of 45 and 64 %, respectively, see **Scheme 2.9**. The work up for both systems was the same, with the reagents being left to stir for ~16 hours, before the solutions were filtered and the solvent removed in vacuo. The resulting solids were then extracted with ether, filtered, and layered with pentanes to crystallize either **18** or **19** as dark orange or dark red crystals respectively. The unit cells of both compounds were nearly the same, with both having one equivalent of ether co-crystallized per asymmetric unit, see **Table B.7** and **Table B.8**. The two complexes are both tetrahedral about the metal centers, having $\tau_4 = 0.707$ and $\tau_4' = 0.645$ for **18**, and $\tau_4 = 0.715$ and $\tau_4' = 0.671$ for **19**,⁷ see **Figure 2.15** and **Figure 2.16**.



Scheme 2.9: Synthesis of $\text{Tp}^{\text{Fc,Me}}\text{FeNHPH}$ (**18**) and $\text{Tp}^{\text{Fc,Me}}\text{CoNHPH}$ (**19**).

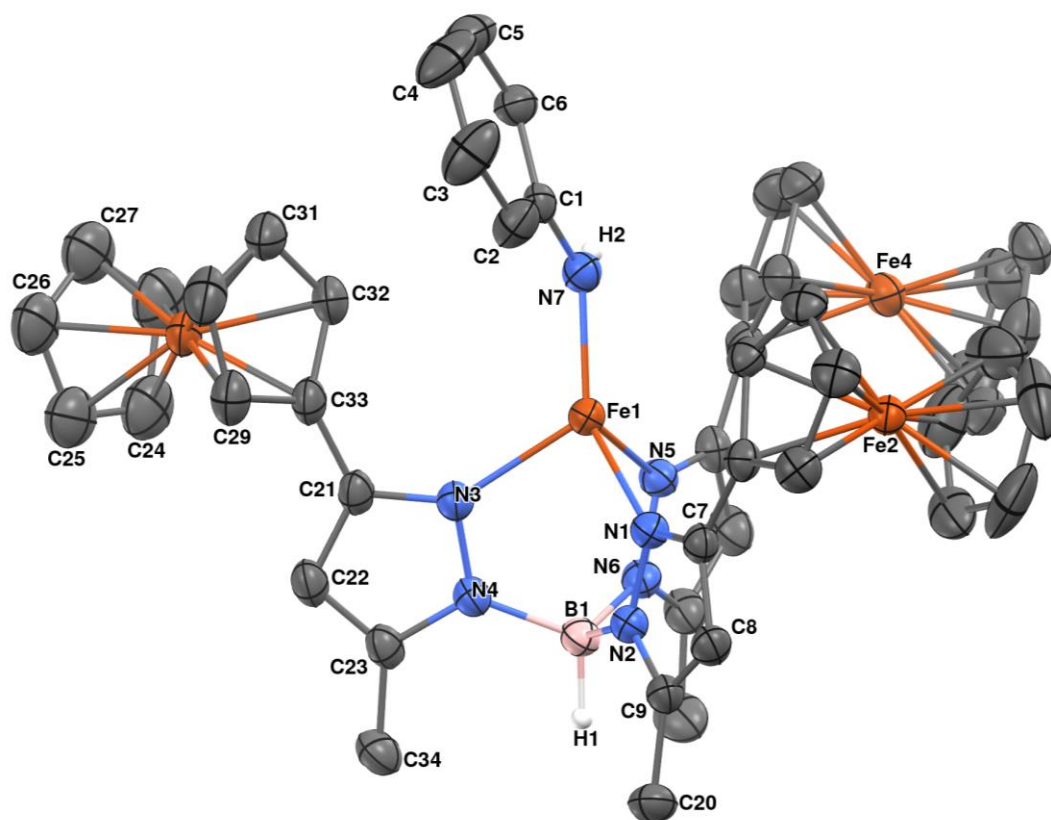


Figure 2.15: Molecular structure of $\text{Tp}^{\text{Fc,Me}}\text{FeNHPPh}$ (18) represented as 50% probability thermal ellipsoids. Hydrogen atoms (with the exception of the hydrogen attached to boron, H1, and the hydrogen attached to N7, H2), and one molecule of ether omitted for clarity.

Table 2.8: Selected interatomic distances (\AA) and angles ($^\circ$) for $\text{Tp}^{\text{Fc,Me}}\text{FeNHPPh}$ (18).

Distances (\AA)			
Fe1-N7	1.936(2)	Fe1-N1	2.0719(19)
Fe1-N5	2.0984(19)	Fe1-N3	2.1135(19)
N1-C7	1.340(3)	N1-N2	1.379(3)
N2-C9	1.350(3)	N2-B1	1.554(3)
N3-C21	1.341(3)	N3-N4	1.369(3)

N4-C23	1.351(3)	N4-B1	1.550(3)
N5-C35	1.338(3)	N5-N6	1.378(3)
N6-C37	1.354(3)	N6-B1	1.544(3)
N7-C1	1.354(3)	C1-C2	1.398(3)
C1-C6	1.423(3)	C2-C3	1.385(4)
C7-C8	1.394(3)	C3-C4	1.381(5)
C8-C9	1.383(3)	C4-C5	1.367(5)
C9-C20	1.490(3)	C5-C6	1.385(4)
C21-C33	1.468(3)	C7-C19	1.456(3)
C24-C25	1.374(5)	C10-C11	1.370(5)
C29-C30	1.419(4)	C21-C22	1.403(3)
C35-C47	1.468(3)	C22-C23	1.370(3)
C38-C39	1.407(5)	C23-C34	1.500(3)
C43-C44	1.428(4)	C24-C28	1.447(5)
C44-C45	1.412(5)	C25-C26	1.386(5)
C45-C46	1.422(4)	C26-C27	1.376(5)
C46-C47	1.421(4)	C27-C28	1.411(5)
C29-C33	1.439(4)	C37-C48	1.491(4)
C30-C31	1.407(5)	C38-C42	1.409(5)
C31-C32	1.425(4)	C39-C40	1.404(5)
C33-C32	1.428(4)	C40-C41	1.405(5)
C35-C36	1.395(4)	C41-C42	1.401(5)
C36-C37	1.381(4)	C43-C47	1.426(4)

Angles (°)

B1-Fe1-N7	162.78(9)	N7-Fe1-N5	112.11(8)
N7-Fe1-N1	140.21(8)	N7-Fe1-N3	120.13(8)
N1-Fe1-N5	87.47(7)	N5-Fe1-N3	94.04(7)
N1-Fe1-N3	90.98(7)	C7-N1-N2	106.49(17)
C9-N2-N1	109.84(19)	C9-N2-B1	129.4(2)
N1-N2-B1	120.57(18)	C21-N3-N4	106.31(18)
C23-N4-N3	110.26(19)	C23-N4-B1	129.2(2)
N3-N4-B1	119.67(18)	C35-N5-N6	106.85(18)
C37-N6-N5	109.54(19)	C37-N6-B1	129.9(2)
N5-N6-B1	120.57(18)	N6-B1-N2	109.35(18)
N6-B1-N4	110.50(19)	N7-C1-C6	122.3(2)
N4-B1-N2	108.61(18)	C3-C2-C1	121.4(3)
N7-C1-C2	122.0(2)	C5-C4-C3	118.5(3)
C2-C1-C6	115.6(2)	C5-C6-C1	121.8(3)
C4-C3-C2	121.6(3)	N1-C7-C19	121.9(2)

C4-C5-C6	120.9(3)	C9-C8-C7	106.0(2)
N1-C7-C8	109.9(2)	N2-C9-C20	123.3(2)
C8-C7-C19	128.0(2)	C18-C19-C15	107.1(2)
N2-C9-C8	107.7(2)	C15-C19-C7	127.9(2)
C8-C9-C20	129.0(2)	N3-C21-C22	109.7(2)
C18-C19-C7	124.7(2)	C22-C21-C33	127.7(2)
N3-C21-C33	122.5(2)	N4-C23-C22	107.8(2)
C23-C22-C21	105.9(2)	C22-C23-C34	129.2(2)
N4-C23-C34	123.0(2)	C32-C33-C21	128.0(2)
C25-C24-C28	106.6(3)	N5-C35-C47	121.5(2)
C24-C25-C26	109.7(3)	C37-C36-C35	106.1(2)
C27-C26-C25	108.7(4)	N6-C37-C48	123.0(2)
C26-C27-C28	108.2(4)	C39-C38-C42	108.1(3)
C27-C28-C24	106.7(3)	C40-C39-C38	108.0(3)
C30-C29-C33	107.7(3)	C45-C44-C43	108.2(3)
C31-C30-C29	108.9(3)	C44-C45-C46	107.8(3)
C30-C31-C32	107.9(3)	C47-C46-C45	108.7(3)
C32-C33-C29	107.1(2)	C46-C47-C43	107.3(2)
C29-C33-C21	124.9(2)	C43-C47-C35	128.1(2)
N5-C35-C36	109.8(2)	C41-C40-C39	107.8(3)
C36-C35-C47	128.8(2)	C42-C41-C40	108.5(3)
N6-C37-C36	107.7(2)	C41-C42-C38	107.6(3)
C36-C37-C48	129.3(2)	C31-C32-C33	108.4(3)
C46-C47-C35	124.6(2)	C47-C43-C44	108.0(2)

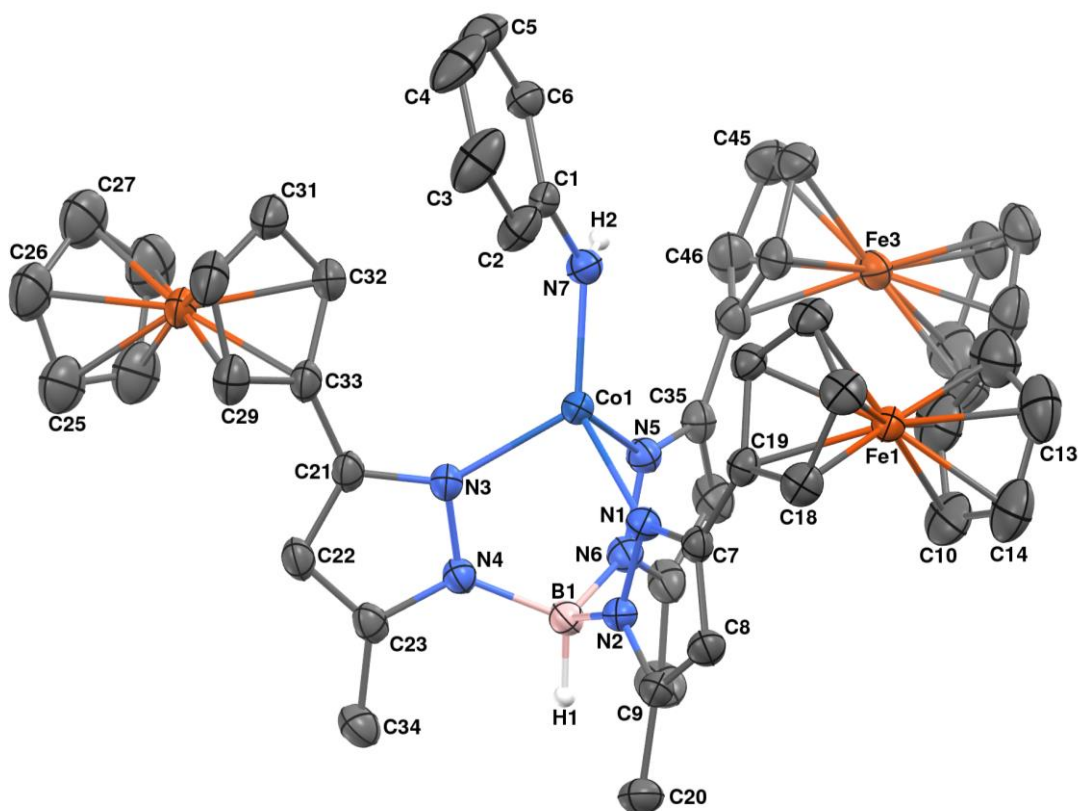


Figure 2.16: Molecular structure of $\text{Tp}^{\text{Fc,Me}}\text{CoNHPh}$ (19) represented as 50% probability thermal ellipsoids. Hydrogen atoms (with the exception of the hydrogen attached to boron, H1, and the hydrogen attached N7, H2), and one molecule of ether omitted for clarity.

Table 2.9: Selected interatomic distances (\AA) and angles ($^\circ$) for $\text{Tp}^{\text{Fc,Me}}\text{CoNHPh}$ (19).

Distances (\AA)			
Co1-N7	1.8961(18)	Co1-N1	2.0379(18)
Co1-N3	2.0438(18)	Co1-N5	2.0663(18)
N1-C7	1.339(3)	N1-N2	1.380(2)
N2-C9	1.351(3)	N2-B1	1.550(3)
N3-C21	1.346(3)	N3-N4	1.371(2)
N4-C23	1.352(3)	N4-B1	1.548(3)

N5-C35	1.339(3)	N5-N6	1.374(2)
N6-C37	1.354(3)	N6-B1	1.548(3)
N7-C1	1.376(3)	C1-C2	1.401(3)
C1-C6	1.407(3)	C2-C3	1.387(4)
C7-C8	1.400(3)	C3-C4	1.374(5)
C8-C9	1.381(3)	C4-C5	1.371(5)
C9-C20	1.490(3)	C5-C6	1.382(4)
C10-C14	1.415(5)	C7-C19	1.459(3)
C11-C12	1.393(5)	C10-C11	1.393(5)
C12-C13	1.358(5)	C15-C16	1.421(3)
C13-C14	1.412(5)	C21-C22	1.402(3)
C15-C19	1.436(3)	C22-C23	1.376(3)
C16-C17	1.419(3)	C23-C34	1.499(3)
C17-C18	1.424(3)	C24-C28	1.450(5)
C18-C19	1.432(3)	C25-C26	1.389(5)
C21-C33	1.465(3)	C26-C27	1.379(5)
C24-C25	1.385(5)	C27-C28	1.417(5)
C29-C30	1.420(4)	C29-C33	1.434(3)
C35-C47	1.466(3)	C30-C31	1.419(4)
C38-C42	1.406(5)	C31-C32	1.426(4)
C43-C47	1.426(3)	C33-C32	1.430(3)
C44-C45	1.409(5)	C35-C36	1.402(3)
C45-C46	1.419(4)	C36-C37	1.378(3)
C46-C47	1.430(3)	C37-C48	1.493(3)

Angles (°)

B1-Co1-N7	162.37(8)	N7-Co1-N3	122.33(8)
N7-Co1-N1	136.78(8)	N7-Co1-N5	108.03(8)
N1-Co1-N3	93.86(7)	N3-Co1-N5	95.72(7)
N1-Co1-N5	88.95(7)	C7-N1-N2	106.60(16)
C7-N1-Co1	141.43(14)	N2-N1-Co1	111.72(12)
C9-N2-N1	109.69(17)	C9-N2-B1	129.58(18)
N1-N2-B1	120.58(16)	C21-N3-N4	106.81(17)
C21-N3-Co1	140.01(15)	N4-N3-Co1	113.06(13)
C23-N4-N3	109.91(18)	C23-N4-B1	129.63(18)
N3-N4-B1	119.59(16)	C35-N5-N6	106.72(17)
C35-N5-Co1	141.34(15)	N6-N5-Co1	111.92(13)
C37-N6-N5	109.87(18)	C37-N6-B1	129.64(19)
N5-N6-B1	120.47(17)	C1-N7-Co1	130.70(15)
N4-B1-N6	110.00(17)	N4-B1-N2	108.78(17)

N6-B1-N2	109.12(17)	N7-C1-C6	122.3(2)
N7-C1-C2	121.0(2)	C3-C2-C1	120.6(2)
C2-C1-C6	116.6(2)	C3-C4-C5	118.4(3)
C4-C3-C2	121.8(3)	C5-C6-C1	121.4(2)
C6-C5-C4	121.1(3)	N1-C7-C19	122.18(18)
N1-C7-C8	109.89(19)	C9-C8-C7	105.85(19)
C8-C7-C19	127.78(19)	N2-C9-C20	123.0(2)
N2-C9-C8	107.94(19)	C11-C10-C14	107.3(3)
C8-C9-C20	129.1(2)	C12-C11-C10	107.9(3)
C18-C19-C7	124.62(19)	C13-C12-C11	109.5(4)
N3-C21-C33	122.47(19)	C12-C13-C14	108.1(3)
C23-C22-C21	106.16(19)	C13-C14-C10	107.2(3)
N4-C23-C34	123.0(2)	C16-C15-C19	107.76(19)
C25-C24-C28	106.7(3)	C17-C16-C15	108.6(2)
C24-C25-C26	109.5(3)	C16-C17-C18	108.0(2)
C27-C26-C25	108.9(3)	C17-C18-C19	108.1(2)
C26-C27-C28	108.3(3)	C18-C19-C15	107.49(19)
C27-C28-C24	106.6(3)	C15-C19-C7	127.57(19)
C30-C29-C33	108.1(2)	N3-C21-C22	109.3(2)
C31-C30-C29	108.3(2)	C22-C21-C33	128.2(2)
C30-C31-C32	108.1(2)	N4-C23-C22	107.87(19)
C32-C33-C29	107.4(2)	C22-C23-C34	129.1(2)
C29-C33-C21	124.8(2)	C32-C33-C21	127.8(2)
N5-C35-C36	109.7(2)	N5-C35-C47	122.0(2)
C36-C35-C47	128.3(2)	C37-C36-C35	106.0(2)
N6-C37-C36	107.7(2)	N6-C37-C48	123.1(2)
C36-C37-C48	129.1(2)	C42-C38-C39	108.2(3)
C46-C47-C35	124.6(2)	C45-C44-C43	108.2(2)
C40-C39-C38	107.8(3)	C44-C45-C46	108.3(2)
C41-C40-C39	107.9(3)	C47-C46-C45	108.2(3)
C40-C41-C42	108.3(3)	C46-C47-C43	107.2(2)
C38-C42-C41	107.8(3)	C43-C47-C35	128.2(2)
C33-C32-C31	108.1(2)	C44-C43-C47	108.2(2)

Neither **18** nor **19** produced the desired imide complexes when reacted with 2,4,6-tri-tert-butylphenoxy radical, which has an O-H BDE of 82.7 Kcal/mol.²⁰ **18**

showed no reactivity at all, while **19** instead produced $\text{Tp}^{\text{Fc,Me}}\text{Co}-(2,4,6\text{-tri-tertbutylphenoxy})$, observed in LIFDI-MS of the reaction mixture, see **Figure 2.17**.

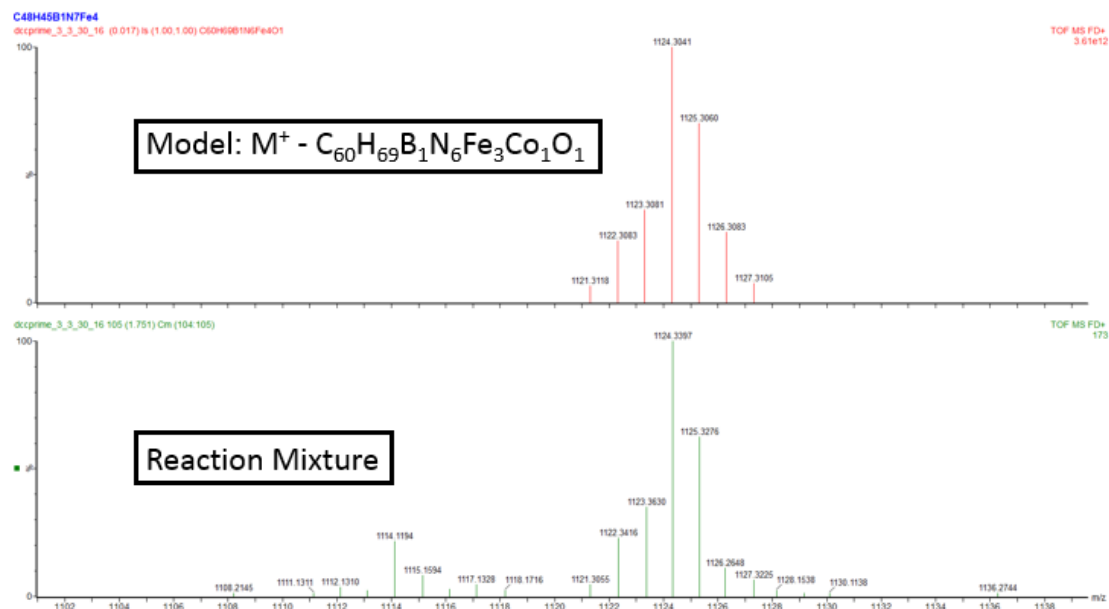


Figure 2.17: LIFDI-MS of the result from a reaction of (19) with 2,4,6-tri-tert-butylphenoxy radical (bottom), calculated isotope pattern for $\text{C}_{60}\text{H}_{69}\text{B}_1\text{N}_6\text{Fe}_3\text{Co}_1\text{O}_1$ (top).

Conclusions

The reactivity of low valent complexes of cobalt and iron supported by the $\text{Tp}^{\text{Fc,Me}}$ ligand system with oxygen atom transfer reagents, including dioxygen gas, has been explored. A novel bridging $\text{Fe}^{\text{II}}/\text{Fe}^{\text{II}}$ oxo complex has been synthesized and is only the second example of such a moiety to have been structurally characterized. This result, taken together with the result that the terminal cobalt superoxide complex with the same ligand does not activate the ferrocenyl C-H bonds, demonstrates the ability of the $\text{Tp}^{\text{Fc,Me}}$ ligand to access novel chalcogenide species. Reactions of the mono-

valent compounds **9** and **10** with organic azide could not produce a terminal imide compound, likely due to the somewhat low steric bulk of the ligand when compared to its $\text{Tp}^{\text{tBu,Me}}$ analogue.

Experimental Section

All reactions were run under a nitrogen atmosphere using standard glovebox and Schlenk techniques, unless otherwise stated. Diethyl ether, pentane, tetrahydrofuran (THF), and toluene were distilled from Na, using benzophenone ketyl as an indicator, while under a nitrogen atmosphere, or by passing the solvent through activated alumina columns followed by a nitrogen purge to remove dissolved oxygen.²¹ Organic chemicals were bought from Fischer, Aldrich, or Acros and all inorganic chemicals were purchased from Strem. Carbon monoxide gas was purchased from Matheson. NMR spectra were obtained on Bruker AVIII-400 or AV-600 spectrometers and were referenced to the residual protons of the solvent (C_6D_6 , 7.16 ppm; THF- D_8 , 3.76, 1.85 ppm). FT-IR spectra were recorded on a Nicolet Magna-IR 560 spectrometers with a resolution of 4 cm^{-1} . Mass spectra (LIFDI-MS) were obtained in the University of Delaware Mass Spectrometry Laboratory, using a Waters GCT Premier high resolution time-of-flight mass spectrometer. X-ray crystallographic studies were conducted in the University of Delaware X-ray crystallographic facility. Molar magnetic susceptibilities (χ_{m}) were measured in the solid state at room temperature using a Johnson Matthey magnetic susceptibility balance, and corrected for diamagnetism using Pascal constants to calculate effective magnetic moments (μ_{eff}).²² Elemental analyses were obtained from Robertson Microlit, Ledgewood, NJ 07852.

General considerations for X-ray diffraction studies: Crystals were selected, sectioned as necessary, and mounted on MiTeGen™ plastic mesh with viscous oil, then flash-cooled to the data collection temperature (200 K). Diffraction data were collected on a Bruker-AXS CCD diffractometer with graphite-monochromated Mo-K α radiation ($\lambda = 0.71073 \text{ \AA}$). The data-sets were treated with absorption corrections based on redundant multi-scan data.²³ The structures were solved using direct methods and refined with full-matrix, least-squares procedures on F^2 . Unit cell parameters were determined by sampling three different sections of the Ewald sphere. Non-hydrogen atoms were refined with anisotropic displacement parameters. Hydrogen atoms were treated as idealized contributions with geometrically calculated positions and with U_{iso} equal to 1.2, or 1.5 for methyl, U_{eq} of the attached atom. Structure factors and anomalous dispersion coefficients are contained in the SHELXTL program library.²⁴

Tp^{Fc,Me}FeO(CPh₃) (13): 200 mg (0.202 mmol) of Tp^{Fc,Me}FeI was added to a solution of 63 mg (0.212 mmol, 1 equiv.) potassium KOCPh₃. The solution color changed steadily from orange to dark orange over the course of 30 minutes of stirring. The volatiles were removed in vacuo, and the orange residue was redissolved in ether and filtered through celite. Crystals were grown by slow evaporation of the ether solution, affording dark orange crystals of the desired Tp^{Fc,Me}FeO(CPh₃) complex, with a total mass of 0.130 g (0.116 mol, 55 % yield). ¹H-NMR (400 MHz, C₆D₆) 53.3 (br, 6H), 47.1 (br, 3H), 43.7 (br, 1H), 42.0 (br, 9H), 13.6 (br, 6H), -1.3 (br, 6H), -8.2 (br, 15H), -9.7 (br, 3H), -25.1 (br, 6H) δ ; IR (KBr): 3091 (m), 3019 (w), 2974 (m), 2924 (m), 2864 (m), 2543 (m, B-H), 1561 (s), 1518 (m), 1487 (w), 1469 (s), 1443 (s), 1428 (s),

1403 (s), 1372 (s), 1362 (s), 1350 (s), 1324 (m), 1181 (vs, br), 1106 (s), 1064 (s), 1028 (s), 1001 (s), 982 (m), 938 (w), 918 (w), 884 (s), 812 (s), 786 (s), 758 (s), 700 (s), 676 (w), 638 (s), 579 (m), 534 (s), 504 (s), 489 (s), 476 (s) cm^{-1} ; m.p. 297 – 299 °C; $\mu_{\text{eff}} = 2.7(1) \mu_{\text{B}}$ (296 K); MS (LIFDI, THF): m/z 1122.2085 [M^+]. Calcd.: 1122.1945 [M^+];

$\text{Tp}^{\text{Fc,Me}}\text{FeS}(\text{CPh}_3)$ (14**):** 1.000 g (1.01 mmol) of **3** was added to a solution of 0.333 g (1.062 mmol, 1 equiv.) of KOCPh_3 . The solution color changed steadily from orange to dark orange over the course of 30 minutes of stirring. The volatiles were removed in vacuo, and the orange residue was redissolved in ether and filtered through celite.

Crystals of the desired complex grew from the ether extract after filtration,

$\text{Tp}^{\text{Fc,Me}}\text{FeS}(\text{CPh}_3)$ was collected as dark orange crystals, with a total mass of 0.660 g (0.576 mmol, 57 % yield). $^1\text{H-NMR}$ (400 MHz, C_6D_6) 57.2 (br, 3H), 44.8 (br, 6H), 30.5 (br, 9H), 27.3 (br, 1H, B-H), 9.4 (br, 3H), 4.3 (br, 15H), 2.1 (br, 6H), -1.8 (br, 6H) δ ; IR (KBr): 3101 (m), 3076 (m), 3050 (m), 3016 (w), 2967 (m), 2928 (m), 2862 (m), 2548 (m, B-H), 1592 (w), 1557 (s), 1516 (m), 1488 (m), 1466 (m), 1440 (sh), 1428 (s), 1402 (s), 1370 (s), 1350 (sh), 1323 (m), 1185 (s), 1176 (sh), 1107 (s), 1060 (s), 1048 (sh), 1001 (s), 982 (s), 927 (w), 883 (s), 815 (s), 791 (s), 767 (sh), 757 (s), 741 (s), 705 (s), 674 (w), 650 (m), 620 (m), 592 (vw), 525 (m), 505 (s), 489 (s), 473 (m), 439 (m) cm^{-1} ; m.p. 234 – 237 °C; $\mu_{\text{eff}} = 4.6(1) \mu_{\text{B}}$ (295 K); MS (LIFDI, THF): m/z 1138.1769 [M^+]. Calcd.: 1138.1716 [M^+]; Anal. Calcd for $\text{C}_{61}\text{H}_{55}\text{B}_1\text{N}_6\text{Fe}_4\text{S}_1$: C, 64.36; H, 4.87; N, 7.38. Found C, 63.48; H, 4.92; N, 7.12.

$[\text{Tp}^{\text{Fc,Me}}\text{Fe}]_2(\mu_2\text{-}\eta^1\text{-}\eta^1\text{-S})$ (15**):** 100 mg (0.088 mmol) of **14** was placed in a flask with 10 ml of benzene, along with 22 mg (0.084 mmol, 1 equiv.) of 18-crown-6. To this

mixture was added 4 mg (0.088 mmol, 1 equiv.) of KH, and the solution was left to stir for 13 hours during which its color darkened significantly, but remained orange. The mixture was filtered and the solvent removed in vacuo. The residue was then extracted with THF and layered with pentane, with the product crystallizing out as dark orange crystals, with a total mass of 31 mg (0.018 mmol, 40 % yield). ¹H-NMR (400 MHz, C₆D₆) 21.5 (br, 6H), 18.4 (br, 18H), 2.8 (br, 12H), 0.6 (br, 30H), -3.5 (br, 12H) δ; IR (KBr): 3095 (m), 3055 (m), 2959 (m), 2924 (m), 2867 (m), 2540 (m, B-H), 1560 (s), 1519 (m), 1467 (s), 1428 (s), 1403 (s), 1363 (s), 1350 (s), 1318 (m), 1255 (w), 1213 (sh), 1188 (s, br), 1106 (s), 1063 (s), 1048 (sh), 1028 (m), 1000 (s), 982 (s), 883 (s), 812 (s), 780 (s), 760 (s), 715 (w), 669 (w), 645 (s), 587 (w), 531 (s), 504 (s), 489 (s), 472 (s), 440 (m) cm⁻¹; m.p. 212 – 215 °C; μ_{eff} = 5.0(1) μ_B (298 K); MS (LIFDI, THF): m/z 1758.0967 [M⁺]. Calcd.: 1758.1375 [M⁺];

[Tp^{Fc,Me}Fe]₂(μ₂-η¹:η¹-O) (16): 18 mg (0.188 mmol) of pyridine-N-oxide was added to a stirred solution of 300 mg (0.171 mmol, 1 equiv.) of **9** dissolved in benzene. The solution was stirred for 30 minutes, during which the solution color became progressively lighter, changing from deep red to orange. The solution also went from opaque to translucent. During this time the mixture effervesced, signifying the release of nitrogen gas. Upon completion of the reaction, the mixture was filtered and layered with pentane to produce crystals of [Tp^{Fc,Me}Fe]₂(μ₂-η¹:η¹-O), with a yield of 170 mg (0.977 mmol, 57 % yield). ¹H-NMR (400 MHz, C₆D₆) 15.0 (br, 18H), 12.3 (br, 6H), 1.24 (br, 12H), 0.13 (br, 30H), -9.6 (br, 2H, B-H) δ; IR (KBr): 3092 (m), 2957 (m), 2923 (m), 2868 (m), 2530 (B-H), 1635 (w), 1562 (s), 1520 (w), 1467 (m), 1429 (s), 1402 (s), 1362 (s), 1322 (m), 1257 (vw), 1185 (s), 1106 (s), 1062 (s), 1046 (s), 1026

(m), 1000 (m), 981 (m), 903 (sh), 882 (s), 814 (s), 780 (s), 716 (w), 678 (w), 646 (m), 591 (vw), 531 (m), 505 (s), 490 (m), 472 (m), 437 (m) cm^{-1} ; m.p. $>315\text{ }^{\circ}\text{C}$; $\mu_{\text{eff}} = 2.9(1)\ \mu_{\text{B}}$ (298 K); MS (LIFDI, THF): m/z 1742.1603 [M^+]. Calcd.: 1742.1509 [M^+]; Anal. Calcd for $\text{C}_{84}\text{H}_{80}\text{N}_{12}\text{B}_2\text{Fe}_8\text{O}$ and 2 benzenes, 2 benzene molecules being present in the crystal structures asymmetric unit: C, 61.38; H, 4.94; N, 8.68. Found C, 61.54; H, 4.97; N, 9.23.

$\text{Tp}^{\text{Fc,Me}}\text{CoN}_4\text{Bn}_2$ (17): 600 mg (0.342 mmol) of **10** was added to a scintillation vial with a magnetic stir bar, and dissolved in 15 ml of THF. To this solution was added 182 mg (1.37 mmol, 4 equiv.) of benzyl azide, dropwise over the course of ~ 2 minutes. The solution became effervescent with the formation of N_2 gas, with the reaction reaching completion after only 5 minutes. The solvent was removed in vacuo, producing a brown residue, which was washed with pentanes and then stirred with ether for several minutes before the ether solution was filtered. Layering of the ether extracts with pentanes overnight afforded the desired product as dark brown crystals, having a total mass of 450 mg (0.411 mmol, 60 % yield). $^1\text{H-NMR}$ (400 MHz, C_6D_6) 7.33 (dd, 4H, $J = 2.4, 7.6\text{ Hz}$), 7.06 (m, 2H), 7.05 (d, 4H, $J = 1.6\text{ Hz}$), 6.43 (s, 3H), 3.90 (s, 15H), 3.8045 (d, 6H, $J = 1.2\text{ Hz}$), 3.79 (br, 6H), 2.30 (s, 4H), 2.27 (s, 9H) δ ; IR (KBr): 3085 (m), 3060 (w), 3028 (w), 2960 (m), 2920 (m), 2860 (m), 2527 (m, B-H), 1555 (s), 1520 (w), 1494 (m), 1454 (s), 1423 (s), 1397 (s), 1362 (s), 1317 (m), 1260 (w), 1209 (s), 1195 (s), 1184 (s, br), 1107 (s), 1066 (s), 1184 (s), 1022 (m), 1001 (s), 978 (sh), 915 (w), 883 (s), 815 (s), 791 (s), 775 (sh), 760 (m), 737 (s), 714 (vw), 699 (s), 677 (w), 640 (m), 529 (m), 503 (s), 489 (s), 473 (s), 438 (m) cm^{-1} ; m.p. 192 – 195 $^{\circ}\text{C}$ dec; MS (LIFDI, THF): m/z 1104.2113 [M]. Calcd.: 1104.2020 [M]; Anal. Calcd

for $C_{56}H_{54}B_1N_{10}Fe_3Co_1$ and 1 Et_2O , the crystals having 1 ether molecule per molecule of **17**: C, 61.15; H, 5.47; N, 11.89. Found C, 60.71; H, 5.48; N, 11.12.

Tp^{Fc,Me}FeN(H)Ph (18): 200 mg (0.202 mmol), of **3** along with 28 mg (0.212 mmol, 1 equiv.) of PhNHK, prepared independently by reaction of NH_2Ph with KH in ether, where placed in a vial with a magnetic stir bar, and 10ml of THF was added. The solution was left to stir for 16 hours, it was then filtered and the volatiles removed in vacuo. The resulting residue was extracted with ether and filtered, then layered with pentane to crystallize the desired product as dark orange crystals, having a total mass of 87 mg (0.091 mmol, 45 % yield). 1H -NMR (400 MHz, C_6D_6) 59.0 (br, 2H), 53.2 (br, 3H), 49.7 (br, 1H), 40.0 (br, 9H), 1.16 (br, 6H), -4.34 (br, 15H), -9.7 (6H), -61.5 (br, 2H) δ ; IR (KBr): 3346 (vw, N-H), 3081 (m), 2977 (m), 2955 (m), 2931 (m), 2544 (m, B-H), 1591 (s), 1562 (s), 1516 (w), 1489 (s), 1468 (s), 1428 (s), 1403 (s), 1358 (s), 1322 (m), 1287 (s), 1222 (w), 1176 (s), 1106 (m), 1059 (vs), 1026 (m), 1000 (m), 985 (m), 886 (s), 814 (s), 786 (s), 749 (s), 717 (w), 691 (m), 637 (m), 598 (w), 529 (m), 503 (s), 490 (s), 474 (m), 437 (w) cm^{-1} ; m.p. 268 – 271 $^{\circ}C$; $\mu_{eff} = 4.9(1) \mu_B$ (298 K); MS (LIFDI, THF): m/z 955.1228 [M]. Calcd.: 955.1318 [M]; This complex is highly sensitive to Oxygen, Anal. Calcd for $C_{48}H_{46}B_1N_7Fe_4O_2$: C, 58.40; H, 4.70; N, 9.93. Found C, 57.81; H, 4.52; N, 10.27.

Tp^(Fc,Me)CoN(H)Ph (19): 200 mg (0.212 mmol), of **4** along with 29 mg (0.222 mmol, 1 equiv.) of PhNHK, prepared independently by reaction of NH_2Ph with KH in ether, were placed in a vial with a magnetic stir bar, and 10ml of THF was added. The solution was left to stir for 16 hours, it was then filtered and the volatiles removed in vacuo. The resulting residue was extracted with ether and filtered, then layered with

pentane to crystallize the desired product as dark red crystals, having a total mass of 130 mg (0.135 mmol, 64 % yield). $^1\text{H-NMR}$ (400 MHz, C_6D_6) 58.0 (br, 3H), 17.5 (br, 9H), 3.98 (br, 2H), 3.39 (br, 6H), 2.37 (br, 2H), 1.66 (br, 15H), -90.8 (br, 1H) δ ; IR (KBr): 3349 (w, N-H), 3091 (m), 2973 (m), 2869 (m), 2542 (m, B-H), 1589 (s), 1561 (s), 1517 (w), 1488 (s), 1465 (s), 1428 (s), 1402 (s), 1350 (s), 1318 (m), 1292 (s), 1174 (vs), 1105 (s), 1061 (vs), 1025 (m), 1000 (m), 986 (m), 882 (s), 816 (s), 784 (s), 750 (s), 715 (w), 690 (m), 645 (m), 601 (w), 571 (w), 531 (m), 504 (s), 489 (s), 468 (m), 439 (w) cm^{-1} ; m.p. 249 – 253 $^\circ\text{C}$; $\mu_{\text{eff}} = 3.8(1) \mu_{\text{B}}$ (298 K); MS (LIFDI, THF): m/z 958.1346 [M]. Calcd.: 958.1243 [M]; Anal. Calcd for $\text{C}_{48}\text{H}_{46}\text{B}_1\text{N}_7\text{Fe}_3\text{Co}$: C, 60.17; H, 4.84; N, 10.23. Found C, 60.45; H, 4.71; N, 10.22.

REFERENCES

1. a) Punniyamurthy, T.; Velusamy, S.; Iqbal, J., *Chem. Rev.*, **2005**, *105*, p. 2329 – 2364; b) Jankowiak, J. T.; Barteau, M. A., *J. Catal.*, **2005**, *236*, p. 366 – 378.
2. Cummins, D. C.; Yap, G. P. A.; Theopold, K. H., *Eur. J. Inorg. Chem.*, **2016**, *15*, p. 2349 – 2356.
3. F. A. Jove, Ph. D. thesis, University of Delaware (Newark, DE), **2008**.
4. Marshman, R. W.; Shapley, P. A., *J. Am. Chem. Soc.*, **1990**, *112*, p. 8369 – 8378.
5. Eikey, R. A.; Abu-Omar, M. M., *Coord. Chem. Rev.*, **2003**, *243*, p. 83.
6. Hartmann, N. J.; Wu, G.; Hayton, T. W., *Angew. Chem. Int. Ed. Engl.*, **2015**, *54*, p. 14956 – 14959.
7. Yang, L.; Powell, D. R.; Houser, R. P., *Dalton Trans.*, **2007**, *0*, p. 955 – 964.
8. Jove, F. A.; Pariya, C.; Scoblete, M.; Yap, G. P. A.; Theopold, K. H., *Chem. Eur. J.*, **2011**, *17*, p. 1310 – 1313.
9. a) Ito, M.; Amagai, H.; Fukui, H.; Kitajima, N.; Moro-oka, Y., *Bull. Chem. Soc. Jpn.*, **1996**, *69*, p. 1937; b) Matsunaga, Y.; Fujisawa, K.; Ibi, N.; Miyashita, Y.; Okamoto, K., *Inorg. Chem.*, **2005**, *44*, p. 325 – 335.
10. Sazama, G. T.; Betley, T., *Inorg. Chem.*, **2014**, *53*, p. 269 – 281.
11. Smith, J. M.; Mayberry, D. E.; Margarit, C. G.; Sutter, J.; Wang, H.; Meyer K.; Bontchev, R. P., *J. Am. Chem. Soc.*, **2012**, *134*, p. 6516 – 6519.
12. Eckert, N. A.; Stoian, S.; Smith, J. M.; Bominaar, E. L.; Münck, E.; Holland, P. L., *J. Am. Chem. Soc.*, **2005**, *127*, p. 9344 – 9345.
13. Comment, CCSD (3-20-17) search returns only 1 Fe^{II}-O-Fe^{II} structure.
14. Waller, B. J.; Lipscomb, J. D., *Chem. Rev.*, **1996**, *96*, p. 2625 – 2658.

15. E. R. Sirianni, Ph. D. thesis, University of Delaware (Newark, DE), USA, **2014**.
16. Addison, A. W.; Rao, N. T.; Reedijk, J.; van Rijn, J.; Verschoor, G. C., *J. Chem. Soc., Dalton Tans.*, **1984**, 0, p. 1349 – 1356.
17. Shay, D. T.; Yap, G. P. A.; Zakharov, L. N.; Rheingold, A. L.; Theopold, K. H., *Angew. Chem. Int. Ed.* **2005**, 44, p. 1508 – 1510.
18. a) Nieto, I.; Ding, F.; Bontchev, R. P.; Wang, H.; Smith, J. M., *J. Am. Chem. Soc.*, **2008**, 130, p. 2716 – 2717; b) Cowley, R. E.; Bontchev, R. P.; Sorrell, J.; Sarracino, O.; Feng, Y.; Wang, H.; Smith, J. M., *J. Am. Chem. Soc.*, **2007**, 129, p. 2424 – 2425.
19. a) Bordwell, F. G.; Algrim, D. J., *J. Am. Chem. Soc.*, **1988**, 110, p. 2965; b) Bordwell, F. G.; Drucker, G. E.; Fried, H. E., *J. Org. Chem.*, **1981**, 46 (3), p. 632 – 635; c) Bordwell, F. G.; Algrim, D.; Vanier, N. R., *J. Org. Chem.*, **1977**, 42 (10), p. 1817 – 1819.
20. Lucarini, M.; Pedulli, G. F., *Chem. Soc. Rev.*, **2010**, 39, p. 2106 – 2119.
21. Pangborn, A. B.; Giardello, M. A.; Grubbs, R. H.; Rosen, R. K.; Timmers, F. J., *Organometallic*, **1996**, 15, p. 1518 – 1520.
22. Bain, G. A.; Berry, J. F., *J. Chem. Educ.*, **2008**, 85, p. 532 – 536.
23. Apex2, Bruker-AXS Inc, Madison, WI, p. 2007.
24. Sheldrick, G.M., *Acta Cryst.*, **2008**, A64, p. 112.

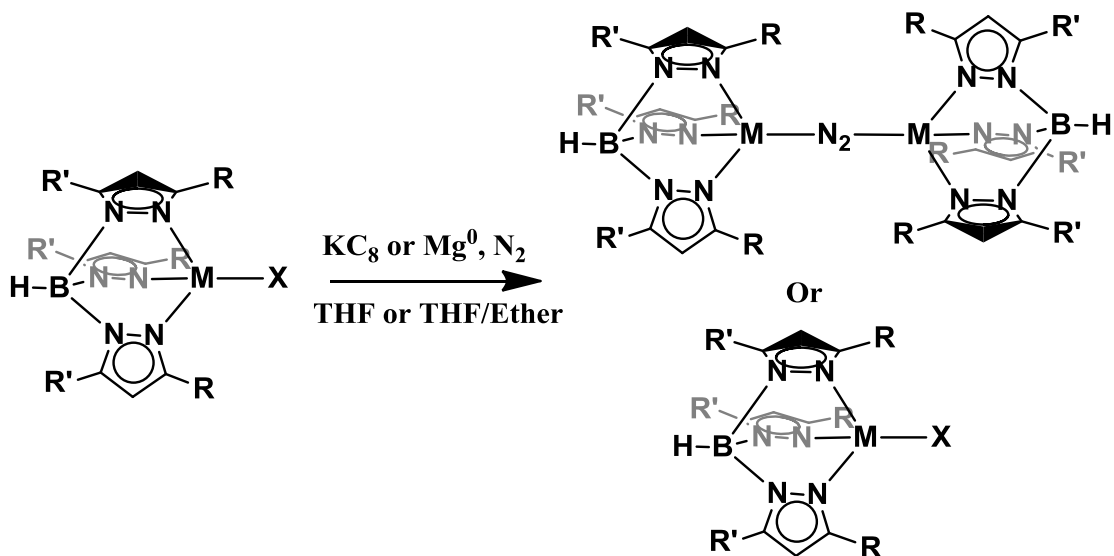
Chapter 4
SYNTHESIS OF NITRIDO COMPLEXES SUPPORTED BY
TRIS(PYRAZOLYL)BORATO LIGANDS, THEIR CHARACTERIZATION
AND REACTIVITY

INTRODUCTION

Nitride complexes of first row transition metals having a formula of M_xN_y possess various useful properties, including semiconductivity, superconductivity, extreme hardness, and they can also be used as diodes in LED lights.¹ Iron nitrides derived from N_2 are also intermediates in the Haber-Bosch Process, used in the industrial production of ammonia.² The Haber-Bosch Process, by which ammonia is produced on an industrial scale, is instrumental in world food production, and is responsible for the food consumed by over 4 billion people since 1908. The industrial production of ammonia accounts for ~.8% of all carbon dioxide produced by industry, as well as 1 – 2% of all global energy consumption. In an effort to better understand the mechanism of nitrogen activation, there has been considerable interest in isolating and studying stable transition metal nitrides over the course of the past 30 years.³

Due to the stable nature of the N_2 molecule, having a bond dissociation enthalpy of 946 kJ/mol, there are few examples of transition metal nitride complexes having been produced from N_2 gas.^{1,4} The difficulty with which N_2 gas can be homolytically cleaved is exemplified by the case of tetrahedral enforcing ligands such

as tris(pyrazolyl)borates, which produce stable di-nitrogen complexes from which N₂ cleavage does not occur under ambient conditions, see **Scheme 3.1**.⁵



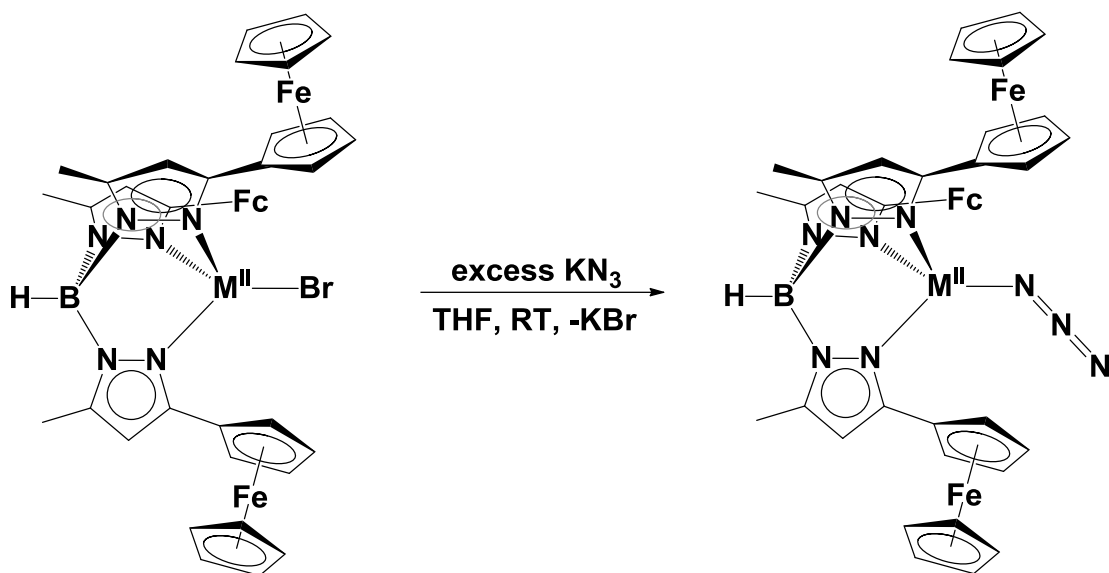
Scheme 3.1: Synthesis of first row transition metal di-nitrogen complexes supported by various hydrotris(3-R,5-R'pyrazolyl)borate ligands, (M = Cr, Mn, Fe, or Co; R = *t*Bu, Me; R' = Me, *i*Pr, or H; X = Cl, I)

The goal of this chapter is to produce a nitride complex of a first row transition metal, supported by a tris(pyrazolyl)borate ligand, and upon success investigate its reactivity and stability. Nitride complexes are known to participate in other reaction pathways to produce commercially relevant complexes, such as ammonia, and low molecular weight imide complexes.⁶ The reactivity of nitrides toward electrophilic substrates will also be explored.

RESULTS AND DISCUSSION

Synthesis of Iron and Cobalt azide complexes supported by $\text{Tp}^{\text{Fc,Me}}$ ligand.

One established method for the production of terminal nitride compounds is the photolysis or thermolysis of ligated transition metal azides, producing the terminal nitride and one equivalent of N_2 . This method is often favored over other means of nitride production, due to the ease of synthesizing the metal azide starting material and requiring no additional or exotic reagents.⁷ With the ultimate goal of producing either an iron or cobalt terminal nitride with metal oxidation state of IV, I set about synthesizing $\text{Tp}^{\text{Fc,Me}}\text{FeN}_3$ (**20**) and $\text{Tp}^{\text{Fc,Me}}\text{CoN}_3$ (**21**). Depending on the desired product, 0.4 g of either $\text{Tp}^{\text{Fc,Me}}\text{FeBr}$ (**2**) or $\text{Tp}^{\text{Fc,Me}}\text{CoBr}$ (**4**) were dissolved in 15 ml of THF, and to that mixture was added four or more equivalents of KN_3 , and the solution was then left to stir for two days at room temperature, see **Scheme 3.2**. For both compounds the solution was filtered and then concentrated, then layered with pentanes to afford the desired product as X-ray quality crystals in yields of 87% for **20** and 63% for **21**.



Scheme 3.2: Synthesis of 20 (M = Fe) and 21 (M = Co).

Compound **20** is light orange in color, and the method for crystallization described above produced two different polymorphs for the complex. One of the two polymorphs has a triclinic cell ($P\bar{1}$) with only one molecule of **20** per asymmetric unit, having 2 disordered positions for the azide group which can be separated into their own free variables at roughly 50% occupancy for each. The second polymorph is orthorhombic ($Pna2_1$), has only one position for the azide, and also contains one molecule of THF per molecule of **20**, and the crystal structure is displayed in **Figure 3.1**. A comparison of the two polymorphs can be found in **Table 3.2**. **20** displays C_{3v} symmetry in solution, as evidenced by its having five chemical shifts between -3 and 59 ppm in its 1H -NMR spectrum, all of which are associated with the $Tp^{Fc,Me}$ ligand system. Its effective magnetic moment, measured in solid state with a Gouy balance at 298 K, was found to be $4.9(1) \mu_B$, consistent with 4 unpaired electrons for a high spin $d^6 Fe^{II}$ metal center. The infrared spectra taken of crystals of the complex in both

of the two crystal systems provides slightly different values for the azide stretching frequency, the triclinic polymorph having an azide stretch at 2100 cm^{-1} and the orthorhombic cell having an azide stretch at 2092 cm^{-1} , see **Figure 3.2**. Either of these show only a minor degree of activation compared to the N-N bonds in the azide moiety, which has an infrared stretching frequency at 2126 cm^{-1} in the case of NaN_3 .⁸

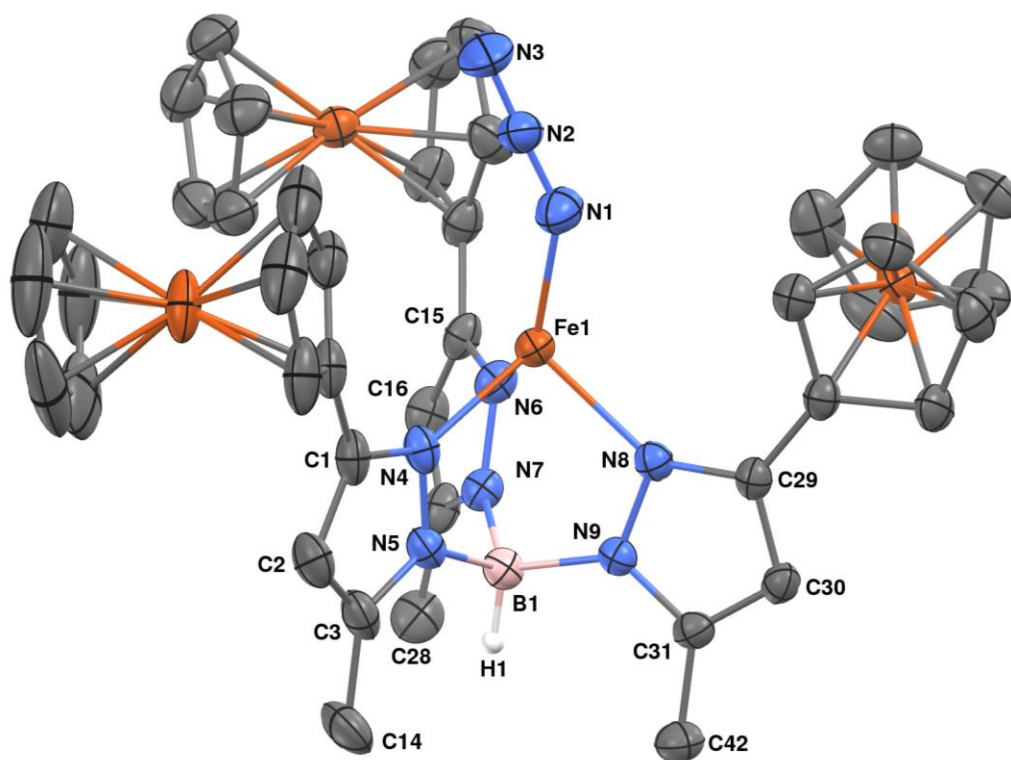


Figure 3.1: Molecular structure of $\text{Tp}^{\text{Fc,Me}}\text{FeN}_3$ (20) represented as 50% probability thermal ellipsoids. Hydrogen atoms (with the exception of the hydrogen attached to boron, H1), and one molecule of THF omitted for clarity.

Table 3.1: Selected interatomic distances (Å) and angles (°) for $\text{Tp}^{\text{Fc,Me}}\text{FeN}_3$ (20).

Distances (Å)			
Fe1-N1	1.932(4)	Fe1-N6	2.063(4)
Fe1-N4	2.083(3)	Fe1-N8	2.091(3)
B1-N5	1.533(6)	B1-N7	1.549(6)
B1-N9	1.555(6)	N1-N2	1.173(6)
N2-N3	1.151(6)	N4-C1	1.342(6)
N4-N5	1.385(5)	N5-C3	1.356(6)
N6-C15	1.338(5)	N6-N7	1.389(5)
N7-C17	1.355(6)	N8-C29	1.350(5)
N8-N9	1.386(5)	N9-C31	1.350(5)
C1-C2	1.398(7)	C1-C13	1.456(7)
C2-C3	1.375(7)	C3-C14	1.505(7)
C15-C16	1.403(6)	C15-C27	1.473(6)
C16-C17	1.373(7)	C17-C28	1.493(7)
C29-C30	1.394(6)	C29-C41	1.469(6)
C30-C31	1.384(6)	C31-C42	1.486(6)

Angles (°)			
B1-Fe1-N1	174.7(2)	N1-Fe1-N4	121.30(17)
N1-Fe1-N6	128.11(17)	N1-Fe1-N8	119.71(16)
N6-Fe1-N4	92.96(14)	N4-Fe1-N8	93.40(14)
N6-Fe1-N8	92.70(14)	N5-B1-N7	109.8(4)
N5-B1-N9	108.8(3)	N7-B1-N9	110.3(4)
N2-N1-Fe1	145.9(4)	N3-N2-N1	178.0(5)
C1-N4-N5	106.9(4)	C1-N4-Fe1	140.8(3)
N5-N4-Fe1	111.7(2)	C3-N5-N4	109.2(4)
C3-N5-B1	129.9(4)	N4-N5-B1	120.7(3)
C15-N6-N7	106.0(4)	C15-N6-Fe1	141.4(3)
N7-N6-Fe1	111.5(2)	C17-N7-N6	110.0(4)
C17-N7-B1	128.7(4)	N6-N7-B1	121.0(3)
C29-N8-N9	106.2(3)	C29-N8-Fe1	142.9(3)
N9-N8-Fe1	110.7(2)	C31-N9-N8	110.0(3)
C31-N9-B1	128.5(3)	N8-N9-B1	121.4(3)
N4-C1-C2	109.5(4)	N4-C1-C13	121.7(4)
C2-C1-C13	128.9(4)	C3-C2-C1	106.4(4)
N5-C3-C2	108.1(4)	N5-C3-C14	122.4(5)

C2-C3-C14	129.5(4)	N6-C15-C27	123.5(4)
N6-C15-C16	110.1(4)	C17-C16-C15	106.3(4)
C16-C15-C27	126.4(4)	N7-C17-C28	123.3(4)
N7-C17-C16	107.6(4)	N8-C29-C41	124.1(4)
N8-C29-C30	109.7(4)	C31-C30-C29	106.5(4)
C30-C29-C41	126.2(4)	N9-C31-C42	123.8(4)
N9-C31-C30	107.6(3)	C30-C31-C42	128.6(4)

Table 3.2: Comparison of triclinic and orthorhombic polymorphs of $\text{Tp}^{\text{Fc,Me}}\text{FeN}_3$ (20).

Space Group	B-Fe-N1 ($^\circ$)	Fe-N1-N2 ($^\circ$)	Fe-N1 (\AA)	N1-N2 (\AA)	N2-N3 (\AA)
$P\bar{1}$	170.0(1)	134.2(5)	1.918(3)	1.05(1)	1.17(2)
$Pna2_1$	174.7(2)	145.8(4)	1.933(5)	1.173(6)	1.151(6)

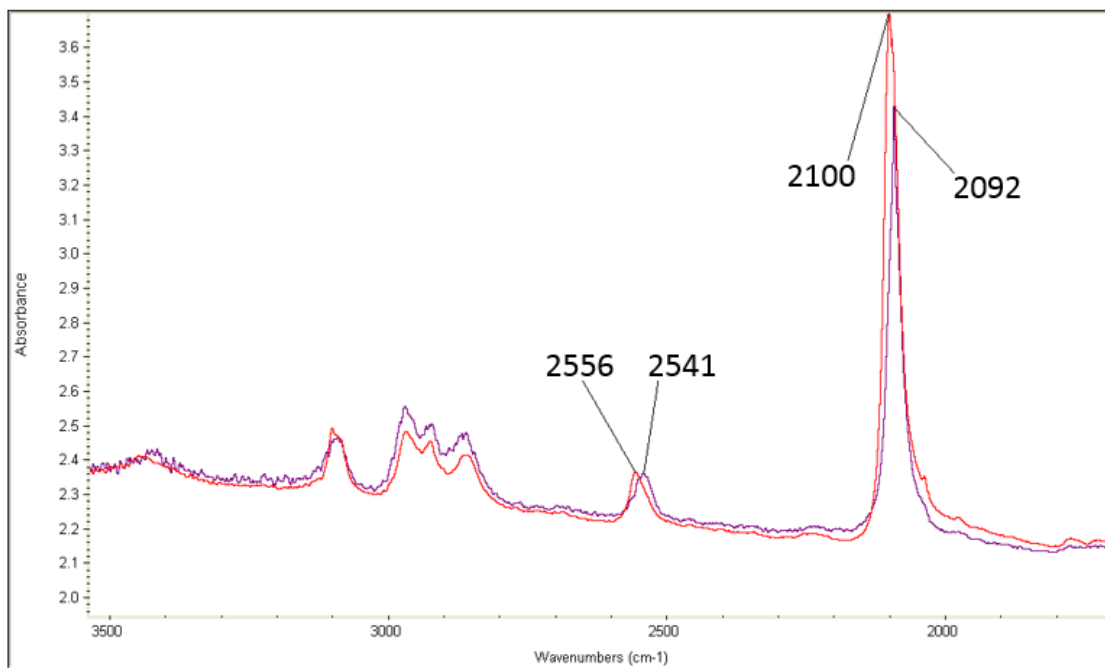


Figure 3.2: IR spectra of both polymorphs of $\text{Tp}^{\text{Fc,Me}}\text{FeN}_3$ (20), triclinic (red, $\nu_{\text{N}_3} = 2100 \text{ cm}^{-1}$) and orthorhombic (purple, $\nu_{\text{N}_3} = 2092 \text{ cm}^{-1}$), with their B-H and N_3 stretching frequencies annotated.

Compound **21** is dark green, and crystallizes with a unit cell that is nearly identical to that of **20**; for this reason a structural determination was foregone. Similarly to **20**, **21** displays five peaks between 0 and 70 ppm in its $^1\text{H-NMR}$ spectrum, with an additional chemical shift at -9.5 ppm assigned to the hydrogen on the boron. The IR spectrum of **21** displays a stretching frequency at 2086 cm^{-1} . **21** had an effective magnetic moment of $3.8(1)\ \mu_{\text{B}}$ at 298 K, which is expected for a high spin $d^7\text{ Co}^{\text{II}}$ metal center.

Attempts to produce a terminal nitride by way of photolysis from either **20** or **21** were unsuccessful. When 0.1g of either complex was placed in 15ml of THF in a 100 ml quartz vessel, and the solution was freeze pump thawed, and exposed to 254 nm radiation, using a Rayonet Photochemical Reactor (Catalog Number RPR – 100), the result was complete decomposition with a 40 % yield of either $\text{Tp}^{\text{Fc,Me}}\text{Fe}(\text{PzH}^{\text{Fc,Me}})(\text{Pz}^{\text{Fc,Me}})$ (**8**) or $\text{Tp}^{\text{Fc,Me}}\text{Co}(\text{PzH}^{\text{Fc,Me}})(\text{Pz}^{\text{Fc,Me}})$ (**A1.2**), depending on which compound was used as starting material. No gas evolution was observed coming from the reaction mixture, and freeze pump thaws using a high vacuum line equipped with a monometer didn't register any gas present in the quartz vessel after the reaction was stopped, leaving the fate of the azide fragment undetermined.

Reactions of nitride transfer reagent with iron and cobalt halides, supported by $\text{Tp}^{\text{Fc,Me}}$ ligand. Following the initial issues encountered with nitride formation using $\text{Tp}^{\text{Fc,Me}}\text{MN}_3$ as starting material, I turned to the use of another nitrogen atom transfer reagent. The compound 2,3:5,6-dibenzo-7-aza bicyclo[2.2.1]hepta-2,5-diene (H-dbabh) and its lithiated variant (Li-dbabh) have been used to produce a number of nitride complexes on chromium and iron metal centers.⁹

Initial attempts at reacting up to 150 mg of either **3** or **4** with Li-dbabh in THF solutions were fraught with issues of transmetalation. Thus, LIFDI-MS taken of the reaction mixture showed the major product to be $\text{Tp}^{\text{Fc,Me}}\text{Li}(\text{THF})$ (**A3.1**), as seen in **Figure 3.3**, without any of the starting material or other high mass compounds being present. After removal of solvent, and recrystallization of product in a mixture of THF and pentanes, **A3.1** was isolated in yields greater than 75%, the structure of this compound can be found in **Figure C.1**.

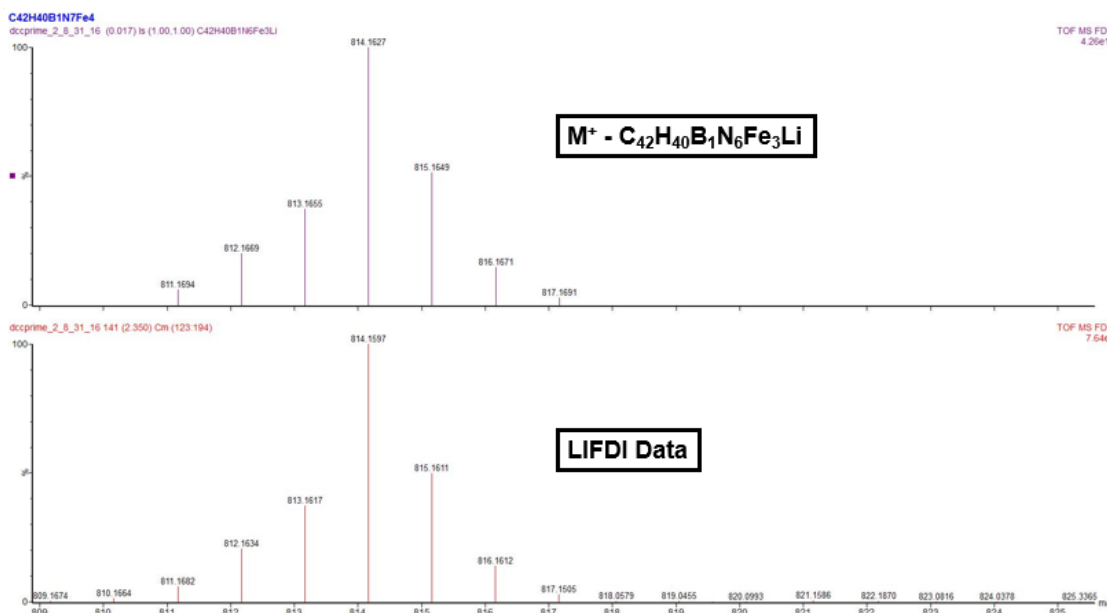
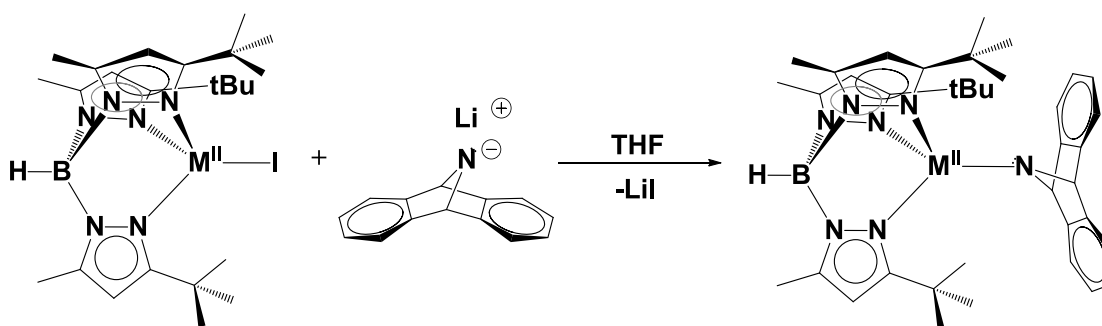


Figure 3.3: LIFDI-MS of the product of a reaction of **3 with Li-dbabh (Bottom), calculated isotope pattern for $\text{Tp}^{\text{Fc,Me}}\text{Li}$ (top, $M^+ - \text{C}_{42}\text{H}_{40}\text{B}_1\text{N}_6\text{Fe}_3\text{Li}$).**

Reactions of Fe and Co complexes supported by $\text{Tp}^{\text{tBu,Me}}$ ligand with dbabh. Because compounds supported by the $\text{Tp}^{\text{tBu,Me}}$ ligand have already been thoroughly investigated, halide and alkyl complexes of Fe and Co have already been described. It was determined that Li salts do not significantly undergo ligand

metathesis to form $\text{Tp}^{\text{tBu,Me}}\text{Li}$, for either $\text{Tp}^{\text{tBu,Me}}\text{Co}$ or $\text{Tp}^{\text{tBu,Me}}\text{Fe}$.¹⁰ Continuing the effort to investigate the utility of Li-dbabh as a means of producing nitride compounds with metals supported by Tp ligands, I prepared $\text{Tp}^{\text{tBu,Me}}\text{FeI}$ and $\text{Tp}^{\text{tBu,Me}}\text{CoI}$, and reacted both with Li-dbabh. In both cases 100 mg of either Tp supported compound was placed in a scintillation vial with a magnetic stir bar and 10 ml of THF; to that mixture was added 1 equiv. of Li-dbabh, see **Scheme 3.3**.



Scheme 3.3: Synthesis of 22 (M = Fe) and 23 (M = Co).

The reaction with $\text{Tp}^{\text{tBu,Me}}\text{FeI}$ changed from colorless to light yellow, with precipitation of LiI salt. The product mixture was found to contain some $\text{Tp}^{\text{tBu,Me}}\text{Li}$, when investigated by LIFDI-MS, but the major product (as determined by independent $^1\text{H-NMR}$ analysis) had a mass that matched the predicted isotope pattern for a $\text{Tp}^{\text{tBu,Me}}\text{Fe-dbabh}$ (**22**), see **Figure 3.4**. Crystals of **22** could be grown from a concentrated solution of the compound in THF, which had been layered with pentanes and cooled to $-35\text{ }^\circ\text{C}$, affording an overall yield of 82%. Analysis by X-ray diffraction revealed the complex is tetrahedral, with a $\tau_4 = 0.739$ and $\tau_4' = 0.725$,¹¹ with an Fe-dbabh bond length of $1.924(2)\text{ \AA}$, see **Figure 3.5** and **Table 3.3**. The compounds solid

state effective magnetic moment was determined to be $5.0(1) \mu_B$ (298 K), indicating that the iron metal center is a high spin d^6 .

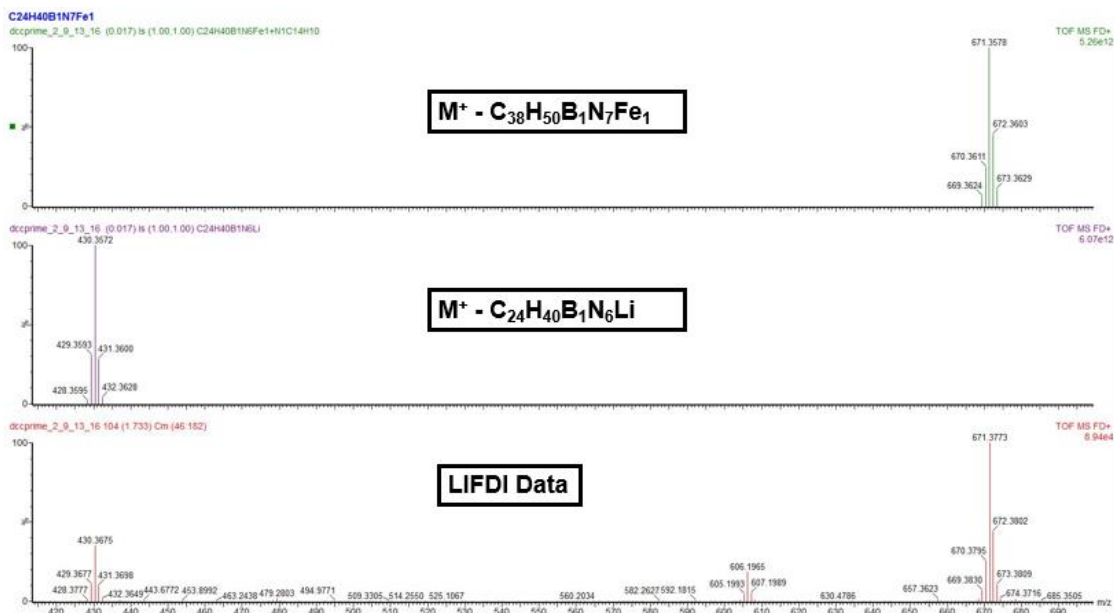


Figure 3.4: LIFDI-MS of the products from a reaction of $\text{Tp}^{\text{tBu,Me}}\text{FeI}$ with dbabh (Bottom), calculated isotope pattern for $\text{Tp}^{\text{tBu,Me}}\text{Li}$ (Middle, $\text{M}^+ - \text{C}_{24}\text{H}_{40}\text{B}_1\text{N}_6\text{Fe}_3\text{Li}$), calculated isotope pattern for $\text{Tp}^{\text{tBu,Me}}\text{Fe-dbabh}$ (top, $\text{M}^+ - \text{C}_{38}\text{H}_{50}\text{B}_1\text{N}_7\text{Fe}_1$).

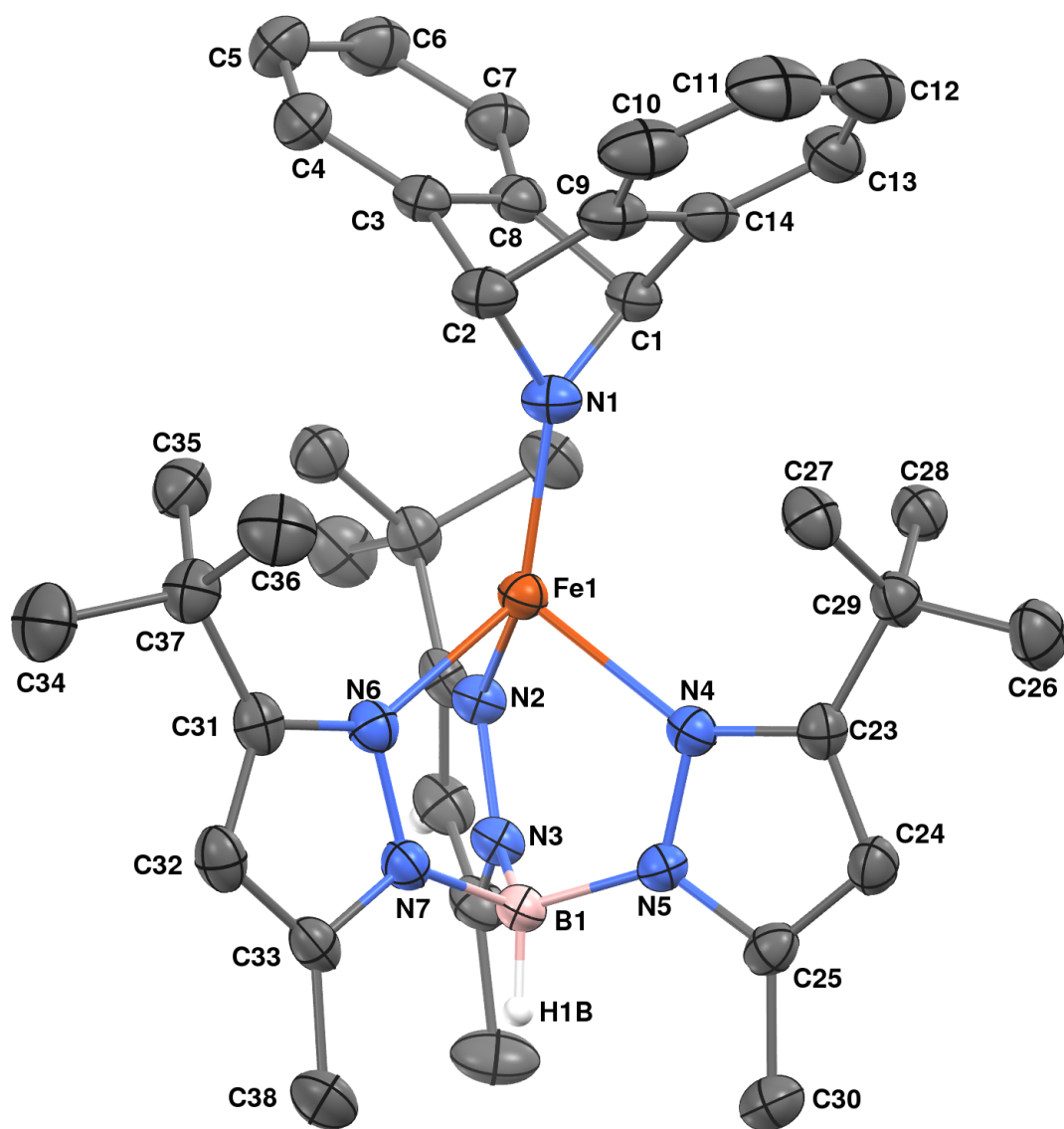


Figure 3.5: Molecular structure of $\text{Tp}^{\text{tBu,Me}}\text{Fe-dbabh}$ (22) represented as 50% probability thermal ellipsoids. Hydrogen atoms (with the exception of the hydrogen attached to boron, H1) were omitted for clarity.

Table 3.3: Selected interatomic distances (Å) and angles (°) for**Tp^{iBu,Me}Fe-dbabh (22).**

Distances (Å)			
Fe1-N1	1.924(2)	Fe1-N6	2.114(2)
Fe1-N2	2.130(2)	Fe1-N4	2.167(2)
N1-C2	1.487(3)	N1-C1	1.492(3)
N2-C15	1.351(3)	N2-N3	1.385(3)
N3-C17	1.345(3)	N3-B1	1.544(4)
N4-C23	1.354(3)	N4-N5	1.379(3)
N5-C25	1.349(3)	N5-B1	1.533(4)
N6-C31	1.350(3)	N6-N7	1.385(3)
N7-C33	1.353(3)	N7-B1	1.544(4)
C1-C8	1.540(4)	C1-C14	1.529(4)
C2-C3	1.526(4)	C2-C9	1.532(4)
C3-C8	1.401(4)	C3-C4	1.374(4)
C9-C14	1.393(4)	C4-C5	1.395(4)
C15-C21	1.512(4)	C5-C6	1.369(5)
C18-C21	1.531(4)	C6-C7	1.397(4)
C19-C21	1.533(4)	C7-C8	1.371(4)
C20-C21	1.542(4)	C9-C10	1.372(4)
C23-C29	1.516(4)	C10-C11	1.397(5)
C26-C29	1.531(4)	C11-C12	1.365(6)
C27-C29	1.534(4)	C12-C13	1.404(5)
C28-C29	1.526(4)	C13-C14	1.378(4)
C31-C37	1.504(4)	C15-C16	1.393(4)
C34-C37	1.539(4)	C16-C17	1.363(4)
C35-C37	1.531(4)	C17-C22	1.508(4)
C36-C37	1.537(4)	C23-C24	1.387(4)
C24-C25	1.370(4)	C32-C33	1.372(4)
C25-C30	1.497(4)	C33-C38	1.505(4)
C31-C32	1.393(4)		
Angles (°)			
B1-Fe1-N1	172.03(8)	N1-Fe1-N2	125.35(9)
N1-Fe1-N6	130.42(9)	N1-Fe1-N4	117.37(9)
N6-Fe1-N2	86.34(8)	N2-Fe1-N4	94.99(8)
N6-Fe1-N4	92.73(8)	C2-N1-Fe1	132.48(17)
C2-N1-C1	94.23(19)	C15-N2-N3	106.4(2)

C1-N1-Fe1	132.81(17)	N3-N2-Fe1	110.75(15)
C15-N2-Fe1	142.76(17)	C17-N3-B1	128.8(2)
C17-N3-N2	109.4(2)	C23-N4-N5	105.6(2)
N2-N3-B1	121.4(2)	N5-N4-Fe1	111.41(15)
C23-N4-Fe1	142.92(17)	C25-N5-B1	128.9(2)
C25-N5-N4	110.4(2)	C31-N6-N7	106.7(2)
N4-N5-B1	120.7(2)	N7-N6-Fe1	111.18(15)
C31-N6-Fe1	141.90(18)	C33-N7-B1	129.5(2)
C33-N7-N6	109.0(2)	N5-B1-N3	110.8(2)
N6-N7-B1	121.16(19)	N3-B1-N7	110.6(2)
N5-B1-N7	109.7(2)	N1-C1-C14	101.3(2)
N1-C1-C8	100.5(2)	C14-C1-C8	104.5(2)
N1-C2-C9	100.9(2)	N1-C2-C3	100.6(2)
C4-C3-C2	135.0(3)	C3-C2-C9	105.5(2)
C3-C4-C5	118.6(3)	C4-C3-C8	120.1(3)
C5-C6-C7	121.1(3)	C8-C3-C2	104.9(2)
C7-C8-C3	121.4(3)	C6-C5-C4	120.9(3)
C3-C8-C1	104.7(2)	C8-C7-C6	117.9(3)
C10-C9-C2	133.9(3)	C7-C8-C1	133.9(3)
C9-C10-C11	117.9(4)	C10-C9-C14	121.0(3)
C11-C12-C13	120.9(3)	C14-C9-C2	105.2(2)
C13-C14-C9	121.2(3)	C12-C11-C10	121.3(3)
C9-C14-C1	104.8(2)	C14-C13-C12	117.6(3)
N2-C15-C21	123.2(2)	C13-C14-C1	134.0(3)
C17-C16-C15	106.8(2)	N2-C15-C16	109.0(2)
N3-C17-C22	122.5(3)	C16-C15-C21	127.8(2)
C15-C21-C18	108.9(2)	N3-C17-C16	108.4(2)
C18-C21-C19	110.5(2)	C16-C17-C22	129.1(3)
C18-C21-C20	108.5(2)	C15-C21-C19	110.7(2)
N4-C23-C24	109.7(2)	C15-C21-C20	109.3(2)
C24-C23-C29	128.0(2)	C19-C21-C20	108.8(2)
N5-C25-C24	107.5(2)	N4-C23-C29	122.3(2)
C24-C25-C30	128.8(3)	C25-C24-C23	106.8(2)
C23-C29-C26	109.6(2)	N5-C25-C30	123.7(2)
C23-C29-C27	110.8(2)	C23-C29-C28	108.0(2)
C26-C29-C27	109.0(2)	C28-C29-C26	108.5(2)
N6-C31-C37	122.7(2)	C28-C29-C27	110.8(2)
C33-C32-C31	106.4(2)	N6-C31-C32	109.4(2)
N7-C33-C38	123.0(2)	C32-C31-C37	127.9(2)

C31-C37-C35	110.8(2)	N7-C33-C32	108.4(2)
C35-C37-C36	110.8(2)	C32-C33-C38	128.6(2)
C35-C37-C34	108.3(2)	C31-C37-C36	108.5(2)
C36-C37-C34	109.2(2)	C31-C37-C34	109.2(2)

The reaction of $\text{Tp}^{\text{tBu,Me}}\text{CoI}$ with Li-dbabh in THF results in a more dramatic change in color from bright blue to brown over the course of 6 hours. After filtration the solvent was removed in vacuo and the residue extracted with ether and then re-filtered. The extract was reddish-brown and upon layering with pentanes and cooling overnight to $-35\text{ }^{\circ}\text{C}$ produced blocky red crystals of $\text{Tp}^{\text{tBu,Me}}\text{Co-dbabh}$ (**23**), in yields varying from 40 to 50 %. **23** was analyzed by X-ray crystallography and found to be in a tetrahedral coordination sphere with a $\tau_4 = 0.790$ and $\tau_4' = 0.788$,¹¹ with an Co-dbabh bond length of $1.897(2)\text{ \AA}$, see **Figure 3.6**. **23** has six resonances in its $^1\text{H-NMR}$ spectrum, three of which can be assigned to the $\text{Tp}^{\text{tBu,Me}}$ ligand and two that are assigned to the dbabh moiety, while the bridgehead protons of the dbabh moiety of **23** can't be located. The effective magnetic moment of **23** was measured in solution, using the Evans method,¹² and found to be $4.0(1)\text{ }\mu_{\text{B}}$ (300 K), consistent with a high spin $d^7\text{ Co}^{\text{II}}$ metal center.

Table 3.4: Selected interatomic distances (Å) and angles (°) for**Tp^{tBu,Me}Co-dbabh (23).**

Distances (Å)			
Co1-N1	1.8967(16)	Co1-N6	2.0858(16)
Co1-N4	2.0912(16)	Co1-N2	2.1268(16)
N1-C2	1.489(3)	N1-C1	1.489(2)
N2-C15	1.348(3)	N2-N3	1.386(2)
N3-C17	1.351(3)	N3-B1	1.541(3)
N4-C23	1.346(2)	N4-N5	1.385(2)
N5-C25	1.349(2)	N5-B1	1.545(3)
N6-C31	1.355(2)	N6-N7	1.379(2)
N7-C33	1.346(2)	N7-B1	1.535(3)
C1-C14	1.534(3)	C1-C8	1.526(3)
C2-C7	1.536(3)	C2-C13	1.537(3)
C3-C4	1.396(3)	C3-C8	1.380(3)
C4-C5	1.372(4)	C9-C14	1.372(3)
C5-C6	1.399(3)	C15-C16	1.394(3)
C6-C7	1.371(3)	C16-C17	1.371(3)
C7-C8	1.399(3)	C17-C22	1.502(3)
C9-C10	1.397(4)	C23-C24	1.397(3)
C10-C11	1.371(4)	C24-C25	1.369(3)
C11-C12	1.397(4)	C25-C30	1.497(3)
C12-C13	1.377(3)	C31-C32	1.392(3)
C13-C14	1.390(3)	C32-C33	1.373(3)
C15-C21	1.513(3)	C33-C38	1.497(3)
C18-C21	1.537(3)	C28-C29	1.536(3)
C19-C21	1.531(3)	C31-C37	1.509(3)
C20-C21	1.536(3)	C34-C37	1.537(3)
C23-C29	1.513(3)	C35-C37	1.532(3)
C26-C29	1.537(3)	C36-C37	1.535(3)
C27-C29	1.532(3)		
Angles (°)			
B1-Co1-N1	177.17(7)	N1-Co1-N4	123.92(7)
N1-Co1-N6	120.71(7)	N1-Co1-N2	124.68(7)
N6-Co1-N4	97.63(6)	N4-Co1-N2	87.06(6)
N6-Co1-N2	94.34(6)	C2-N1-Co1	131.10(12)
C2-N1-C1	94.41(14)	C15-N2-N3	106.08(16)

C1-N1-Co1	134.38(14)	N3-N2-Co1	108.99(11)
C15-N2-Co1	144.74(14)	C17-N3-B1	128.64(17)
C17-N3-N2	109.62(16)	C23-N4-N5	106.59(15)
N2-N3-B1	121.43(16)	N5-N4-Co1	109.24(11)
C23-N4-Co1	144.04(13)	C25-N5-B1	128.39(17)
C25-N5-N4	109.35(16)	C31-N6-N7	105.72(15)
N4-N5-B1	121.85(15)	N7-N6-Co1	111.68(12)
C31-N6-Co1	142.50(13)	C33-N7-B1	129.44(16)
C33-N7-N6	110.55(16)	N7-B1-N3	109.92(16)
N6-N7-B1	119.99(15)	N3-B1-N5	110.43(16)
N7-B1-N5	110.23(16)	N1-C1-C8	100.38(16)
N1-C1-C14	100.88(16)	C8-C1-C14	104.91(17)
N1-C2-C13	101.08(16)	N1-C2-C7	100.75(16)
C5-C4-C3	121.3(2)	C7-C2-C13	104.55(15)
C7-C6-C5	117.8(2)	C8-C3-C4	118.1(2)
C6-C7-C2	133.96(19)	C4-C5-C6	120.9(2)
C3-C8-C7	120.3(2)	C6-C7-C8	121.63(19)
C7-C8-C1	105.33(17)	C8-C7-C2	104.41(17)
C11-C10-C9	121.0(2)	C3-C8-C1	134.4(2)
C13-C12-C11	117.7(3)	C14-C9-C10	118.0(3)
C12-C13-C2	134.0(2)	C10-C11-C12	121.0(3)
C9-C14-C13	121.0(2)	C12-C13-C14	121.3(2)
C13-C14-C1	105.33(18)	C14-C13-C2	104.68(18)
N2-C15-C21	123.14(18)	C9-C14-C1	133.7(2)
C17-C16-C15	106.32(18)	N2-C15-C16	109.79(18)
N3-C17-C22	123.20(19)	C16-C15-C21	127.05(19)
C15-C21-C19	110.53(17)	N3-C17-C16	108.16(18)
C19-C21-C18	108.28(19)	C16-C17-C22	128.6(2)
C19-C21-C20	111.59(19)	C15-C21-C18	109.59(18)
N4-C23-C24	109.22(18)	C15-C21-C20	108.04(18)
C24-C23-C29	127.03(18)	C18-C21-C20	108.79(19)
N5-C25-C24	108.21(18)	N4-C23-C29	123.75(17)
C24-C25-C30	128.77(19)	C25-C24-C23	106.61(18)
C23-C29-C26	109.77(17)	N5-C25-C30	123.0(2)
C23-C29-C28	110.12(17)	C23-C29-C27	109.30(17)
C26-C29-C28	109.15(18)	C27-C29-C26	108.41(18)
N6-C31-C37	122.65(17)	C27-C29-C28	110.07(17)
C33-C32-C31	106.72(17)	N6-C31-C32	109.50(17)
N7-C33-C38	123.51(18)	C32-C31-C37	127.82(17)

C31-C37-C35	108.15(16)	N7-C33-C32	107.52(17)
C35-C37-C36	108.60(17)	C32-C33-C38	128.97(19)
C35-C37-C34	110.75(17)	C31-C37-C36	109.91(17)
C36-C37-C34	108.84(17)	C31-C37-C34	110.57(16)

Complexes of dbabh are rare and are unstable when the metal complex has available d electrons to reduce the nitrogen atom. Such compounds often favor elimination of anthracene to increase the metals oxidation state by two. Representative LM-dbabh compounds include $(NAr_F)_2Cr^{VI}(N)(dbabh)$ and $PhBP^{iPr}_3Mn(dbabh)$ prepared by Mindiola and Peters respectively.^{9a,13} The chromium complex remains stable due to lack of available electrons, however the stability of the manganese complex is the apparent result of other factors. A comparison between the bond lengths and angles of these LM-dbabh complexes is available in **Table 3.5** below.

Table 3.5: Comparison of bond lengths and angles for LM(dbabh) complexes (M= Cr, Mn, Fe, or Co)

	α ($^\circ$)	M-N(anthracene) (\AA)	N-C(anthracene) (\AA)
$Tp^{tBu,Me}Fe(dbabh)$ 22	172.03(8)	1.924(2)	1.489(3)
$Tp^{tBu,Me}Co(dbabh)$ 23	177.17(7)	1.897(2)	1.487(3), 1.492(4)
$(NAr_F)_2Cr(N)(dbabh)^{9a}$	N.A.	1.814(4)	1.494(6), 1.495(5)
$PhBP^{iPr}_3Mn(dbabh)^{11}$	177.68(5)	1.948(1)	1.484(2), 1.481(2)

It has been observed in the case of the $PhBP^{iPr}_3Fe(dbabh)$ complex that the elimination of anthracene is dependent on temperature.^{9b} In an attempt to produce nitride compounds both **22** and **23** were heated. **22** was placed in an NMR tube and dissolved in C_6D_6 , then heated to 75 $^\circ C$ for 24 hours. This resulted in all of the material decomposing, leaving only resonances associated with free ligand and no

apparent formation of anthracene, see **Figure 3.7**. The lack of resonances associated with anthracene indicates that **22** decomposes through a mechanism that does not produce a nitride as an intermediate. Some $\text{Tp}^{\text{tBu,Me}}\text{FeI}$ was also present in the NMR after the completion of the reaction (~4%), this was later found to be present in trace quantities crystallizing along with the sample of **22** that was used.

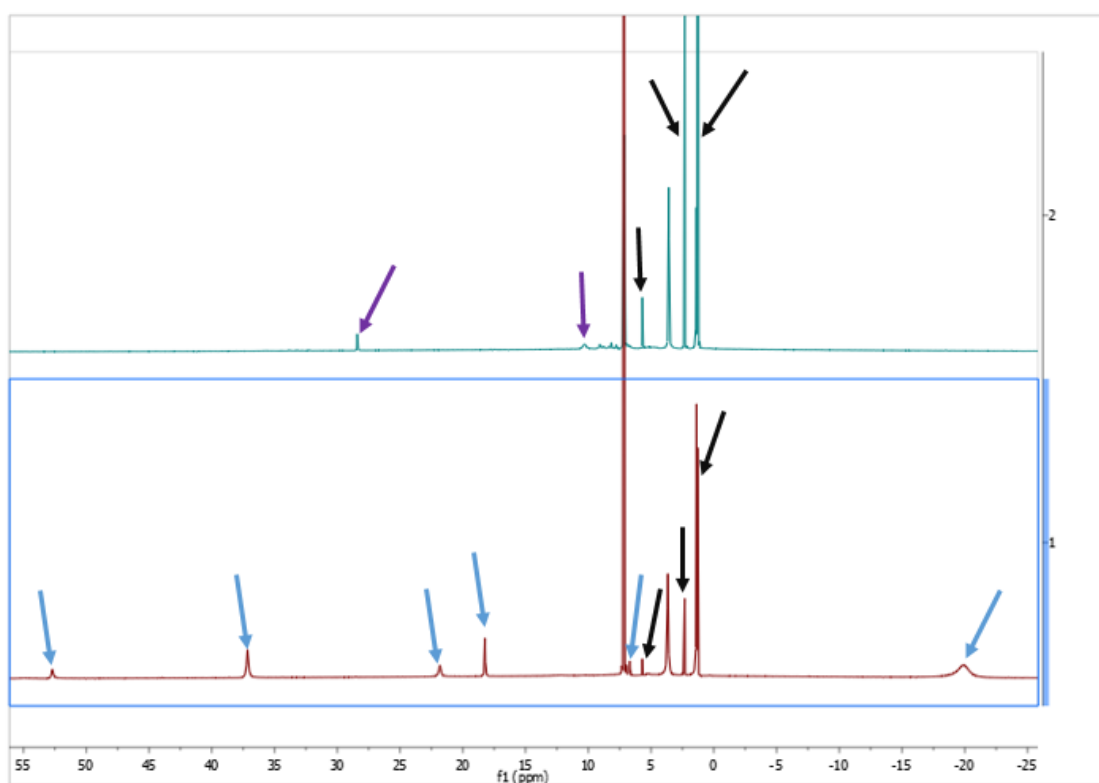


Figure 3.7: ¹H-NMR spectrum of the starting material, **22** (bottom), and the resulting spectrum after heating the material at 75 °C for 24 hours (Top), (**22** = blue arrows, $\text{Tp}^{\text{tBu,Me}}\text{FeI}$ = purple arrows, free $\text{Tp}^{\text{tBu,Me}}$ = black arrows).

When **23** was similarly heated, no reaction was observed, even when the temperature was increased to 110 °C and the material was left for a longer period of time, see **Figure 3.8**. Similar to the previous example, the complete removal of all $\text{Tp}^{\text{tBu,Me}}\text{CoI}$ from the product of its reaction with Li-dbabh was difficult and trace quantities still remain observable by $^1\text{H-NMR}$.

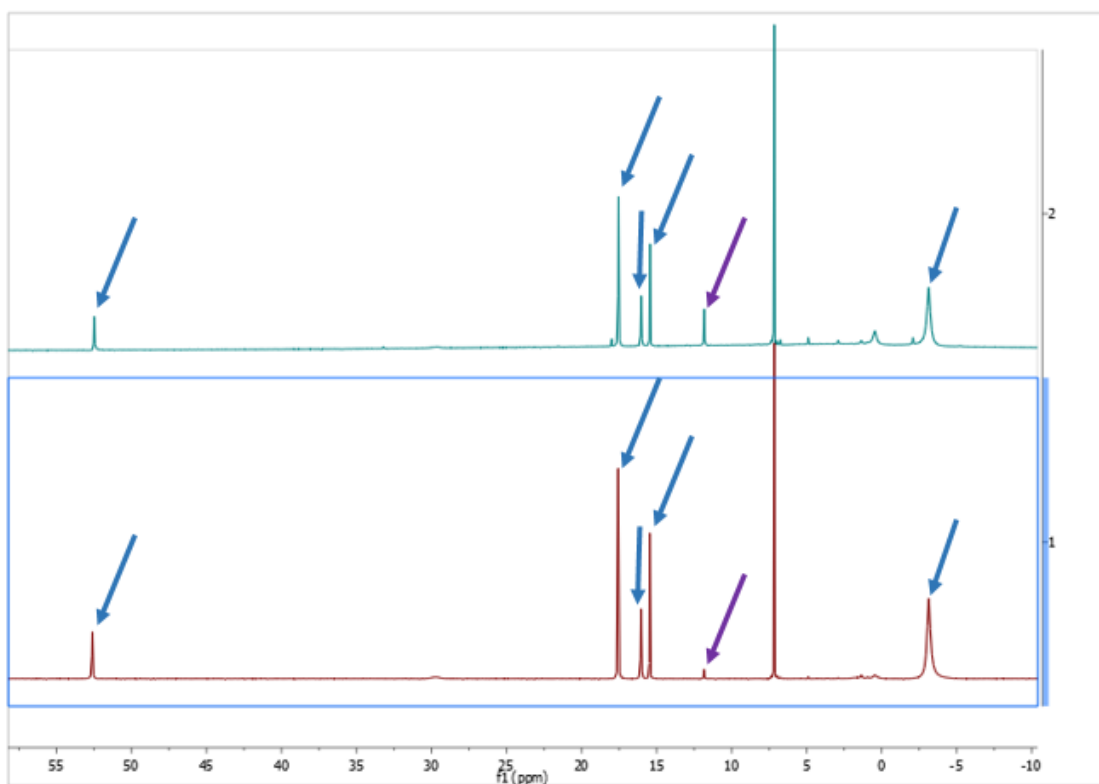
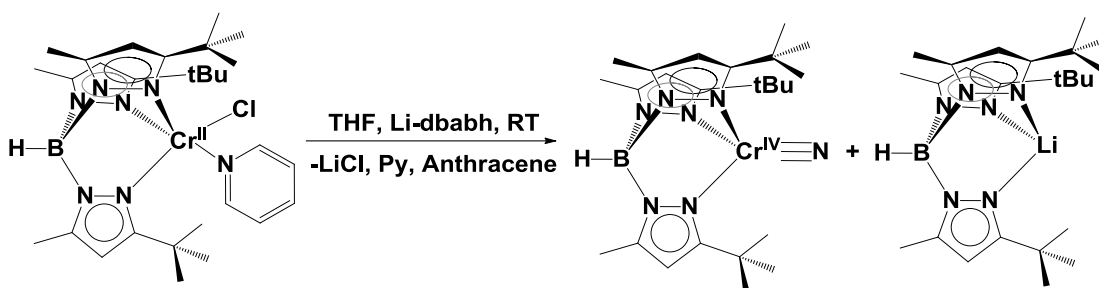


Figure 3.8: $^1\text{H-NMR}$ spectrum of the starting material, $\text{Tp}^{\text{tBu,Me}}\text{Co-dbabh}$ (**23**) (bottom), and the resulting spectrum after heating the material at 100 °C for 24 hours (Top), (**23** = blue arrows, $\text{Tp}^{\text{tBu,Me}}\text{CoI}$ = purple arrows).

Reactions of Li-dbabh and H-dbabh with $\text{Tp}^{\text{tBu,Me}}\text{CrCl}$ and $\text{Tp}^{\text{tBu,Me}}\text{CrEt}$, synthesis of $\text{Tp}^{\text{tBu,Me}}\text{CrN}$. Given precedent for producing chromium nitride compounds using the dbabh moiety, I resolved to produce a nitride complex supported by the more readily oxidizable chromium metal center. I chose the compound $\text{Tp}^{\text{tBu,Me}}\text{Cr}(\text{Cl})(\text{Py})$ as a starting material, given its relative ease of synthesis and purification.¹⁴ The reaction of the chromium halide with Li-dbabh was examined by ¹H-NMR and found to produce a mixture of compounds, including $\text{Tp}^{\text{tBu,Me}}\text{Li}$, anthracene, an unidentified chromium dbabh complex, and $\text{Tp}^{\text{tBu,Me}}\text{CrN}$ (**24**), see **Scheme 3.4** and **Figure 3.9**.



Scheme 3.4: Reaction of $\text{Tp}^{\text{tBu,Me}}\text{Cr}(\text{Cl})(\text{Py})$ with Li-dbabh.

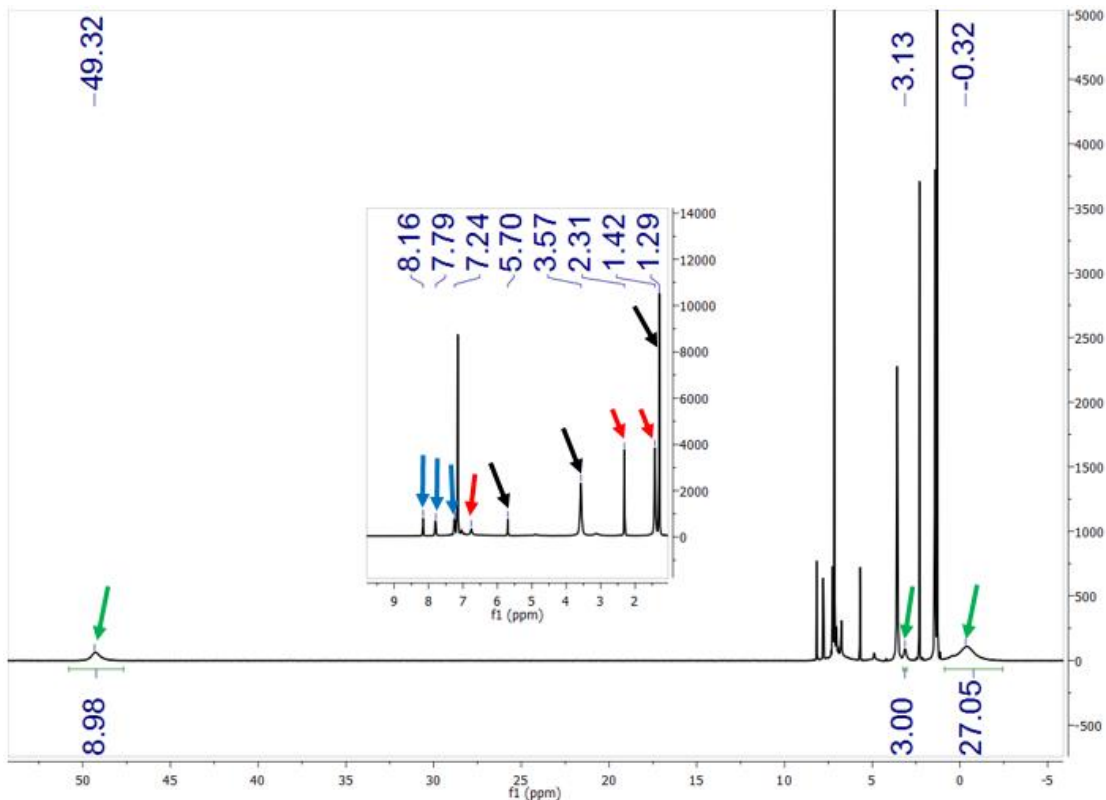


Figure 3.9: $^1\text{H-NMR}$ spectrum of solid residue from reaction of $\text{Tp}^{\text{tBu,Me}}\text{Cr}(\text{Cl})(\text{Py})$ with Li-dbabh in C_6D_6 (24** = green arrows, Anthracene = blue arrows, $\text{Tp}^{\text{tBu,Me}}\text{Li}$ = black arrows, unidentified Cr dbabh complex = red arrows).**

Due to the presence of $\text{Tp}^{\text{tBu,Me}}\text{Li}$ in the product mixture, acquiring pure samples of **24** was exceptionally difficult, even when extracting the nitride complex with pentanes. Pure samples of **24** can be produced, however, by 3 or more crystallizations from diethyl ether layered with pentanes and left to sit at $-35\text{ }^\circ\text{C}$, and a final crystallization from a slow evaporation of a pentanes solution. This results in small yellow/orange blocky crystals, which when analyzed by X-ray diffraction are shown to have a monoclinic unit cell, and an asymmetric unit made up of half a molecule of **24**, bifurcated by a mirror plane. The crystal structure reveals a well

behaved pseudo tetrahedral coordination sphere, with a $\tau_4 = 0.804$ and $\tau_4' = 0.798$,¹¹ and a Cr-N bond length of 1.544 Å, see **Figure 3.10**. ¹H-NMR of **24** show 3 peaks at 50.32, 3.02, and -0.45 ppm, associated with the Tp^{tBu,Me} ligand, indicating it displays C₃ symmetry in solution.

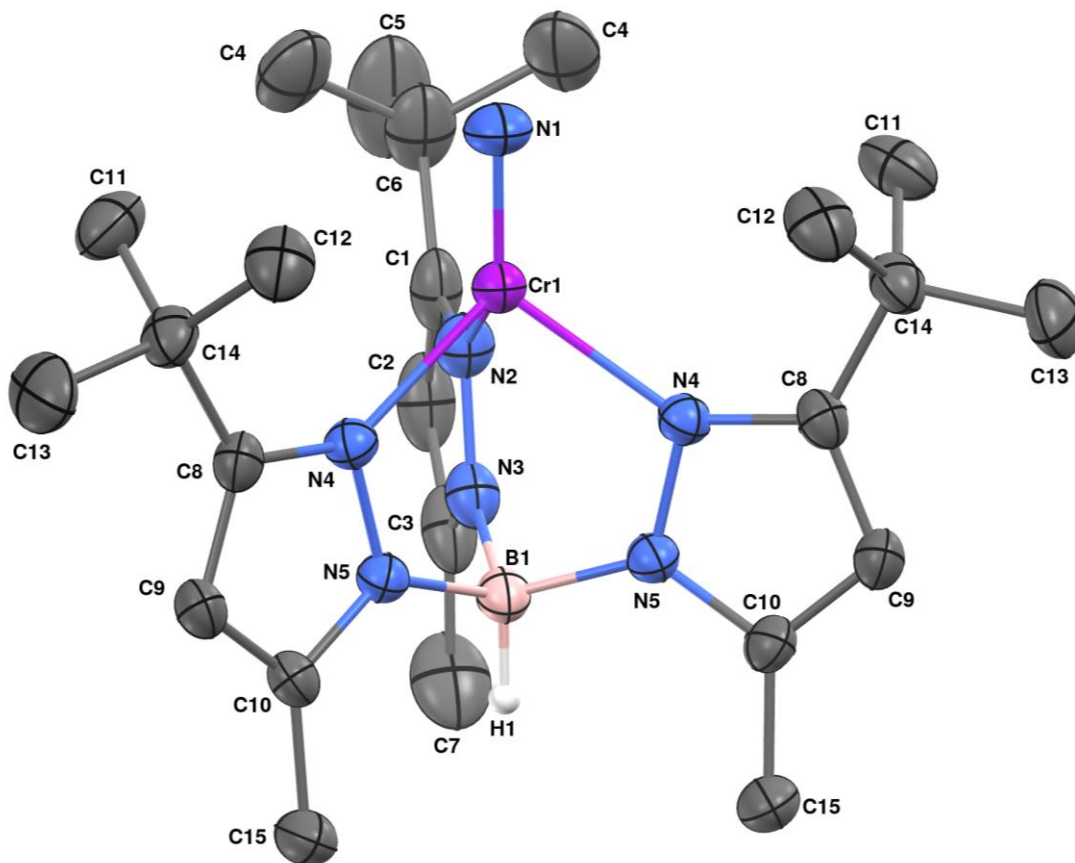


Figure 3.10: Molecular structure of Tp^{Fc,Me}Cr (**24**) represented as 50% probability thermal ellipsoids. Hydrogen atoms (with the exception of the hydrogen attached to boron, H1) were omitted for clarity.

Table 3.6: Selected interatomic distances (Å) and angles (°) for $\text{Tp}^{\text{tBu,Me}}\text{CrN}$ (24).

Distances (Å)			
Cr1-N1	1.544(3)	Cr1-N2	2.076(4)
Cr1-N4	2.0989(19)	Cr1-N4	2.0989(19)
N2-C1	1.338(5)	N2-N3	1.388(5)
N3-C3	1.357(5)	N3-B1	1.535(6)
N4-C8	1.339(3)	N4-N5	1.378(3)
N5-C10	1.353(3)	N5-B1	1.547(3)
B1-N5	1.547(3)	C1-C6	1.519(7)
C1-C2	1.396(7)	C4-C6	1.527(5)
C2-C3	1.382(7)	C5-C6	1.532(7)
C3-C7	1.478(7)	C6-C4	1.527(5)
C8-C14	1.516(4)	C8-C9	1.397(4)
C11-C14	1.539(4)	C9-C10	1.376(4)
C12-C14	1.520(4)	C10-C15	1.505(4)
C13-C14	1.532(4)		
Angles (°)			
B1-Cr1-N1	178.4	N1-Cr1-N4	122.32(9)
N1-Cr1-N2	124.28(18)	N4-Cr1-N4	96.29(10)
N2-Cr1-N4	91.65(9)	C1-N2-Cr1	142.2(3)
C1-N2-N3	107.5(3)	C3-N3-N2	108.8(3)
N3-N2-Cr1	110.3(2)	N2-N3-B1	121.8(3)
C3-N3-B1	129.4(4)	C8-N4-Cr1	142.14(17)
C8-N4-N5	107.22(19)	C10-N5-N4	109.46(19)
N5-N4-Cr1	110.54(14)	N4-N5-B1	121.1(2)
C10-N5-B1	129.4(2)	N3-B1-N5	109.9(2)
N3-B1-N5	109.9(2)	N2-C1-C6	121.3(4)
N5-B1-N5	110.0(3)	C3-C2-C1	106.6(4)
N2-C1-C2	109.2(4)	N3-C3-C7	122.3(5)
C2-C1-C6	129.5(4)	C1-C6-C4	109.4(2)
N3-C3-C2	107.9(4)	C4-C6-C4	111.1(5)
C2-C3-C7	129.8(4)	C4-C6-C5	108.9(3)
C1-C6-C4	109.4(2)	N4-C8-C9	109.0(2)
C1-C6-C5	109.1(5)	C9-C8-C14	128.6(2)
C4-C6-C5	108.9(3)	N5-C10-C9	107.6(2)
N4-C8-C14	122.4(2)	C9-C10-C15	130.0(2)
C10-C9-C8	106.7(2)	C8-C14-C13	109.7(2)
N5-C10-C15	122.4(2)	C8-C14-C11	109.3(2)

C8-C14-C12	110.7(2)	C13-C14-C11	108.8(3)
C12-C14-C13	108.7(3)	C12-C14-C11	109.8(3)

As previously stated, chromium nitride complexes in tetrahedral coordination environments are not entirely uncommon, with a CSD search returning 48 known structures of 4-coordinate chromium nitrides. A histogram of their bond lengths is shown in **Figure 3.11**. All of those complexes possess a chromium center with oxidation state of either V or VI, however the effective magnetic moment of **24** was found to be $2.9(1) \mu_B$ when measured in the solid state at 294 K, consistent with a high spin $d^2 \text{Cr}^{\text{IV}}$ metal center.

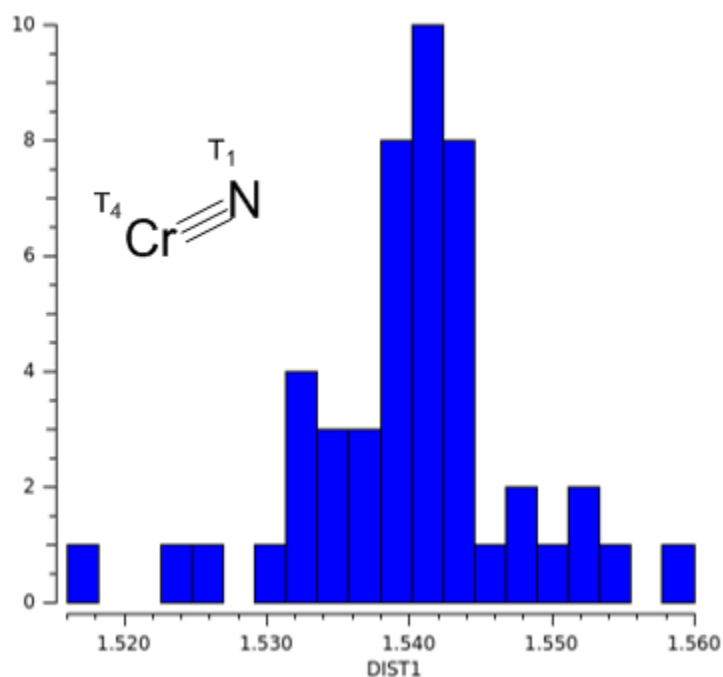
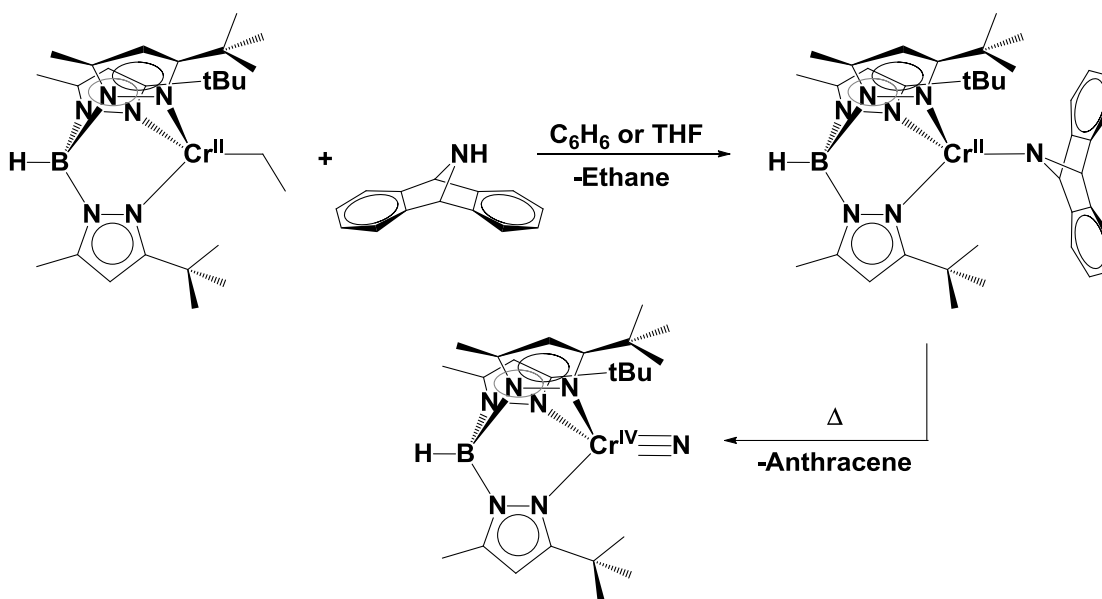


Figure 3.11: Histogram of chromium bond lengths, using the search query drawn in the upper left, Avg. = 1.539 Å, Std. Dev. = 0.008 Å, Range = 1.516 – 1.560 Å, the Cr-N bond length of $\text{Tp}^{\text{tBu,Me}}\text{CrN}$ (24**) is 1.544(3) Å.**

In an effort to eliminate the concern of $\text{Tp}^{\text{tBu,Me}}\text{Li}$ being present in the product mixture, I moved to use $\text{Tp}^{\text{tBu,Me}}\text{CrEt}$ as a starting material and H-dbabh as the nitride delivering reagent.¹⁴ This reaction was carried out in THF, and produced **24** cleanly with elimination of ethane and anthracene. The production of anthracene was observed to coincide with the loss of an intermediate when the reaction is monitored by ^1H -NMR spectroscopy, see **Figure 3.12**. Because the disappearance of the intermediate was seen coinciding with the production of anthracene, it was reasonable to assume that intermediate was $\text{Tp}^{\text{tBu,Me}}\text{Cr-dbabh}$, see **Scheme 3.5**, and that it has three ^1H -NMR resonances at 47.3, 4.5, and an exceptionally broad resonance at -4.5 ppm.



Scheme 3.5: Reaction of $\text{Tp}^{\text{tBu,Me}}\text{CrEt}$ with H-dbabh.

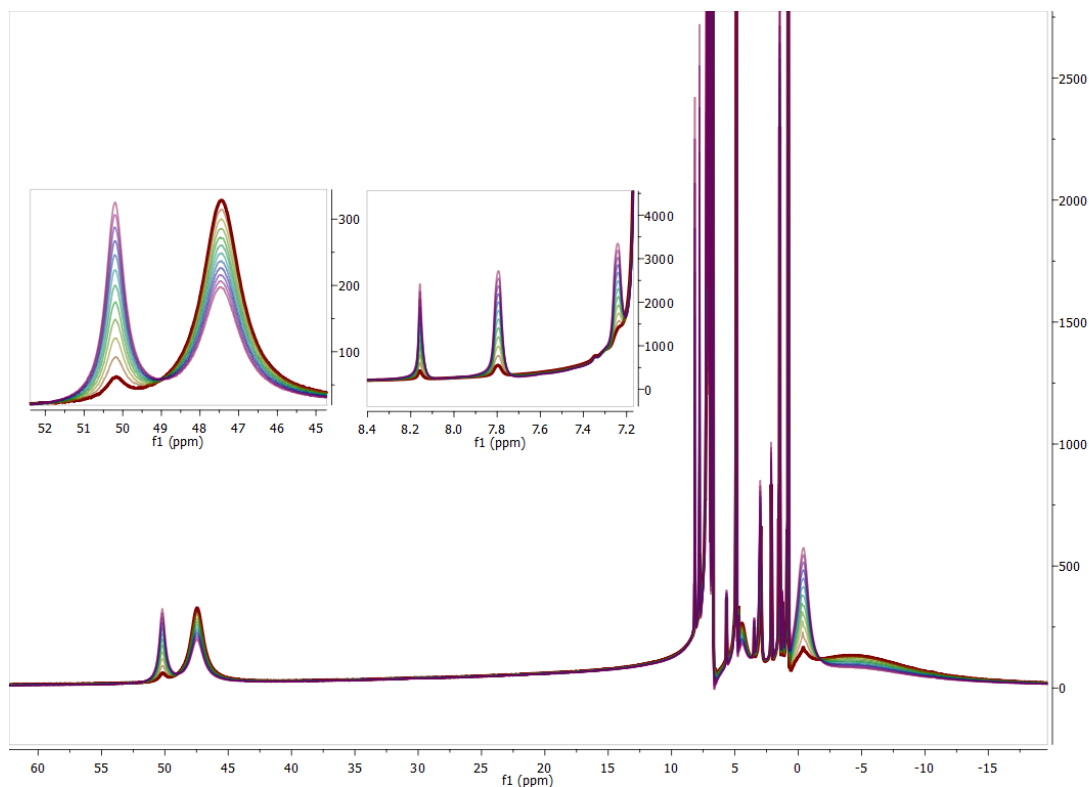


Figure 3.12: $^1\text{H-NMR}$ of the reaction of $\text{Tp}^{\text{tBu,Me}}\text{CrEt}$ with H-dbabh in C_6D_6 , starting 5 minutes after transfer of solvent, with spectra taken every 10 minutes. **Inset (left):** disappearance of intermediate chemical shift at 47.3 ppm and growth of **24** chemical shift at 50.3 ppm; **Inset (right):** growth of anthracene chemical shifts at 8.2, 7.8, and 7.2 ppm.

Acquiring large quantities of pure **24** for further study and analysis was still complicated by the presence of 1 equiv. of anthracene in the product mixture, which is soluble in pentanes to such a degree as to preclude extraction of **24** with that solvent. A pure sample of **24**, isolated in the manner previously described for producing X-ray quality crystals, was heated in C_6D_6 and monitored by $^1\text{H-NMR}$ spectroscopy,

whereupon it was discovered that the compound is stable at temperatures up to 110 °C in solution. This allows for the removal of anthracene from the product mixture by sublimation, which can be achieved at 110 °C under a vacuum with a pressure lower than $1 \cdot 10^{-7}$ mbar, which can be achieved through use of a TMH071 Turbo-molecular Drive Pump, available from Pfeiffer Vacuum.¹⁵ After purification in this manner, pure quantities of **24** can be produced with a yield of 84 % after 1 crystallization from a mixture of ether and pentanes, see **Figure 3.13**.

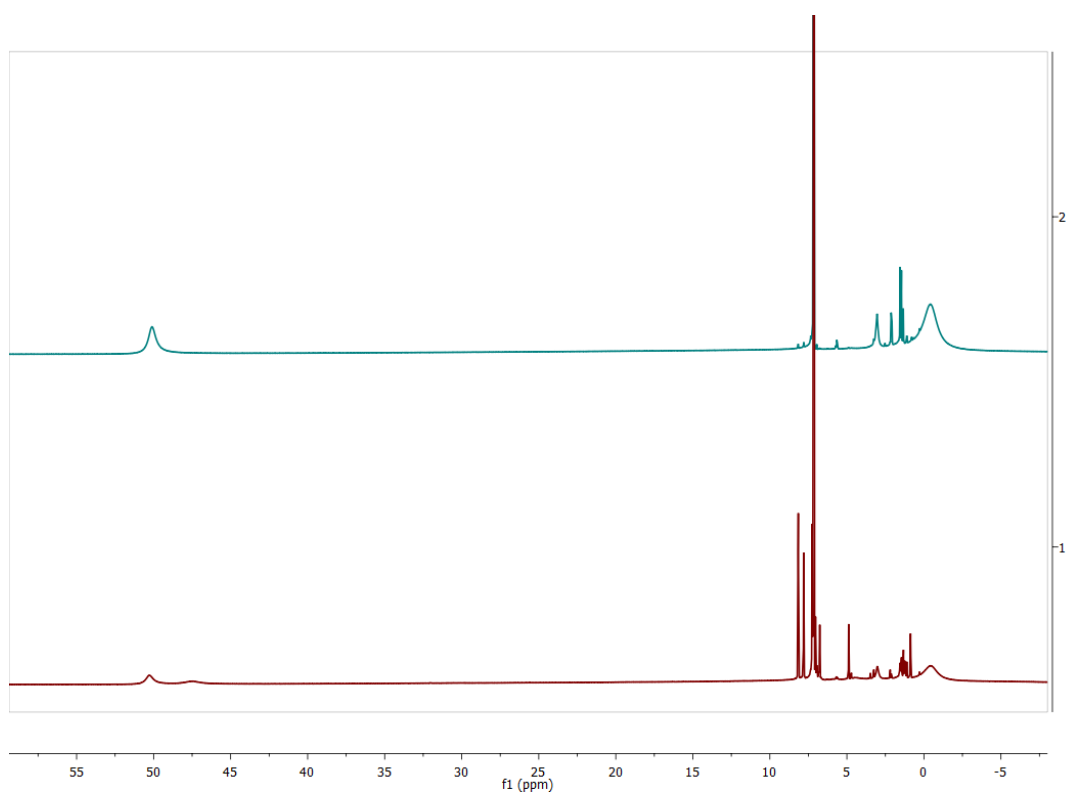
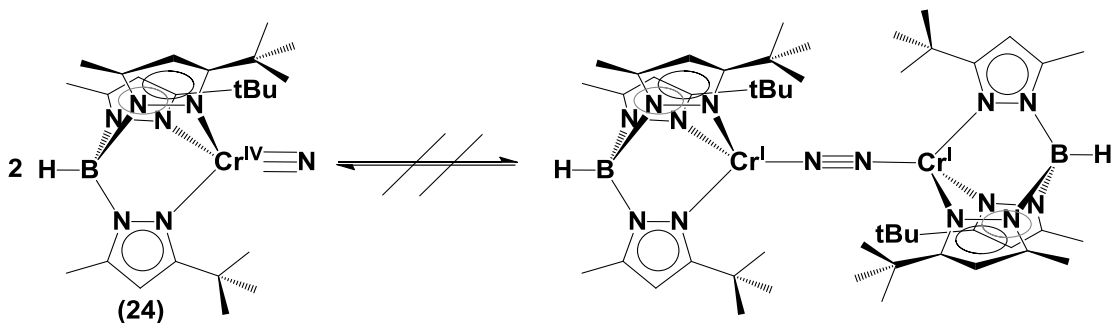


Figure 3.13: ^1H -NMR spectra before (bottom) and after sublimation done at 110 °C for 6 hours and one crystallization from a solution of **24** in ether and pentane (top).

Kinetic and thermodynamic data related to $\text{Tp}^{\text{tBu,Me}}\text{CrN}$. It is of significant note that $[\text{Tp}^{\text{tBu,Me}}\text{Cr}^{\text{I}}]_2(\mu\text{-}\eta^1\text{:}\eta^1\text{-N}_2)$ has been isolated and is stable.¹⁶ However, even at high temperatures $\text{Tp}^{\text{tBu,Me}}\text{CrN}$ (**24**) does not convert to the monovalent chromium dinitrogen complex, see **Scheme 3.6**. This is especially significant, given the observation by Peters et. al. regarding the compound $\text{PhBP}^{\text{iPr}}_3\text{FeN}$, which is unstable at ambient temperatures, coupling to form a monovalent iron dinitrogen complex.^{9b}



Scheme 3.6: Expected equilibrium of **24** with $[\text{Tp}^{\text{tBu,Me}}\text{Cr}^{\text{I}}]_2(\mu\text{-}\eta^1\text{:}\eta^1\text{-N}_2)$, which is observed to not occur.

Furthermore, $\text{Tp}^{\text{tBu,Me}}\text{M-dbabh}$ ($\text{M} = \text{Fe}$ (**22**) and Co (**23**)) complexes are stable despite the readiness of the chromium dbabh complex to decompose via a 2 electron oxidation of the metal center. In the hopes of better understanding why **24** is stable despite the inability to produce nitride complexes of Co and Fe on the same $\text{Tp}^{\text{tBu,Me}}$ ligand, I produced an Eyring plot for the conversion of $\text{Tp}^{\text{tBu,Me}}\text{Cr-dbabh}$ to **24**, see **Figure 3.15**. Rate constants, at temperatures ranging from 5 to 55 °C, were determined by measuring the rate of disappearance of the intermediate, $\text{Tp}^{\text{tBu,Me}}\text{Cr-dbabh}$, which

had a λ_{\max} at 830 nm in UV-Vis Spectroscopy. The spectra showed an isosbestic point at 645 nm observable when the reaction of $\text{Tp}^{\text{tBu,Me}}\text{CrEt}$ with H-dbabh is monitored by Uv-Vis spectrometry, see **Figure 3.14**. The values relevant to the Eyring plot are available in **Table 3.7**.

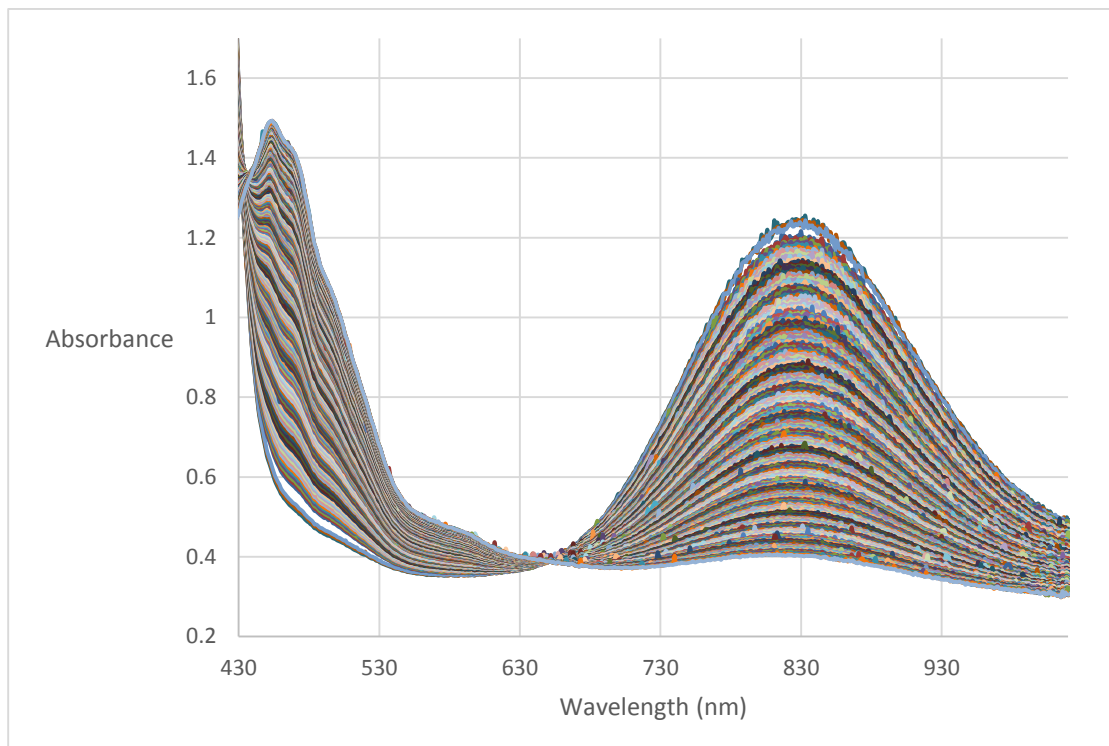


Figure 3.14: Stacked plot of UV-Vis data showing the loss of the intermediate ($\lambda_{\max} = 830$ nm), growth of 24 ($\lambda_{\max} = 455$ nm), and isosbestic point at 645 nm.

Table 3.7: Rate constants taken at temperatures between 278.15 K and 328.15 K for the decomposition of $\text{Tp}^{\text{tBu,Me}}\text{Cr-dbabh}$ to $\text{Tp}^{\text{tBu,Me}}\text{CrN}$ (24), ($R = 8.31446$ J/Kmol, $h = 6.626 \cdot 10^{-34}$ Js, $K_b = 1.38065 \cdot 10^{-23}$ J/K).

T	k (S^{-1})	$1/t$	$R \ln((kh)/(K_b T))$
278.15	$1.98 \cdot 10^{-5}$ (2)	0.003595	-334.375
286.15	$3.55 \cdot 10^{-5}$ (4)	0.003495	-329.653
298.15	$7.51 \cdot 10^{-5}$ (11)	0.003354	-323.073
308.15	$1.70 \cdot 10^{-4}$ (3)	0.003245	-317.039
318.15	$4.29 \cdot 10^{-4}$ (13)	0.003143	-309.753
328.15	$9.11 \cdot 10^{-4}$ (7)	0.003047	-303.919

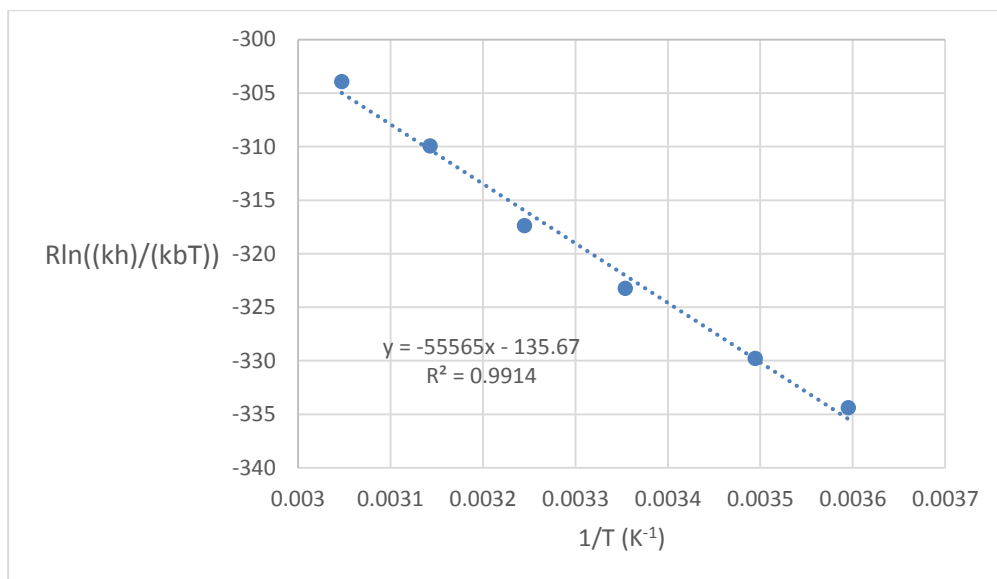


Figure 3.15: Eyring plot for the decomposition of $\text{Tp}^{\text{tBu,Me}}\text{Cr-dbabh}$ to $\text{Tp}^{\text{tBu,Me}}\text{CrN}$, plotted as $R \ln((kh)/(K_b T))$ vs $1/T$, ($R = 8.31446$ J/Kmol, $h = 6.626 \cdot 10^{-34}$ Js, $K_b = 1.38065 \cdot 10^{-23}$ J/K).

Using the Eyring Equation, shown below, the activation parameters for the reaction can be determined from the above plot, giving values of $\Delta H^\ddagger = 55.6(7)$ kJ/mol and $\Delta S^\ddagger = 135.7(7)$ J/Kmol.

$$\text{Eyring Equation: } -R \ln \left(\frac{kh}{K_b T} \right) = \Delta H^\ddagger \frac{1}{T} + \Delta S^\ddagger$$

The relatively large positive entropy gives some indication as to why **22** and **23** remain stable while the chromium complex decomposes readily at room temperature. Iron and cobalt are both far less stable in high oxidation states, so even though the their decompositions should have similar ΔS^\ddagger parameters, the ΔH^\ddagger for such a 2 electron oxidation must be considerably higher.¹⁷ Given the high change in entropy associated with this transformation, **22** and **23** should eventually decompose into the nitride and anthracene at high enough temperatures, but instead decompose through some other pathway at a 110 °C.

Reactivity of $\text{Tp}^{\text{tBu,Me}}\text{CrN}$ (24**) with various substrates, general considerations.** Nitride complexes of late transitional metals are often reactive toward small molecules and electrophilic substrates.^{9b-d} The range of reactivity of the iron nitride supported by the phenyltris(1-mesitylimidazol-2-ylidene)borato ($\text{PhB}(\text{mesIm})_3$) ligand includes spontaneous reactivity with phosphines, olefins, and both alkyl radicals as well as hydrogen atom donor molecules.¹⁸ With this in mind I set about investigating complimentary reactivity with **24**, as well other potential pathways to further functionalize the complex.

Initial reactions with dihydroanthracene (DHA) resulted in no reaction. When monitored by ¹H-NMR a sample of **24** in C₆D₆ was heated to 70 °C in the presence of

either ~0.9 atm of H₂, ethylene, or CO gas, and no apparent loss of the starting material or appearance of new chemical shifts were observed. The reaction of **24** with excess DHA did not result in any additional resonances between -5 and 15 ppm. The mixture was then heated to 75 °C for 14 hours, also without the production of any additional resonances in the diamagnetic region, but with some resonances that correspond to anthracene, see **Figure 3.16**. This may be due to decomposition of DHA to anthracene by way of the release of H₂.¹⁹

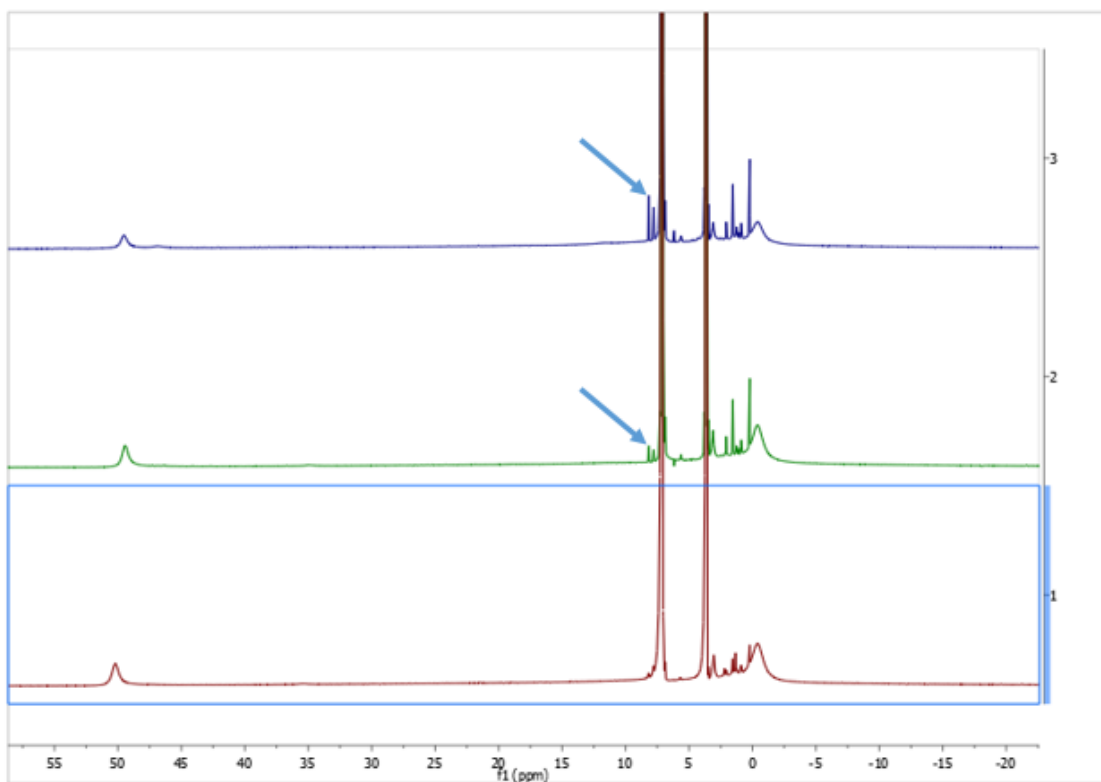


Figure 3.16: ¹H-NMR spectra of the reaction of Tp^{tBu,Me}CrN (**24**) with 9,10-dihydroanthracene, with chemical shifts for anthracene marked with blue arrows (bottom – starting material, middle – 7 hours at 75 °C, top – 7 additional hours at 75 °C).

Given the attenuated reactivity of **24** in comparison to that of $\text{PhB}(\text{mesIm})_3\text{FeN}$,²⁰ we set out to functionalize **24** by way of either reduction or oxidation of the complex. Reaction of **24** with O_2 , PhIO , or NO resulted in apparent decomposition, with LIFDI-MS indicating the major chromium containing product is a $\text{Tp}^{\text{tBu,Me}}\text{Cr}(\text{N})(\text{Pz}^{\text{tBu,Me}})$ complex, having a pyrazolate being apparently bound to the metal center with some free $\text{HPz}^{\text{tBu,Me}}$ being evident in the ^1H -NMR spectrum, see **Figures 3.17** and **3.18**.

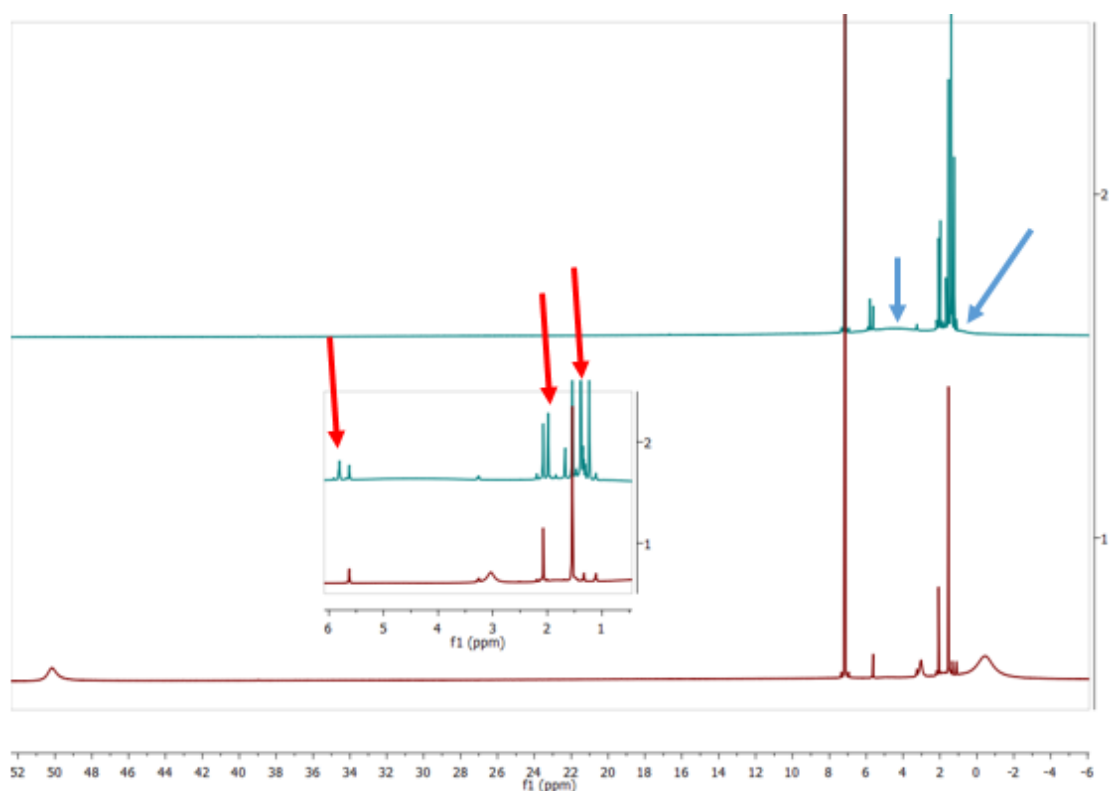


Figure 3.17: ^1H -NMR for the reaction of $\text{Tp}^{\text{tBu,Me}}\text{CrN}$ (**24**) (bottom) with 1 atm of NO (top), ($\text{HPz}^{\text{tBu,Me}}$ highlighted with red arrows [inset], chromium containing product highlighted with blue arrows).

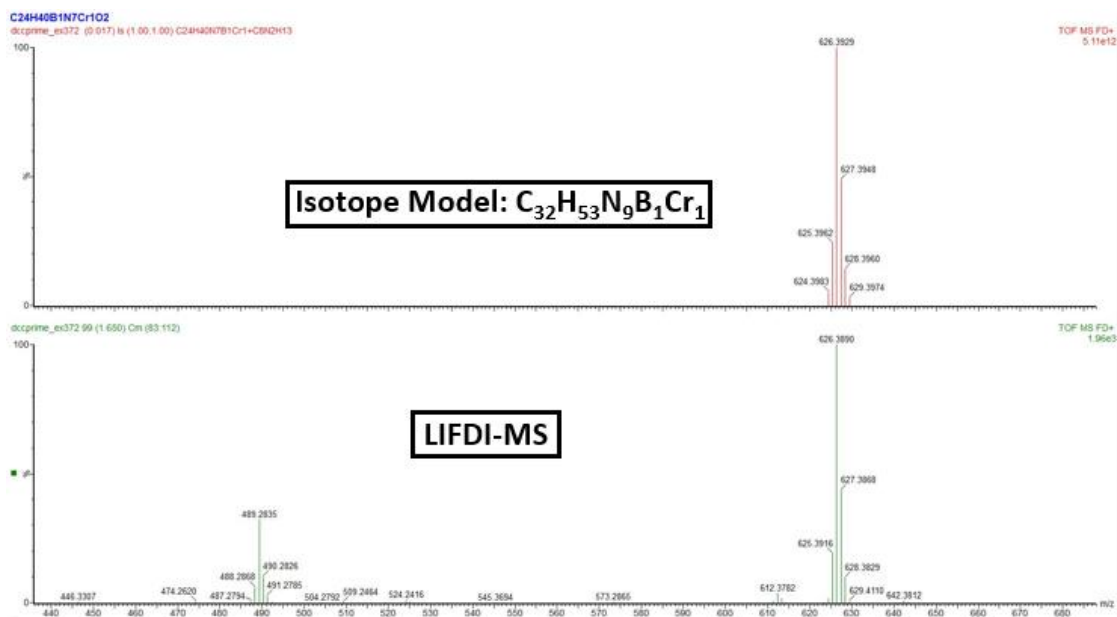


Figure 3.18: LIFDI-MS for the result of the reaction of $\text{Tp}^{\text{tBu,Me}}\text{CrN}$ (24**) with 1 atm of NO (bottom), with isotope model for a compound have the formula corresponding to $\text{Tp}^{\text{tBu,Me}}\text{Cr}(\text{N})(\text{Pz}^{\text{tBu,Me}})$ (top).**

I attempted to reduce **24** with KC_8 , but only isolated $\text{Tp}^{\text{tBu,Me}}\text{K}$, with the fate of the chromium and nitride left undetermined. To better understand this, cyclic voltammograms were taken of two samples of **24** prepared in THF with $\text{N}^{\text{tBu}}\text{Bu}_4\text{BF}_4$ as an electrolyte, with one having ferrocene to act as an internal standard. The complex showed an irreversible oxidation with a voltage max of 1.0 V vs SHE, and 2 irreversible reductions with voltage maxima at -1.85 and -2.24 V vs SHE. The irreversibility of both of these events indicates a chemical change, meaning that either oxidation state III or V for the nitride as an ionic salt or in a tetrahedral coordination sphere is likely impossible, requiring instead either a change of ligand or coordination sphere about the metal center.

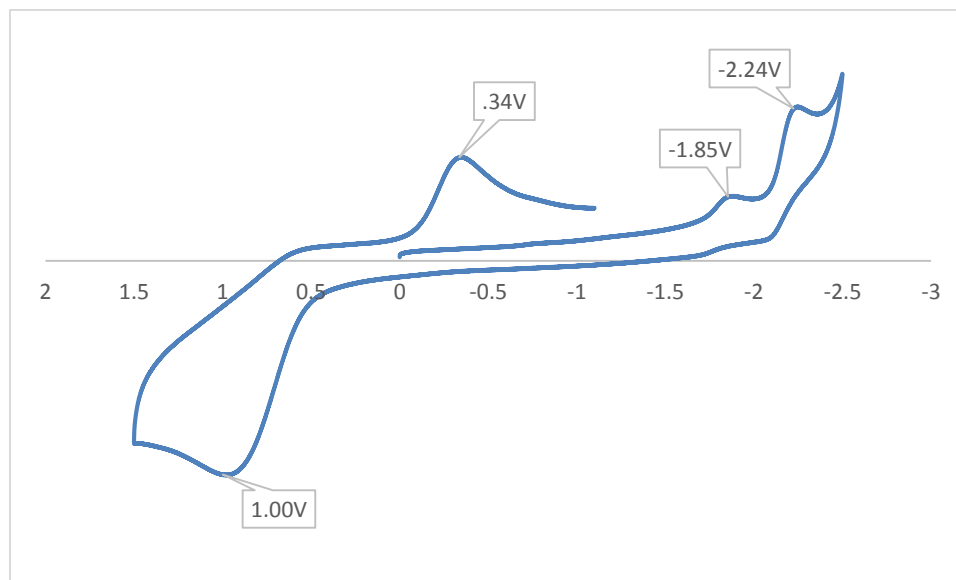


Figure 3.19: Cyclic voltammogram of $\text{Tp}^{\text{tBu,Me}}\text{CrN}$ (24**), in 0.1 M THF solution of $[\text{NnBu}_4]\text{PF}_6$ referenced with Fc^+/Fc to SHE at $V = 0$, (working electrode = GC, reference electrode = Ag/Ag^+ , Counter electrode = Pt)**

Previous examples of iron and rhenium terminal nitride complexes have demonstrated reactivity toward electrophiles, undergoing nucleophilic addition to electron poor alkyl substrates.²⁰ Seeking to further explore the reactivity of **24**, I investigated its interaction with electrophilic alkyl substrates, focusing on methyl compounds in an effort to produce low molecular weight imides. It has been shown previously that imide complexes can be accessed by treatment of monovalent $\text{Tp}^{\text{tBu,Me}}\text{Cr}$ substrates with organic azides.²¹ Such reactions with low molecular weight azides have not been significantly investigated, as those azides are often temperature sensitive explosives, making their synthesis and handling difficult.²² The first reagent I used was methyl triflate (MeOTf), which reacted rapidly with 1 equiv. of **24** in ether at

room temperature, resulting in a color change from yellow to green over the course of several minutes. $^1\text{H-NMR}$ of the solution indicated a mixture of products, and when analyzed with LIFDI-MS it was determined that one of those products had a mass corresponding to that expected for $\text{Tp}^{\text{tBu,Me}}\text{CrNMe}$, either as a Cr^{IV} ion having lost its accompanying triflate, or as Cr^{III} imide.

This was encouraging, but given that the compound was only produced in small quantities (<10 % yield), I began utilizing methyl iodide (MeI) as an alkylating reagent, in the hopes that the reactivity of a less electrophilic methyl donor would be easier to control. Mixtures of **24** with 1 equiv. of MeI at room temperature showed little evidence of reactivity. However, a mixture of excess MeI (4 equiv.) with **24** in THF heated to 45 °C for 5 days, showed no evidence of any remaining starting material and as many as 3 paramagnetic compounds when analyzed with $^1\text{H-NMR}$ spectroscopy. After removal of the solvent in vacuo and extraction with pentane, a yellow residue remained insoluble. The yellow solid could be dissolved with stirring in ether, and after filtration and layering with pentanes, yellow crystals of $\text{Tp}^{\text{tBu,Me}}\text{Cr}^{\text{V}}(\text{N})(\text{I})$ (**25**) were formed in yields between 38 and 44 %. The crystals were analyzed using X-ray diffraction and the compound was found to be roughly trigonal bipyramidal, see **Figure 3.20**, having a geometry index $\tau_5 = 0.646$.²³ The Cr-N bond distance of **25**, 1.532(3) Å, is the same within error as that observed in **24**. The Cr-I bond distance, 2.7005(6) Å, is consistent with other Cr-I bond lengths previously reported.²⁴ The effective magnetic moment, measured by Evans Method at 300 K, was found to be 1.9(1) μ_{B} , indicating **25** has a d^1 Cr^{V} metal center. **25** can also be produced with yields between 82 and 87 % by the reaction of **24** with excess I_2 in THF.

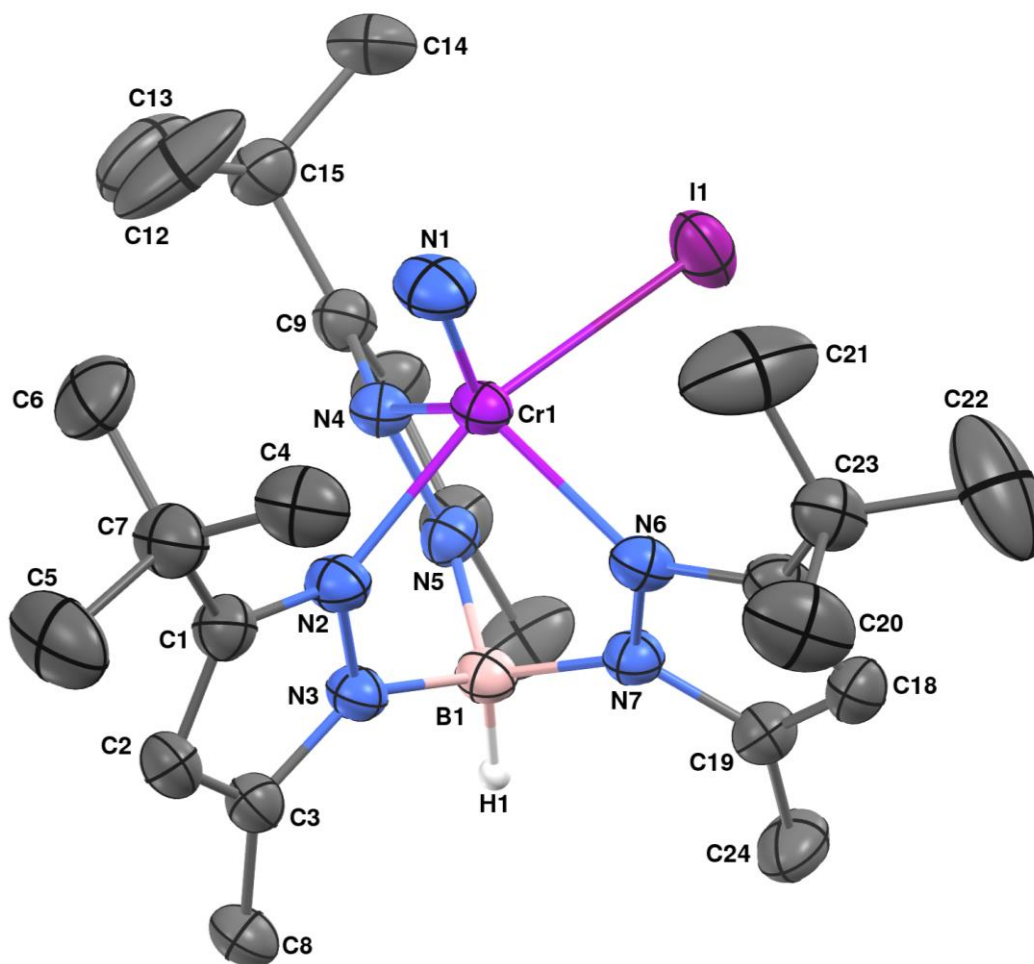


Figure 3.20: Molecular structure of $\text{Tp}^{\text{tBu,Me}}\text{Cr}(\text{N})(\text{I})$ (25) represented as 50% probability thermal ellipsoids. Hydrogen atoms (with the exception of the hydrogen attached to boron, H1) omitted for clarity.

Table 3.8: Selected interatomic distances (Å) and angles (°) for $\text{Tp}^{\text{tBu,Me}}\text{Cr}(\text{N})(\text{I})$ (25).

Distances (Å)			
Cr1-N1	1.532(3)	Cr1-N4	2.037(3)
Cr1-N6	2.045(3)	Cr1-N2	2.077(3)
Cr1-I1	2.7005(6)	N2-C1	1.347(5)

N2-N3	1.375(4)	N3-C3	1.350(4)
N3-B1	1.535(5)	N4-C9	1.341(4)
N4-N5	1.402(4)	N5-C11	1.352(4)
N5-B1	1.554(4)	N6-C17	1.347(4)
N6-N7	1.392(4)	N7-C19	1.355(4)
N7-B1	1.561(4)	C1-C7	1.528(5)
C1-C2	1.397(5)	C4-C7	1.539(6)
C2-C3	1.377(5)	C5-C7	1.541(6)
C3-C8	1.490(5)	C6-C7	1.516(6)
C9-C10	1.388(5)	C9-C15	1.524(5)
C10-C11	1.377(5)	C12-C15	1.509(7)
C11-C16	1.489(5)	C13-C15	1.525(6)
C17-C18	1.400(5)	C14-C15	1.511(7)
C18-C19	1.372(5)	C17-C23	1.510(5)
C19-C24	1.501(5)	C20-C23	1.511(6)
C22-C23	1.514(7)	C21-C23	1.515(6)

Angles (°)

N1-Cr1-N4	118.32(16)	N1-Cr1-N6	121.82(16)
N4-Cr1-N6	119.86(10)	N1-Cr1-N2	102.45(15)
N4-Cr1-N2	85.20(11)	N6-Cr1-N2	82.61(11)
N1-Cr1-I1	96.98(13)	N4-Cr1-I1	86.40(8)
N6-Cr1-I1	86.44(8)	N2-Cr1-I1	160.55(8)
C1-N2-N3	107.0(3)	C1-N2-Cr1	144.5(2)
N3-N2-Cr1	108.1(2)	C3-N3-N2	110.1(3)
C3-N3-B1	132.0(3)	N2-N3-B1	117.9(3)
C9-N4-N5	106.7(3)	C9-N4-Cr1	142.3(2)
N5-N4-Cr1	99.11(18)	C11-N5-N4	108.7(3)
C11-N5-B1	129.3(3)	N4-N5-B1	121.3(3)
C17-N6-N7	107.2(3)	C17-N6-Cr1	144.3(2)
N7-N6-Cr1	101.61(17)	C19-N7-N6	108.9(3)
C19-N7-B1	129.0(3)	N6-N7-B1	121.9(2)
N3-B1-N5	106.8(3)	N3-B1-N7	107.7(3)
N5-B1-N7	113.1(3)	N2-C1-C7	124.1(3)
N2-C1-C2	108.6(3)	C3-C2-C1	107.2(3)
C2-C1-C7	127.3(3)	N3-C3-C8	122.9(3)
N3-C3-C2	107.1(3)	C6-C7-C1	109.3(3)
C2-C3-C8	130.0(3)	C1-C7-C4	110.9(3)
C6-C7-C4	110.9(4)	C1-C7-C5	108.3(3)
C6-C7-C5	110.0(4)	N4-C9-C10	109.6(3)

C4-C7-C5	107.4(4)	C10-C9-C15	126.5(3)
N4-C9-C15	123.9(3)	N5-C11-C10	108.1(3)
C11-C10-C9	106.9(3)	C10-C11-C16	130.8(3)
N5-C11-C16	121.1(3)	C12-C15-C9	111.1(3)
C12-C15-C14	112.1(5)	C12-C15-C13	107.4(5)
C14-C15-C9	109.4(3)	C9-C15-C13	108.9(3)
C14-C15-C13	107.8(5)	N6-C17-C23	125.0(3)
N6-C17-C18	108.7(3)	C19-C18-C17	107.1(3)
C18-C17-C23	126.1(3)	N7-C19-C24	123.0(3)
N7-C19-C18	108.1(3)	C17-C23-C20	107.6(3)
C18-C19-C24	128.8(3)	C20-C23-C22	108.6(4)
C17-C23-C22	108.8(4)	C20-C23-C21	108.1(4)
C17-C23-C21	113.3(3)	C22-C23-C21	110.4(5)

The pentane extract of the reaction of **24** with MeI was purple in color, and yielded purple crystals when cooled to -35 °C for several days. ¹H-NMR of the crystals presented 7 paramagnetic chemical shifts, see **Figure 3.21**, indicating more than one Tp^{tBu,Me}Cr complex co-crystallized. The LIFDI-MS of the crystals displayed masses that correspond to the molecular ions of both Tp^{tBu,Me}Cr^{III}NMe (**26**) and Tp^{tBu,Me}Cr^{II}I, see **Figure 3.22**. Tp^{tBu,Me}Cr^{II}I is not a known compound, but apart from the mass spectrometry data its identity is further supported by the distribution of its ¹H-NMR chemical shifts being 22.5, 13.1, and -7.7 ppm with integrations of roughly 9, 27 and 3 H respectively. The proposed chromium iodide also displays behavior and color that are similar to the known compound Tp^{tBu,Me}CrCl, both being soluble in pentanes, both reacting with pyridine to form a complex soluble in ether, and both being a pale green color.²⁷ The formation of **26** suggests an intermediate [Tp^{tBu,Me}Cr^{IV}NMe]⁺[I]⁻ reacted with remaining starting material, which resulted in Tp^{tBu,Me}Cr^V(N)(I) (**25**) and Tp^{tBu,Me}Cr^{III}NMe (**26**) both being formed. The means through which Tp^{tBu,Me}CrI is produced remains ambiguous, see **Scheme 3.7**.

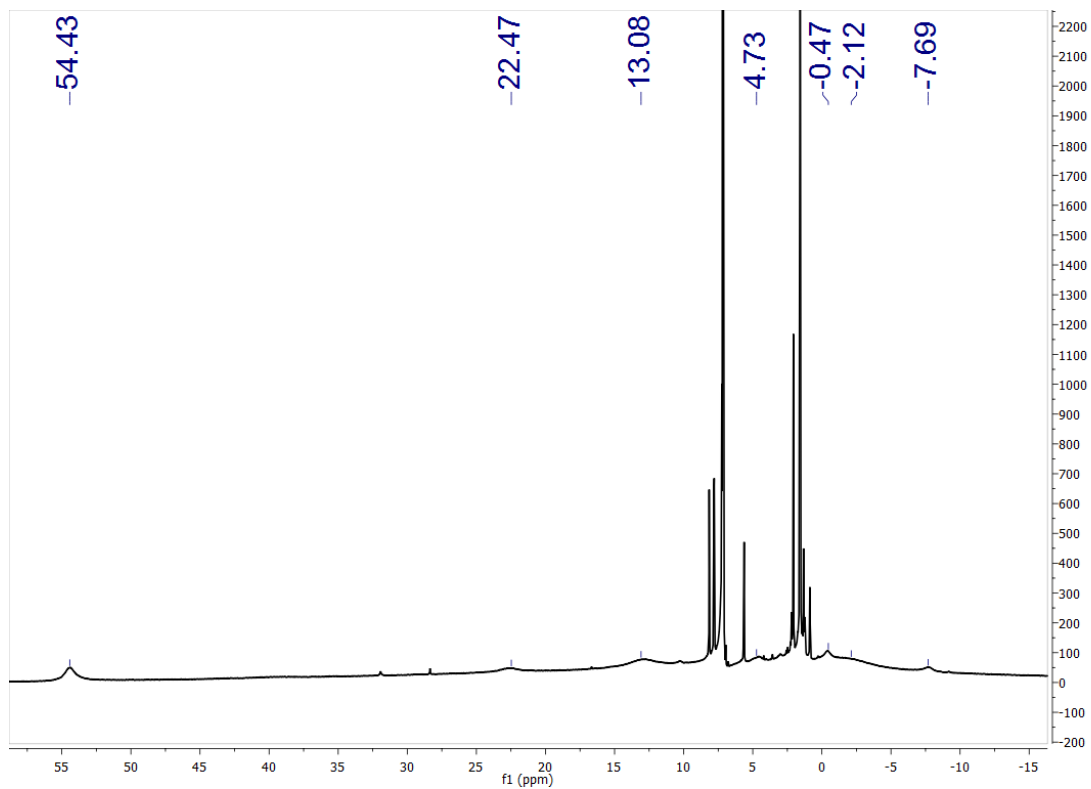


Figure 3.21: ^1H -NMR spectrum of crystals grown from pentane, from the reaction of $\text{Tp}^{\text{tBu,Me}}\text{CrN}$ with MeI, showing 7 broad paramagnetic chemical shifts, with some anthracene having also been present in the unit cell.

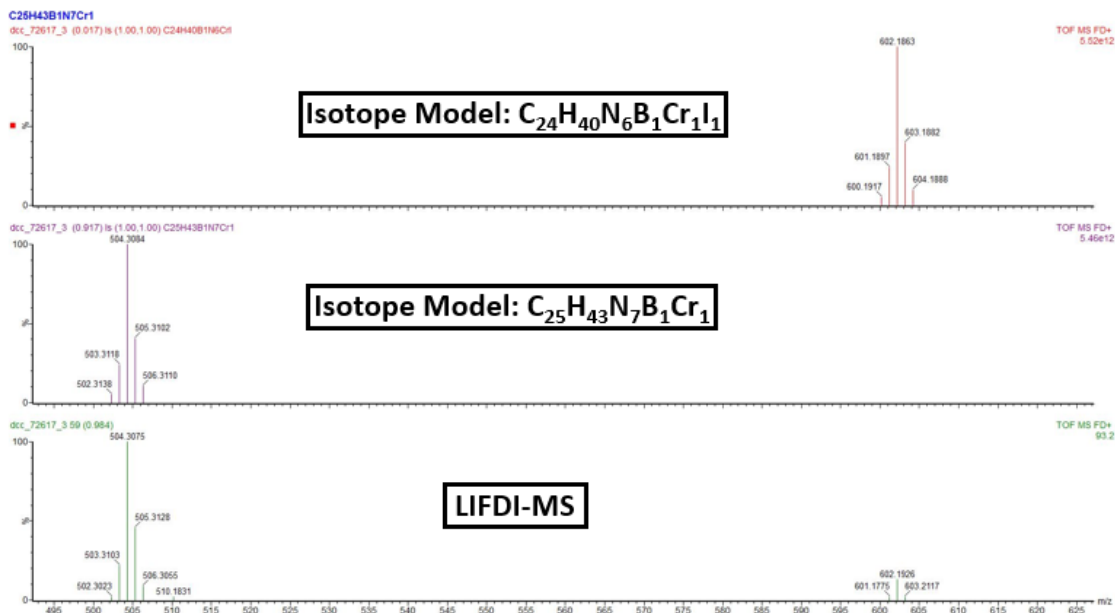
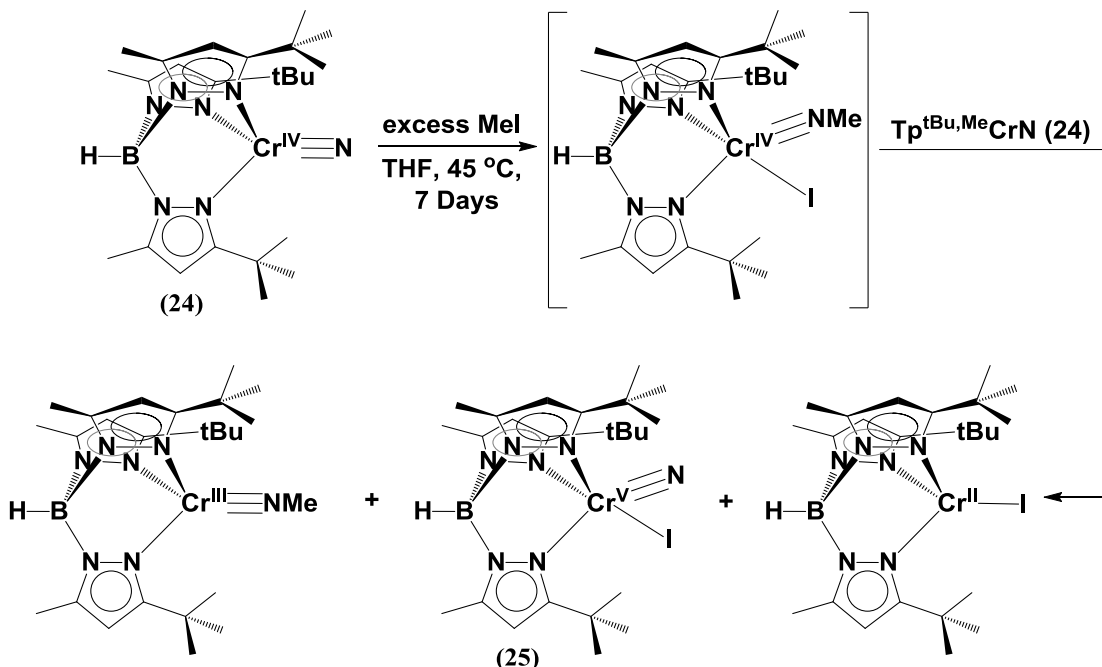


Figure 3.22: LIFDI-MS spectrum of the pentane extract from the reaction of $\text{Tp}^{\text{tBu},\text{Me}}\text{CrN}$ (24) with MeI (bottom), predicted isotope pattern for a complex with a formula corresponding to $\text{Tp}^{\text{tBu},\text{Me}}\text{CrNMe}$ ($\text{C}_{25}\text{H}_{43}\text{N}_7\text{B}_1\text{Cr}_1$ middle), and the predicted isotope pattern complex with a formula corresponding to $\text{Tp}^{\text{tBu},\text{Me}}\text{CrI}$ ($\text{C}_{24}\text{H}_{40}\text{N}_6\text{B}_1\text{Cr}_1\text{I}_1$ top).



Scheme 3.7: Reaction of $\text{Tp}^{\text{tBu,Me}}\text{CrN}$ (24) with MeI, synthesis of $\text{Tp}^{\text{tBu,Me}}\text{Cr(N)(I)}$ (25), $\text{Tp}^{\text{tBu,Me}}\text{CrNMe}$, and $\text{Tp}^{\text{tBu,Me}}\text{CrI}$.

The similar solubility of $\text{Tp}^{\text{tBu,Me}}\text{CrI}$ and **26** make the separation of the two compounds difficult. However, the analogous complex $\text{Tp}^{\text{tBu,Me}}\text{CrCl}$ was observed to react with pyridine (Py) to produce $\text{Tp}^{\text{tBu,Me}}\text{Cr(Cl)(Py)}$, a compound that is nearly completely insoluble in pentanes solutions.²⁷ Armed with this knowledge, I added Py to a mixture of **26** and $\text{Tp}^{\text{tBu,Me}}\text{CrI}$ in pentanes solution, after which the formation of a precipitate was observed. Upon filtration and concentration, the remaining purple solution was placed in a $-35\text{ }^{\circ}\text{C}$ freezer for 4 days, during which time purple crystals of **26** grew, affording a 42 % isolated yield. The magnetic moment of **26** was measured using Evans Method, and found to be $3.8(1)\ \mu_{\text{B}}$, consistent with high spin Cr^{III} metal center. Its structure was determined using X-ray crystallography, and found to be

tetrahedral with $\tau_4 = 0.745$, and $\tau_4' = 0.733$,¹¹ having a Cr-N-Me bond angle of $174.4(5)^\circ$, see **Figure 3.23** and **Table 3.9**.

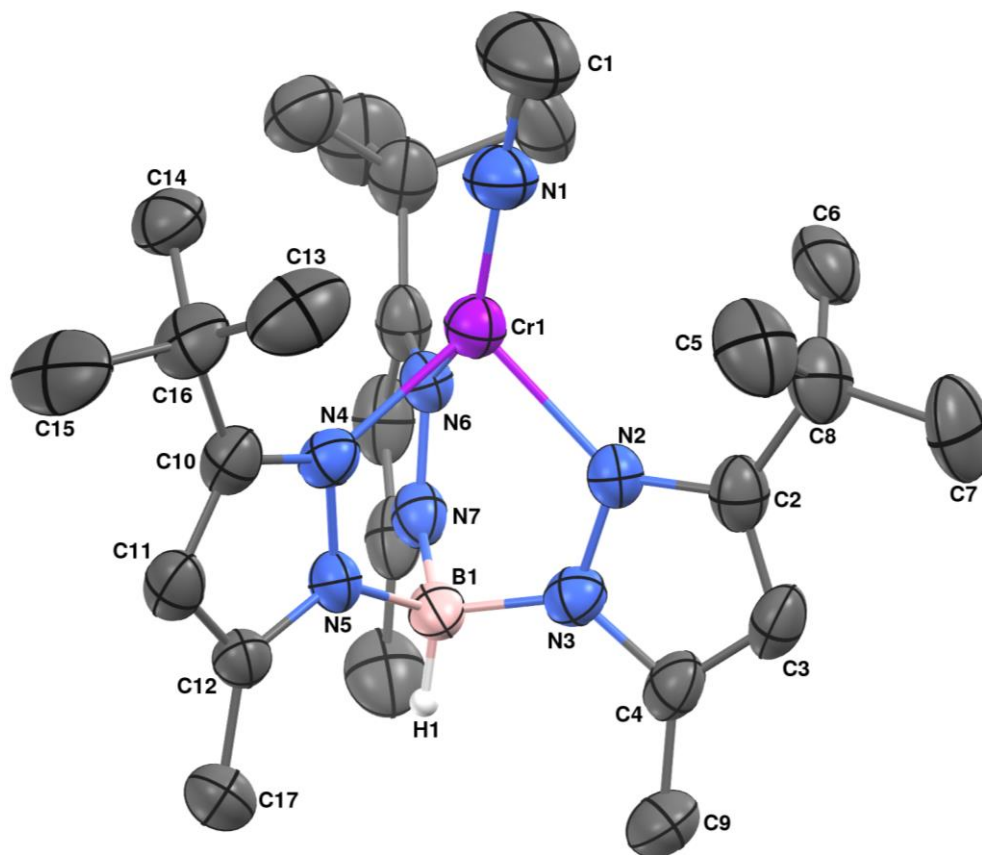


Figure 3.23: Molecular structure of $\text{Tp}^{\text{tBu,Me}}\text{CrNMe}$ (26) represented as 50% probability thermal ellipsoids. Hydrogen atoms (with the exception of the hydrogen attached to boron, H1) omitted for clarity.

Table 3.9: Selected interatomic distances (Å) and angles (°) for**Tp^{tBu,Me}CrNMe (26).**

Distances (Å)			
Cr1-N1	1.673(4)	Cr1-N2	2.099(3)
Cr1-N4	2.110(3)	Cr1-N6	2.113(4)
N1-C1	1.433(7)	N2-C2	1.351(5)
N2-N3	1.383(5)	N3-C4	1.370(5)
N3-B1	1.550(6)	N4-C10	1.333(5)
N4-N5	1.385(5)	N5-C12	1.347(5)
N5-B1	1.540(6)	N6-C18	1.339(5)
N6-N7	1.380(5)	N7-C20	1.357(5)
N7-B1	1.532(6)	C2-C3	1.382(6)
C2-C8	1.547(6)	C3-C4	1.379(6)
C5-C8	1.542(7)	C4-C9	1.483(6)
C6-C8	1.494(7)	C10-C11	1.404(6)
C7-C8	1.524(7)	C11-C12	1.379(6)
C10-C16	1.524(6)	C12-C17	1.491(6)
C13-C16	1.527(8)	C15-C16	1.536(7)
C14-C16	1.529(7)		
Angles (°)			
N1-Cr1-N2	123.32(17)	N1-Cr1-N4	125.44(17)
N2-Cr1-N4	90.55(13)	N1-Cr1-N6	129.51(17)
N2-Cr1-N6	89.29(14)	N4-Cr1-N6	86.69(13)
C1-N1-Cr1	174.4(5)	C2-N2-N3	105.9(3)
C2-N2-Cr1	138.1(3)	N3-N2-Cr1	115.9(2)
C4-N3-N2	110.0(3)	C4-N3-B1	130.4(4)
N2-N3-B1	119.6(3)	C10-N4-N5	107.0(3)
C10-N4-Cr1	137.6(3)	N5-N4-Cr1	115.3(2)
C12-N5-N4	109.7(3)	C12-N5-B1	130.2(3)
N4-N5-B1	120.0(3)	C18-N6-N7	106.9(3)
C18-N6-Cr1	137.7(3)	N7-N6-Cr1	115.3(2)
C20-N7-N6	109.8(4)	C20-N7-B1	129.9(4)
N6-N7-B1	120.3(3)	N7-B1-N5	109.8(3)
N7-B1-N3	109.9(3)	N5-B1-N3	108.5(3)
N2-C2-C8	122.0(4)	N2-C2-C3	110.1(4)

C4-C3-C2	107.3(4)	C3-C2-C8	127.9(4)
N3-C4-C9	123.2(4)	N3-C4-C3	106.7(4)
C6-C8-C7	109.2(4)	C3-C4-C9	130.1(4)
C7-C8-C5	107.9(4)	C6-C8-C5	112.3(5)
C7-C8-C2	109.1(4)	C6-C8-C2	111.7(4)
N4-C10-C11	109.2(4)	C5-C8-C2	106.5(4)
C11-C10-C16	127.9(4)	N4-C10-C16	122.9(4)
N5-C12-C11	107.6(4)	C12-C11-C10	106.5(4)
C11-C12-C17	128.7(4)	N5-C12-C17	123.7(4)
C10-C16-C14	111.3(4)	C10-C16-C13	109.1(4)
C10-C16-C15	107.8(4)	C13-C16-C14	110.4(4)
C14-C16-C15	107.9(4)	C13-C16-C15	110.2(5)

Conclusion

A terminal nitride complex of a first row transition metal supported by a tris(pyrazolyl)borate has been described and characterized in the form of $\text{Tp}^{\text{tBu,Me}}\text{Cr}^{\text{IV}}\text{N}$ (**24**). The complex is stable at high temperatures and under U.V. radiation, without any evidence of the formation of the known complex $[\text{Tp}^{\text{tBu,Me}}\text{Cr}]_2(\mu_2\text{-}\eta^1\text{:}\eta^1\text{-N}_2)$. It was determined that the same means of synthesis was not viable for analogous nitride complexes of either Fe or Co, which decompose by ways other than the formation of nitride at high temperatures. **24** was found to be only somewhat stable in the face of oxidative or reductive environments, decomposing when exposed to oxidants such as O_2 and PhIO. **24** does participate in reactions as a nucleophile, reacting with electrophilic methylating substrates, producing the imide $\text{Tp}^{\text{tBu,Me}}\text{Cr}^{\text{III}}\text{NMe}$ (**26**).

Experimental Section

All reactions were run under a nitrogen atmosphere using standard glovebox and Schlenk techniques, unless otherwise stated. Diethyl ether, pentane,

tetrahydrofuran (THF), and toluene were distilled over Na using benzophenone ketyl as an indicator while under a nitrogen atmosphere, or by passing the solvent through activated alumina columns followed by a nitrogen purge to remove dissolved oxygen.²⁵ Organic chemicals were bought from Fischer, Aldrich, or Acros and all inorganic chemicals were purchased from Strem. Li-dbabh and H-dbabh were synthesized according to literature procedures.^{9a,26} Samples of $\text{Tp}^{\text{tBu,Me}}\text{CrEt}$, $\text{Tp}^{\text{tBu,Me}}\text{FeI}$, and $\text{Tp}^{\text{tBu,Me}}\text{CoI}$ were prepared using literature procedures.²⁷ Carbon monoxide gas was purchased from Matheson. NMR spectra were obtained on Bruker AVIII-400 or AV-600 spectrometers and were referenced to the residual protons of the solvent (C_6D_6 , 7.16 ppm; THF-D_8 , 3.76, 1.85 ppm). FT-IR spectra were recorded on a Nicolet Magna-IR 560 spectrometers with a resolution of 4 cm^{-1} . Mass spectra (LIFDI-MS) were obtained in the University of Delaware Mass Spectrometry Laboratory, using a Waters GCT Premier high resolution time-of-flight mass spectrometer. X-ray crystallographic studies were conducted in the University of Delaware X-ray crystallographic facility. Unless otherwise stated, molar magnetic susceptibilities (χ_m) were acquired in the solid state at room temperature using a Johnson Matthey magnetic susceptibility balance, and corrected for diamagnetism using Pascal constants to give effective magnetic moments (μ_{eff}).²⁸ Elemental analyses were obtained from Robertson Microlit, Ledgewood, NJ 07852.

General considerations for X-ray diffraction studies: Crystals were selected, sectioned as necessary, and mounted on MiTeGen™ plastic mesh with viscous oil, then flash-cooled to the data collection temperature (200 K). Diffraction data were collected on a Bruker-AXS CCD diffractometer with graphite-

monochromated Mo-K α radiation ($\lambda = 0.71073 \text{ \AA}$). The data-sets were treated with absorption corrections based on redundant multi-scan data.²⁹ The structures were solved using direct methods and refined with full-matrix, least-squares procedures on F^2 . Unit cell parameters were determined by sampling three different sections of the Ewald sphere. Non-hydrogen atoms were refined with anisotropic displacement parameters. Hydrogen atoms were treated as idealized contributions with geometrically calculated positions and with U_{iso} equal to 1.2, or 1.5 for methyl, U_{eq} of the attached atom. Structure factors and anomalous dispersion coefficients are contained in the SHELXTL program library.³⁰

Tp^{Fc,Me}FeN₃ (20): 200 mg (0.212 mmol) of Tp^{Fc,Me}FeBr was dissolved in 15ml of THF, and 55 mg (0.849 mmol, 4 equiv.) of NaN₃ was added. The solution was left to stir at room temperature for 60 hours. The solution was filtered, and all volatile material removed in vacuo. The remaining solid residue was dissolved in a minimal quantity of THF and the resulting solution was layered with pentanes, affording orange crystals of the desired Tp^{Fc,Me}FeN₃ complex, yield 170 mg (0.185 mmol, 87 %). ¹H-NMR (400 MHz, C₆D₆) 58.7 (br, 3H), 40.1 (br, 9H), 2.74 (br, 6H), -0.89 (br, 6H), -2.58 (br, 15H) δ ; IR (KBr): 3093 (m), 2969 (m), 2922 (m), 2867 (m), 2544 (m, B-H), 2097 (vs, N₃), 1564 (s), 1513 (w), 1466 (m), 1427 (m), 1404 (m), 1357 (m), 1326 (w), 1190 (s), 1104 (sharp), 1066 (s), 995 (m), 894 (m), 813 (s), 762 (m), 653 (m), 528 (w), 505 (m), 470 (w), 435 (w) cm⁻¹; m.p. 272 – 275 °C (dec); $\mu_{\text{eff}} = 4.9(1) \mu_{\text{B}}$ (296 K); MS (LIFDI, THF): m/z 905.0876 [M⁺]. Calcd.: 905.0909 [M⁺]; Anal. Calcd for C₄₂H₄₀B₁N₉Fe₄: C, 55.74; H, 4.45; N, 13.93. Found C, 54.59; H, 4.33; N, 13.37. Uv/Vis (λ_{max} (THF), ϵ): 440, 1084 (nm, cm⁻¹ M⁻¹).

Tp^{Fc,Me}CoN₃ (21): 450 mg (0.476 mmol) of Tp^{Fc,Me}CoBr was added to 15ml of THF and stirred for 20 minute, then 220 mg (2.72 mmol, 5.2 equiv.) of KN₃ was added, and the solution allowed to stir overnight (24 hours). During that time the solution colored changed from forest green to slightly lighter green, and a colorless precipitate formed in solution. The mixture was filtered, and all volatiles removed in vacuo, the solid residue was dissolved in a minimal quantity of THF and layered with pentanes, affording bright green crystals of the desired Tp^{Fc,Me}CoN₃ complex, 270 mg yield (3.0*10⁻⁴ mol, 63 %). ¹H-NMR (400 MHz, C₆D₆) 70.22 (br, 3H), 15.15 (br, 9H), 9.44 (br, 6H), 3.77 (br, 15H), 3.53 (br, 6H), -9.25 (br, 1H, B-H) δ; IR (KBr): 3100 (m), 2971 (m), 2918 (m), 2856 (m), 2559 (m, B-H), 2086 (vs, N₃), 1559 (s), 1516 (w), 1469 (m), 1429 (s), 1402 (s), 1361 (s), 1316 (w), 1185 (s), 1105 (s), 1060 (s), 1029 (w), 1001 (m), 984 (m), 887 (m), 810 (s), 794 (s), 786 (s), 756 (s), 718 (w), 674 (w), 643 (s), 593 (w), 533 (m), 499 (s), 472 (s), 438 (w) cm⁻¹; m.p. 273 – 274 °C (dec); μ_{eff} = 3.8(2) μ_B (298 K); MS (LIFDI, THF): m/z 908.0918 [M⁺]. Calcd.: 908.0891 [M⁺]; Anal. Calcd for C₄₂H₄₀B₁N₉Fe₃Co: C, 55.55; H, 4.44; N, 13.88. Found C, 55.30; H, 4.40; N, 13.63.

Tp^{tBu,Me}FeN(C₁₄H₁₀) (22): 100 mg (0.165 mmol) of Tp^{tBu,Me}FeI was dissolved in 10 ml of THF, to this solution was added 33 mg (0.165 mmol, 1 equiv.) of lithium-dbabh. The solution turned from colorless to pale yellow after 30 minutes, at which time the volatiles were removed in vacuo and the resulting residue was triturated with 7 ml of ether. The ether solution was separated by filtration, and layered with pentane to afford yellow crystals of Tp^{tBu,Me}FeN(C₁₄H₁₀), yield 91 mg, (0.135 mmol, 82 %). ¹H-

NMR (400 MHz, C₆D₆) 52.7 (br, 3H), 37.2 (br, 9H), 21.8 (br, 4H), 18.2 (br, 4H), -20.0 (br, 27H) δ ; IR (KBr): 2958 (s), 2929 (s), 2864 (m), 2553 (m, B-H), 1541 (s), 1459 (s), 1424 (s), 1382 (m), 1363 (s), 1339 (sh), 1292 (w), 1242 (m), 1187 (s), 1140 (w), 1066 (s), 1028 (m), 986 (m), 920 (w), 842 (m), 785 (sh), 767 (s), 748 (m), 714 (w), 681 (w), 649 (s), 598 (m), 562 (m), 519 (w), 446 (w) cm⁻¹; m.p. 217 – 220 °C; $\mu_{\text{eff}} = 5.0(1) \mu_{\text{B}}$ (298 K); MS (LIFDI, THF): m/z 671.3757 [M⁺]. Calcd.: 671.3578 [M⁺];

Tp^{tBu,Me}CoN(C₁₄H₁₀) (23): 150 mg (0.247 mmol) of Tp^{tBu,Me}CoI was dissolved in 10ml of THF, to this solution was added 50 mg (0.247 mmol, 1 equiv.) of lithium-dbabh. The solution color changed from blue to reddish brown after 4 hours, at which time the volatiles were removed in vacuo and the resulting residue was triturated with 15 ml of ether, and the remaining residue was dissolved in THF. The THF solution was filtered, and layered with pentane to afford red crystals of Tp^{tBu,Me}CoN(C₁₄H₁₀), yield 80 mg (0.119 mmol, 48.2 %). ¹H-NMR (400 MHz, C₆D₆) 52.61 (br, 3H), 29.90 (br, 1H, B-H), 17.57 (br, 9H), 16.04 (br, 4H), 15.45 (br, 4H), -3.15 (br, 27H) δ ; IR (KBr): 3066 (m), 2962 (s), 2929 (m), 2865 (m), 2553 (m, B-H), 1544 (s), 1465 (s), 1456 (s), 1433 (s), 1420 (s), 1381 (m), 1359 (s), 1314 (m), 1254 (m), 1193 (s, br), 1140 (w), 1128 (w), 1065 (s), 1025 (m), 985 (w), 968 (w), 935 (s), 853 (w), 811 (w), 796 (s), 766 (s), 738 (m), 714 (m), 679 (w), 639 (s), 615 (m), 592 (w), 569 (w), 519 (w), 471 (m), 452 (w) cm⁻¹; m.p. 242 – 244 °C; $\mu_{\text{eff}} = 4.0(1) \mu_{\text{B}}$ (300 K, Evans method);¹² MS (LIFDI, THF): m/z 674.3529 [M]. Calcd.: 674.3560 [M]; Anal. Calcd for C₃₈H₅₀B₁N₇Co₁ : C, 67.66; H, 7.47; N, 14.53. Found C, 67.38; H, 7.38; N, 14.43.

Tp^{tBu,Me}CrN (24): 300 mg (0.596 mmol) of Tp^{tBu,Me}CrEt was added to a 12ml of Et₂O with stirring, 115 mg (0.596 mmol, 1 equiv.) of H-dbabh was added and the solution was left to stir for 14 hours. The volatiles were removed in vacuo, and the solid transferred to a sublimation apparatus under high vacuum, then heated to 110 °C for 6 hours. Upon complete sublimation of anthracene the remaining solid residue was dissolved in ether which was then layered with pentane and left at -35 °C to afford bright orange crystals of the desired Tp^{tBu,Me}CrN, yield 260 mg (0.532 mmol, 89.6 %). ¹H-NMR (400 MHz, C₆D₆) 50.32 (br, 9H), 3.02 (br, 3H), -.45 (br, 27H) δ; IR (KBr): 2962 (s), 2932 (m), 2907 (m), 2866 (m), 2564 (m, br, B-H) 1539 (s), 1463 (m), 1426 (m), 1381 (w), 1362 (s), 1342 (w), 1242 (w), 1181 (s), 1126 (w), 1065 (s), 1040 (s, Cr-Nitride), 1029 (w, sh), 1018 (w), 981 (w), 935 (w), 853 (w), 850 (w), 786 (m), 764 (s), 730 (w), 678 (w), 646 (s), 524 (w) cm⁻¹; m.p. 253 – 255 °C; μ_{eff} = 2.8(1) μ_B (294 K); MS (LIFDI, THF): m/z 489.2809 [M⁺]. Calcd.: 489.2849 [M⁺]; Anal. Calcd for C₂₄H₄₀B₁N₇Cr₁: C, 58.9; H, 8.24; N, 20.03. Found C, 58.33; H, 7.87; N, 19.05. Uv/Vis (λ_{max}(THF), ε): 280, 1316.7; 325, 730.0; 455, 243.7 (nm, cm⁻¹ M⁻¹).

Tp^{tBu,Me}Cr(I)(N) (25): 200 mg (0.409 mmol) of Tp^{tBu,Me}CrN was added to 15 ml of THF, and placed in a schlenk ampule with a magnetic stir bar. To that solution was added 4 equiv. of MeI, and the mixture was then stirred for 7 days at 45 °C. During this time the solution color darkens considerably to a brown/orange, signaling the completion of the reaction. The ampule was brought into a glove box and all volatile materials were removed in vacuo, producing an orange residue. The solid was triturated with pentane by stirring for several minutes until a bright yellow solid was all that remains undissolved, that solid is then collected by filtration and dissolved in

ether. The ether solution was layered with approximately twice the quantity of pentane as the ether that was used and the mixture left at -35 °C, resulting in the growth of crystals of $\text{Tp}^{\text{tBu,Me}}\text{Cr}(\text{N})(\text{I})$ as bright yellow blocks, yield 101 mg (40 %, 0.164 mmol). $^1\text{H-NMR}$ (400 MHz, C_6D_6) 1.98 (br, 27 H), 1.04 (br, 9H) δ ; IR (KBr): 2965 (s), 2930 (m), 2906 (m), 2867 (m), 2550 (m, B-H), 1541 (s), 1475 (s), 1461 (sh), 1430 (s), 1356 (s), 1328 (w), 1242 (m), 1197 (s), 1166 (m), 1147 (m), 1131 (m), 1049 (s, Cr-N ?), 1029 (w), 979 (w), 855 (w), 819 (m), 804 (w), 794 (m), 756 (s), 723 (w), 675 (w), 653 (w), 639 (m), 535 (vw), 524 (vw), 476 (vw) cm^{-1} ; m.p. 248 – 250 °C; $\mu_{\text{eff}} = 1.9(1) \mu_{\text{B}}$ (300 K, Evans method);¹² MS (LIFDI, THF): m/z 489.2944 [M^+]. Calcd.: 616.1894 [M^+], 489.2849 [$\text{M}^+ - \text{I}$]; Anal. Calcd. for $\text{C}_{24}\text{H}_{40}\text{B}_1\text{N}_7\text{Cr}_1\text{I}_1$: C, 46.77; H, 6.50; N, 15.66. Found C, 46.55; H, 6.54; N, 15.91.

$\text{Tp}^{\text{tBu,Me}}\text{CrNMe}$ (26): 200 mg (0.409 mmol) of $\text{Tp}^{\text{tBu,Me}}\text{CrN}$ was added to 15 ml of THF, and placed in a Schlenk ampule with a magnetic stir bar. To that solution was added an 4 equiv. of MeI, and the mixture was then stirred for 7 days at 45 °C. During this time the solution color darkened considerably to a brown/orange, signaling the completion of the reaction. The ampule was brought into a glove box and all volatile materials were removed in vacuo, producing an orange residue. The solid was triturated with pentane by stirring for several minutes until a bright yellow solid was all that remains undissolved, the solution was then separated by filtration and pyridine was added to remove $\text{Tp}^{\text{tBu,Me}}\text{CrI}$ which fell out of solution as a pale green solid. The pentane solution was filtered and then the solvent removed in vacuo, with the resulting purple residue then re-dissolved in a minimal amount of pentanes and the resulting solution placed in a -35 °C freezer for several hours. This resulted in the formation of

blocky purple crystals of $\text{Tp}^{\text{tBu,Me}}\text{CrNMe}$, yield 58 mg (0.115 mmol, 28 %). $^1\text{H-NMR}$ (400 MHz, C_6D_6) 55.0 (br, 9H), 50.5 (br, 1H), -0.54 (br, 3H), -1.88 (br, 27H) δ ; IR (KBr): 2959 (s), 2928 (s), 2906 (s), 2864 (s), 2817 (m), 2733 (w), 2539 (m, B-H), 1540 (s), 1473 (m), 1425 (s), 1381 (m), 1360 (s), 1340 (m), 1242 (w), 1186 (vs), 1129 (w), 1066 (s), 1027 (m), 985 (w), 935 (vw), 880 (w), 858 (w), 842 (w), 812 (w), 787 (s), 768 (s), 731 (w), 679 (w), 647 (s), 589 (w), 520 (w) cm^{-1} ; m.p. 245 – 247 $^\circ\text{C}$; $\mu_{\text{eff}} = 3.8(1) \mu_{\text{B}}$ (300 K, Evans method);¹² MS (LIFDI, THF): m/z 504.3075 [M^+]. Calcd.: 504.3084 [M^+]; Anal. Calcd. for $\text{C}_{25}\text{H}_{43}\text{B}_1\text{N}_7\text{Cr}_1$: C, 59.52; H, 8.59; N, 19.44. Found C, 59.54; H, 8.42; N, 17.51.

REFERENCES

1. a) Oyama, S. T., ed. (1996). *The Chemistry of Transition Metal Carbides and Nitrides*. Blackie Academic; b) Salamat, A.; Hector, A. L.; Kroll, P.; McMillan, P. F., *Coordin. Chem. Rev.*, **2013**, p. 2063 – 2072.
2. Rodriguez, M. M.; Bill, E.; Brennesel, W. W.; Holland, P. L., *Science*, **2011**, *334*, p. 780 – 783.
3. Lan, R.; Alkhazmi, K. A.; Amar, I. A.; Tao, S., *Appl. Catal., B*, **2014**, *152 – 153*, p. 212 – 217.
4. a) Laplaza, C. E.; Johnson, M. J. A.; Peters, J. C.; Odom, A. L.; Kim, E.; Cummins, C. C.; George, G. N.; Pickering, I. J., *J. Am. Chem. Soc.*, **1996**, *118* (36), p. 8623 – 8638; b) González-Moreiras, M.; Mena, M.; Pérez-Redondo, A.; Yélamos, C., *Chem. Eur. J*, **2017**, *23*, p. 3558 – 3561; c) Laplaza, C. E.; Johnson, A. R.; Cummins, C. C., *J. Am. Chem. Soc.*, **1996**, *118* (3), p. 709 – 710.
5. Cummins, D. C.; Yap, G. P. A.; Theopold, K. H., *Euro. J. Inor. Chem.*, **2016**, (15-16), p. 2349 – 2356.
6. a) Bucinsky, L.; Breza, M.; Lee, W.-T.; Hickey, A.K.; Dickie, D.A.; Nieto, I.; Harris, T.D.; Meyer, K.; Krzystek, J.; Ozarowski, A.; Nehr Korn, J.; Schnegg, A.; Holldack, K.; Herber, R.H.; Telser, J.; Smith, J.M., *Inorg. Chem.* **2017**, *56*, p. 4752 – 4769; b) Klopsch, I.; Finger, M.; Wgrtele, C.; Milde, B.; Werz, D. B.; Schneider, S.; *J. Am. Chem. Soc.*, **2014**, *136*, p. 6881 – 6883.
7. a) Choi, J.; Gillian, E. G., *J. Am. Chem. Soc.*, **2005**, *44*, p. 7385; b) Walstrom, A.; Pink, M.; Yang, X.; Tomaszewski, J.; Baik, M. H.; Caulton, K., *J. Am. Chem. Soc.*, **2005**, *127*, p. 5330; c) Vogel, C.; Heinemann, F. W.; Sutter, J.; Anthon, C.; Meyer, K., *Angew. Chem.*, **2008**, *47*, p. 2681; d) Scepaniak, J. J.; Vogel, C. S.; Khusniyarov, M. M.; Heinemann, F. W.; Meyer, K.; Smith J. M., *Science*, **2011**, *331*, p. 1049.

8. Nyquist, R. A.; Putzig, C. L.; Leugers, M. A., *The Handbook of Infrared and Raman Spectra of Inorganic Compounds and Organic Salts*, Academic Press, **1997**, p. 22.
9. a) Mendiola, D. J.; Cummins, C. C., *Angew. Chem. Int. Ed.*, **1998**, *37*, p. 945 – 946; b) Betley, T. A.; Peters, J. C., *J. Am. Chem. Soc.*, **2004**, *126*, p. 6252 – 6254; c) Adhikari, D.; Basuli, F.; Fan, H.; Huffman, J. C.; Pink, M. Mendiola, D. J., *Inorg. Chem.*, **2008**, *47*, p. 4439 – 4441; d) Bowman, A. C.; Bart, S. C.; Heinemann, F. W.; Meyer, K.; Chirik, P. J., *Inorg. Chem.*, **2009**, *48*, p. 5587 – 5589.
10. a) Jove, F. A.; Pariya, C.; Scobleto, M.; Yap, G. P. A.; Theopold, K. H., *Chem. Euro. J.*, **2011**, *17*, p. 1310; c) Egan, J. W. Jr.; Haggerty, B. S.; Rheingold, A. L.; Sendlinger, S. C.; Theopold, K. H., *J. Am. Chem. Soc.*, **1990**, *112*, p. 2445.
11. Yang, L.; Powell, D. R.; Houser, R. P., *Dalton Trans.*, **2007**, *0*, p. 955 – 964.
12. Evans, D. F., *J. Chem. Soc.*, **1959**, p. 2003 - 2005.
13. Lu, C. C.; Peters, J., *Inorg. Chem.*, **2006**, *45*, p. 8597.
14. Kersten, J. L.; Kucharczyk, R. R.; Yap, G. P. A.; Rheingold, A. L.; Theopold, K. H., *Chem. Eur. J.*, **1997**, *3*, p. 1668 – 1674.
15. a) Siddiqi, M. A.; Siddiqui, R. A.; Atakan, B., *J. Chem. Eng. Data*, **2009**, *54* (10), p. 2795 – 2802 ; b) Operations manual, Turbomolekular- Drag-Pumpe mit Antriebselektronik TC 100, TMH071, Pfeiffer Vacuum, available from www.pfeiffer-vacuum.net.
16. Akturk, E. S.; Yap, G. P. A.; Theopold, K. H.; *Chem. Commun.*, **2015**, *51*, p. 15402 – 15405.
17. Brown, G. (2012). *The Inaccessible Earth: An integrated view to its structure and composition*. Springer Science & Business Media. p. 88.
18. a) Muñoz, III, S.B.; Lee, W.-T.; Dickie, D.A.; Scepaniak, J.J.; Subedi, D.; Pink, M.; Johnson, M.D.; Smith, J.M., *Angew. Chem. Int. Ed.*, **2015**, *54*, p. 10600 – 10603; b) Lin, H.-J.; Siretanu, D.; Dickie, D.A.; Subedi, D.; Scepaniak, J.J.; Mitcov, D.; Clérac, R.; Smith, J.M., *J. Am. Chem. Soc.* **2014**, *136*, p. 13326 – 13332; c) Lee, W.-T.; Juarez, R.A.; Scepaniak, J.J.; Muñoz, S.B.; Dickie, D.A.; Wang, H.; Smith, J.M., *Inorg. Chem.*, **2014**, *53*, p. 8425 – 8430; d) Scepaniak, J.J.; Margarit,

- C.G.; Harvey, J.N.; Smith, J.M., *Inorg. Chem.* **2011**, *50*, 9508-9517.; e) Scepaniak, J.J.; Young, J.A; Bontchev, R.P.; Smith, J.M., *Angew. Chem. Int. Ed.* **2009**, *48*, p. 3158 – 3160.
19. Pajares, J. A.; Tascón, J. M. D., ed. (1995). *Coal Science*. Elsevier Science B. V.
 20. a) Klopsch, I.; Finger, M.; Wgrtele, C.; Milde, B.; Werz, D. B.; Schneider, S., *J. Am. Chem. Soc.*, **2014**, *136*, p. 6881–6883; b) Bucinsky, L.; Breza, M.; Lee, W. T.; Hickey, A. K.; Dickie, D. A.; Nieto, I.; Harris, T. D.; Meyer, K.; Krzystek, J.; Ozarowski, A.; Nehrkorn, J.; Schnegg, A.; Holldack, K.; Herber, R. H.; Telsler, J.; Smith, J. M., *Inorg. Chem.*, **2017**, *56*, p. 4752 – 4769.
 21. E. S. Akturk, Ph. D. Thesis, University of Delaware, (Newark, DE), USA, **2016**.
 22. a) Urben, P. G., ed. (2006). *Bretherick's Handbook of Reactive Chemical Hazards* (7th ed.). Elsevier.; b) Burns, M. E.; Smith, R. H., *Chem. Eng. News*, **1984**, *62* (2), p. 2.
 23. Addison, A. W.; Rao, N. T.; Reedijk, J.; van Rijn, J.; Verschoor, G. C., *J. Chem. Soc., Dalton Tans.*, **1984**, *0*, p. 1349 – 1356.
 24. Monillas, W. H.; Yap, G. P. A.; Theopold, K. H., *J. Chem. Cryst.*, **2009**, *39*, p. 73.
 25. Pangborn, A. B.; Giardello, M. A.; Grubbs, R. H.; Rosen, R. K.; Timmers, F. J., *Organometallic*, **1996**, *15*, p. 1518 – 1520.
 26. Carpino, L. A.; Padykula, R. E.; Barr, D. E.; Hall, F. H.; Krause, J. G.; Dufresne, R. F.; Thoman, C. J., *J. Org. Chem.*, **1988**, *53* (11), p. 2565 – 2572.
 27. Kersten, J. L.; Kucharczyk, R. R.; Yap, G. P. A.; Rheingold, A. L.; Theopold, K. H., *Chem. Eur. J.*, **1997**, *3*, p. 1968
 28. Bain, G. A.; Berry, J. F., *J. Chem. Educ.*, **2008**, *85*, No. 4, p. 532 – 536.
 29. Apex2, Bruker-AXS Inc, Madison, WI, p. 2007.
 30. Sheldrick, G.M., *Acta Cryst.*, **2008**, *A64*, p. 112.

Appendix A

SYNTHESIS AND CHARACTERIZATION OF MONO-VALENT IRON AND COBALT COMPLEXES OF FERROCENYL SUBSTITUTED TRIS(PRAZOLYL)BORATE LIGANDS

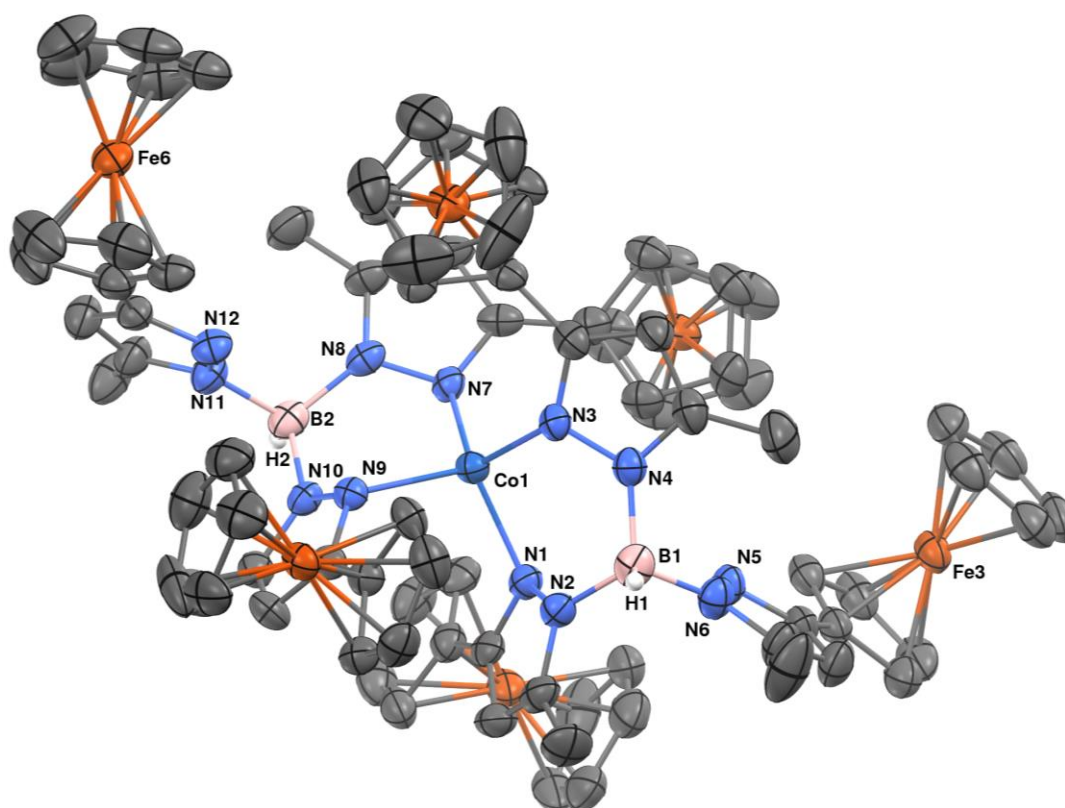


Figure A.1: Molecular structure of $[\text{Tp}^{\text{Fc,Me}}]_2\text{Co}$ (A1.2) represented as 50% probability thermal ellipsoids. Hydrogen atoms (with the exception of the hydrogens attached to the boron, H1 and H2), have been omitted for clarity.

Table A.1: Selected interatomic distances (Å) and angles (°) for [Tp^{Fe,Me}]₂Co**(A1.2).****Distances (Å)**

Co1-N3	1.989(4)	Co1-N7	1.991(4)
Co1-N1	2.002(4)	Co1-N9	2.006(4)
N7-N8	1.388(5)	N1-N2	1.387(5)
N8-B2	1.551(7)	N2-B1	1.556(7)
N9-N10	1.386(5)	N3-N4	1.388(5)
N10-B2	1.575(7)	N4-B1	1.563(7)
N11-N12	1.377(5)	N5-N6	1.383(5)
N12-C70	1.353(6)	N6-B1	1.519(7)
N11-B2	1.541(7)		

Angles (°)

N3-Co1-N7	111.89(16)	N3-Co1-N1	97.13(17)
N7-Co1-N1	126.04(16)	N3-Co1-N9	123.99(15)
N7-Co1-N9	96.26(16)	N1-Co1-N9	103.86(16)
N12-N11-B2	117.2(4)	N1-N2-B1	122.1(4)
N6-B1-N2	108.6(4)	N3-N4-B1	123.9(4)
N2-B1-N4	112.0(4)	N5-N6-B1	118.6(4)
N11-B2-N10	106.9(4)	N7-N8-B2	123.6(4)
N11-B2-N8	110.1(4)	N9-N10-B2	123.2(4)
N8-B2-N10	111.2(4)	N6-B1-N4	110.0(4)

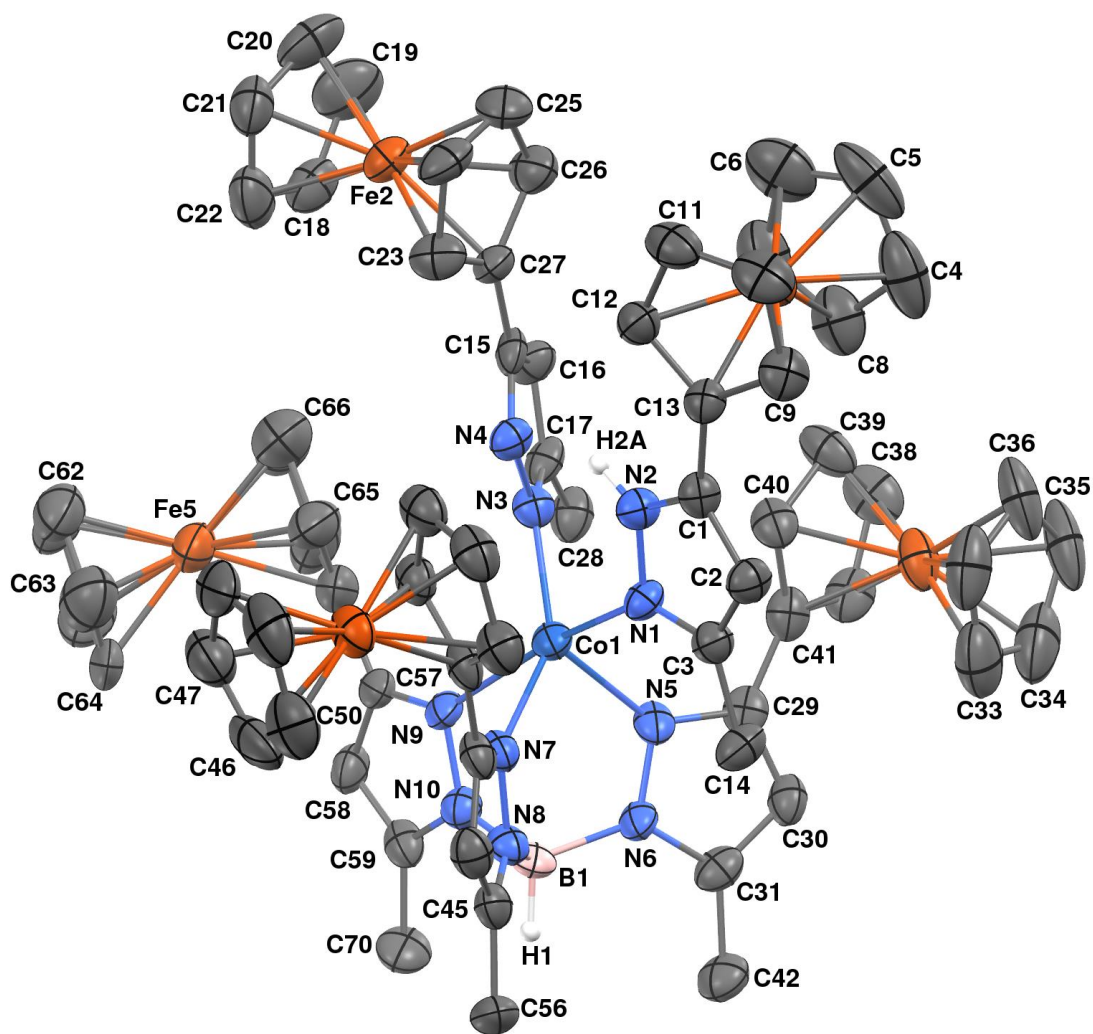


Figure A.2: Molecular structure of $\text{Tp}^{\text{Fc,Me}}\text{Co}(\text{PzH}^{\text{Fc,Me}})(\text{Pz}^{\text{Fc,Me}})$ (A1.3) represented as 50% thermal ellipsoids. Hydrogen atoms (with the exception of the hydrogens attached to the boron, H1, and to N2, H2A), and 1 molecule of THF and n-Pentane have been omitted for clarity.

Table A.2: Selected interatomic distances (Å) and angles (°) for **$\text{Tp}^{\text{Fc,Me}}\text{Co}(\text{PzH}^{\text{Fc,Me}})(\text{Pz}^{\text{Fc,Me}})$ (A1.3).**

Distances (Å)			
Co1-N3	1.976(5)	Co1-N7	2.053(5)
Co1-N5	2.072(5)	Co1-N1	2.135(5)
Co1-N9	2.304(5)	B1-N10	1.502(9)
B1-N8	1.545(9)	B1-N6	1.579(8)
N1-N2	1.361(6)	N1-C3	1.344(7)
N3-N4	1.377(6)	N2-C1	1.351(7)
N5-C29	1.348(7)	N3-C17	1.342(7)
N6-C31	1.358(7)	N4-C15	1.349(7)
N7-N8	1.368(6)	N5-N6	1.367(6)
N9-C57	1.323(8)	N8-C45	1.328(7)
N10-C59	1.372(7)	N9-N10	1.375(6)
C1-C13	1.482(8)	C3-C14	1.510(8)
C4-C8	1.411(10)	C4-C5	1.404(12)
C9-C13	1.432(8)	C5-C6	1.396(12)
C15-C16	1.401(8)	C6-C7	1.397(11)
C16-C17	1.377(8)	C7-C8	1.382(10)
C17-C28	1.501(8)	C11-C12	1.433(8)
C18-C19	1.416(10)	C12-C13	1.416(8)
C19-C20	1.376(10)	C15-C27	1.469(8)
C20-C21	1.398(10)	C18-C22	1.425(9)
C21-C22	1.421(10)	C23-C27	1.418(8)
C25-C26	1.422(9)	C29-C30	1.387(8)
C26-C27	1.431(8)	C30-C31	1.368(8)
C29-C41	1.475(8)	C31-C42	1.511(8)
C37-C38	1.417(9)	C33-C34	1.398(11)
C45-C56	1.516(8)	C34-C35	1.404(12)
C46-C50	1.423(11)	C35-C36	1.439(11)
C52-C53	1.414(9)	C37-C41	1.428(8)
C65-C66	1.384(11)	C40-C41	1.432(8)
C59-C70	1.513(8)	C46-C47	1.415(11)
C62-C63	1.377(11)	C57-C58	1.372(8)
C63-C64	1.395(12)	C58-C59	1.353(8)

Angles (°)

N3-Co1-N7	146.8(2)	N3-Co1-N5	115.6(2)
N7-Co1-N5	96.8(2)	N3-Co1-N1	94.9(2)
N7-Co1-N1	88.0(2)	N5-Co1-N1	96.54(19)
N3-Co1-N9	95.1(2)	N7-Co1-N9	80.6(2)
N5-Co1-N9	84.10(18)	N1-Co1-N9	168.6(2)
N10-B1-N6	109.3(6)	N10-B1-N8	110.8(5)
N10-B1-H1	109.1	N8-B1-N6	109.5(5)
N6-B1-H1	109.1	N8-B1-H1	109.1
C3-N1-Co1	137.0(4)	C3-N1-N2	103.4(5)
C1-N2-N1	112.5(5)	N2-N1-Co1	119.7(4)
N1-N2-H2A	123.7	C1-N2-H2A	123.7
C17-N3-Co1	135.9(4)	C17-N3-N4	108.3(5)
C15-N4-N3	106.9(5)	N4-N3-Co1	115.5(4)
C29-N5-Co1	136.9(4)	C29-N5-N6	105.5(5)
C31-N6-N5	110.9(5)	N6-N5-Co1	116.1(4)
N5-N6-B1	118.8(5)	C31-N6-B1	130.0(5)
C45-N8-N7	110.0(5)	N8-N7-Co1	118.7(4)
N7-N8-B1	117.5(5)	C45-N8-B1	132.4(6)
C57-N9-Co1	142.5(5)	C57-N9-N10	105.4(5)
C59-N10-N9	109.4(5)	N10-N9-Co1	111.4(4)
N9-N10-B1	121.2(5)	C59-N10-B1	129.4(6)
N2-C1-C13	122.0(6)	C12-C13-C1	126.7(6)
N1-C3-C14	120.5(6)	N4-C15-C27	119.2(6)
C8-C4-C5	106.0(9)	C17-C16-C15	104.1(6)
C6-C5-C4	109.3(9)	N3-C17-C28	121.7(6)
C7-C6-C5	107.2(10)	C22-C18-C19	108.5(7)
C8-C7-C6	108.4(9)	C20-C19-C18	107.7(8)
C7-C8-C4	109.0(9)	C19-C20-C21	109.5(8)
C13-C12-C11	108.1(6)	C20-C21-C22	108.4(7)
C12-C13-C9	109.2(6)	C18-C22-C21	105.9(7)
C9-C13-C1	124.0(6)	C25-C26-C27	108.6(6)
N4-C15-C16	110.2(5)	C23-C27-C26	106.3(6)
C16-C15-C27	130.6(6)	C26-C27-C15	126.3(6)
N3-C17-C16	110.5(6)	N5-C29-C30	110.1(6)
C16-C17-C28	127.8(6)	C30-C29-C41	126.9(6)
N6-C31-C30	106.9(6)	C30-C31-C42	129.3(6)
C23-C27-C15	127.3(6)	C37-C41-C29	122.8(6)
N5-C29-C41	122.7(6)	N8-C45-C56	122.9(6)

C31-C30-C29	106.7(6)	C47-C46-C50	110.7(8)
N6-C31-C42	123.7(6)	N9-C57-C58	111.5(6)
C35-C34-C33	108.9(9)	C58-C59-N10	107.2(6)
C34-C35-C36	106.9(8)	N10-C59-C70	122.1(6)
C38-C37-C41	108.7(6)	C40-C41-C29	130.9(6)
C37-C41-C40	106.2(6)		

Table A.3: Crystal data and structure refinement for $\text{Tp}^{\text{Fc,Me}}\text{FeCl}$ (1).

Identification code	kla0578	
Chemical formula	$\text{C}_{42}\text{H}_{40}\text{BClFe}_4\text{N}_6$	
Formula weight	898.46 g/mol	
Temperature	225(2) K	
Wavelength	0.71073 Å	
Crystal size	0.066 x 0.165 x 0.198 mm	
Crystal system, Space group	triclinic, $P-1$	
Unit cell dimensions	$a = 12.9765(15)$ Å	$\alpha = 106.834(2)^\circ$
	$b = 13.3042(16)$ Å	$\beta = 109.768(2)^\circ$
	$c = 13.4255(16)$ Å	$\gamma = 108.008(2)^\circ$
Volume	$1862.4(4)$ Å ³	
Z, Density (calculated)	2, 1.602 g/cm ³	
Absorption coefficient	1.640 mm ⁻¹	
F(000)	920	
Theta range for data collection	1.79 to 27.59°	
Index ranges	$-16 \leq h \leq 16$, $-17 \leq k \leq 17$, $-17 \leq l \leq 17$	
Reflections collected / unique	28513 / 8522 [R(int) = 0.0976]	
Completeness to theta = 25.000	98.70%	
Max. and min. transmission	0.7456 and 0.6628	
Absorption corrections	Semi-empirical from equivalents	
Structure solution technique	direct methods	
Structure solution program	SHELXS-97 (Sheldrick 2008)	
Refinement method	Full-matrix least-squares on F^2 SHELXL-2014/7 (Sheldrick,	
Refinement program	2014)	
Function minimized	$\sum w(F_o^2 - F_c^2)^2$	
Data / restraints / parameters	8522 / 0 / 490	
Goodness-of-fit on F^2	0.862	
Final R indices	4442 data; $l > 2\sigma(l)$	$R1 = 0.0582$, $wR2 = 0.1320$
	all data	$R1 = 0.1423$, $wR2 = 0.1822$
Weighting scheme	$w = 1/[\sigma^2(F_o^2) + (0.1000P)^2]$, where $P = (F_o^2 + 2F_c^2)/3$	
Largest diff. peak and hole	0.495 and -0.553 eÅ ⁻³	
R.M.S. deviation from mean	0.113 eÅ ⁻³	

Table A.4: Crystal data and structure refinement for $\text{Tp}^{\text{Fc,Me}}\text{CoBr}$ (4).

Identification code	kla0608	
Chemical formula	$\text{C}_{42}\text{H}_{40}\text{BBrCoFe}_3\text{N}_6$	
Formula weight	946.00 g/mol	
Temperature	200(2) K	
Wavelength	0.71073 Å	
Crystal size	0.174 x 0.193 x 0.327 mm	
Crystal system, Space group	triclinic, $P-1$	
Unit cell dimensions	$a = 13.0130(7)$ Å	$\alpha = 106.407(2)^\circ$
	$b = 13.3329(7)$ Å	$\beta = 110.042(2)^\circ$
	$c = 13.4301(7)$ Å	$\gamma = 107.954(2)^\circ$
Volume	1875.82(18) Å ³	
Z, Density (calculated)	2, 1.675 g/cm ³	
Absorption coefficient	2.677 mm ⁻¹	
F(000)	958	
Theta range for data collection	1.78 to 27.70°	
Index ranges	-16 ≤ h ≤ 16, -17 ≤ k ≤ 17, -17 ≤ l ≤ 17	
Reflections collected / unique completeness to theta = 25.000	55545 / 8684 [R(int) = 0.0878] 98.80%	
absorption correction	Semi-empirical from equivalents	
Max. and min. transmission	0.7456 and 0.5893	
Structure solution technique	direct methods	
Structure solution program	SHELXS-97 (Sheldrick 2008)	
Refinement method	Full-matrix least-squares on F ²	
Refinement program	SHELXL-2014/7 (Sheldrick, 2014)	
Function minimized	$\sum w(F_o^2 - F_c^2)^2$	
Data / restraints / parameters	8684 / 0 / 493	
Goodness-of-fit on F²	1.091	
$\Delta/\sigma_{\text{max}}$	0.001	
Final R indices	5883 data; $l > 2\sigma(l)$	R1 = 0.0447, wR2 = 0.0943
	all data	R1 = 0.0812, wR2 = 0.1081
Weighting scheme	$w = 1/[\sigma^2(F_o^2) + (0.0421P)^2]$, where $P = (F_o^2 + 2F_c^2)/3$	
Largest diff. peak and hole	0.628 and -0.404 eÅ ⁻³	
R.M.S. deviation from mean	0.107 eÅ ⁻³	

Table A.5: Crystal data and structure refinement for $\text{Tp}^{\text{Fc,Me}}\text{FeBn}$ (5).

Identification code	kla0640	
Chemical formula	$\text{C}_{56}\text{H}_{55}\text{BFe}_4\text{N}_6$	
Formula weight	1046.27	
Temperature	200(2) K	
Wavelength	0.71073 Å	
Crystal size	0.414 x 0.640 x 0.674 mm	
Crystal habit	orange block	
Crystal system, Space group	monoclinic, $P2_1/c$	
Unit cell dimensions	$a = 12.025(2)$ Å	$\alpha = 90^\circ$
	$b = 18.768(3)$ Å	$\beta = 99.925(4)^\circ$
	$c = 21.783(4)$ Å	$\gamma = 90^\circ$
Volume	$4842.5(15)$ Å ³	
Z, Density (calculated)	4, 1.435 g/cm ³	
Absorption coefficient	1.219 mm ⁻¹	
F(000)	2168	
Theta range for data collection	1.44 to 27.63°	
Index ranges	$-15 \leq h \leq 15$, $-24 \leq k \leq 24$, $-28 \leq l \leq 28$	
Reflections collected / unique	74025 / 11199 [R(int) = 0.0399]	
Completeness to theta = 25.000	99.30%	
Absorption correction	multi-scan	
Max. and min. transmission	0.7456 and 0.6105	
Structure solution technique	direct methods	
Structure solution program	SHELXS-97 (Sheldrick 2008)	
Refinement method	Full-matrix least-squares on F^2	
Refinement program	SHELXL-2014 (Sheldrick, 2014)	
Function minimized	$\sum w(F_o^2 - F_c^2)^2$	
Data / restraints / parameters	11199 / 147 / 599	
Goodness-of-fit on F^2	1.014	
$\Delta/\sigma_{\text{max}}$	0.001	
Final R indices	8947 data; $l > 2\sigma(l)$	R1 = 0.0395, wR2 = 0.1030
	all data	R1 = 0.0535, wR2 = 0.1126
Weighting scheme	$w = 1/[\sigma^2(F_o^2) + (0.0586P)^2 + 3.7198P]$, where $P = (F_o^2 + 2F_c^2)/3$	
Largest diff. peak and hole	0.898 and -0.631 eÅ ⁻³	
R.M.S. deviation from mean	0.066 eÅ ⁻³	

Table A.6: Crystal data and structure refinement for $\text{Tp}^{\text{Fc,Me}}\text{FeEt}$ (6).

Identification code	kla0895	
Chemical formula	$\text{C}_{44}\text{H}_{45}\text{BFe}_4\text{N}_6$	
Formula weight	892.07 g/mol	
Temperature	200(2) K	
Wavelength	0.71073 Å	
Crystal size	0.200 x 0.238 x 0.400 mm	
Crystal habit	orange block	
Crystal system, Space group	triclinic, $P-1$	
Unit cell dimensions	a = 11.3371(6) Å	$\alpha = 109.8304(10)^\circ$
	b = 13.5104(7) Å	$\beta = 108.4746(10)^\circ$
	c = 14.2446(8) Å	$\gamma = 91.1377(10)^\circ$
Volume	1926.74(18) Å ³	
Z, Density (calculated)	2, 1.538 g/cm ³	
Absorption coefficient	1.517 mm ⁻¹	
F(000)	920	
Theta range for data collection	1.62 to 27.68°	
Index ranges	-14 ≤ h ≤ 14, -17 ≤ k ≤ 17, -18 ≤ l ≤ 18	
Reflections collected / unique	41576, 8990 [R(int) = 0.0345]	
Completeness to theta = 25.000	99.60%	
Absorption correction	multi-scan	
Max. and min. transmission	0.7456 and 0.6597	
Structure solution technique	direct methods	
Structure solution program	SHELXS-97 (Sheldrick 2008)	
Refinement method	Full-matrix least-squares on F ²	
Refinement program	SHELXL-2014/7 (Sheldrick, 2014)	
Function minimized	$\Sigma w(F_o^2 - F_c^2)^2$	
Data / restraints / parameters	8990 / 0 / 502	
Goodness-of-fit on F²	0.975	
$\Delta/\sigma_{\text{max}}$	0.001	
Final R indices	7305 data; $l > 2\sigma(l)$	R1 = 0.0366, wR2 = 0.0883
	all data	R1 = 0.0479, wR2 = 0.0945
Weighting scheme	$w = 1/[\sigma^2(F_o^2) + (0.0490P)^2 + 1.1044P]$, where $P = (F_o^2 + 2F_c^2)/3$	
Largest diff. peak and hole	0.625 and -0.251 eÅ ⁻³	
R.M.S. deviation from mean	0.069 eÅ ⁻³	

Table A.7: Crystal data and structure refinement for $\text{Tp}^{\text{Fc,Me}}\text{Fe}(\text{CO})$ (7).

Identification code	kla0644	
Chemical formula	$\text{C}_{43}\text{H}_{40}\text{BFe}_4\text{N}_6\text{O}$	
Formula weight	891.02 g/mol	
Temperature	200(2) K	
Wavelength	0.71073 Å	
Crystal size	0.100 x 0.231 x 0.233 mm	
Crystal system, Space group	triclinic, <i>P</i> -1	
Unit cell dimensions	a = 13.1524(9) Å	$\alpha = 107.2910(10)^\circ$
	b = 13.2859(9) Å	$\beta = 110.4320(10)^\circ$
	c = 13.3740(9) Å	$\gamma = 107.4480(10)^\circ$
Volume	1866.2(2) Å ³	
Z, Density (calculated)	2, 1.586 g/cm ³	
Absorption coefficient	1.569 mm ⁻¹	
F(000)	914	
Theta range for data collection	1.80 to 27.57°	
Index ranges	-17 ≤ h ≤ 17, -17 ≤ k ≤ 17, -17 ≤ l ≤ 17	
Reflections collected / unique	30637 / 8606 [R(int) = 0.0399]	
Completeness to theta = 25.000	99.70%	
Absorption correction	multi-scan	
Max. and min. transmission	0.7456 and 0.6619	
Structure solution technique	direct methods	
Structure solution program	SHELXS-97 (Sheldrick 2008)	
Refinement method	Full-matrix least-squares on F ²	
Refinement program	SHELXL-2014/7 (Sheldrick, 2014)	
Function minimized	$\sum w(F_o^2 - F_c^2)^2$	
Data / restraints / parameters	8606 / 0 / 502	
Goodness-of-fit on F²	1.031	
$\Delta/\sigma_{\text{max}}$	0.001	
Final R indices	6832 data; I > 2σ(I)	R1 = 0.0341, wR2 = 0.0742
	all data	R1 = 0.0488, wR2 = 0.0810
Weighting scheme	w = 1/[σ ² (F _o ²) + (0.0330P) ² + 0.6546P], where P = (F _o ² + 2F _c ²)/3	
Largest diff. peak and hole	0.355 and -0.353 eÅ ⁻³	
R.M.S. deviation from mean	0.072 eÅ ⁻³	

Table A.8: Crystal data and structure refinement for $\text{Tp}^{\text{Fc,Me}}\text{Fe}(\text{PzH}^{\text{Fc,Me}})(\text{Pz}^{\text{Fc,Me}})$

(8).

Identification code	kla0442	
Chemical formula	$\text{C}_{74}\text{H}_{77}\text{BFe}_6\text{N}_{10}\text{O}$	
Formula weight	1468.36	
Temperature	200(2) K	
Wavelength	0.71073 Å	
Crystal size	0.155 x 0.176 x 0.286 mm	
Crystal system, Space group	triclinic, <i>P</i> -1	
Unit cell dimensions	$a = 13.058(4)$ Å	$\alpha = 88.533(5)^\circ$
	$b = 15.377(5)$ Å	$\beta = 73.911(5)^\circ$
	$c = 19.440(6)$ Å	$\gamma = 68.416(5)^\circ$
Volume	$3474.8(19)$ Å ³	
Z, Density (calculated)	2, 1.403 g/cm ³	
Absorption coefficient	1.271 mm ⁻¹	
F(000)	1520	
Theta range for data collection	1.43 to 23.49°	
Index ranges	$-14 \leq h \leq 14, -17 \leq k \leq 17, -21 \leq l \leq 21$	
Reflections collected / unique	32311 / 10177 [R(int) = 0.0371]	
Completeness to theta = 25.000	99.10%	
Absorption correction	multi-scan	
Max. and min. transmission	0.7449 and 0.6501	
Structure solution technique	direct methods	
Structure solution program	SHELXS-97 (Sheldrick 2008)	
Refinement method	Full-matrix least-squares on F ²	
Refinement program	SHELXL-2014/7 (Sheldrick, 2014)	
Function minimized	$\sum w(F_o^2 - F_c^2)^2$	
Data / restraints / parameters	10177 / 0 / 844	
Goodness-of-fit on F²	1.024	
$\Delta/\sigma_{\text{max}}$	0.004	
Final R indices	8191 data; $l > 2\sigma(l)$	R1 = 0.0343, wR2 = 0.0797
	all data	R1 = 0.0465, wR2 = 0.0860
Weighting scheme	$w = 1/[\sigma^2(F_o^2) + (0.0381P)^2 + 1.5470P]$, where $P = (F_o^2 + 2F_c^2)/3$	
Largest diff. peak and hole	0.459 and -0.411 eÅ ⁻³	
R.M.S. deviation from mean	0.053 eÅ ⁻³	

Table A.9: Crystal data and structure refinement for [Tp^{Fc,Me}Fe]₂(μ-η¹:η¹-N₂) (9).

Identification code	klA0660	
Chemical formula	C _{95.50} H ₁₀₆ B ₂ Fe ₈ N ₁₄ O	
Formula weight	1934.36	
Temperature	200(2) K	
Wavelength	0.71073 Å	
Crystal size	0.318 x 0.513 x 0.538 mm	
Crystal system, Space group	orthorhombic, <i>Pccn</i>	
Unit cell dimensions	a = 27.0666(9) Å	α = 90°
	b = 41.4766(13) Å	β = 90°
	c = 16.0276(5) Å	γ = 90°
Volume	17993.1(10) Å ³	
Z, Density (calculated)	8, 1.428 g/cm ³	
Absorption coefficient	1.307 mm ⁻¹	
F(000)	8024	
Theta range for data collection	1.50 to 27.50°	
Index ranges	-35 ≤ h ≤ 35, -42 ≤ k ≤ 53, -20 ≤ l ≤ 19	
Reflections collected / unique	134194 / 20643 [R(int) = 0.0796]	
Completeness to theta = 25.000	99.80%	
Absorption correction	multi-scan	
Max. and min. transmission	0.7456 and 0.5928	
Structure solution technique	direct methods	
Structure solution program	SHELXS-97 (Sheldrick 2008)	
Refinement method	Full-matrix least-squares on F ²	
Refinement program	SHELXL-2014/6 (Sheldrick, 2014)	
Function minimized	Σ w(F _o ² - F _c ²) ²	
Data / restraints / parameters	20643 / 195 / 1081	
Goodness-of-fit on F²	1.073	
Δ/σ_{max}	0.002	
Final R indices	13326 data; I > 2σ(I)	R1 = 0.0738, wR2 = 0.1690
	all data	R1 = 0.1199, wR2 = 0.1901
Weighting scheme	w = 1/[σ ² (F _o ²) + (0.0672P) ² + 48.0149P], where P = (F _o ² + 2F _c ²)/3	
Largest diff. peak and hole	1.327 and -0.806 eÅ ⁻³	
R.M.S. deviation from mean	0.096 eÅ ⁻³	

Table A.10: Crystal data and structure refinement for [Tp^{Fc,Me}Co]₂(μ-η¹:η¹-N₂)

(10).

Identification code	klA0646	
Chemical formula	C ₁₂₄ H ₁₆₀ B ₂ Co ₂ Fe ₆ N ₁₄ O ₁₀	
Formula weight	2481.23	
Temperature	200(2) K	
Wavelength	0.71073 Å	
Crystal size	0.110 x 0.185 x 0.238 mm	
Crystal system, Space group	triclinic, <i>P</i> -1	
Unit cell dimensions	a = 14.2293(6) Å	α = 102.552(2)°
	b = 20.3076(8) Å	β = 90.407(2)°
	c = 21.2943(9) Å	γ = 96.181(2)°
Volume	5968.3(4) Å ³	
Z, Density (calculated)	2, 1.381 g/cm ³	
Absorption coefficient	1.042 mm ⁻¹	
F(000)	2604	
Theta range for data collection	0.98 to 27.56°	
Index ranges	-18 ≤ h ≤ 18, -26 ≤ k ≤ 26, -27 ≤ l ≤ 27	
Reflections collected / unique	176157 / 27465 [R(int) = 0.1076]	
Completeness to theta = 25.000	99.50%	
Absorption correction	multi-scan	
Max. and min. transmission	0.7456 and 0.6591	
Structure solution technique	direct methods	
Structure solution program	SHELXS-97 (Sheldrick 2008)	
Refinement method	Full-matrix least-squares on F ²	
Refinement program	SHELXL-2014 (Sheldrick, 2014)	
Function minimized	Σ w(F _o ² - F _c ²) ²	
Data / restraints / parameters	27465 / 120 / 979	
Goodness-of-fit on F²	1.011	
Δ/σ_{max}	0.027	
Final R indices	15087 data; I > 2σ(I)	R1 = 0.0488, wR2 = 0.1106
	all data	R1 = 0.1072, wR2 = 0.1284
Weighting scheme	w = 1/[σ ² (F _o ²) + (0.0554P) ²], where P = (F _o ² + 2F _c ²)/3	
Largest diff. peak and hole	0.422 and -0.378 eÅ ⁻³	
R.M.S. deviation from mean	0.070 eÅ ⁻³	

Table A.11: Crystal data and structure refinement for [Tp^{Fc,Me}Co]₂(μ-η¹:η¹-N₂)

(10).

Identification code	kIa0654	
Chemical formula	C ₈₉ H ₉₂ B ₂ Co ₂ Fe ₆ N ₁₄	
Formula weight	1832.34	
Temperature	200(2) K	
Wavelength	0.71073 Å	
Crystal size	0.490 x 0.530 x 0.550 mm	
Crystal system, Space group	triclinic, <i>P</i> -1	
Unit cell dimensions	a = 15.0360(10) Å	α = 75.1146(16)°
	b = 16.0654(11) Å	β = 70.3400(16)°
	c = 19.8808(14) Å	γ = 65.4306(15)°
Volume	4074.4(5) Å ³	
Z, Density (calculated)	2, 1.494 g/cm ³	
Absorption coefficient	1.489 mm ⁻¹	
F(000)	1888	
Theta range for data collection	1.64 to 27.52°	
Index ranges	-19 ≤ h ≤ 19, -20 ≤ k ≤ 20, -25 ≤ l ≤ 25	
Reflections collected / unique	92133 / 18644 [R(int) = 0.0555]	
Completeness to theta = 25.000	99.40%	
Absorption correction	multi-scan	
Max. and min. transmission	0.7456 and 0.5775	
Structure solution technique	direct methods	
Structure solution program	SHELXS-97 (Sheldrick 2008)	
Refinement method	Full-matrix least-squares on F ²	
Refinement program	SHELXL-2014/6 (Sheldrick, 2014)	
Function minimized	Σ w(F _o ² - F _c ²) ²	
Data / restraints / parameters	18644 / 31 / 1019	
Goodness-of-fit on F²	1.026	
Δ/σ_{max}	0.001	
Final R indices	13189 data; I > 2σ(I)	R1 = 0.0452, wR2 = 0.1093
	all data	R1 = 0.0755, wR2 = 0.1270
Weighting scheme	w = 1/[σ ² (F _o ²) + (0.0558P) ² + 5.1677P], where P = (F _o ² + 2F _c ²)/3	
Largest diff. peak and hole	1.181 and -0.624 eÅ ⁻³	
R.M.S. deviation from mean	0.092 eÅ ⁻³	

Table A.12: Crystal data and structure refinement for $\text{Bp}^{\text{Fc,Me}}(\text{Me-pz-CpFe}(\text{C}_5\text{H}_4))\text{Co}$ (11).

Identification code	kla0653	
Chemical formula	$\text{C}_{44.50}\text{H}_{45}\text{BCoFe}_3\text{N}_6$	
Formula weight	901.15	
Temperature	200(2) K	
Wavelength	0.71073 Å	
Crystal size	0.070 x 0.184 x 0.423 mm	
Crystal habit	green needle	
Crystal system, Space group	monoclinic, $P2_1/n$	
Unit cell dimensions	$a = 10.7658(6)$ Å	$\alpha = 90^\circ$
	$b = 16.0450(8)$ Å	$\beta = 98.9912(13)^\circ$
	$c = 22.9248(12)$ Å	$\gamma = 90^\circ$
Volume	$3911.3(4)$ Å ³	
Z, Density (calculated)	4, 1.530 g/cm ³	
Absorption coefficient	1.549 mm ⁻¹	
F(000)	1856	
Theta range for data collection	1.55 to 27.58°	
Index ranges	-14 ≤ h ≤ 13, -20 ≤ k ≤ 20, -26 ≤ l ≤ 29	
Reflections collected / unique	59098 / 9008 [R(int) = 0.0783]	
Completeness to theta = 25.000	99.60%	
Absorption correction	multi-scan	
Max. and min. transmission	0.7456 and 0.6552	
Structure solution technique	direct methods	
Structure solution program	SHELXS-97 (Sheldrick 2008)	
Refinement method	Full-matrix least-squares on F ²	
Refinement program	SHELXL-2014/6 (Sheldrick, 2014)	
Function minimized	$\Sigma w(F_o^2 - F_c^2)^2$	
Data / restraints / parameters	9008 / 105 / 507	
Goodness-of-fit on F²	1.022	
$\Delta/\sigma_{\text{max}}$	0.017	
Final R indices	5844 data; $l > 2\sigma(l)$	R1 = 0.0478, wR2 = 0.1115
	all data	R1 = 0.0891, wR2 = 0.1320
Weighting scheme	$w = 1/[\sigma^2(F_o^2) + (0.0588P)^2 + 2.4902P]$, where $P = (F_o^2 + 2F_c^2)/3$	
Largest diff. peak and hole	0.679 and -0.609 eÅ ⁻³	
R.M.S. deviation from mean	0.084 eÅ ⁻³	

Table A.13: Crystal data and structure refinement for BpFc,Me(Me-pz-CpFe(C5H4))Co(CO) (12).

Identification code	kla0871	
Chemical formula	C ₄₅ H ₄₄ BCoFe ₃ N ₆ O _{1.50}	
Formula weight	930.15 g/mol	
Temperature	200(2) K	
Wavelength	0.71073 Å	
Crystal size	0.200 x 0.287 x 0.820 mm	
Crystal system, Space group	monoclinic, <i>P2₁/n</i>	
Unit cell dimensions	a = 12.7668(9) Å	α = 90°
	b = 10.5840(7) Å	β = 91.4250(10)°
	c = 29.656(2) Å	γ = 90°
Volume	4006.0(5) Å ³	
Z, Density (calculated)	4, 1.542 g/cm ³	
Absorption coefficient	1.518 mm ⁻¹	
F(000)	1912	
Theta range for data collection	1.72 to 27.73°	
Index ranges	-16 ≤ h ≤ 16, -13 ≤ k ≤ 13, -38 ≤ l ≤ 38	
Reflections collected / unique	58785 / 9360 [R(int) = 0.0410]	
Completeness to theta = 25.000	99.30%	
Absorption correction	multi-scan	
Max. and min. transmission	0.7456 and 0.5388	
Structure solution technique	direct methods	
Structure solution program	SHELXS-97 (Sheldrick 2008)	
Refinement method	Full-matrix least-squares on F ²	
Refinement program	SHELXL-2014/7 (Sheldrick, 2014)	
Function minimized	Σ w(F _o ² - F _c ²) ²	
Data / restraints / parameters	9360 / 60 / 545	
Goodness-of-fit on F²	1.039	
Δ/σ_{max}	0.001	
Final R indices	7627 data; I > 2σ(I)	R1 = 0.0391, wR2 = 0.0960
	all data	R1 = 0.0510, wR2 = 0.1025
Weighting scheme	w = 1 / [σ ² (F _o ²) + (0.0546P) ² + 1.8121P], where P = (F _o ² + 2F _c ²) / 3	
Largest diff. peak and hole	0.874 and -0.316 eÅ ⁻³	
R.M.S. deviation from mean	0.071 eÅ ⁻³	

Table A.14: Crystal data and structure refinement for $\text{Tp}^{\text{Fc,Me}*}\text{MgMe}$ (A1.1).

Identification code	kIa0452	
Chemical formula	$\text{C}_{43}\text{H}_{43}\text{BFe}_3\text{MgN}_6$	
Formula weight	846.5	
Temperature	200(2) K	
Wavelength	0.71073 Å	
Crystal size	0.102 x 0.158 x 0.231 mm	
Crystal system, Space group	triclinic, <i>P</i> -1	
Unit cell dimensions	a = 11.013(12) Å	$\alpha = 65.156(12)^\circ$
	b = 14.009(15) Å	$\beta = 70.269(13)^\circ$
	c = 14.893(16) Å	$\gamma = 77.388(14)^\circ$
Volume	1955.(4) Å ³	
Z, Density (calculated)	2, 1.438 g/cm ³	
Absorption coefficient	1.154 mm ⁻¹	
F(000)	876	
Theta range for data collection	1.57 to 27.41°	
Index ranges	-14 ≤ h ≤ 14, -18 ≤ k ≤ 18, -19 ≤ l ≤ 19	
Reflections collected / unique	18780 / 8802 [R(int) = 0.1149]	
Completeness to theta = 25.000	98.80%	
Absorption correction	multi-scan	
Max. and min. transmission	0.7455 and 0.5711	
Structure solution technique	direct methods	
Structure solution program	SHELXS-97 (Sheldrick 2008)	
Refinement method	Full-matrix least-squares on F ²	
Refinement program	SHELXL-2014/6 (Sheldrick, 2014)	
Function minimized	$\sum w(F_o^2 - F_c^2)^2$	
Data / restraints / parameters	8802 / 0 / 487	
Goodness-of-fit on F²	0.963	
$\Delta/\sigma_{\text{max}}$	0.001	
Final R indices	3515 data; $ I > 2\sigma(I)$	
	all data	R1 = 0.0773, wR2 = 0.1520
	$w=1/[\sigma^2(F_o^2)+(0.0781P)^2]$, where $P=(F_o^2+2F_c^2)/3$	R1 = 0.2115, wR2 = 0.2084
Weighting scheme		
Largest diff. peak and hole	0.795 and -0.492 eÅ ⁻³	
R.M.S. deviation from mean	0.098 eÅ ⁻³	

Table A.15: Crystal data and structure refinement for [Tp^{Fc,Me}]₂Co (A1.2).

Identification code	kla0623	
Chemical formula	C ₄₆ H ₄₈ BCo _{0.50} Fe ₃ N ₆ O	
Formula weight	908.73 g/mol	
Temperature	200(2) K	
Wavelength	0.71073 Å	
Crystal size	0.082 x 0.261 x 0.270 mm	
Crystal system, Space group	Monoclinic, <i>P</i> 2 ₁ / <i>c</i>	
Unit cell dimensions	a = 15.2545(15) Å	
	b = 23.522(2) Å	α = 90°
	c = 23.434(2) Å	β = 101.470(2)°
		γ = 90°
Volume	8240.6(14) Å ³	
Z, Density (calculated)	8, 1.465 g/cm ³	
Absorption coefficient	1.281 mm ⁻¹	
F(000)	3764	
Theta range for data collection	1.61 to 27.54°	
Index ranges	-19 ≤ h ≤ 19, -30 ≤ k ≤ 30, -30 ≤ l ≤ 30	
Reflections collected / unique	124401 / 18919 [R(int) = 0.1355]	
Completeness to theta = 25.000	99.50%	
Absorption correction	multi-scan	
Max. and min. transmission	0.7456 and 0.6500	
Structure solution technique	direct methods	
Structure solution program	SHELXS-97 (Sheldrick 2008)	
Refinement method	Full-matrix least-squares on F ²	
Refinement program	SHELXL-2014/7 (Sheldrick, 2014)	
Function minimized	Σ w(F _o ² - F _c ²) ²	
Data / restraints / parameters	18919 / 72 / 1018	
Goodness-of-fit on F²	1.033	
Δ/σ_{max}	0.001	
Final R indices	9492 data; I > 2σ(I)	R1 = 0.0624, wR2 = 0.1429
	all data	R1 = 0.1480, wR2 = 0.1804
Weighting scheme	w = 1/[σ ² (F _o ²) + (0.0735P) ² + 2.7690P], where P = (F _o ² + 2F _c ²)/3	
Largest diff. peak and hole	1.131 and -0.572 eÅ ⁻³	
R.M.S. deviation from mean	0.095 eÅ ⁻³	

Table A.16: Crystal data and structure refinement for



Identification code	k1a0701	
Chemical formula	$\text{C}_{70}\text{H}_{67}\text{BCoFe}_5\text{N}_{10}$	
Formula weight	1397.32 g/mol	
Temperature	200(2) K	
Wavelength	0.71073 Å	
Crystal size	0.110 x 0.115 x 0.166 mm	
Crystal system, Space group	triclinic, <i>P</i> -1	
Unit cell dimensions	$a = 12.996(3)$ Å	$\alpha = 88.360(6)^\circ$
	$b = 15.398(4)$ Å	$\beta = 74.039(6)^\circ$
	$c = 19.482(5)$ Å	$\gamma = 68.587(6)^\circ$
Volume	3478.3(15) Å ³	
Z, Density (calculated)	2, 1.334 g/cm ³	
Absorption coefficient	1.294 mm ⁻¹	
F(000)	1438	
Theta range for data collection	1.72 to 27.58°	
Index ranges	-16 ≤ h ≤ 16, -19 ≤ k ≤ 20, -25 ≤ l ≤ 25	
Reflections collected / unique	38146 / 15959 [R(int) = 0.1267]	
Completeness to theta= 25.000	99.20%	
Absorption correction	multi-scan	
Max. and min. transmission	0.7456 and 0.6606	
Structure solution technique	direct methods	
Structure solution program	SHELXS-97 (Sheldrick 2008)	
Refinement method	Full-matrix least-squares on F ²	
Refinement program	SHELXL-2014/7 (Sheldrick, 2014)	
Function minimized	$\sum w(F_o^2 - F_c^2)^2$	
Data / restraints / parameters	15959 / 120 / 790	
Goodness-of-fit on F²	1.003	
Final R indices	5793 data; $l > 2\sigma(l)$	R1 = 0.0732, wR2 = 0.1245
	all data	R1 = 0.2172, wR2 = 0.1632
Weighting scheme	$w = 1/[\sigma^2(F_o^2) + (0.0321P)^2]$, where $P = (F_o^2 + 2F_c^2)/3$	
Largest diff. peak and hole	0.625 and -0.471 eÅ ⁻³	
R.M.S. deviation from mean	0.096 eÅ ⁻³	

Appendix B

REACTIONS OF LOW VALENT IRON AND COBALT COMPLEXES SUPPORTED BY HYDROTRIS(3-FERROCENYL-5-METHYL)PYRAZOLYL BORATO LIGANDS WITH OXO AND IMIDO TRANSFER REAGENTS

Pz^{Fc,Me}Bp^{Fc,Me}FeN₄Ad₂ (A2.1): 150 mg (0.085 mmol) of **9** was added to 10 ml of THF and then chilled to -35 °C. To this solution, with stirring, was added 60 mg (0.343 mmol, 4 equiv.) of N₃Ad, which led to immediate and vigerous effervescence of the solution. The solvent was removed in vacuo, and the remaining solid residue was then dissolved in a minimal quantity of ether and place in a -35 °C freezer, affording the desired complex as blocky orange crystals, with a total mass of 12 mg (0.010 mmol, 12 % yield). ¹H-NMR (400 MHz, C₆D₆) 59.6 (br, 2H), 34.7 (br, 6H), 27.4 (br, 1H), 25.1 (br, 4H), 11.2 (br, 4H), 5.33 (br, 5H), 5.20 (br, 2H), 3.46 (br, 6H), 3.14 (br, 10H), 1.48 (br, 2H), -6.02 (br, 3H) δ; IR (KBr): 3101 (s), 3093 (m), 3084 (m), 3077 (m), 2976 (m), 2861 (w), 2539 (m, B-H), 1561 (s), 1534 (m), 1466 (s), 1431 (s), 1424 (s), 1371 (s), 1324 (m), 1294 (m), 1223 (w), 1181 (s), 1175 (s), 1163 (m), 1105 (s), 1091 (w), 1062 (s), 1030 (m), 999 (s), 983 (w), 967 (w), 882 (s), 821 (s), 804 (s), 788 (m), 752 (m), 714 (w), 674 (w), 643 (s), 530 (m), 509 (s), 503 (s), 492 (s), 481 (s), 473 (m), 457 (w), 441 (m) cm⁻¹;

Tp^{Fc,Me}Co(TEMPO) (A2.2): 1.000 g (0.569 mmol) of **10** was added to 10 ml of THF, along with a magnetic stir bar. To that mixture was added 0.177 g (1.138 mmol, 2 equiv.) of (2,2,6,6-Tetramethylpiperidin-1-yl)oxyl radical, and solution was then

Figure B.1: Molecular structure of $\text{Tp}^{\text{Fc,Me}}\text{Co}(\text{TEMPO})$ (A2.2) represented as 50% probability thermal ellipsoids. Hydrogen atoms (with the exception of the hydrogen attached to boron, H1), and one molecule of Ether omitted for clarity.

Table B.1: Selected interatomic distances (Å) and angles (°) for $\text{Tp}^{\text{Fc,Me}}\text{Co}(\text{TEMPO})$ (A2.2).

Distances (Å)			
Co1-O1	1.857(2)	Co1-N4	2.055(3)
Co1-N2	2.094(3)	Co1-N6	2.107(3)
N1-O1	1.443(3)	N1-C5	1.480(4)
N1-C1	1.491(4)	N2-C10	1.347(4)
N2-N3	1.380(3)	N3-C12	1.357(4)
N3-B1	1.542(5)	N4-C24	1.345(4)
N4-N5	1.382(3)	N5-C26	1.348(4)
N5-B1	1.544(5)	N6-C38	1.352(4)
N6-N7	1.382(4)	N7-C40	1.354(4)
N7-B1	1.535(4)	C1-C2	1.534(5)
C3-C4	1.498(5)	C2-C3	1.525(5)
C10-C11	1.399(5)	C4-C5	1.546(5)
C11-C12	1.369(5)	C10-C17	1.457(5)
C12-C23	1.498(4)	C24-C25	1.391(5)
C24-C31	1.462(4)	C25-C26	1.367(5)
C27-C28	1.415(5)	C26-C37	1.492(5)
C32-C33	1.407(6)	C27-C31	1.419(5)
C33-C34	1.415(6)	C28-C29	1.397(6)
C34-C35	1.407(5)	C29-C30	1.421(5)
C35-C36	1.409(5)	C30-C31	1.435(5)
C38-C39	1.382(5)	C32-C36	1.400(6)
C39-C40	1.371(5)	C38-C45	1.461(5)
C40-C51	1.488(5)	C41-C42	1.418(5)
C41-C45	1.421(5)	C43-C44	1.413(5)
C42-C43	1.406(5)	C44-C45	1.434(5)
Angles (°)			
B1-Co1-O1	169.4(1)	O1-Co1-N2	117.43(10)
O1-Co1-N4	117.02(11)	O1-Co1-N6	133.38(10)

N4-Co1-N2	88.57(11)	N2-Co1-N6	93.16(10)
N4-Co1-N6	96.65(11)	O1-N1-C5	107.9(2)
O1-N1-C1	108.4(2)	C5-N1-C1	117.7(3)
C10-N2-N3	106.1(3)	C10-N2-Co1	142.6(2)
N3-N2-Co1	111.23(19)	C12-N3-N2	110.2(3)
C12-N3-B1	129.2(3)	N2-N3-B1	120.6(3)
C24-N4-N5	106.0(3)	C24-N4-Co1	142.2(2)
N5-N4-Co1	111.56(19)	C26-N5-N4	109.7(3)
C26-N5-B1	129.5(3)	N4-N5-B1	119.5(3)
C38-N6-N7	105.7(3)	C38-N6-Co1	140.5(2)
N7-N6-Co1	108.86(18)	C40-N7-N6	109.9(3)
C40-N7-B1	126.3(3)	N6-N7-B1	122.7(3)
N1-O1-Co1	115.50(17)	N7-B1-N3	108.0(3)
N7-B1-N5	111.8(3)	N3-B1-N5	109.1(3)
N1-C1-C2	107.2(3)	N1-C1-C7	107.2(3)
N1-C1-C6	115.0(3)	C7-C1-C2	108.2(3)
C2-C1-C6	110.8(3)	C7-C1-C6	108.2(3)
N1-C5-C4	107.7(3)	C3-C2-C1	113.6(3)
N1-C5-C8	115.2(3)	C4-C3-C2	109.0(3)
C4-C5-C8	109.5(3)	C3-C4-C5	113.7(3)
N2-C10-C17	123.6(3)	N1-C5-C9	106.8(3)
C12-C11-C10	106.8(3)	C9-C5-C4	109.3(3)
N3-C12-C23	122.7(3)	C9-C5-C8	108.2(3)
C14-C13-C17	108.1(3)	N2-C10-C11	109.5(3)
C15-C14-C13	108.6(3)	C11-C10-C17	126.9(3)
C14-C15-C16	107.7(3)	N3-C12-C11	107.4(3)
C15-C16-C17	108.4(3)	C11-C12-C23	129.9(3)
N4-C24-C25	109.9(3)	N4-C24-C31	121.5(3)
C25-C24-C31	128.4(3)	C26-C25-C24	106.2(3)
N5-C26-C25	108.2(3)	N5-C26-C37	123.1(3)
C25-C26-C37	128.7(3)	C28-C27-C31	108.4(4)
N6-C38-C45	124.6(3)	C29-C28-C27	108.7(3)
C40-C39-C38	106.7(3)	C28-C29-C30	108.0(3)
N7-C40-C51	122.8(3)	C29-C30-C31	108.1(3)
C42-C41-C45	108.4(3)	N6-C38-C39	110.0(3)
C43-C42-C41	108.0(3)	C39-C38-C45	125.3(3)
C43-C44-C45	108.1(3)	N7-C40-C39	107.6(3)
C41-C45-C44	106.9(3)	C39-C40-C51	129.6(3)
C44-C45-C38	123.3(3)	C41-C45-C38	129.5(3)

Table B.2: Crystal data and structure refinement for $\text{Tp}^{\text{Fc,Me}}\text{FeO}(\text{CPh}_3)$ (13).

Identification code	kla0814	
Chemical formula	$\text{C}_{130}\text{H}_{130}\text{B}_2\text{Fe}_8\text{N}_{12}\text{O}_4$	
Formula weight	2392.87 g/mol	
Temperature	200(2) K	
Wavelength	0.71073 Å	
Crystal size	0.314 x 0.487 x 0.687 mm	
Crystal system, Space group	triclinic, <i>P</i> -1	
Unit cell dimensions	a = 14.6464(13) Å b = 18.5223(17) Å c = 23.295(2) Å	$\alpha = 98.600(2)^\circ$ $\beta = 106.723(2)^\circ$ $\gamma = 93.913(2)^\circ$
Volume	5942.8(9) Å ³	
Z, Density (calculated)	2, 1.337 g/cm ³	
Absorption coefficient	1.005 mm ⁻¹	
F(000)	2488	
Theta range for data collection	0.93 to 27.58°	
Index ranges	-19 ≤ h ≤ 19, -24 ≤ k ≤ 24, -30 ≤ l ≤ 30	
Reflections collected / Unique	122436 / 27449 [R(int) = 0.0814]	
Completeness to theta = 25.000	99.80%	
Absorption correction	multi-scan	
Max. and min. transmission	0.7430 and 0.5450	
Structure solution technique	direct methods	
Structure solution program	SHELXS-97 (Sheldrick 2008)	
Refinement method	Full-matrix least-squares on F ²	
Refinement program	SHELXL-2014/7 (Sheldrick, 2014)	
Function minimized	$\sum w(F_o^2 - F_c^2)^2$	
Data / restraints / parameters	27449 / 60 / 1321	
Goodness-of-fit on F²	0.879	
$\Delta/\sigma_{\text{max}}$	0.003	
Final R indices	14238 data; $l > 2\sigma(l)$ all data	R1 = 0.0461, wR2 = 0.0983 R1 = 0.0944, wR2 = 0.1150
Weighting scheme	$w = 1/[\sigma^2(F_o^2) + (0.0506P)^2]$, where $P = (F_o^2 + 2F_c^2)/3$	

Largest diff. peak and hole 0.707 and -0.341 eÅ⁻³

Table B.3: Crystal data and structure refinement for Tp^{Fc,Me}FeS(CPh₃) (14).

Identification code	kIa0811	
Chemical formula	C ₆₁ H ₅₅ BFe ₄ N ₆ S	
Formula weight	1138.38 g/mol	
Temperature	200(2) K	
Wavelength	0.71073 Å	
Crystal size	0.404 x 0.411 x 0.590 mm	
Crystal system, Space group	monoclinic, P2 ₁ /c	
Unit cell dimensions	a = 20.9179(10) Å	α = 90°
	b = 21.0588(11) Å	β = 105.1110(10)°
	c = 12.1814(6) Å	γ = 90°
Volume	5180.4(4) Å ³	
Z, Density (calculated)	4, 1.460 g/cm ³	
Absorption coefficient	1.185 mm ⁻¹	
F(000)	2352	
Theta range for data collection	1.01 to 27.59°	
Index ranges	-27 ≤ h ≤ 26, -27 ≤ k ≤ 27, -14 ≤ l ≤ 15	
Reflections collected / unique	78940 / 11963 [R(int) = 0.0383]	
Completeness to theta = 25.000	99.70%	
Absorption correction	multi-scan	
Max. and min. transmission	0.7456 and 0.6679	
Structure solution technique	direct methods	
Structure solution program	SHELXS-97 (Sheldrick 2008)	
Refinement method	Full-matrix least-squares on F ²	
Refinement program	SHELXL-2014/7 (Sheldrick, 2014)	
Function minimized	Σ w(F _o ² - F _c ²) ²	
Data / restraints / parameters	11963 / 180 / 659	
Goodness-of-fit on F ²	1.011	
Δ/σ _{max}	0.002	
Final R indices	8934 data; I > 2σ(I)	R1 = 0.0542, wR2 = 0.1386
	all data	R1 = 0.0759, wR2 = 0.1542
Weighting scheme	w=1/[σ ² (F _o ²)+(0.0768P) ² +6.4031P], where P=(F _o ² +2F _c ²)/3	
Largest diff. peak and hole	1.845 and -0.555 eÅ ⁻³	

R.M.S. deviation from mean 0.080 eÅ⁻³

**Table B.4: Crystal data and structure refinement for [Tp^{Fe,Me}Fe]₂(μ₂-η¹:η¹-S)
(15).**

Identification code	kla0831	
Chemical formula	C ₈₈ H ₉₀ B ₂ Fe ₈ N ₁₂ OS	
Formula weight	1832.19 g/mol	
Temperature	200(2) K	
Wavelength	0.71073 Å	
Crystal size	0.314 x 0.346 x 0.575 mm	
Crystal system, Space group	triclinic, <i>P</i> -1	
Unit cell dimensions	a = 15.1852(10) Å	α = 97.8410(10)°
	b = 17.4387(12) Å	β = 111.2870(10)°
	c = 19.2740(13) Å	γ = 105.6940(10)°
Volume	4419.0(5) Å ³	
, Density (calculated)	2, 1.377 g/cm ³	
Absorption coefficient	1.349 mm ⁻¹	
F(000)	1888	
Theta range for data collection	1.53 to 27.68°	
Index ranges	-19 ≤ h ≤ 19, -22 ≤ k ≤ 22, -25 ≤ l ≤ 25	
Reflections collected / unique	74265 / 20537 [R(int) = 0.0359]	
Completeness to theta = 25.000	99.40%	
Absorption correction	multi-scan	
Max. and min. transmission	0.7456 and 0.6830	
Structure solution technique	direct methods	
Structure solution program	SHELXS-97 (Sheldrick 2008)	
Refinement method	Full-matrix least-squares on F ²	
Refinement program	SHELXL-2014/7 (Sheldrick, 2014)	
Function minimized	Σ w(F _o ² - F _c ²) ²	
Data / restraints / parameters	20537 / 180 / 1016	
Goodness-of-fit on F²	1.053	
Δ/σ_{max}	0.001	
Final R indices	13285 data; l > 2σ(l)	R1 = 0.0681, wR2 = 0.1904
	all data	R1 = 0.1034, wR2 = 0.2160

Weighting scheme	$w=1/[\sigma^2(F_o^2)+(0.1062P)^2+6.1297P]$, where $P=(F_o^2+2F_c^2)/3$
Largest diff. peak and hole	1.856 and -1.701 eÅ ⁻³
R.M.S. deviation from mean	0.089 eÅ ⁻³

Table B.5: Crystal data and structure refinement for [Tp^{Fc,Me}Fe]₂(μ₂-η¹:η¹-O)

(16).

Identification code	kIa0686	
Chemical formula	C ₉₂ H ₉₆ B ₂ Fe ₈ N ₁₂ O ₃	
Formula weight	1886.22	
Temperature	200(2) K	
Wavelength	0.71073 Å	
Crystal size	0.194 x 0.320 x 0.709 mm	
Crystal system, Space group	triclinic, <i>P</i> -1	
Unit cell dimensions	a = 15.3459(8) Å	α = 93.9270(10)°
	b = 16.8844(9) Å	β = 97.5240(10)°
	c = 17.2774(10) Å	γ = 107.9090(10)°
Volume	4194.9(4) Å ³	
Z, Density (calculated)	2, 1.493 g/cm ³	
Absorption coefficient	1.401 mm ⁻¹	
F(000)	1948	
Theta range for data collection	1.41 to 27.50°	
Index ranges	-19 ≤ h ≤ 19, -21 ≤ k ≤ 21, -22 ≤ l ≤ 22	
Reflections collected / Unique	81570 / 19220 [R(int) = 0.0567]	
Coverage of independent reflections	99.80%	
Absorption correction	multi-scan	
Max. and min. transmission	0.7456 and 0.6385	
Structure solution technique	direct methods	
Structure solution program	SHELXS-97 (Sheldrick 2008)	
Refinement method	Full-matrix least-squares on F ²	
Refinement program	SHELXL-2014/7 (Sheldrick, 2014)	
Function minimized	Σ w(F _o ² - F _c ²) ²	
Data / restraints / parameters	19220 / 100 / 1036	
Goodness-of-fit on F ²	1.005	
Δ/σ _{max}	0.001	
Final R indices	13070 data; I > 2σ(I)	R1 = 0.0486, wR2 = 0.1193
	all data	R1 = 0.0818, wR2 = 0.1383
Weighting scheme	$w=1/[\sigma^2(F_o^2)+(0.0628P)^2+4.1215P]$, where $P=(F_o^2+2F_c^2)/3$	

Largest diff. peak and hole	0.979 and -0.892 eÅ ⁻³
R.M.S. deviation from mean	0.084 eÅ ⁻³

Table B.6: Crystal data and structure refinement for Tp^{Fc,Me}CoN₄Bn₂ (17).

Identification code	kla0847	
Chemical formula	C ₁₂₄ H ₁₃₂ B ₂ Co ₂ Fe ₆ N ₂₀ O ₃	
Formula weight	2425.07 g/mol	
Temperature	200(2) K	
Wavelength	0.71073 Å	
Crystal size	0.064 x 0.180 x 0.342 mm	
Crystal system, Space group	triclinic, <i>P</i> -1	
Unit cell dimensions	a = 16.410(2) Å	α = 91.141(3)°
	b = 18.748(2) Å	β = 106.721(3)°
	c = 20.280(3) Å	γ = 94.835(3)°
Volume	5947.8(12) Å ³	
Z, Density (calculated)	2, 1.354 g/cm ³	
Absorption coefficient	1.041 mm ⁻¹	
F(000)	2520	
Theta range for data collection	1.48 to 27.56°	
Index ranges	-21 ≤ h ≤ 21, -24 ≤ k ≤ 24, -26 ≤ l ≤ 26	
Reflections collected / unique	91895 / 27402 [R(int) = 0.1084]	
Completeness to theta = 25.000	99.60%	
Absorption correction	multi-scan	
Max. and min. transmission	0.7456 and 0.6550	
Structure solution technique	direct methods	
Structure solution program	SHELXS-97 (Sheldrick 2008)	
Refinement method	Full-matrix least-squares on F ²	
Refinement program	SHELXL-2014/7 (Sheldrick, 2014)	
Function minimized	Σ w(F _o ² - F _c ²) ²	
Data / restraints / parameters	27402 / 192 / 1285	
Goodness-of-fit on F ²	1.002	
Δ/σ _{max}	0.001	
Final R indices	12830 data; I > 2σ(I)	R1 = 0.0638, wR2 = 0.1033
	all data	R1 = 0.1547, wR2 = 0.1263
Weighting scheme	w = 1/[σ ² (F _o ²) + (0.0300P) ²], where P = (F _o ² + 2F _c ²)/3	
Largest diff. peak and hole	0.435 and -0.331 eÅ ⁻³	
R.M.S. deviation from mean	0.072 eÅ ⁻³	

Table B.7: Crystal data and structure refinement for $\text{Tp}^{\text{Fc,Me}}\text{FeNHPPh}$ (18).

Identification code	kla0796	
Chemical formula	$\text{C}_{50}\text{H}_{51}\text{BFe}_4\text{N}_7\text{O}_{0.50}$	
Formula weight	992.18 g/mol	
Temperature	200(2) K	
Wavelength	0.71073 Å	
Crystal size	0.262 x 0.383 x 0.436 mm	
Crystal system, Space group	triclinic, <i>P</i> -1	
Unit cell dimensions	a = 10.9098(9) Å	$\alpha = 109.8791(14)^\circ$
	b = 14.0615(11) Å	$\beta = 107.0123(14)^\circ$
	c = 16.8662(14) Å	$\gamma = 95.3290(14)^\circ$
Volume	2272.9(3) Å ³	
Z, Density (calculated)	2, 1.450 g/cm ³	
Absorption coefficient	1.296 mm ⁻¹	
F(000)	1026	
Theta range for data collection	1.37 to 27.73°	
Index ranges	-14 ≤ h ≤ 14, -18 ≤ k ≤ 18, -22 ≤ l ≤ 21	
Reflections collected / unique	61826 / 10626 [R(int) = 0.0371]	
Completeness to theta = 25.000	99.40%	
Absorption correction	multi-scan	
Max. and min. transmission	0.7456 and 0.6625	
Structure solution technique	direct methods	
Structure solution program	SHELXS-97 (Sheldrick 2008)	
Refinement method	Full-matrix least-squares on F ²	
Refinement program	SHELXL-2014/7 (Sheldrick, 2014)	
Function minimized	$\sum w(F_o^2 - F_c^2)^2$	
Data / restraints / parameters	10626 / 105 / 590	
Goodness-of-fit on F²	1.147	
$\Delta/\sigma_{\text{max}}$	0.001	
Final R indices	8669 data; I > 2σ(I)	R1 = 0.0428, wR2 = 0.1159
	all data	R1 = 0.0538, wR2 = 0.1237
Weighting scheme	w = 1/[σ ² (F _o ²) + (0.0693P) ² + 0.6109P], where P = (F _o ² + 2F _c ²)/3	
Largest diff. peak and hole	1.176 and -0.640 eÅ ⁻³	
R.M.S. deviation from mean	0.078 eÅ ⁻³	

Table B.8: Crystal data and structure refinement for $\text{Tp}^{\text{Fc,Me}}\text{CoNHPPh}$ (19).

Identification code	k1a0795	
Chemical formula	$\text{C}_{50}\text{H}_{51}\text{BCoFe}_3\text{N}_7\text{O}_{0.50}$	
Formula weight	995.26 g/mol	
Temperature	200(2) K	
Wavelength	0.71073 Å	
Crystal size	0.514 x 0.586 x 0.852 mm	
Crystal system, Space group	triclinic, $P-1$	
Unit cell dimensions	$a = 10.8973(9)$ Å	$\alpha = 109.6630(10)^\circ$
	$b = 14.0670(12)$ Å	$\beta = 106.8230(10)^\circ$
	$c = 16.7954(14)$ Å	$\gamma = 95.4280(10)^\circ$
Volume	2267.5(3) Å ³	
Z, Density (calculated)	2, 1.458 g/cm ³	
Absorption coefficient	1.345 mm ⁻¹	
F(000)	1028	
Theta range for data collection	1.65 to 27.66°	
Index ranges	-14 ≤ h ≤ 14, -18 ≤ k ≤ 18, -21 ≤ l ≤ 21	
Reflections collected / unique	35590 / 10500 [R(int) = 0.0246]	
Completeness to Theta = 25.000	99.20%	
Absorption correction	multi-scan	
Max. and min. transmission	0.7456 and 0.5170	
Structure solution technique	direct methods	
Structure solution program	SHELXS-97 (Sheldrick 2008)	
Refinement method	Full-matrix least-squares on F ²	
Refinement program	SHELXL-2014/7 (Sheldrick, 2014)	
Function minimized	$\sum w(F_o^2 - F_c^2)^2$	
Data / restraints / parameters	10500 / 120 / 590	
Goodness-of-fit on F²	1.008	
$\Delta/\sigma_{\text{max}}$	0.001	
Final R indices	9257 data; $ I > 2\sigma(I)$	R1 = 0.0386, wR2 = 0.1016
	all data	R1 = 0.0445, wR2 = 0.1070
Weighting scheme	$w = 1/[\sigma^2(F_o^2) + (0.0590P)^2 + 2.3934P]$, where $P = (F_o^2 + 2F_c^2)/3$	
Largest diff. peak and hole	1.201 and -0.747 eÅ ⁻³	
R.M.S. deviation from mean	0.076 eÅ ⁻³	

Table B.9: Crystal data and structure refinement for $\text{Pz}^{\text{Fc,Me}}\text{Bp}^{\text{Fc,Me}}\text{FeN}_4\text{Ad}_2$

(A2.1).

Identification code	kIa0682	
Chemical formula	$\text{C}_{35.50}\text{H}_{44}\text{BFe}_2\text{N}_5\text{O}$	
Formula weight	679.26 g/mol	
Temperature	200(2) K	
Wavelength	0.71073 Å	
Crystal size	0.190 x 0.423 x 0.536 mm	
Crystal system, Space group	triclinic, <i>P</i> -1	
Unit cell dimensions	a = 10.6844(7) Å	$\alpha = 72.7820(10)^\circ$
	b = 14.0059(9) Å	$\beta = 87.787(2)^\circ$
	c = 23.6279(18) Å	$\gamma = 74.7910(10)^\circ$
Volume	3256.1(4) Å ³	
Z, Density (calculated)	4, 1.386 g/cm ³	
Absorption coefficient	0.928 mm ⁻¹	
F(000)	1428	
Theta range for data collection	1.57 to 27.60°	
Index ranges	-13 ≤ h ≤ 13, -18 ≤ k ≤ 18, -30 ≤ l ≤ 30	
Reflections collected / unique	60286 / 15047 [R(int) = 0.0453]	
Completeness to theta = 25.000	99.70%	
Absorption correction	multi-scan	
Max. and min. transmission	0.7456 and 0.6644	
Structure solution technique	direct methods	
Structure solution program	SHELXS-97 (Sheldrick 2008)	
Refinement method	Full-matrix least-squares on F ²	
Refinement program	SHELXL-2014/7 (Sheldrick, 2014)	
Function minimized	$\sum w(F_o^2 - F_c^2)^2$	
Data / restraints / parameters	15047 / 0 / 725	
Goodness-of-fit on F²	1.025	
$\Delta/\sigma_{\text{max}}$	0.002	
Final R indices	10900 data; $ I > 2\sigma(I)$	R1 = 0.0447, wR2 = 0.1096
	all data	R1 = 0.0686, wR2 = 0.1219
Weighting scheme	$w = 1/[\sigma^2(F_o^2) + (0.0622P)^2 + 0.9135P]$, where $P = (F_o^2 + 2F_c^2)/3$	
Largest diff. peak and hole	1.900 and -0.436 eÅ ⁻³	
R.M.S. deviation from mean	0.067 eÅ ⁻³	

Table B.10: Crystal data and structure refinement for $\text{Tp}^{\text{Fc,Me}}\text{Co}(\text{TEMPO})$

(A2.2).

Identification code	klA0707	
Chemical formula	$\text{C}_{57.50}\text{H}_{74}\text{BCoFe}_3\text{N}_7\text{O}_2$	
Formula weight	1132.52	
Temperature	200(2) K	
Wavelength	0.71073 Å	
Crystal size	0.162 x 0.220 x 0.315 mm	
Crystal system, Space group	triclinic, $P-1$	
Unit cell dimensions	$a = 11.0395(10)$ Å	$\alpha = 85.542(2)^\circ$
	$b = 15.8294(15)$ Å	$\beta = 71.509(2)^\circ$
	$c = 16.7461(16)$ Å	$\gamma = 81.893(2)^\circ$
Volume	$2745.8(4)$ Å ³	
Z, Density (calculated)	2, 1.370 g/cm ³	
Absorption coefficient	1.121 mm ⁻¹	
F(000)	1188	
Theta range for data collection	1.79 to 27.52°	
Index ranges	$-14 \leq h \leq 14, -20 \leq k \leq 20, -21 \leq l \leq 21$	
Reflections collected / unique	54227 / 12600 [R(int) = 0.0820]	
Max. and min. transmission	0.7456 and 0.6737	
Structure solution technique	direct methods	
Structure solution program	SHELXS-97 (Sheldrick 2008)	
Refinement method	Full-matrix least-squares on F^2	
Refinement program	SHELXL-2014/7 (Sheldrick, 2014)	
Function minimized	$\sum w(F_o^2 - F_c^2)^2$	
Data / restraints / parameters	12600 / 55 / 657	
Goodness-of-fit on F^2	1.023	
$\Delta/\sigma_{\text{max}}$	0.001	
Final R indices	7640 data; $I > 2\sigma(I)$	R1 = 0.0490, wR2 = 0.1043
	all data	R1 = 0.0995, wR2 = 0.1259
Weighting scheme	$w = 1/[\sigma^2(F_o^2) + (0.0505P)^2 + 0.2406P]$, where $P = (F_o^2 + 2F_c^2)/3$	
Largest diff. peak and hole	0.549 and -0.507 eÅ ⁻³	
R.M.S. deviation from mean	0.081 eÅ ⁻³	

Appendix C

SYNTHESIS OF NITRIDO COMPLEXES SUPPORTED BY TRIS(PYRAZOLYL)BORATO LIGANDS, THEIR CHARACTERIZATION AND REACTIVITY

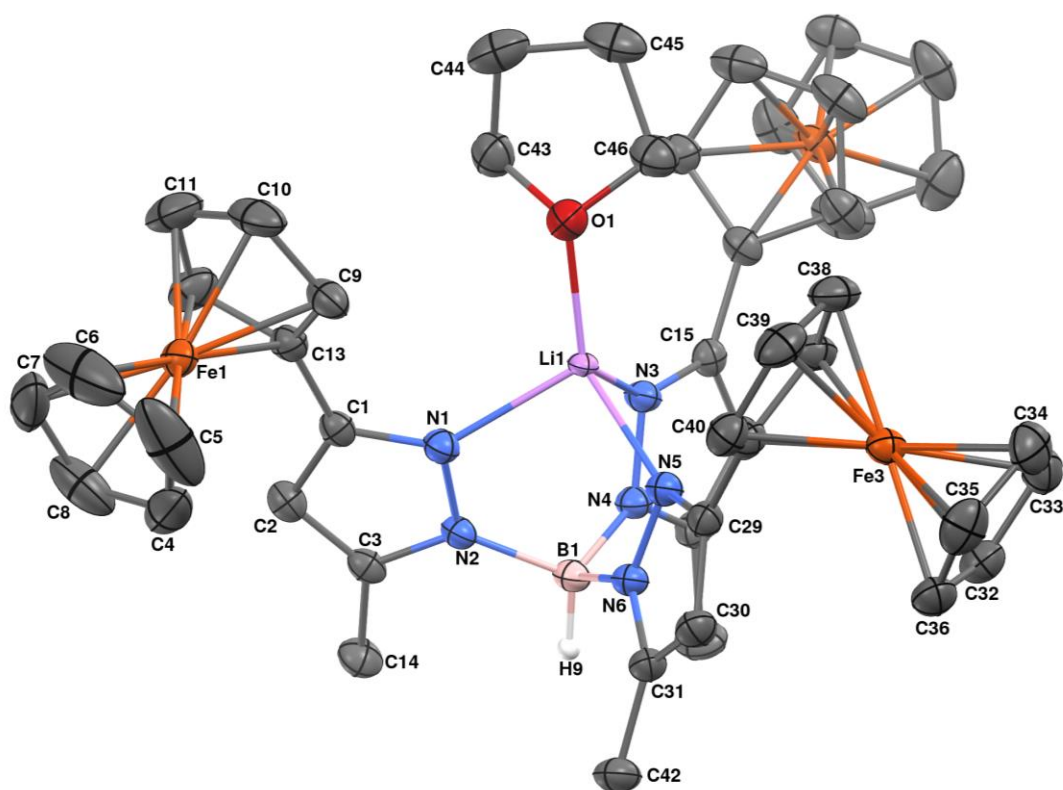


Figure C.1: Molecular structure of $\text{Tp}^{\text{Fc,Me}}\text{Li}(\text{THF})$ (A3.1) represented as 50% probability thermal ellipsoids. Hydrogen atoms (with the exception of the hydrogen attached to boron, H1) omitted for clarity.

Table C.1: Selected interatomic distances (Å) and angles (°) for $\text{Tp}^{\text{Fc,Me}}\text{Li}(\text{THF})$ **(A3.1).**

Distances (Å)			
Li1-O1	1.910(3)	Li1-N5	2.055(3)
Li1-N3	2.063(3)	Li1-N1	2.081(3)
N1-C1	1.336(3)	N1-N2	1.377(2)
N2-C3	1.359(2)	N2-B1	1.552(3)
N3-C15	1.338(2)	N3-N4	1.371(2)
N4-C17	1.355(2)	N4-B1	1.552(3)
N5-C29	1.333(2)	N5-N6	1.378(2)
N6-C31	1.358(2)	N6-B1	1.549(3)
C1-C13	1.467(3)	C1-C2	1.408(3)
C3-C14	1.501(3)	C2-C3	1.381(3)
C4-C8	1.368(5)	C4-C5	1.366(6)
C5-C6	1.381(6)	C9-C10	1.422(3)
C6-C7	1.371(6)	C15-C16	1.403(3)
C7-C8	1.382(5)	C16-C17	1.381(3)
C9-C13	1.428(3)	C17-C28	1.501(3)
C10-C11	1.422(4)	C18-C22	1.420(4)
C11-C12	1.417(4)	C19-C20	1.407(4)
C12-C13	1.432(3)	C20-C21	1.410(4)
C15-C27	1.477(3)	C21-C22	1.407(3)
C18-C19	1.414(4)	C23-C27	1.428(3)
C23-C24	1.415(3)	C24-C25	1.419(4)
C29-C30	1.403(3)	C25-C26	1.425(3)
C30-C31	1.380(3)	C26-C27	1.432(3)
C31-C42	1.496(3)	C29-C41	1.467(3)
C32-C33	1.416(3)	C32-C36	1.415(3)
C33-C34	1.419(4)	C37-C38	1.429(3)
C34-C35	1.417(4)	C43-O1	1.431(3)
C35-C36	1.413(4)	C44-C45	1.520(4)
C37-C41	1.433(3)	C46-O1	1.417(3)
C38-C39	1.419(4)	C43-C44	1.500(3)
C39-C40	1.416(3)	C45-C46	1.518(3)
C40-C41	1.431(3)		

Angles (°)

O1-Li1-N3	118.28(15)	O1-Li1-N5	132.92(16)
O1-Li1-N1	114.07(15)	N5-Li1-N3	91.31(13)
N3-Li1-N1	98.65(13)	N5-Li1-N1	94.57(13)
C1-N1-Li1	140.31(16)	C1-N1-N2	106.08(15)
C3-N2-N1	110.15(16)	N2-N1-Li1	107.45(14)
N1-N2-B1	120.40(15)	C3-N2-B1	129.43(16)
C15-N3-Li1	141.30(15)	C15-N3-N4	106.28(15)
C17-N4-N3	110.38(15)	N4-N3-Li1	109.79(13)
N3-N4-B1	120.30(15)	C17-N4-B1	128.92(16)
C29-N5-Li1	139.56(16)	C29-N5-N6	106.04(15)
C31-N6-N5	110.22(16)	N6-N5-Li1	107.85(14)
N5-N6-B1	120.91(15)	C31-N6-B1	128.69(16)
N6-B1-N4	109.58(16)	N6-B1-N2	109.56(16)
N1-C1-C13	121.36(17)	N2-B1-N4	109.76(15)
C3-C2-C1	105.18(17)	N1-C1-C2	110.68(18)
N2-C3-C14	122.85(18)	C2-C1-C13	127.96(18)
C5-C4-C8	107.2(3)	N2-C3-C2	107.90(17)
C4-C5-C6	109.4(3)	C2-C3-C14	129.26(18)
C7-C6-C5	106.9(3)	C9-C13-C1	126.87(19)
C6-C7-C8	108.1(3)	N3-C15-C27	118.98(17)
C4-C8-C7	108.5(3)	C17-C16-C15	105.71(17)
C10-C9-C13	108.4(2)	N4-C17-C28	122.96(18)
C11-C10-C9	107.7(2)	C19-C18-C22	108.0(2)
C12-C11-C10	108.4(2)	C20-C19-C18	107.7(2)
C11-C12-C13	108.1(2)	C19-C20-C21	108.5(2)
C9-C13-C12	107.3(2)	C22-C21-C20	108.1(2)
C12-C13-C1	125.9(2)	C21-C22-C18	107.7(2)
N3-C15-C16	110.15(17)	C24-C23-C27	108.7(2)
C16-C15-C27	130.61(18)	C23-C24-C25	107.9(2)
N4-C17-C16	107.48(17)	C24-C25-C26	108.3(2)
C16-C17-C28	129.56(19)	C25-C26-C27	107.9(2)
C23-C27-C15	127.51(18)	C23-C27-C26	107.11(18)
N5-C29-C41	119.94(17)	C26-C27-C15	124.99(18)
C31-C30-C29	105.57(18)	N5-C29-C30	110.62(18)
N6-C31-C42	123.23(19)	C30-C29-C41	129.38(18)
C36-C32-C33	107.8(2)	N6-C31-C30	107.52(17)
C32-C33-C34	108.2(2)	C30-C31-C42	129.25(19)
C35-C34-C33	107.7(2)	C40-C41-C29	126.07(19)

C36-C35-C34	108.2(2)	C46-O1-Li1	122.31(16)
C35-C36-C32	108.1(2)	C39-C40-C41	108.5(2)
C38-C37-C41	108.11(19)	C40-C41-C37	107.16(19)
C39-C38-C37	107.9(2)	C37-C41-C29	126.76(18)
C40-C39-C38	108.4(2)	O1-C43-C44	103.53(19)
C43-O1-Li1	119.55(16)	C43-C44-C45	102.5(2)
C46-C45-C44	104.2(2)	C46-O1-C43	107.83(17)
O1-C46-C45	106.7(2)		

Table C.2: Crystal data and structure refinement for $\text{Tp}^{\text{Fc,Me}}\text{FeN}_3$ (20).

Identification code	kIa0631	
Chemical formula	$\text{C}_{42}\text{H}_{40}\text{BFe}_4\text{N}_9$	
Formula weight	905.04	
Temperature	200(2) K	
Wavelength	0.71073 Å	
Crystal size	0.248 x 0.355 x 0.441 mm	
Crystal system, Space group	triclinic, $P-1$	
Unit cell dimensions	a = 13.2864(7) Å	$\alpha = 106.6524(11)^\circ$
	b = 13.3629(7) Å	$\beta = 112.4624(11)^\circ$
	c = 13.4127(7) Å	$\gamma = 106.3029(11)^\circ$
Volume	1892.58(17) Å ³	
Z, Density (calculated)	2, 1.588 g/cm ³	
Absorption coefficient	1.548 mm ⁻¹	
F(000)	928	
Theta range for data collection	1.77 to 27.48°	
Index ranges	-17 ≤ h ≤ 17, -17 ≤ k ≤ 17, -17 ≤ l ≤ 17	
Reflections collected, unique	29190, 8643 [R(int) = 0.0365]	
Completeness to theta = 25.000	99.70%	
Absorption correction	multi-scan	
Max. and min. transmission	0.7456 and 0.6031	
Structure solution technique	direct methods	
Structure solution program	SHELXS-97 (Sheldrick 2008)	
Refinement method	Full-matrix least-squares on F ²	
Refinement program	SHELXL-2014 (Sheldrick, 2014)	
Function minimized	$\Sigma w(F_o^2 - F_c^2)^2$	
Data / restraints / parameters	8643 / 81 / 527	
Goodness-of-fit on F²	1.015	
$\Delta/\sigma_{\text{max}}$	0.001	
Final R indices	6731 data; $l > 2\sigma(l)$	R1 = 0.0375, wR2 = 0.0994
	all data	R1 = 0.0538, wR2 = 0.1100
Weighting scheme	$w = 1/[\sigma^2(F_o^2) + (0.0650P)^2]$, where $P = (F_o^2 + 2F_c^2)/3$	
Absolute structure parameter	0.0(0)	
Largest diff. peak and hole	0.626 and -0.405 eÅ ⁻³	
R.M.S. deviation from mean	0.073 eÅ ⁻³	

Table C.3: Crystal data and structure refinement for $\text{Tp}^{\text{Fc,Me}}\text{FeN}_3$ (20).

Identification code	kIa0633	
Chemical formula	$\text{C}_{46}\text{H}_{48}\text{BFe}_4\text{N}_9\text{O}$	
Formula weight	977.14 g/mol	
Temperature	200(2) K	
Wavelength	0.71073 Å	
Crystal size	0.342 x 0.438 x 0.664 mm	
Crystal system, Space group	orthorhombic, $Pna2_1$	
Unit cell dimensions	a = 12.0604(4) Å	$\alpha = 90^\circ$
	b = 22.4098(8) Å	$\beta = 90^\circ$
	c = 15.8863(5) Å	$\gamma = 90^\circ$
Volume	4293.6(2) Å ³	
Z, Density (calculated)	4, 1.512 g/cm ³	
Absorption coefficient	1.373 mm ⁻¹	
F(000)	2016	
Theta range for data collection	1.57 to 27.54°	
Index ranges	-15 ≤ h ≤ 15, -26 ≤ k ≤ 29, -20 ≤ l ≤ 20	
Reflections collected / unique	47674 / 9835 [R(int) = 0.0434]	
Max. and min. transmission	0.7456 and 0.6072	
Completeness to theta = 25.000	99.80%	
Structure solution technique	direct methods	
Structure solution program	SHELXS-97 (Sheldrick 2008)	
Refinement method	Full-matrix least-squares on F ²	
Refinement program	SHELXL-2017/1 (Sheldrick, 2017)	
Function minimized	$\sum w(F_o^2 - F_c^2)^2$	
Data / restraints / parameters	9835 / 121 / 544	
Goodness-of-fit on F ²	1.029	
$\Delta/\sigma_{\text{max}}$	0.004	
Final R indices	8571 data; $l > 2\sigma(l)$	R1 = 0.0360, wR2 = 0.0844
	all data	R1 = 0.0451, wR2 = 0.0890
Weighting scheme	$w = 1/[\sigma^2(F_o^2) + (0.0450P)^2 + 1.0554P]$, where $P = (F_o^2 + 2F_c^2)/3$	
Absolute structure parameter	-0.005(7)	
Largest diff. peak and hole	0.511 and -0.393 eÅ ⁻³	
R.M.S. deviation from mean	0.061 eÅ ⁻³	

Table C.4: Crystal data and structure refinement for $\text{Tp}^{\text{tBu,Me}}\text{Fe-dbabh}$ (22).

Identification code	klA0860	
Chemical formula	$\text{C}_{38}\text{H}_{50}\text{BFeN}_7$	
Formula weight	671.51 g/mol	
Temperature	200(2) K	
Wavelength	0.71073 Å	
Crystal size	0.138 x 0.263 x 0.366 mm	
Crystal system, Space group	monoclinic, $P2_1/c$	
Unit cell dimensions	a = 15.3498(16) Å	$\alpha = 90^\circ$
	b = 9.8378(11) Å	$\beta = 96.073(2)^\circ$
	c = 24.389(3) Å	$\gamma = 90^\circ$
Volume	3662.3(7) Å ³	
Z, Density (calculated)	4, 1.218 g/cm ³	
Absorption coefficient	0.448 mm ⁻¹	
F(000)	1432	
Theta range for data collection	1.68 to 27.58°	
Index ranges	-19 ≤ h ≤ 18, -12 ≤ k ≤ 12, -31 ≤ l ≤ 31	
Reflections collected / unique	31807 / 8460 [R(int) = 0.0539]	
Completeness to theta = 25.000	99.80%	
Absorption correction	multi-scan	
Max. and min. transmission	0.7456 and 0.6548	
Structure solution technique	direct methods	
Structure solution program	SHELXS-97 (Sheldrick 2008)	
Refinement method	Full-matrix least-squares on F ²	
Refinement program	SHELXL-2014/7 (Sheldrick, 2014)	
Function minimized	$\sum w(F_o^2 - F_c^2)^2$	
Data / restraints / parameters	8460 / 0 / 437	
Goodness-of-fit on F²	1.028	
$\Delta/\sigma_{\text{max}}$	0.004	
Final R indices	6084 data; $I > 2\sigma(I)$	R1 = 0.0545, wR2 = 0.1193
	all data	R1 = 0.0813, wR2 = 0.1303
Weighting scheme	$w = 1/[\sigma^2(F_o^2) + (0.0359P)^2 + 4.4411P]$, where $P = (F_o^2 + 2F_c^2)/3$	
Largest diff. peak and hole	0.586 and -0.310 eÅ ⁻³	
R.M.S. deviation from mean	0.061 eÅ ⁻³	

Table C.5: Crystal data and structure refinement for $\text{Tp}^{\text{tBu,Me}}\text{Co-dbabh}$ (23).

Identification code	kla0887	
Chemical formula	$\text{C}_{38}\text{H}_{50}\text{BCoN}_7$	
Formula weight	674.59 g/mol	
Temperature	200(2) K	
Wavelength	0.71073 Å	
Crystal size	0.240 x 0.264 x 0.275 mm	
Crystal habit	clear light brown-red Block	
Crystal system, Space group	monoclinic, $P2_1/c$	
Unit cell dimensions	$a = 15.3437(7)$ Å	$\alpha = 90^\circ$
	$b = 9.8366(4)$ Å	$\beta = 95.8260(10)^\circ$
	$c = 24.3022(11)$ Å	$\gamma = 90^\circ$
Volume	$3649.0(3)$ Å ³	
Z, Density (calculated)	4, 1.228 g/cm ³	
Absorption coefficient	0.507 mm ⁻¹	
F(000)	1436	
Theta range for data collection	1.69 to 27.66°	
Index ranges	$-19 \leq h \leq 20$, $-12 \leq k \leq 12$, $-31 \leq l \leq 31$	
Reflections collected / unique	74862 / 8457 [R(int) = 0.0723]	
Completeness to Theta = 25.000	99.40%	
Absorption correction	multi-scan	
Max. and min. transmission	0.7456 and 0.7016	
Structure solution technique	direct methods	
Structure solution program	SHELXS-97 (Sheldrick 2008)	
Refinement method	Full-matrix least-squares on F^2	
Refinement program	SHELXL-2014/7 (Sheldrick, 2014)	
Function minimized	$\sum w(F_o^2 - F_c^2)^2$	
Data / restraints / parameters	8457 / 0 / 439	
Goodness-of-fit on F^2	1.008	
$\Delta/\sigma_{\text{max}}$	0.001	
Final R indices	6470 data; $l > 2\sigma(l)$	R1 = 0.0445, wR2 = 0.1051
	all data	R1 = 0.0650, wR2 = 0.1160
Weighting scheme	$w = 1/[\sigma^2(F_o^2) + (0.0561P)^2 + 1.5205P]$, where $P = (F_o^2 + 2F_c^2)/3$	
Largest diff. peak and hole	0.375 and -0.319 eÅ ⁻³	
R.M.S. deviation from mean	0.068 eÅ ⁻³	

Table C.6: Crystal data and structure refinement for $\text{Tp}^{\text{tBu,Me}}\text{CrN}$ (24).

Identification code	kla0877	
Chemical formula	$\text{C}_{12}\text{H}_{20}\text{B}_{0.50}\text{Cr}_{0.50}\text{N}_{3.50}$	
Formula weight	244.72 g/mol	
Temperature	200(2) K	
Wavelength	0.71073 Å	
Crystal size	0.096 x 0.230 x 0.404 mm	
Crystal system, Space group	orthorhombic, <i>Ama</i> 2	
Unit cell dimensions	a = 16.6393(14) Å	$\alpha = 90^\circ$
	b = 15.8199(13) Å	$\beta = 90^\circ$
	c = 10.3901(8) Å	$\gamma = 90^\circ$
Volume	2735.0(4) Å ³	
Z, Density (calculated)	8, 1.189 g/cm ³	
Absorption coefficient	0.442 mm ⁻¹	
F(000)	1048	
Theta range for data collection	2.35 to 27.61°	
Index ranges	-21 ≤ h ≤ 21, -20 ≤ k ≤ 20, -13 ≤ l ≤ 13	
Reflections collected / unique	20675 / 3289 [R(int) = 0.0396]	
Completeness to Theta = 25.000	99.90%	
Absorption correction	multi-scan	
Max. and min. transmission	0.7456 and 0.6660	
Structure solution technique	direct methods	
Structure solution program	SHELXS-97 (Sheldrick 2008)	
Refinement method	Full-matrix least-squares on F ²	
Refinement program	SHELXL-2014/7 (Sheldrick, 2014)	
Function minimized	$\sum w(F_o^2 - F_c^2)^2$	
Data / restraints / parameters	3289 / 1 / 172	
Goodness-of-fit on F²	1.037	
Final R indices	2971 data; $l > 2\sigma(l)$	R1 = 0.0321, wR2 = 0.0815
	all data	R1 = 0.0377, wR2 = 0.0844
Weighting scheme	$w = 1 / [\sigma^2(F_o^2) + (0.0518P)^2]$, where $P = (F_o^2 + 2F_c^2) / 3$	
Absolute structure parameter	-0.0(0)	
Largest diff. peak and hole	0.434 and -0.158 eÅ ⁻³	
R.M.S. deviation from mean	0.039 eÅ ⁻³	

Table C.7: Crystal data and structure refinement for $\text{Tp}^{\text{tBu,Me}}\text{Cr}(\text{N})(\text{I})$ (25).

Identification code	kIa0921	
Chemical formula	$\text{C}_{24}\text{H}_{40}\text{BCrIN}_7$	
Formula weight	616.34 g/mol	
Temperature	200(2) K	
Wavelength	0.71073 Å	
Crystal size	0.136 x 0.148 x 0.185 mm	
Crystal habit	clear intense yellow Block	
Crystal system, Space group	monoclinic, $P2_1/c$	
Unit cell dimensions	$a = 9.7587(8)$ Å	$\alpha = 90^\circ$
	$b = 13.1948(10)$ Å	$\beta = 95.085(2)^\circ$
	$c = 22.6589(18)$ Å	$\gamma = 90^\circ$
Volume	$2906.2(4)$ Å ³	
Z, Density (calculated)	4, 1.409 g/cm ³	
Absorption coefficient	1.480 mm ⁻¹	
F(000)	1260	
Theta range for data collection	1.80 to 27.66°	
Index ranges	-12 ≤ h ≤ 12, -17 ≤ k ≤ 17, -29 ≤ l ≤ 27	
Reflections collected / unique	43551 / 6763 [R(int) = 0.0644]	
Completeness to theta = 25.000	99.50%	
Absorption correction	multi-scan	
Max. and min. transmission	0.7456 and 0.5882	
Structure solution technique	direct methods	
Structure solution program	SHELXS-97 (Sheldrick 2008)	
Refinement method	Full-matrix least-squares on F^2	
Refinement program	SHELXL-2014/7 (Sheldrick, 2014)	
Function minimized	$\sum w(F_o^2 - F_c^2)^2$	
Data / restraints / parameters	6763 / 0 / 322	
Goodness-of-fit on F^2	1.022	
Final R indices	5231 data; $l > 2\sigma(l)$	R1 = 0.0456, wR2 = 0.1207
	all data	R1 = 0.0628, wR2 = 0.1318
Weighting scheme	$w = 1/[\sigma^2(F_o^2) + (0.0722P)^2 + 2.5325P]$, where $P = (F_o^2 + 2F_c^2)/3$	
Largest diff. peak and hole	1.970 and -1.100 eÅ ⁻³	
R.M.S. deviation from mean	0.100 eÅ ⁻³	

Table C.8: Crystal data and structure refinement for $\text{Tp}^{\text{tBu,Me}}\text{CrNMe}$ (26).

Identification code	kla0943	
Chemical formula	$\text{C}_{25}\text{H}_{43}\text{BCrN}_7$	
Formula weight	504.47 g/mol	
Temperature	200(2) K	
Wavelength	0.71073 Å	
Crystal size	0.110 x 0.197 x 0.294 mm	
Crystal habit	translucent intense purple-violet Block	
Crystal system, Space group	trigonal, $R3c$	
Unit cell dimensions	$a = 30.730(3)$ Å	$\alpha = 90^\circ$
	$b = 30.730(3)$ Å	$\beta = 90^\circ$
	$c = 19.420(2)$ Å	$\gamma = 120^\circ$
Volume	15882.(4) Å ³	
Z, Density (calculated)	18, 0.949 g/cm ³	
Absorption coefficient	0.344 mm ⁻¹	
F(000)	4878	
Theta range for data collection	2.23 to 27.63°	
Index ranges	-39 ≤ h ≤ 39, -39 ≤ k ≤ 39, -25 ≤ l ≤ 25	
Reflections collected / unique	59714 / 8160 [R(int) = 0.1126]	
Completeness to theta = 25.000	99.80%	
Max. and min. transmission	0.7456 and 0.5465	
Structure solution technique	direct methods	
Structure solution program	SHELXS-97 (Sheldrick 2008)	
Refinement method	Full-matrix least-squares on F ²	
Refinement program	SHELXL-2014/7 (Sheldrick, 2014)	
Function minimized	$\sum w(F_o^2 - F_c^2)^2$	
Data / restraints / parameters	8160 / 1 / 320	
Goodness-of-fit on F²	1.007	
$\Delta/\sigma_{\text{max}}$	0.006	
Final R indices	5254 data; $l > 2\sigma(l)$	R1 = 0.0481, wR2 = 0.1029
	all data	R1 = 0.0912, wR2 = 0.1198
Weighting scheme	$w = 1/[\sigma^2(F_o^2) + (0.0531P)^2]$, where $P = (F_o^2 + 2F_c^2)/3$	
Absolute structure parameter	-0.0(0)	
Largest diff. peak and hole	0.394 and -0.261 eÅ ⁻³	
R.M.S. deviation from mean	0.038 eÅ ⁻³	